Technical Report

UCAM-CL-TR-261
ISSN 1476-2986

Number 261

UNIVERSITY OF CAMBRIDGE
Computer Laboratory

Image resampling

Neil Anthony Dodgson

August 1992

15 JJ Thomson Avenue
Cambridge CB3 0FD
United Kingdom
phone +44 1223 763500

http://www.cl.cam.ac.uk/

This technical report is based on a dissertation submitted by the author for the degree of Doctor of Philosophy to the University of Cambridge, Wolfson College.

Technical reports published by the University of Cambridge Computer Laboratory are freely available via the Internet:

http://www.cl.cam.ac.uk/TechReports/

ISSN 1476-2986

Summary

Image resampling is the process of geometrically transforming digital images. This dissertation considers several aspects of the process.

We begin by decomposing the resampling process into three simpler sub-processes: reconstruction of a continuous intensity surface from a discrete image, transformation of that continuous surface, and sampling of the transformed surface to produce a new discrete image. We then consider the sampling process, and the subsidiary problem of intensity quantisation. Both these are well understood, and we present a summary of existing work, laying a foundation for the central body of the dissertation where the sub-process of reconstruction is studied.

The work on reconstruction divides into four parts, two general and two specific:

1. Piecewise local polynomials: the most studied group of reconstructors. We examine these, and the criteria used in their design. One new derivation is of two piecewise local quadratic reconstructors.

2. Infinite extent reconstructors: we consider these and their local approximations, the problem of finite image size, the resulting edge effects, and the solutions to these problems. Amongst the reconstructors discussed are the interpolating cubic B-spline and the interpolating Bezier cubic. We derive the filter kernels for both of these, and prove that they are the same. Given this kernel we demonstrate how the interpolating cubic B-spline can be extended from a one-dimensional to a two-dimensional reconstructor, providing a considerable speed improvement over the existing method of extension.

3. Fast Fourier transform reconstruction: it has long been known that the fast Fourier transform (FFT) can be used to generate an approximation to perfect scaling of a sample set. Donald Fraser (in 1987) took this result and generated a hybrid FFT reconstructor which can be used for general transformations, not just scaling. We modify Fraser's method to tackle two major problems: its large time and storage requirements, and the edge effects it causes in the reconstructed intensity surface.

4. *A priori* knowledge reconstruction: first considering what can be done if we know how the original image was sampled, and then considering what can be done with one particular class of image coupled with one particular type of sampling. In this latter case we find that exact reconstruction of the image is possible. This is a surprising result as this class of images cannot be exactly reconstructed using classical sampling theory.

The final section of the dissertation draws all of the strands together to discuss transformations and the resampling process as a whole. Of particular note here is work on how the quality of different reconstruction and resampling methods can be assessed.

About this document

This report is, apart from some cosmetic changes, the dissertation which I submitted for my PhD degree. I performed the research for this degree over the period January 1989 through May 1992.

The page numbering is different in this version to versions prior to 2005 because I have been able to incorporate many of the photographs which were previously unavailable in the online version.

Figures 1.4, 2.1, 2.2, 4.34, 7.9, and 7.10 are either incomplete or missing, owing to the way in which the original manuscript was prepared. Appendix C is also missing for the same reason.

Acknowledgements

I would like to thank my supervisor, Neil Wiseman, for his help, advice, and listening ear over the course of this research. I am especially grateful for his confidence in me, even when I had little of my own, and for reading this dissertation and making many helpful comments.

I would also like to thank David Wheeler and Paul Heckbert for useful discussions about image resampling and related topics, which clarified and stimulated my research.

Over the last three and a third years several bodies have given me financial assistance. The Cambridge Commonwealth Trust paid my fees and maintenance for the first three years, for which I am grateful. Wolfson College, through the kind offices of Dr Rudolph Hanka, and the Computer Laboratory, have both contributed towards travel, conference, and typing expenses; and I am grateful for these too. Finally, I am extremely grateful to my wife, Catherine Gibbs, for her financial support, without which that last third of a year would have been especially difficult.

This dissertation was typed in by four people, not a pleasant task. Many thanks go to Lynda Murray, Eileen Murray, Annemarie Gibbs, and Catherine Gibbs for taking this on, and winning!

The Rainbow graphics research group deserve many thanks for their support and friendship over my time in Cambridge; they have made the research much more enjoyable. Thanks go to Olivia, Stuart, Jeremy, Heng, Alex, Adrian, Dan, Tim, Rynson, Nicko, Oliver, Martin, Jane, and Neil. Equal, if not more, thanks go to Margaret Levitt and Eileen Murray, who have helped to keep me sane; and also to the other inmates of Austin 4 and 5 for the interesting working environment they provide.

Final heartfelt thanks go to my parents and to Catherine, to whom this dissertation is dedicated. Their support, and encouragement, has been invaluable in getting me to this point.

Contents

Notation **8**

Preface **9**

1 Resampling **11**

1.1 Introduction 11

1.2 Images 11

1.3 Sources of discrete images 13

1.4 Resampling: the geometric transformation of discrete images 16

1.5 The practical uses of resampling 16

1.6 Optical image warping 18

1.7 Decomposition 18

1.8 How it really works 27

1.9 The literature 29

1.10 Summary 31

2 Sampling **33**

2.1 Converting the continuous into the discrete 33

2.2 The problem of discrete intensities 33

2.3 Producing a discrete image 37

2.4 The sampling process 39

2.5 Area *vs* point sampling 43

2.6 Practical considerations 46

2.7 Anti-aliasing 48

2.8 Sampling which considers the reconstruction method 49

2.9 Summary 50

3 Reconstruction **52**

3.1 Classification 52

3.2 Skeleton reconstruction 55

3.3 Perfect interpolation . . . 58
3.4 Piecewise local polynomials . . . 59
3.5 What should we look for in a NAPK reconstructor? . . . 72
3.6 Cubic functions . . . 87
3.7 Higher orders . . . 95
3.8 Summary . . . 96

4 Infinite Extent Reconstruction 98
4.1 Introduction to infinite reconstruction . . . 98
4.2 Edge effects . . . 98
4.3 Sinc and other perfect interpolants . . . 117
4.4 Gaussian reconstructors . . . 123
4.5 Interpolating cubic B-spline . . . 125
4.6 Local approximations to infinite reconstructors . . . 142
4.7 Summary . . . 144

5 Fast Fourier Transform Reconstruction 145
5.1 The reconstructed intensity surface . . . 145
5.2 DFT sample rate changing . . . 148
5.3 FFT intensity surface reconstruction . . . 154
5.4 Problems with the FFT reconstructor . . . 156
5.5 Summary . . . 169

6 *A priori* knowledge reconstruction 171
6.1 Knowledge about the sampler . . . 171
6.2 Knowledge about the image content . . . 174
6.3 One-dimensional sharp edge reconstruction . . . 175
6.4 Two-dimensional sharp edge reconstruction . . . 191
6.5 Summary . . . 210

7 Transforms & Resamplers 211
7.1 Practical resamplers . . . 211
7.2 Transform dimensionality . . . 213
7.3 Evaluation of reconstructors and resamplers . . . 215
7.4 Summary . . . 227

8 Summary & Conclusions 228
8.1 Major results . . . 228
8.2 Other results . . . 229

8.3 Future work 229

A Literature Analysis **230**

B Proofs **238**

B.1 The inverse Fourier transform of a box function 238

B.2 The Fourier transform of the sinc function 238

B.3 Derivation of $a = -2 + \sqrt{3}$ 239

B.4 The Straightness Criteria 241

B.5 A signal cannot be bandlimited in both domains 242

B.6 The Fourier transform of a finite-extent comb 244

B.7 The not-a-knot end-condition for the B-spline 245

B.8 Timing calculations for the B-spline kernel 245

B.9 The error in edge position due to quantisation 246

C Graphs **248**

D Cornsweet's figures **262**

Glossary **266**

Bibliography **268**

Notation

There is little specialised notation in this thesis. We draw your attention to the following notational conventions:

Spatial domain functions tend to be represented by lowercase letters, for example: g and $f(x)$, or by lowercase words, for example: $\mathrm{sinc}(x)$. Frequency domain functions tend to be represented by the equivalent uppercase letters, for example: G and $F(\nu)$, or by capitalised words, for example: $\mathrm{Box}(\nu)$.

Domains are represented by calligraphic uppercase letters, for example: $\mathcal{Z}$ (the integers) and $\mathcal{R}$ (the real numbers). This non-standard notation is due to the inability of our typesetter to generate the correct notation.

We use three functions which generate an integer from a real number: $\mathrm{ceiling}(x)$ gives the nearest integer greater than, or equal to, x; $\mathrm{floor}(x)$ gives the nearest integer less than, or equal to, x; $\mathrm{round}(x)$ gives the nearest integer to x. These are represented in equations as shown below:

$$\begin{aligned} \mathrm{ceiling}(x) &= \lceil x \rceil \\ \mathrm{floor}(x) &= \lfloor x \rfloor \\ \mathrm{round}(x) &= \langle x \rangle \end{aligned}$$

Some of the derivations required the use of a book of tables. We used Dwight [1934]. References to Dwight are written thus: [Dwight, 850.1], giving the number of the appropriate entry in Dwight's book.

The term *continuous* is used in this dissertation in a non-standard way: a *continuous function* is one that is defined at all points in the real plane, but is not necessarily continuous in the mathematical sense. A more rigourous description for this use of *continuous* would be *everywhere defined*. The concept of mathematical continuity is represented in this dissertation by the term *C0-continuous*.

There is a glossary of terms at the back of the dissertation, just before the bibliography.

Preface

Digital image resampling is a field that has been in existence for over two decades. However, when we began this research in 1989, all work on image resampling existed in conference proceedings, journals, and technical reports. Since that time, the subject has come more into the public eye. Heckbert's Masters thesis, "Fundamentals of Texture Mapping and Image Warping" [Heckbert, 1989], brought many of the ideas together, concentrating on two-dimensional geometric mappings (specifically affine, bilinear and projective) and on the necessary anti-aliasing filters.

Wolberg's "Digital Image Warping" [Wolberg, 1990], is the first book on the subject. Its strength is that it draws most of the published work together in one place. Indeed, it grew out of a survey paper [Wolberg, 1988] on geometric transformation techniques for digital images. The book has a computational slant to it, being aimed at people who need to implement image resampling algorithms.

The same year saw the publication of the long awaited successor to Foley and van Dam's "Fundamentals of Interactive Computer Graphics", [1982]. Foley, van Dam, Feiner and Hughes [1990] contains a good summary of several image resampling concepts and techniques [*ibid.* pp.611, 614, 617–646, 741–745, 758–761, 815–834, 851, 910, 976–979] in contrast with its predecessor which does not mention resampling at all.

In the face of this flurry of publicity what can we say of image resampling. Certainly it has been in use for over twenty years, and is now used regularly in many fields. Many of the problems have been overcome and the theory behind resampling has been more to the fore in recent years.

What place, then, is there for research in the field? Much: image resampling is a complicated process. Many factors must be taken into account when designing a resampling algorithm. A framework is required which can be used to classify and analyse resampling methods. Further, there are holes in the coverage of the subject. Certain topics have not been studied because they are not perceived as important, because the obvious or naive answer has always been used, or because no-one has yet thought to study them.

In this dissertation we produce a framework which is useful for analysing and classifying resampling methods, and we fit the existing methods into it. We continue by studying the parts of the framework in detail, concentrating on the reconstruction sub-process. Thus we look at piecewise quadratic reconstructors, edge effects, the interpolating Bezier cubic, the kernel of the interpolating cubic B-spline, Fraser's [1987, 1989a, 1989b] FFT method and its extensions, and *a priori* knowledge reconstructors; whilst not ignoring the well-trod ground of, for example, piecewise cubic reconstructors and classical sampling theory.

The dissertation is divided into eight chapters, arranged as follows:

1. Resampling — we introduce the concepts of a digital image, a continuous image, and the resampling process. Resampling is decomposed into three sub-processes: reconstruction of a continuous intensity surface from a discrete image, transformation of that continuous surface, and sampling of the transformed surface to produce a new discrete image. This decomposition underpins the rest of the dissertation.

2. Sampling — the concepts of sampling are introduced, laying a foundation for the work on reconstruction and resampling as a whole. As a side issue we discuss the problem of intensity quantisation as it relates to image resampling.

3. Reconstruction — an introduction to reconstruction. Most of the chapter is given over to a discussion of piecewise local polynomial reconstructors, and the factors involved in their design.

4. Infinite Extent Reconstruction — sinc, Gaussian, interpolating cubic B-spline, and interpolating Bezier cubic are all theoretically infinite. We discuss these, their local approximations, and the problem of a finite image. The latter problem applies to local reconstructors, as well as infinite extent ones.

5. Fast Fourier Transform Reconstruction — a method of implementing an approximation to sinc reconstruction, developed by Donald Fraser [1987]. We describe his method, and then present improvements which solve two of its major problems.

6. *A priori* knowledge reconstruction — in the preceding three chapters we assumed that we had no *a priori* knowledge about how the image was sampled, or about its contents. In this chapter we briefly consider what can be achieved given *a priori* knowledge about how the image was sampled. The bulk of this chapter, however, is an analysis of what can be achieved given a particular set of intensity surfaces (those with areas of constant intensity separated by sharp edges) and one particular type of sampling (exact area sampling).

7. Transforms and Resamplers — where we consider transforms, and the resampling process as a whole. An important section in this chapter is the discussion of how to measure the quality of a reconstructor and of a resampler.

8. Summary and Conclusions — where all our results are drawn into one place.

Chapter 1

Resampling

1.1 Introduction

Digital image resampling occupies a small but important place in the fields of image processing and computer graphics. In the most basic terms, resampling is the process of geometrically transforming digital images.

Resampling finds uses in many fields. It is usually a step in a larger process, seldom an end in itself and is most often viewed as a means to an end. In computer graphics resampling allows texture to be applied to surfaces in computer generated imagery, without the need to explicitly model the texture. In medical and remotely sensed imagery it allows an image to be registered with some standard co-ordinate system, be it another image, a map, or some other reference. This is primarily done to prepare for further processing.

1.2 Images

There are two basic types of image: continuous and discrete. Continuous images have a real intensity at every point in the real plane. The image that is presented to a human eye or to a video camera, before any processing is done to it, is a continuous image. Discrete images only have intensity values at a set of discrete points and these intensities are drawn from a set of discrete values. The image stored in a computer display's frame buffer is a discrete image. The discrete values are often called 'pels' or 'pixels' (contractions of 'picture elements').

There are intermediate types of image, which are continuous in some dimensions but discrete in others. Wolberg [1990, p.12] gives two examples of these: where the image is continuous in space but discrete in intensity, or where it is continuous in intensity but discrete in space. A television signal is an interesting third case: it is continuous in intensity and in one spatial dimension (horizontally) but it is discrete in the other spatial dimension (vertically).

A digital computer, being a discrete device, can deal only with discrete images. What we perceive in the real world are invariably continuous images (which our eyes discretise for processing). For a human to perceive a discrete image it must be displayed as a continuous image, thus always putting us one step away from the data on which the computer operates. We must accept (and compensate for) this limitation if we wish to use the power of digital computers to process images.

Binkley [1990] discusses some of the philosophical problems of digital imagery. He states that 'digital image' is an oxymoron: "If a digital image is something one can see (by experiencing it with one's eyes), one cannot compute it; but if one can apply mathematical operations to it, then it has no intrinsic visual manifestation." Resampling is essentially a mathematical operation

Figure 1.1: The same image represented in three different ways: (1) displayed on a monitor.

Figure 1.2: The same image represented in three different ways: (2) rendered in halftone by a laser printer.

mapping one collection of numbers into another. The important point here is that what is seen by a human to be the input to and output from the resampling process are continuous representations of the underlying discrete images. There are many different ways of reconstructing a continuous image from a discrete one. We must be careful about the conclusions we draw from the continuous representations of discrete images. Binkley's figures 2 and 3 show how different two continuous representations of the same discrete image can be. Figure 1.1 and figure 1.2 are based on Binkley's figures, and show that the same image can give rise to very different continuous representations. Figure 1.3 shows the discrete representation that is stored in the computer's memory.

The images we deal with are thus discrete. In general any practical discrete image that we meet will be a rectangular array of intensity values. Experimental and theoretical work is being done on hexagonal arrays [Mersereau, 1979; Wüthrich, Stucki and Ghezal, 1989; Wüthrich and Stucki, 1991] but, at present, all practical image resampling is performed on rectangular arrays.

148	151	153	151	150	151	151	···	6	1	0	0	0	0
149	148	151	152	151	149	147	···	0	0	0	3	7	5
145	146	152	152	150	150	147	···	0	0	1	9	19	11
145	144	148	149	149	149	148	···	4	0	1	14	26	15
143	144	145	147	147	146	147	···	7	0	3	13	15	6
144	146	144	147	146	147	146	···	0	0	4	13	13	5
145	143	146	146	148	148	149	···	0	0	4	11	10	5
139	141	144	143	149	148	144	···	0	0	2	18	14	5
⋮	⋮	⋮	⋮	⋮	⋮	⋮	⋱	⋮	⋮	⋮	⋮	⋮	⋮
57	66	59	56	58	67	71	···	136	137	137	133	129	127
31	38	42	36	37	53	60	···	138	138	136	134	128	128
23	46	49	37	35	47	49	···	133	134	134	132	130	127
40	64	53	38	45	54	70	···	131	127	129	126	125	126

Figure 1.3: The same image represented in three different ways: (3) the array of numbers held in the computers memory.

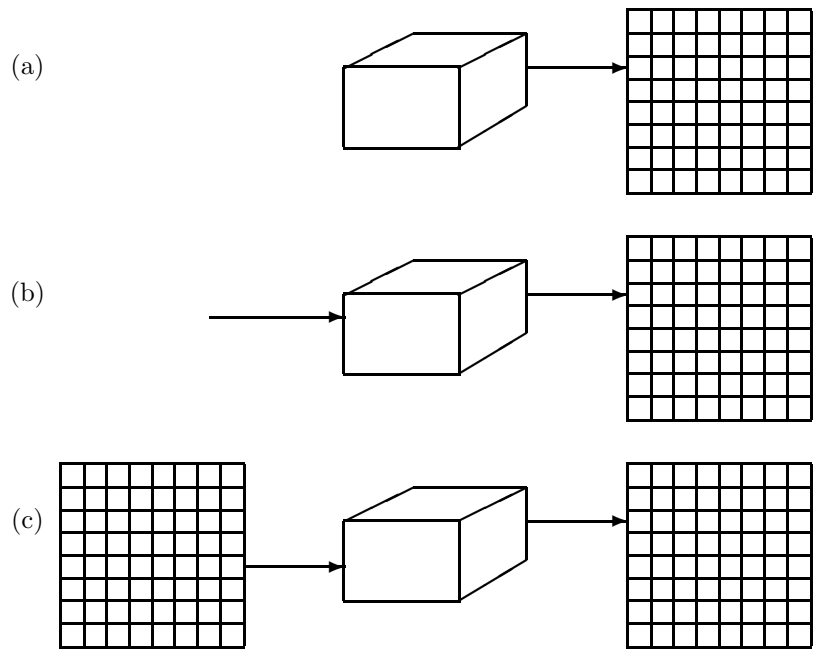

Figure 1.4: The three ways of producing an image: (a) capturing a real world scene; (b) rendering a scene description; and (c) processing an existing image.

1.3 Sources of discrete images

There are three distinct ways of producing such a rectangular array of numbers for storage in a computer. These can be succinctly described as capturing, rendering, or processing the discrete image (figure 1.4):

Image capture is where some real-world device (for example: a video camera, digital x-ray

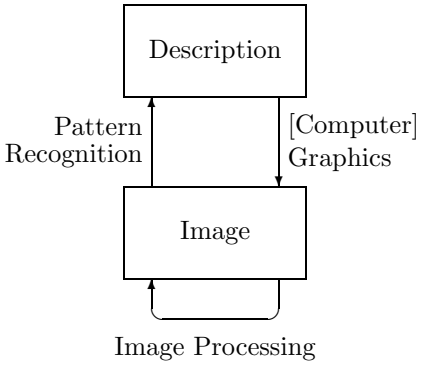

Figure 1.5: Pavlidis [1982] figure 1.1, showing the relationship between image processing, pattern recognition (image analysis), and computer graphics.

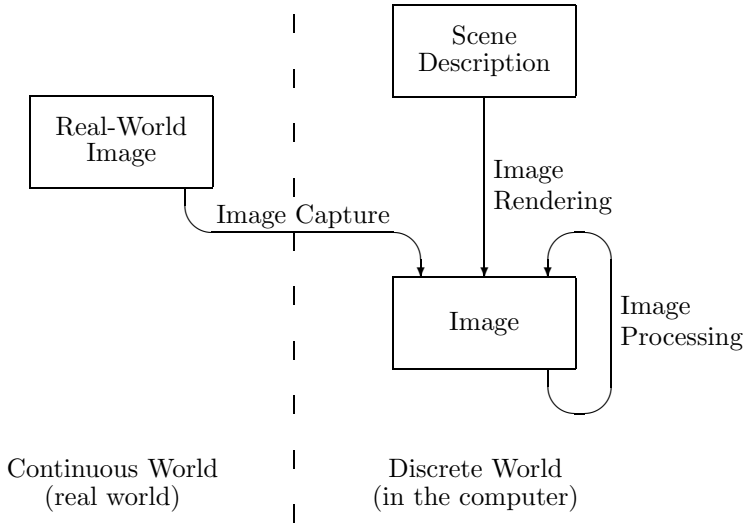

Figure 1.6: The three sources of discrete imagery shown as processes.

scanner, or fax machine) is used to capture and discretise some real-world (continuous) image.

Image rendering is where some description of a scene is stored within the computer and this description is converted into an image by a rendering process (for example: ray-tracing). The field of *computer graphics* is generally considered as encompassing all the aspects of this rendering process.

Image processing is where a previously generated discrete image is processed in some way to produce a new discrete image (for example: thresholding, smoothing, or resampling).

Pavlidis [1982] produced a simple diagram, reproduced in figure 1.5, showing the links between discrete images and scene descriptions. Based on his diagram, we produce figure 1.6 which shows the three sources of discrete imagery:

In order for us to evaluate digital imagery we must add ourselves into the picture (figure 1.7). Here we see that, to perceive a discrete image, we need to display that image in some continuous form (be it on a cathode ray tube (CRT), on photographic film, on paper, or wherever) and then use our visual system on that continuous image.

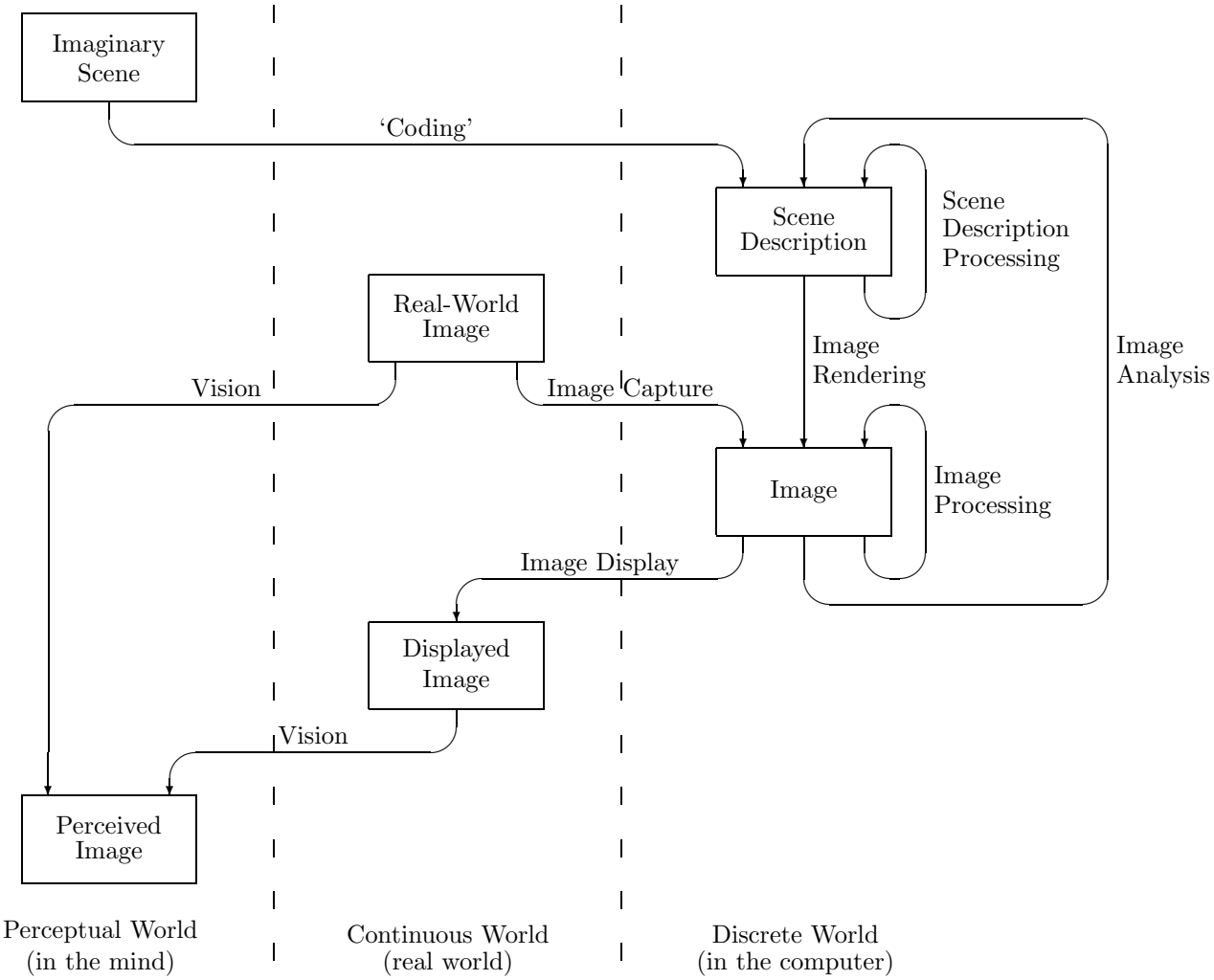

Figure 1.7: The complete diagram, showing the connection between images in the discrete, continuous, and perceptual worlds.

To complete the diagram, consider the scene description. Such a description could be generated from an image by an image analysis process [see, for example, Rosenfeld, 1988]; or it could be generated from another scene description (for example: by converting a list of solid objects into a set of polygons in preparation for rendering, as in the Silicon Graphics pipeline machines; or Bley's [1980] cleaning of a 'picture graph' to give a more compact description of the image from which the graph was created). Mantas [1987] suggests that pattern recognition is partially image analysis and partially scene description processing. A third way of generating a scene description is for a human being to physically enter it into the computer, basing the description on some imagined scene (which could itself be related to some perceived scene, a process not shown in the figures). Adding these processes to figure 1.6 gives us figure 1.7 which illustrates the relationships between these processes and the various image representations.

To avoid confusion between continuous and discrete images in this dissertation, we have chosen to call a continuous image an *intensity surface*. It is a function mapping each point in the real plane to an intensity value, and can be thought of as a surface in three dimensions, with intensity being the third dimension. We can thus take it that, when the word 'image' appears with no qualification, it means 'discrete image'.

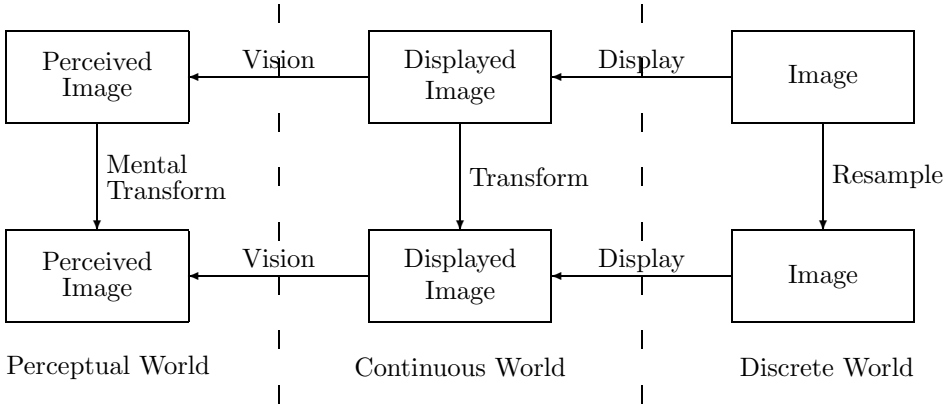

Figure 1.8: The relationship between the resampled and the original images. The two continuous versions must be perceived as transformed versions of one another.

1.4 Resampling: the geometric transformation of discrete images

In image resampling we are given a discrete image and a transformation. The aim is to produce a second discrete image which looks as if it was formed by applying the transformation to the original discrete image. What is meant by 'looks as if' is that the continuous image generated from the second discrete image, to all intents and purposes, appears to be identical to a transformed version of the continuous image generated from the first discrete image, as is illustrated in figure 1.8. What makes resampling difficult is that, in practice, it is impossible to generate the second image by *directly* applying the mathematical transformation to the first (except for a tiny set of special case transformations).

The similarity between the two images can be based on visual (perceptual) criteria or mathematical criteria, as we shall see in section 3.5. If based on perceptual criteria then we should consider the perceptual images, which are closely related to the continuous images. If based on mathematical criteria the perceptual images are irrelevant and we concentrate on the similarities between the continuous images and/or between the discrete images.

Whatever the ins and outs of how we think about image resampling, it reduces to a single problem: determining a suitable intensity value for each pixel in the final image, given an initial image and a transformation[1].

1.5 The practical uses of resampling

Resampling initially appears to be a redundant process. It seems to beg the question: "why not re-capture or re-render the image in the desired format rather than resampling an already existing image to produce a (probably) inferior image?"

Resampling is used in preference to re-capturing or re-rendering when it is either:

- the only available option; or
- the preferential option.

[1] c.f. Fiume's definition of rendering, 1989, p.2.

The first case occurs where it is impossible to capture or render the image that we require. In this situation we must 'make do' with the image that we have got and thus use resampling to transform the image that we have got into the image that we want to have.

The second case occurs where it *is* possible to capture or render the required image but it is easier, cheaper or faster to resample from a different representation to get the required image.

Various practical uses of image resampling are[2]:

- distortion compensation of optical systems. Fraser, Schowengerdt and Briggs [1985] give an example of compensating for barrel distortion in a scanning electron microscope. Gardner and Washer [1948] give an example of how difficult it is to compensate for distortion using an optical process rather than a digital one (this example is covered in more detail in section 1.6).
- registration to some standard projection.
- registration of images from different sources with one another; for example registering the different bands of a satellite image with one another for further processing.
- registering images for time-evolution analysis. A good example of this is recorded by Herbin *et al* [1989] and Venot *et al* [1988] where time-evolution analysis is used to track the healing of lesions over periods of weeks or months.
- geographical mapping; changing from one projection to another.
- photomosaicing; producing one image from many smaller images. This is often used to build up a picture of the surface of a planet from many photographs of parts of the planet's surface. A simpler example can be found in Heckbert [1989] figures 2.9 and 2.10.
- geometrical normalisation for image analysis.
- television and movie special effects. Warping effects are commonplace in certain types of television production; often being used to enhance the transition between scenes. They are also used by the movie industry to generate special effects. Wolberg [1990, sec. 7.5] discusses the technique used by Industrial Light and Magic, the special effects division of Lucasfilm Ltd. This technique has been used to good effect, for example, in the movies: *Willow*[3], *Indiana Jones and the Last Crusade*[4], and *The Abyss*[5]. Smith [1986, ch. 10] gives an overview of Industrial Light and Magic's various digital image processing techniques.
- texture mapping; a technique much used in computer graphics. It involves taking an image and applying it to a surface to control the shading of that surface in some way. Heckbert [1990b] explains that it can be applied so as to modify the surface's colour (the more narrow meaning of texture mapping), its normal vector ('bump mapping'), or in a myriad of other ways. Wolberg [1990, p.3] describes the narrower sense of texture mapping as mapping a two-dimensional image onto a three-dimensional surface which is then projected back on to a two-dimensional viewing screen. Texture mapping provides a way of producing visually rich and complicated imagery without the overhead of having to explicitly model every tiny feature

[2]Based on a list by Braccini and Marino, [1980, p.27].

[3]One character (Raziel) changes shape from a tortoise, to an ostrich, to a tiger, to a woman. Rather than simply cross-dissolve two sequences of images, which would have looked unconvincing, two sequences of *resampled* images were cross-dissolved to make the character appear to change shape as the transformation was made from one animal to another.

[4]The script called for a character (Donovan) to undergo rapid decomposition in a close-up of his head. In practice, three model heads were used, in various stages of decomposition. A sequence for each head was recorded and then resampled so that, in a cross-dissolve, the decomposition appeared smooth and continuous.

[5]At one point in the movie, a creature composed of seawater appears. Image resampling was used in the generation of the effect of a semi-transparent, animated object: warping what could be seen through the object so that there appeared to be a transparent object present.

in the scene [Smith, 1986, p.208]. Image resampling, as described in this dissertation, can be taken to refer to texture mapping in its narrow sense (that of mapping images onto surfaces). The other forms of texture mapping described by Heckbert [1990b] produce different visual effects and so the discussion will have little relevance to them.

1.6 Optical image warping

Image warping need not be performed digitally. The field of optical image warping has not been completely superseded by digital image warping [Wolberg, 1990, p.1]. However optical systems are limited in control and flexibility. A major *advantage* of optical systems is that they work at the speed of light. For example Chiou and Yeh [1990] describe an optical system which will produce multiple scaled or rotated copies of a source image in less than a millionth of a second. These images can be used as input to an optical pattern recognition system. There is no way that such images could be digitally transformed this quickly, but there is a limited use for the output of this optical process.

The *problems* of using an optical system for correction of distortion in imagery are well illustrated by Gardner and Washer [1948]. In the early 1940s, Zeiss, in Germany, developed a lens with a large amount of negative distortion, specifically for aerial photography. The negative distortion was designed into the lens in order that a wide field of view (130°) could be photographed without the extreme loss of illumination which would occur near the edges of the field if no distortion were present in the lens.

A photograph taken with this lens will appear extremely distorted. To compensate, Zeiss developed (in parallel with the lens) a copying or rectifying system by which an undistorted copy of the photograph could be obtained from the distorted negative.

For the rectification to be accurate the negative has to be precisely centred in the rectifying system. Further, and more importantly, the particular rectifying system tested did not totally correct the distortion. Gardner and Washer suggest the possibility that camera lens and rectifier were designed to be selectively paired for use (that is: each lens must have its own rectifier, rather than being able to use a general purpose rectifier) and that the lens and rectifier they tested may not have been such a pair. However, they also suggest that it would be difficult to actually make such a lens/rectifier pair so that they accurately compensate for one another.

The advent of digital image processing has made such an image rectification process far simpler to achieve. Further, digital image processing allows a broader range of operations to be performed on images. One example of such processing power is in the Geosphere project, where satellite photographs of the Earth, taken over a ten month period, were photomosaiced to produce a cloudless satellite photograph of the entire surface of the Earth [van Sant, 1992][6].

1.7 Decomposition

Image resampling is a complex process. Many factors come into play in a resampling algorithm. Decomposing the process into simpler parts provides a framework for analysing, classifying, and evaluating resampling methods, gives a better understanding of the process, and facilitates the design and modification of resampling algorithms. One of the most important features of any useful decomposition is that the sub-processes are independent of one another. Independence of the sub-processes allows us to study each in isolation and to analyse the impact of changing one sub-process whilst holding the others constant. In chapter 7 we will discuss the equivalence

[6] An interesting artifact is visible in the Antarctic section of this photomosaic: the Antarctic continent is so stretched by the projection used that resampling artifacts are visible there. However, the rest of the mosaic looks just like a single photograph — no artifacts are visible.

Figure 1.9: A two part decomposition of resampling into reconstruction and sampling.

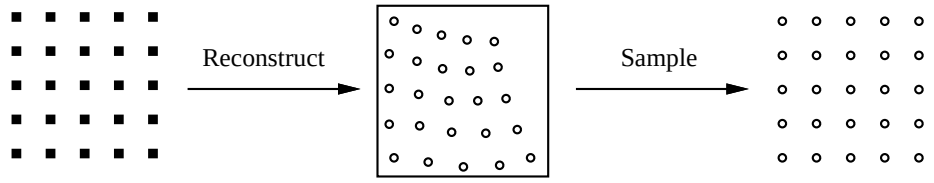

Figure 1.10: An example of a two-part decomposition (figure 1.9). The squares are the original image's sample points which are reconstructed to make the intensity surface. The open circles are the resampled images sample points which are not evenly spaced in the reconstructed intensity surface, but are evenly spaced in the resampled image.

of resamplers; that is, how two dissimilar decompositions of a resampling method can produce identical results.

The simplest decomposition is into two processes: reconstruction, where a continuous intensity surface is reconstructed from the discrete image data; and sampling, where a new discrete image is generated by taking samples off this continuous intensity surface. Figure 1.9 shows this decomposition.

Mitchell and Netravali [1988] follow this view as a part of the cycle of sampling and reconstruction that occurs in the creation of an image. Take, for example, a table in a ray-traced image, texture-mapped with a real wooden texture. First, some wooden texture is sampled by an image capture device to produce a digital texture image. During the course of the ray-tracing this image is reconstructed and sampled to produce the ray-traced pixel values. The ray-traced image is subsequently reconstructed by the display device to produce a continuous image which is then sampled by the retinal cells in the eye. Finally, the brain processes these samples to give us the perceived image, which may or may not be continuous depending on quite what the brain does. These many processes may be followed in figure 1.7, except that image resampling is a single process there, rather than being decomposed into two separate ones.

This decomposition into reconstruction and sampling has also been proposed by Wolberg [1990, p.10], Ward and Cok [1989, p.260], Parker, Kenyon and Troxel [1983, pp.31–32], and Hou and Andrews [1978, pp.508–509]. It has been alluded to in many places, for example: by Schreiber and Troxel [1985].

It is important to note that all of these people (with the exception of Wolberg) used only single point sampling in their resampling algorithms. This decomposition becomes complicated when more complex methods of sampling are introduced and Wolberg introduces other decompositions in order to handle these cases, as explained below. Figure 1.10 gives an example of a resampling decomposed into these two sub-processes.

A second simple decomposition into two parts is that espoused by Fraser, Schowengerdt and Briggs [1985, pp.23–24] and Braccini and Marino [1980, p.130]; it is also mentioned by Foley, van Dam, Feiner and Hughes [1990, pp.823–829] and Wolberg [1990]. The first part is to transform the source or destination pixels into their locations in the destination or source image (respectively). The second part is to interpolate between the values of the source pixels near each destination pixel to provide a value for each destination pixel. This decomposition is shown in figure 1.11.

Figure 1.11: A two part decomposition into transformation and interpolation.

The interpolation step could be thought of as a reconstruction followed by a point sample at the (transformed) destination pixel, but this further decomposition is not explicit in this model of resampling[7]. Note that point sampling is assumed in the model of the resampling process and thus any more complicated sampling method cannot easily be represented.

Both of these two part models are valid and useful decompositions of resampling. However, both contain the implicit assumption that only single point sampling will be used. Many resampling processes do exclusively use single point sampling. However, those which do not will not fit into these models. A more general model of resampling is required if we are to use it to classify and analyse all resampling methods.

It may not be immediately apparent why these models cannot embrace other sampling methods. In the case of the second decomposition, there is no place for any other sampling method. Single point sampling is built into the model. The sampling is performed as part of the interpolation step, and the assumption is that interpolation is done at a single point from each sample value. It is possible to simulate other forms of sampling by modifying the interpolation method, but such modification is transform-specific and thus destroys the independence of the two sub-processes in the model.

The first decomposition can be expanded to include other sampling methods, but there are difficulties. To illustrate this let us look at exact-area sampling using a square kernel the size of one pixel. This resampling model (figure 1.9) has the transform implicitly built into the sampling stage. This works well with point sampling. A transformed point is still a point. With area sampling we have two choices: either we transform the centre of the pixel and apply the area sampler's kernel 'as is' (as in figure 1.12(a)) or we transform the whole area and apply the transformed kernel (as in figure 1.12(b)).

The former method is equivalent to changing the reconstructor[8] in a transformation-independent way and then using point sampling. This is not what is desired. We would get the same results by retaining point sampling and using a different reconstructor.

The latter method is what is wanted, the whole area is warped by the transformation. Unfortunately, the sampler is now transform-dependent (remember that transforming a point produces a point, so a point sampler is transform-independent: although the positions of the point samples change, the shape of the sampling kernel (a point) does not; in area sampling, the position and shape of the kernel change and thus the area sampler is transform-dependent). Therefore, neither method of expanding the reconstruct/sample decomposition is particularly helpful.

To produce an all-encompassing decomposition we need to split resampling into three parts.

1.7.1 A three-part decomposition

Fiume [1989, pp.36-38; 1986, pp.28-30] discusses texture mapping using a continuous texture function defined over a texture space [see p.37 of Fiume, 1989]. He comments: "In practice, texture mapping consists of two distinct (but often interleaved) parts: the geometric texture mapping technique itself... and rendering". Rendering is a sampling process (Fiume discusses rendering in

[7]The 'interpolation' need not be a true interpolation but may be an 'approximation', that is a function which does not interpolate the data points but still produces an intensity surface which reflects the shape implied by the data points.

[8]A reconstructor is a reconstruction method.

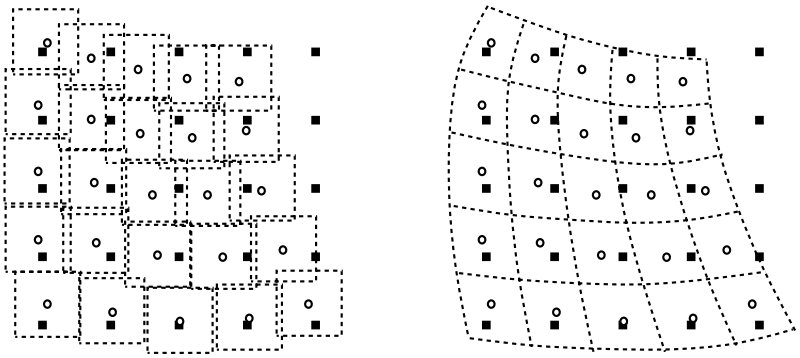

(a) (b)

Figure 1.12: Two ways of extending two-part decomposition to cope with area sampling. The squares are the original image's pixels on a regular grid. The open circles are the resampled image's pixels at the locations they would be if they were generated by taking point samples off the intensity surface (figure 1.10). As an example, we have taken a square area sampler centred at this point. This can be implemented in two ways: (a) transform-independent sampling, the sample filter shape does not change; (b) transform-dependent sampling, the sample filter shape changes.

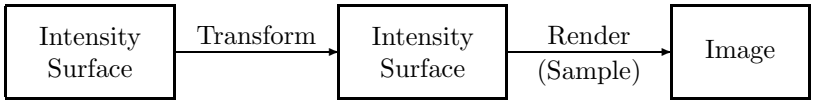

Figure 1.13: Fiume's [1989] decomposition of resampling. He does not, however, start with an image, but with an intensity surface. Some extra process is required to produce the intensity surface from an image.

great detail in his chapter 3 [Fiume, 1989, pp.67-121]). Figure 1.13 shows Fiume's decomposition. Compare this with Mitchell and Netravali's 'reconstruct/sample' decomposition (figure 1.9).

These two decompositions do not have the same starting point. Fiume is interested in the generation of digital images from scene specifications (the rendering process in figure 1.13(b)), thus he starts with some continuous intensity surface. He states that this continuous intensity surface could itself be generated procedurally from some scene specification or it could be generated from a digital image but gives no further comment on the process required to generate a continuous intensity surface from a digital image. The required process is reconstruction, as found in Mitchell and Netravali's decomposition. Fiume, however, splits Mitchell and Netravali's sampling step into two parts: the geometric transformation and the sampling, where 'sampling' can be any type of sampling, not just single point sampling. He comments: "The failure to distinguish between these [two] parts can obscure the unique problems that are a consequence of each."

The three part decomposition thus developed from these two-part decompositions is shown in figure 1.14.

1.7.2 Description of the parts

A discrete image, consisting of discrete samples, is reconstructed in some way to produce a continuous intensity surface. The actual intensity surface that is produced depends solely on the image being reconstructed and on the reconstruction method. There are many different reconstruction methods so a given image can give rise to many different intensity surfaces.

This intensity surface is then transformed to produce another intensity surface. This is a well-understood and simple idea, but it is the heart of resampling. Resampling itself, the geometric

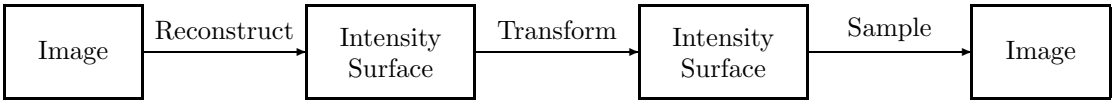

Figure 1.14: The three part decomposition of resampling into reconstruction, transformation, and sampling.

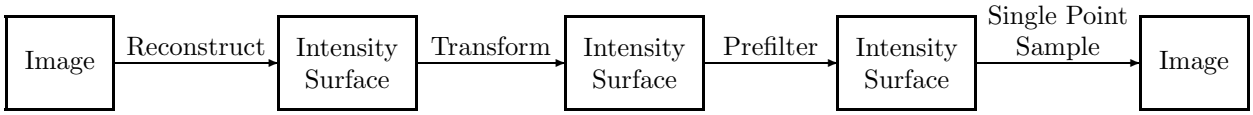

Figure 1.15: Smith's [1982] four part decomposition of resampling.

transformation of one digital image into another (or, rather the illusion of such a transformation, as described in section 1.4) is a complex process. The transformation stage in this decomposition is applying that geometric transform to a continuous intensity surface, and is a much simpler idea.

Mathematically an intensity surface can be thought of as a function, $I(x, y)$, defined over the real plane. The function value $I(x, y)$ is the intensity at the point (x, y). When we say that the intensity surface is transformed we mean that every point, (x, y), in the real plane is transformed and that the intensity values move with the points. Thus a transform τ will move the point (x, y) to $\tau(x, y)$ and the transformed intensity surface, $I_\tau(x, y)$ will bear the following relation to the original intensity surface:

$$I_\tau(\tau(x, y)) = I(x, y)$$

This holds for one-to-many and one-to-one transforms. For many-to-one transforms some arbiter is needed to decide which of the many points mapping to a single point should donate its intensity value to that point (or whether there should be some sort of mixing of values). Catmull and Smith [1980] call this the 'foldover' problem because it often manifests itself in an image folding over on top of itself, perhaps several times. An example of such a transform is mapping a rectangular image of a flag into a picture of a flag flapping in the breeze.

Whatever the transform, the end result is a new intensity surface, $I_\tau(x, y)$. The final stage in this decomposition is to sample off this new surface to produce a new, resampled image. Any sampling method can be used, whether it is single point, multiple point, or area (filtered) sampling.

This decomposition is general. All three parts are essential to a resampling method. It is our hypothesis that virtually any resampling method can be decomposed into these three stages. Appendix A lists the resamplers discussed in around fifty of the resampling research papers, and decomposes them into these three parts.

It is, however, possible to decompose resampling further. The two four-part decompositions which have been proposed are described in the following section.

1.7.3 Further decomposition

The two decompositions discussed here have more parts than those discussed above and are not as general as the three-part decomposition. They can each be used to classify only a subset of all resamplers, although in the first case this subset is large.

Smith and Heckbert's four part decomposition

Smith [1982] proposed this decomposition in the early eighties and Heckbert [1989, pp.42–45] subsequently used it with great effect in his development of the idea of a 'resampling filter'.

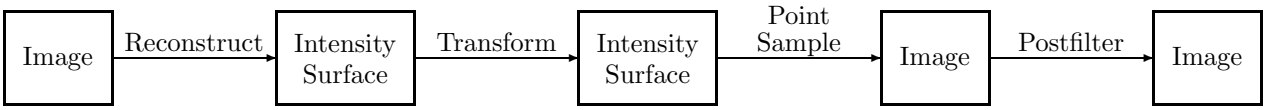

Figure 1.16: The super-sampling, or postfiltering decomposition.

Smith's decomposition is shown in figure 1.15. It arose out of sampling theory where it is considered desirable to prefilter an intensity surface before point sampling to remove any high frequencies which would alias in the sampling process.

The two stages of *prefilter* and *single point sample* replace the single *sample* stage in the three-part decomposition. Not all samplers can be split up easily into a prefilter followed by single point sampling. Such a split is appropriate for area samplers, which Heckbert [1989] uses exclusively [*ibid.*, sec. 3.5.1]. For multiple point samplers this split is inappropriate, especially for such as jittered sampling [Cook, 1986] and the adaptive super-sampling method.

Heckbert [1989 pp.43–44] slightly alters Smith's model by assuming that the reconstruction is one that can be represented by a filter. The majority of reconstructors can be represented as reconstruction filters, but a few cannot and so are excluded from Heckbert's model. Two examples of these exceptions are the sharp edge reconstruction method described in section 6.4, and Olsen's [1990] method for smoothing enlarged monochrome images. However, the idea of a reconstruction filter and a prefilter are important ones in the development of the concept of a resampling filter. This decomposition is useful for those resamplers where the filter idea is appropriate. See section 1.8.2 for a discussion of resampling filters.

The super-sampling or postfiltering decomposition

This decomposition is only appropriate for resamplers which use point sampling. It consists of the same reconstruction and transformation stages as the three-part decomposition with the sampling stage replaced by point sampling at a high resolution and then postfiltering the high resolution signal to produce a lower resolution output [Heckbert, 1989, pp.46–47]. This is illustrated in figure 1.16.

This can be considered to be a decomposition in two separate resampling processes. In the first, the transformed intensity surface is sampled at high resolution, while in the second (the postfiltering) this high resolution image is resampled to a low resolution image.

Area sampling does not fit into this model, although high resolution single point sampling and postfiltering is used as an approximation to area sampling. As the number of points tends to infinity, point sampling plus postfiltering tends towards area sampling, but using an infinite number of point samples is not a practicable proposition. Certain types of multi-point sampling do not fit into this model either, notably adaptive super-sampling. Therefore this decomposition, while useful for a subset of resampling methods, is not useful as a general decomposition.

1.7.4 Advantages of the three-part decomposition

Our view is that the three-part decomposition is the most useful general decomposition for the study of resampling. This is justified below. Accordingly this thesis is divided in much the same way with chapters associated with each of the three parts.

This decomposition is fairly intuitive to a person taking an overview of all resampling methods, but is not explicitly stated elsewhere. Wolberg [1990, p.6] mentions "the three components that comprise all geometric transformations in image warping: spatial transformations, resampling and antialiasing"; but these are not the three parts we have described, and it is odd that 'resampling' (the whole process) is considered to be a part of the whole by Wolberg. Foley *et al* [1990, p.820],

on the other hand, describe a decomposition as follows: "we wish to reconstruct the abstract image, to translate it, and to sample this translated version." This is our three-part decomposition (figure 1.14), but for translation rather than general transformation. Other transforms naturally follow, Foley *et al* discuss these without explicitly generalising the decomposition.

The three-part decomposition into reconstruct, transform and sample has several advantages over other decompositions:

Independence of parts. Most resamplers can be split into these three independent parts so that changing any one part does not affect the other two. This means that neither the reconstructor nor the sampler is dependent on the transform, and that the reconstructor is the same for all parts of the original image and the sampler the same for all parts of the resampled image.

In any resampling method, some constituents of the method will depend on position in relation to the original sampling grid and some in relation to the resampled sampling grid. Placing the former in the reconstructor and the latter in the sampler makes them independent of whatever transform is applied. The transform itself is left in splendid isolation as a simple mathematical process.

There exist resampling methods where the sampler or reconstructor cannot be made independent of the transform because some part of one or the other depends on both the original and the resampled images' sampling grids. One such method is Williams' [1983] pyramidal resampling scheme where the level in the pyramid is selected based on how an area in the resampled image plane maps into the original image plane. The choice of level for any given point (whether in the original or resampled image's plane) is transform-dependent and thus either the reconstructor or the sampler (or perhaps both) must be transform-dependent. The transform itself still remains a simple mathematical process of mapping one plane into the other (for further discussion of Williams' method see section 7.1.1.)

It is helpful for analysis of reconstruction and sampling methods that they be transform-independent. It is also necessary that, having discussed and analysed these sub-processes, the resampling process as a whole is considered to see the overall effect produced by all three sub-processes. It is useful to be able to alter one sub-process without affecting or being affected by either of the other sub-processes. This aids immensely in analysing the sub-processes and various resampling methods.

Equivalence of sampling grids. By extracting the transformation as a separate step between reconstruction and sampling we allow the original and resampled images' sampling grids to be identical. The main problem with the two-part reconstruct/sample decomposition (figure 1.9) is that the sampling takes place on a non-uniform grid. As pointed out in the discussion of this decomposition, this non-uniform sampling makes area sampling (and some point sampling) a complex business. Further, virtually all sampling theory and practice is directed at sampling on a regular grid (even the stochastic sampling methods are based on regular sampling grids). Keeping the transform separate from the sampler allows the sampler to be based on a regular sampling grid. The fact that the sampling grids which produce the original and resampled images are identical, simplifies and unifies the discussion and analysis of the sampling process.

It also alleviates us of needing to consider transform-dependent sampling methods. These change as one moves around the (non-uniform) sampling grid and are tricky things to deal with. By allowing us to always use a uniform sampling grid the three-part decomposition frees us from this difficult area and makes for clear, simple theory.

A *resampler* will be spatially-variant, except in the case of very simple transformations (affine transforms and scaling transforms). This decomposition removes the spatial variance from the reconstruction and sampling stages so that we need only consider their spatially invariant cases, greatly simplifying the analysis of resampling techniques.

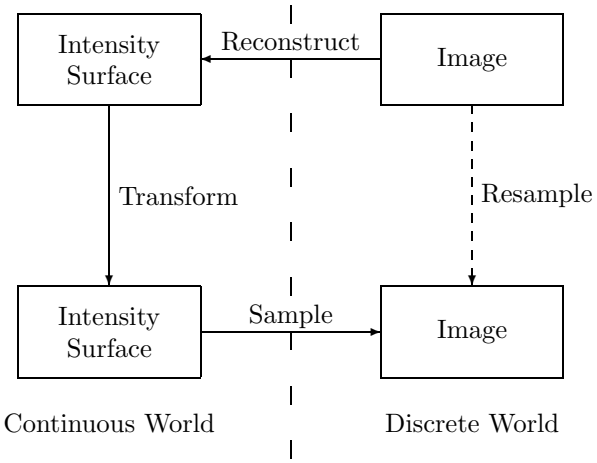

Figure 1.17: The original image (at top) is reconstructed to give an intensity surface. This is then transformed to produce the transformed intensity surface, which is sampled, giving the resampled image. In a digital computer the entire process is performed in the discrete world, shown by the dotted arrow in this figure.

Separation of format conversion. Reconstruction and sampling are opposites. Reconstruction converts a discrete image into a continuous intensity surface. Sampling converts a continuous intensity surface into a discrete image.

Resampling is the complex process of geometrically transforming one digital image to produce another (see figure 1.8). This decomposition replaces that transformation with the conceptually much simpler transformation from one continuous intensity surface to another, and it adds processes to convert from the discrete image to the continuous intensity surface (reconstruction) and back again (sampling). Thus the decomposition separates the format conversion (discrete to continuous, and continuous to discrete) from the transform (the core of the process). This whole process is illustrated in figure 1.17.

Generality of the decomposition. Almost all resamplers can be split into these three parts, but decomposing resampling into more parts limits the types of resamplers that can be represented, as illustrated in section 1.7.3. Appendix A lists many of the resamplers that have been discussed in the literature and decomposes them into these three parts.

1.7.5 One-dimensional and multi-pass resampling

Multi-pass resampling can mean a sequence of two-dimensional resampling stages to produce the desired result. An example of this is the decomposition in figure 1.16 which can be thought of as one resampling followed by another. Such methods fit easily into our framework by considering them to be a sequence of resamplings with each resampling being decomposed individually into its three component stages.

Multi-pass resampling, however, usually refers to a sequence of two or more one-dimensional resamplings. For example, each horizontal scan-line in the image may be resampled in the first pass and each vertical scan-line in the second. The overall effect is that of a two-dimensional resampling. Catmull and Smith [1980] deal with this type of resampling; other researchers have suggested three- [Paeth, 1986, 1990] and four- [Weiman, 1980] pass one-dimensional resampling.

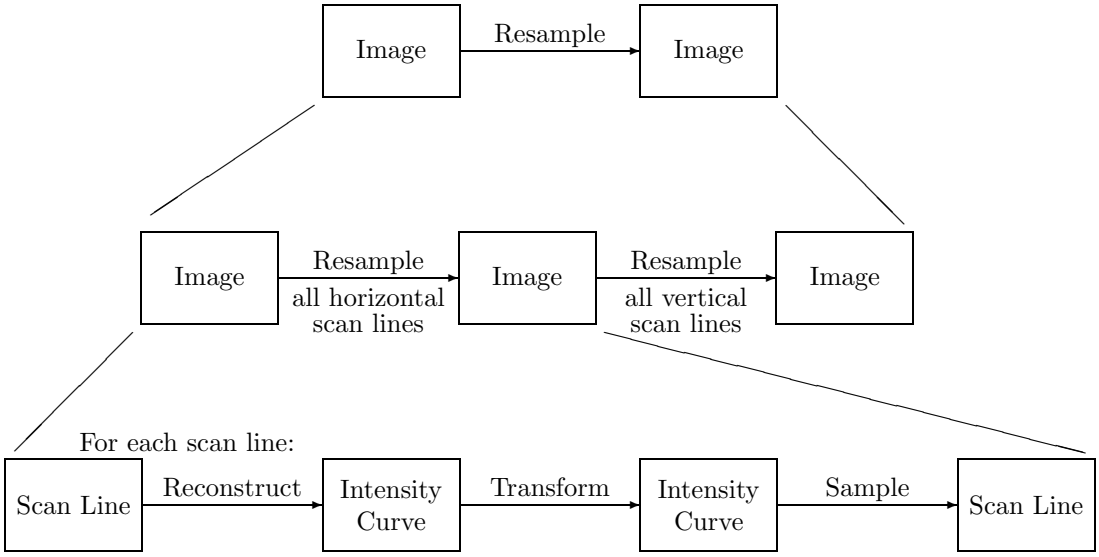

Figure 1.18: The decomposition of resampling for a two-pass one-dimensional resampler. The whole resampling decomposes into two sets of resamplings, one resampling per scan line. These then decompose into the three parts, as before.

To include such resampling methods in our framework we note that the overall resampling consists of two or more resampling stages. In each of these stages each one of a set of scan-lines undergoes a one-dimensional resampling which can be decomposed into reconstruction, transformation and sampling. An example of this decomposition for a two-pass resampling is given in figure 1.18. Thus the decomposition is quite valid for multi-pass one-dimensional resampling methods. Indeed, many two-dimensional reconstructors are simple extrapolations of one-dimensional ones (for example: see section 3.4.2).

Multi-pass, one-dimensional resampling tends to be faster to implement than the same two-dimensional resampling. In general, though, the one-dimensional version produces a more degraded resampled image than the two-dimensional one. Fraser [1989b] and Maisel and Morden [1981] are amongst those who have examined the difference in quality between one-pass, two-dimensional and multi-pass, one-dimensional resampling.

1.7.6 Three dimensions and mixed dimensional cases

Resampling theory can be simply extended to three or more dimensions (where an intensity volume or hyper-volume is reconstructed). There are still the same three sub-processes. Multi-pass resampling also generalises: three dimensional resampling, for example, can be performed as a multi-pass one-dimensional process [Hanrahan, 1990].

Finally, some resamplers involve the reconstruction of an intensity surface (or volume) of higher dimension than the image. One example is the $1\frac{1}{2}$-dimensional reconstruction of a one-dimensional image, discussed in section 7.2. Another is Williams' [1983] resampler: reconstructing a three dimensional intensity volume from a two dimensional image. This is discussed in detail in section 7.1.1.

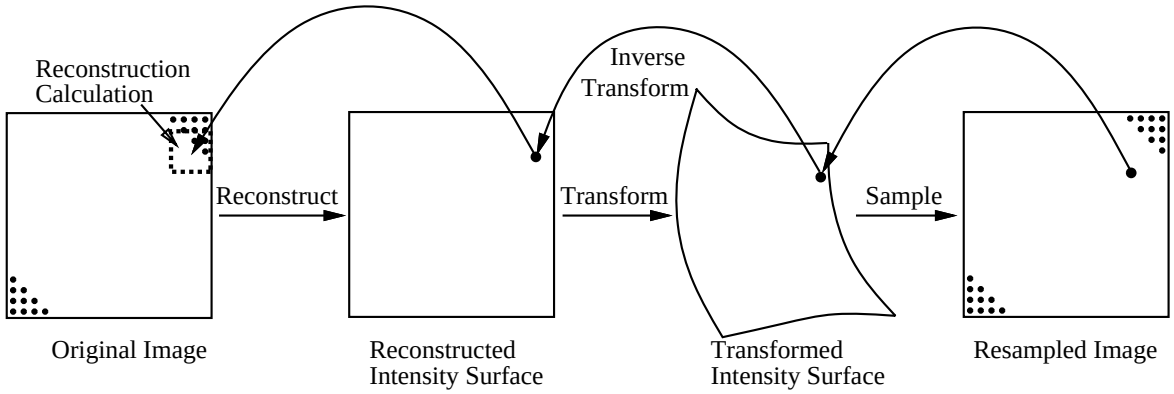

Figure 1.19: How resampling is implemented when it involves point sampling. For each point sample required in the process, the point is inverse transformed into the original image's space and a reconstruction calculation performed for the point from the original image's samples in the region of the inverse transformed point.

1.8 How it really works

The theory is that a digital image is reconstructed to a continuous intensity surface, which is transformed, and then sampled on a regular grid to produce a new digital image (figure 1.14). In practice resampling cannot be done this way because a digital computer cannot contain a continuous function. Thus practical resampling methods avoid the need to contain a continuous function, instead calculating values from the original image's data values only at the relevant points.

Conceptually, the usual method of implementation is to push the sampling method back through the transformation so that no continuous surface need be created. Whilst this process is conceptually the same for an area sampler as for a point sampler, the former is practically more complicated and so we will discuss the two cases separately.

1.8.1 The usual implementation of a point sampler

Each point sample that must be taken is taken at a single point on the transformed intensity surface. This point usually corresponds to exactly one point on the original intensity surface. Remember that for many-to-one transformations some arbiter must be included to decide which one of the many takes priority, or to decide how to mix the many reconstructed intensities to produce a single intensity[9].

The value of the intensity surface at this point (or points) in the original image can then be computed from the original image's data values. This process is illustrated in figure 1.19.

For a single point sampler this value is assigned to the appropriate pixel in the final image. For a multi-point sampler, several such samples are combined in some way to produce a pixel value.

Thus to get the value of a point sample the following process is used:

1. Inverse transform the location of the point from the final image's space to the original image's space.
2. Calculate the value of the intensity surface at this point in the original image's space.

[9]The situation where a final intensity surface point has no corresponding original intensity surface point is discussed in the section on edge effects (section 4.2).

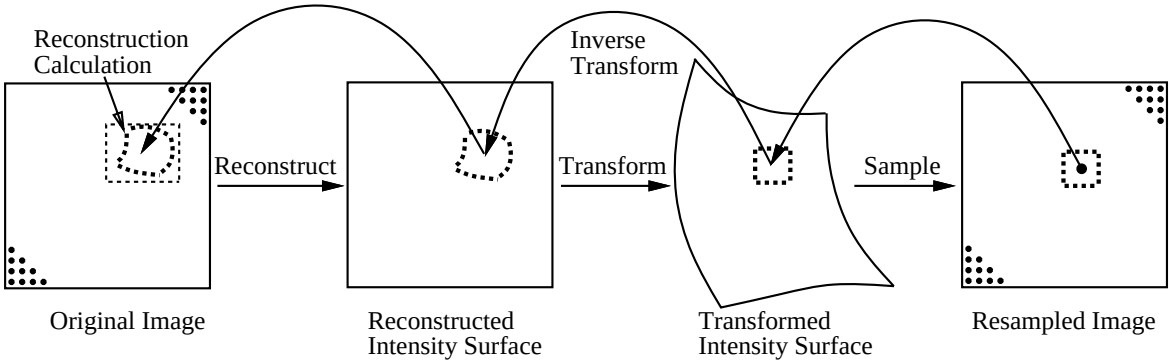

Figure 1.20: How resampling is implemented when it involves area sampling. For each area sample required in the process, the area is inverse transformed into the original image's space and a reconstruction calculation performed for the whole area from the original image's samples in the region of the inverse transformed area.

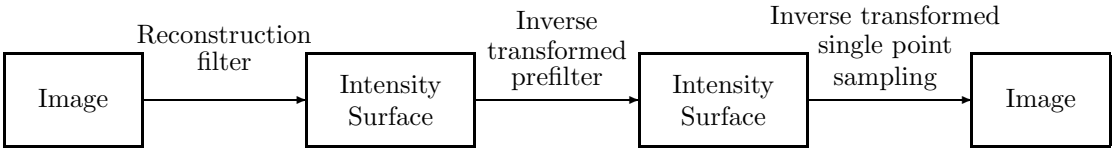

Figure 1.21: An equivalent decomposition of an area sampler. Rather than use a transform-invariant area sampler, here we use an inverse transformed prefilter, followed by inverse transformed single point sampling. These two steps combine to produce the same effect as a transform followed by area sampling.

1.8.2 The usual implementation of an area sampler

Analogous to the point sampling case, the area of the sample is inverse transformed (taking with it, of course, the weighting information for every point in the area). This inverse transformed area will now be spatially-variant as it is now transformation-dependent. The same shaped area in different parts of the final image's space will inverse transform to differently shaped areas in the original image's space.

Somehow this spatially-variant area sampler is combined with the spatially-invariant reconstructor to produce a calculation which will give a single value for each final image pixel. The process is illustrated in figure 1.20.

Heckbert [1989] explains how this combination can be achieved in the case where the reconstructor can be represented as a filter:

Heckbert's resampling filter

An area sampler can be thought of as a filter (called a 'prefilter') followed by single point sampling. Thus the three-part decomposition becomes four part (see figure 1.15). If both sampling stages are pushed back through the transform we get the situation shown in figure 1.21. The space-invariant reconstruction filter can now be convolved with the generally space-variant inverse transformed prefilter to produce what Heckbert calls the resampling filter, shown in figure 1.22. The right hand process is a point sampler and so the intensity surface values need only be generated at those points — in a similar way to the point sampling case. Thus the area sampling resampler can be implemented as a point sampling resampler.

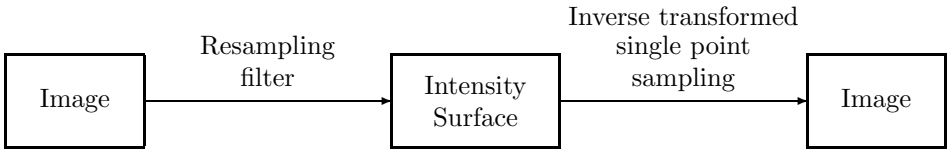

Figure 1.22: Heckbert's [1989] resampling filter. The whole resampling is decomposed into two stages for implementation: a resampling filter composed of the convolution of the reconstruction filter and the inverse transformed prefilter, and inverse transformed single point sampling.

1.8.3 Comparison

The major difference between a point and an area sampling process is that the calculation to produce a value is space-invariant in the former case and generally space-variant in the latter. Only in the case of an affine transform will the area-sampling case produce a space-invariant calculation [Heckbert, 1989, p.46, sec. 3.4.4]. The added complexity of space-variance makes area sampling much more difficult to implement than point sampling. This disadvantage must be weighed against the advantages of area sampling.

1.8.4 Other implementations

Whilst those shown here are the most common implementations, it is possible to generate others. For those, relatively rare, reconstructors which cannot be represented as filters, Heckbert's 'resampling filter' is not a viable implementation. Some other way of combining the reconstructor and area sampler would need to be found if such a reconstructor were to be used with an area sampler (the alternative is that this reconstructor could only ever be used with point sampling methods).

On a different tack, resamplers could be found for which the following implementation would prove possible:

> The original digital image is analysed to produce a digital 'image description' which describes an intensity surface. This image description is transformed, producing another image description which describes the transformed intensity surface. This image description can then be rendered, potentially by any sampler, to produce the final image (see figure 1.23).

Such reconstruction methods are discussed in chapter 6.

1.8.5 Comments

However we think of a particular resampling process: whether as a single process; as a resampling filter that is point sampled; as reconstruction followed by sampling; or as reconstruct, transform, sample; it is the same resampler producing the same results. The implementation may appear totally different to the theoretical description, but the results are the same.

1.9 The literature

Digital image resampling is useful in many fields and so the literature relating to it is in many disparate places. Medical imaging, remote sensing, computer vision, image processing and computer graphics all make use of resampling. The practitioners in the various fields all have their own views on the subject, driven by the uses to which they put resampling. Thus we find, for example, that

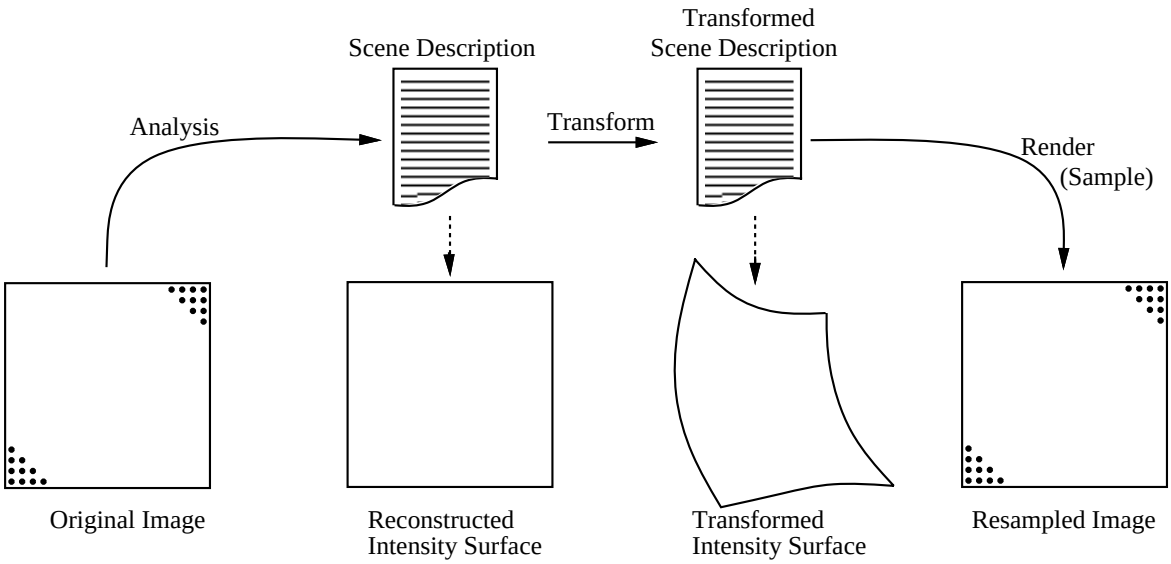

Figure 1.23: An alternative method of resampling. The image is analysed to give a scene description, which is transformed, and the transformed version rendered to produce the resampled image.

in one field (computer graphics), where distortion can be very high in resampled imagery, greater emphasis is placed on sampling methods than in another field (registering medical images) where distortion is mild [Heckbert, 1989; Wolberg, 1990].

Digital image resampling has its beginnings in the early '70s. Catmull [1974] was the first in the field of computer graphics to work on texture mapping, when he discovered a way to map images onto curved surfaces. Rifman, McKinnon, and Bernstein [Keys, 1981; Park and Schowengerdt, 1983] did some of the first work on resampling for correction of remotely sensed image data (satellite imagery) around the same time.

However none of this work made its way into the standard textbooks on image processing [Pratt, 1978; Gonzalez and Wintz, 1977; Rosenfeld and Kak, 1982] or computer graphics [Foley and van Dam, 1982] which were all produced around 1980. The exception to this is Newman and Sproull's [1979] "Principles of Interactive Computer Graphics", but even they only mention the subject in passing [*ibid.*, p.265]. The image processing texts do spend time on image restoration, which is related to *a priori* knowledge reconstruction (chapter 6), but none on resampling.

It was in the eighties that far more interest was paid to digital image resampling (only three of the 54 references listed in appendix A were published before 1980). The rush of publications was probably due to increased computer power and increased interest in raster displays; both for geometrical correction of digital images and for generation of realistic synthetic images.

Heckbert [1986a] presented a good survey of texture mapping as it was to date. He built on this foundation in his masters thesis [Heckbert, 1989], which is a valuable reference for those working in texture mapping.

The work on image resampling reached a milestone in 1990. In that year the first book [Wolberg, 1990] was published on the subject and the new standard texts [Foley *et al* 1990; Pratt, 1991] included sections on image resampling and its related topics.

"Digital Image Warping" by George Wolberg [1990] is the only existing book on digital image resampling. Prior to its publication the only source of information on image resampling was a myriad of articles scattered through technical journals and conference proceedings across half a dozen fields. Wolberg's book draws much of this material into one place providing a "conceptually

unified, interdisciplinary survey of the field" [Heckbert, 1991a].

Wolberg's book is not, however, the final word on image resampling. His specific aim was to emphasise the computational techniques involved rather than any theoretical framework [Wolberg, 1991]. "Digital Image Warping" has its good points [McDonnell, 1991] and its bad [Heckbert, 1991b] but as the only available text it is a useful resource for the study of resampling (for a review of the book see Heckbert [1991a]; the discussion sparked by this review may be found in Wolberg [1991], McDonnell [1991] and Heckbert [1991b]).

The most recent standard text, Foley, van Dam, Feiner and Hughes [1990] "Computer Graphics: Principles and Practice", devotes some considerable space to image resampling and its related topics. Its predecessor [Foley and van Dam, 1982] made no mention at all of the subject. This reflects the change in emphasis in computer graphics from vector to raster graphics over the past decade. The raster display is now the most common 'soft-copy' output device [Sproull, 1986; Fournier and Fussell,1988], cheap raster displays having been developed in the mid nineteen-seventies as an offshoot of the contemporary television technology [Foley and van Dam, 1982]. Today it is true to say that "with only a few specialised exceptions, line [vector] graphics has been subsumed by... raster graphics" [Fiume, 1986, p.2].

A number of the myriad articles on resampling are analysed in appendix A. The resamplers in each article have been decomposed into their three constituent parts, which are listed in the table there. This produces some insights into research in resampling. Over half the articles consider only single point sampling, concentrating instead on different reconstructors or transforms. Many articles examine only one of the three parts of the decomposition, keeping the other two constant. There are a significant number which consider only a scaling transform and single point sampling. There are others which concentrate on the transforms. It is only a minority that consider the interaction between all parts of the resampler, and these are mostly in the computer graphics field where distortions tend to be highest and hence the resampler has to be better (the higher the distortion the harder it is to resample well).

Most of the resamplers surveyed fit neatly into our three part decomposition, having three independent parts. A few fit less neatly, in that the three parts cannot be made independent. This latter set of resamplers are those in which area sampling is approximated. They depend on an approximation in original image space to an area in resampled image space transformed back into original image space. Because of the approximation either the reconstructor or the sampler must be transformation-dependent. Only one of the resamplers in appendix A does not fit well into the decomposition. This is Namane and Sid-Ahmed's [1990] method of binary image scaling. Their method cannot be said to produce any kind of continuous intensity surface and has thus proven difficult to fit into the three-part decomposition.

One 'resampler' not listed in the table is Kornfeld's [1985, 1987] image prism. This device only performs a limited set of orthogonal transformations which exactly map pixels onto pixels. Therefore no resampling is required.

In the following chapters many of these articles will be referred to in the discussion of the three parts of resampling. At the end we will draw the strands together and consider resampling as a whole.

1.10 Summary

The concept of digital image resampling has been introduced. It is a process which find uses in many fields. We have seen how it fits into the larger framework of operations on images, and how the continuous image we view differs from the discrete image that the computer operates on.

Several decompositions of resampling have been considered. We favour the three-part decomposition into reconstruction, transformation, and sampling. The remainder of this dissertation is

organised around this decomposition.

We concluded the chapter by considering how a resampler can be implemented, and by briefly looking at the history and literature of digital image resampling.

We now go on to consider the third of the sub-processes: sampling.

Chapter 2

Sampling

Sampling is the process of converting a continuous intensity surface into a discrete representation. As well as being the third sub-process of resampling, it is the process by which the original image is generated. Thus sampling is important in its own right as a sub-process, and also in how it it affects the original image and subsequent reconstruction from that image. Conventional sampling theory deals with a regular grid of point samples, with each sample in the image being generated by a single one of these point samples. In this dissertation 'sampling' refers to many sampling methods besides this single point sample method. In this chapter we discuss these sampling methods and their applicability to various sampling tasks.

2.1 Converting the continuous into the discrete

Sampling takes a continuous signal, one defined over all space, and produces a discrete signal, one defined over only a discrete set of points. In practice the two signals are only defined within a region of interest. Discussion of what lies outside this region is left until chapter 4. In our case, the continuous signal is an intensity surface; that is: a three-dimensional function with two spatial dimensions and one intensity dimension where each point in the spatial plane has a single intensity. When dealing with colour, the number of dimensions increases, typically to three colour dimensions (but still only two spatial dimensions). When dealing with one or three spatial dimensions the situation also changes but the underlying principle is the same: for every spatial point there is a single intensity or colour. An intensity surface is a many-to-one mapping from a spatial domain into an intensity (or colour) domain.

The discrete signal in our case is an image. It has the same number of spatial and intensity (colour) dimensions as the intensity surface but is discrete in the spatial domain. A digital computer cannot represent a continuous quantity and so the image will be discrete in intensity as well. In practice we find that spatial discreteness is central to the resampling problem, whilst intensity discreteness is a peripheral problem which can, for the most part, be safely ignored. Why this is so is discussed in the next section.

2.2 The problem of discrete intensities

Ideally, infinite precision in recorded intensity is desirable, no errors would then arise from slightly imprecise intensity values. In practice, intensities are recorded to finite precision which leads to errors in the reconstructed intensity surface, whether on the screen or in the resampling process.

These errors are most noticeable when only a few discrete intensity levels are available, and most

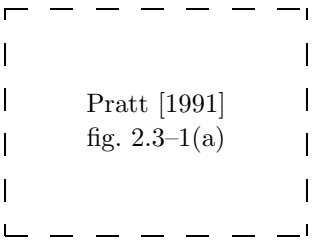

Figure 2.1: The minimum noticeable intensity difference ($\Delta I/I$) as a function of intensity (I) [Pratt, 1991, fig. 2.3–1(a)]. It is 2% for much of the range, rising to higher values for very dark or very light intensities.

image processing texts include an example showing the effect on a displayed image of allowing a larger or smaller number of intensity levels [see, for example, Rosenfeld and Kak, 1982, pp.107–8 figs. 14 and 15; Gonzalez and Wintz, 1977, fig. 2.8]. The extreme case is where there are only two levels: black and white. Such an image takes comparatively little storage (one bit per pixel) but has a limited usefulness. With digital half-toning techniques it can be made to simulate a wide range of grey shades, but, for resampling, it is preferable to have true shades of grey rather than simulated ones.

The general case, then, is one where a significant number of discrete intensity levels are used to represent a continuous range of intensities. But how many intensity levels are sufficient?

The minium necessary number of intensity levels

The human visual system is limited in how small an intensity change it can detect. Research suggests that, for two large areas of constant intensity, a two percent difference can be just detected [Crow, 1978, p.4]. The minimum difference that can be detected rises to a higher value for very dark or very bright areas [Pratt, 1978, pp.17–18] (see figure 2.1). It also rises when comparing small areas of constant intensity [*ibid.*, pp.18–19, fig. 2.5]. When dealing with colour images the minimum noticeable differences for pure colour information (that is with no intensity component) are much larger than those for intensity information, hence broadcast television has an intensity channel with high spatial resolution and two channels carrying the colour information at low spatial resolution [NMFPT, 1992]. Here, we shall consider only intensity. The number of intensity levels required to produce a faithful representation of an original intensity surface depends on the image itself [Gonzalez and Wintz, pp.27-28] and on the type of reconstruction.

If we wish to display any image on a 'reasonable' display device then how many levels are required? Many researchers have answered this question and their results are given below. We are working with binary digital computers and so, sensibly, most of the answers are powers of two.

Crow [1978, p.4] says that between six and eight bits (64 to 256 intensity levels) are required, depending on the quality of the display. He also calculates that the typical display would need about 162 intensity levels. This calculation is reproduced and explained later.

Gonzalez and Wintz [1977, pp.19 and 26] suggest that 64 levels (six bits) may be sufficient in some cases but say that "to obtain displays that will appear reasonably smooth to the eye for a large class of image types, a range of over 100 intensity levels is generally required."

Rosenfeld and Kak [1982, p.106] also suggest that more than 100 levels may be needed for some applications.

Finally, Foley and van Dan [1982, p.594] and Pavlidis [1982, p.39] both agree that 64 levels are generally adequate but that 256 levels may be needed for some images (Pavlidis hints that 256

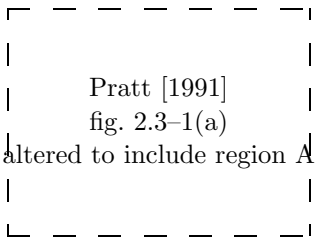

Figure 2.2: The minimum noticable intensity difference ($\Delta I/I$) as a function of intensity (I); in region A $\Delta I/I$ is higher that 2.35%. So long as the darkest possible intensity falls in this region, 1024 linearly spaced intensity levels will be sufficient for all images (after [Pratt, 1991, fig. 2.3–1(a)]).

levels may not be enough for a small number of images).

The consensus appears to be that many images require only 64 intensity levels and virtually none need more than 256.

If we wish *all* images that we could possibly display to exhibit no artifacts due to intensity quantisation then we must take into account those images with large areas of slowly changing intensity at the dark ¡end of the intensity range. Crow [1978, p.4] performs a 'back of the envelope' calculation to see how many intensity levels are required, given the two percent minimum perceivable intensity difference mentioned earlier. He notes that the most intense spot that a typical cathode ray tube (CRT) can produce is 25 times more intense than the dimmest. If the intensity levels are exponentially distributed (that is, each is two percent brighter than the previous level) then about $\frac{\log 25}{\log 1.02} = 163$ intensity levels are required.

However, for work in image resampling it is important that the intensities are distributed linearly. This means that the average of two intensities is a third intensity that is perceptually halfway between the two. Thus a checkerboard of squares in any two intensities, viewed from sufficient distance that the individual checks are imperceptible, will appear like a plane of constant intensity of the average of the two intensities. This property is important because virtually all resampling work involves taking the weighted average of a number of intensities and this must produce the perceptually correct result. (An exponential distribution could be used if it were transformed to the linear domain before any calculations and transformed back afterwards. This is a tremendous overhead for a resampling operation and should thus be avoided.)

With linearly distributed intensity levels all adjacent levels are the same distance apart, say ΔI, in intensity space. If, as above, the brightest level is 25 times as bright as the darkest and the total number of levels is n then ΔI will be:

$$\Delta I = \frac{25 - 1}{n - 1}$$

ΔI must be such that the second darkest level is two percent brighter than the darkest, therefore, in the above formula, $\Delta I = 0.02$. This means that the number of levels, n, is around $n = 1201$. 1200 is considerably more than the 256 quoted earlier, and is slightly more than 2^{10} (1024). Ten bits should however be sufficient, because the minimum perceivable intensity difference for the darkest levels is known to be higher than two percent. With 1024 levels the difference between the darkest and second darkest levels is 2.35%. This should be small enough provided that the darkest intensity on the screen is dark enough to be in the area of the response curve which rises above the two percent level (region A in figure 2.2). With 256 levels (eight bits) the difference is 9.41%, which may be too large. Observations on an eight bit, linearly distributed display show that it *is* too large: false contouring can be seen in areas of slowly varying dark intensity.

Blinn [1990, p.85] notes the same effect in digital video. In his discussion of digital video format D1 he says: "Digital video sounds like the world of the future, but I understand there's still a bit of a problem: 8 bits don't really give enough resolution in the darker areas to prevent contouring or banding."

Murch and Weiman [1991] have performed experiments which show that ten is the maximum number of bits required to make intensity differences between adjacent levels imperceptible, with the possible exceptions of CRTs with an extremely high maximum intensity.

For any image without large areas of slowly varying dark intensities, ten bits of intensity information is too much, and so, for many images, if the intensity values are stored to a precision of eight bits, few visible errors will result from the quantisation of intensity. If they are stored to a precision of ten bits or more, practically no visible errors will arise.

2.2.1 Extra precision

Resampling involves the manipulation of intensity values. As these values are used in calculations, a little extra precision may be desirable to absorb any numerical inaccuracies which arise. This is illustrated in the following diagram:

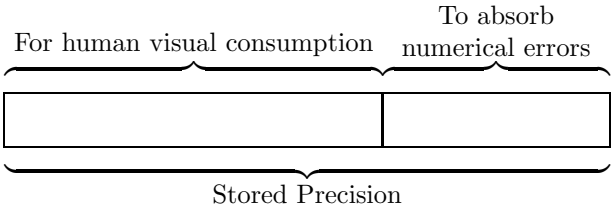

In calculations it is also possible for intensities to be produced that are 'whiter than white'. Such supra-white intensities have values brighter than the brightest that can be represented. Extra bits should be provided at the top of the intensity value to catch such overflow, otherwise the calculation can wrap around and produce spurious wrong intensities.

Underflow will produce negative intensities which, while physically unrealisable, are a possible outcome of resampling calculations. Thus the intensities need to be stored as a signed quantity to catch such sub-black intensities, for the same reasons we needed to catch supra-white values. A sign bit must be included. This amends our diagram to:

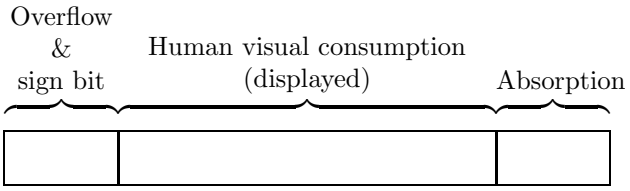

Such a representation cannot catch all overflows, underflows, or numerical inaccuracies, but it will help immensely in catching most of them.

As a practical example, our experimental image processing system has a generous bit allocation scheme. It uses 32 bit integers and an 8 bit display: overflow is allocated seven bits plus the sign bit, absorption is given fourteen and the lowest two of the ten bits required for correct display cannot be displayed:

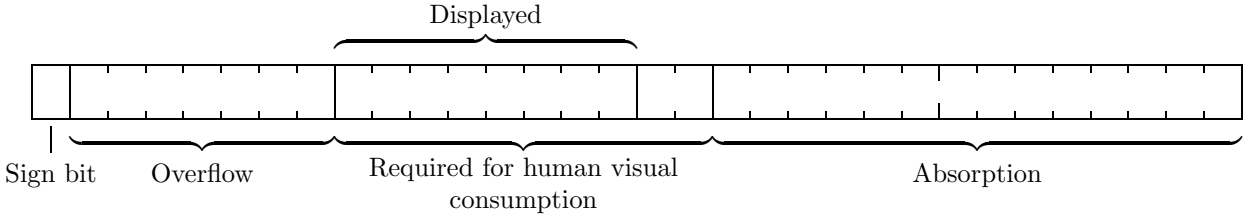

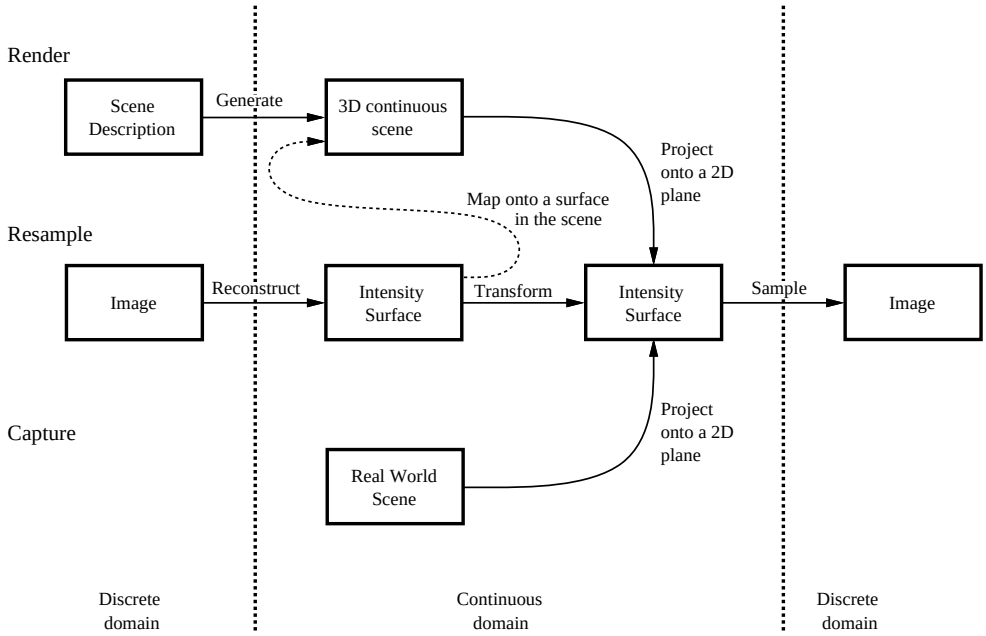

Figure 2.3: The three image creation processes subdivided. On the right is the image that is created. In each case it is generated from an intensity surface by a sampling sub-process. This intensity surface is generated in a different way for each creation process.

To conclude: with these precautions it can be seen that little, if any, visible errors or artifacts will arise from intensity quantisation. Thus the fact that the intensity values are quantised can be largely ignored in our discussion. We may now proceed to discuss the more important problem of spatial discreteness.

2.3 Producing a discrete image

Sampling occurs in three distinct processes: image capture, image rendering and image resampling. These are the three image creation processes described in section 1.3. In each of these a continuous intensity surface is sampled to produce a discrete image. The continuous intensity surface is generated in a different way in each process but the sampling is fundamentally the same in all three cases, as illustrated in figure 2.3.

In *image capture* some physical device is used to sample a real world scene. Such devices include video cameras, scanners and fax machines. Figure 2.3 divides the image capture process into two parts. This subdivision can be thought of in two ways:

(a) the theoretical two-dimensional intensity surface is generated by the optics of the capture device and occurs immediately in front of the light sensors (figure 2.4(a));

(b) the theoretical two-dimensional intensity surface exists just in front of the entire capture device and the entire device, optics and light sensors included, form part of the sampling process (figure 2.4(b)).

Some capture devices have no optics, in which case (a) and (b) are identical.

(b) has the disadvantage that depth effects caused by the optics of the system cannot be modelled as pointing the capture device at a two-dimensional intensity surface because depth effects (for

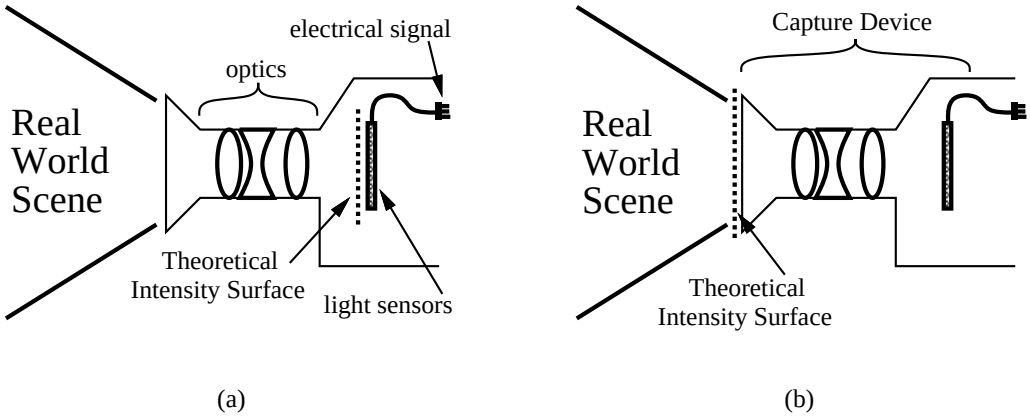

Figure 2.4: The two ways of subdividing the image capture process: (a) a theoretical two-dimensional intensity surface is generated by the optics of the capture device, just before it is captured by the light sensors; (b) a theoretical two-dimensional intensity surface is assumed to occur just before the entire capture device, and this intensity surface is sampled by the whole device.

example, depth of field) depend on the three-dimensional layout of the real-world scene. On the other hand (a) models all effects because the intensity surface is placed after the optics which process the scene into a two-dimensional function. In (b) the intensity surface could be reasonably thought of as a two-dimensional window into the three-dimensional scene.

The big disadvantage of (a) is that part of the capture device is included in the sampling process and part is not. It is far preferable for the entire device to be included in the sampling process as all parts of the device can affect the samples that are produced. For this reason (b) is the preferred way of thinking of this theoretical division of capture into two parts. Note that atmospheric effects are here part of the scene, not of the sampling process.

Wolberg and Boult [1992] discuss image creation, subdividing the process into five parts: warping before entering the capture device, blurring by the optics of the capture device, warping by the optics of the capture device, blurring by the light sensors and single point sampling. This subdivision can be placed in our diagram as follows: the warping before entering the device is considered part of the real world scene, the blurring and warping by the optics, blurring by the light sensors, and single point sampling are all part of the sampling sub-process. Alternatively, if we were to use (a) rather than (b); the blurring and warping caused by the optics would be part of the process of generating the two-dimensional intensity surface and only the blurring by the image sensors and the single point sampling would be included in the sampling process. This latter assumption is used by Boult and Wolberg in their generation of a reconstructor which corrects for the capture device's sampling method (see section 6.1).

Image rendering takes a digital scene description and generates a continuous, usually three-dimensional, scene from this description. As in image capture, this three-dimensional scene is projected to a theoretical two-dimensional intensity surface which is then sampled. Again, if the sampling method generates depth effects then this model is not totally accurate. However, it is a useful approximation.

In *image resampling* there are no problems with depth effects, the entire process takes place in two dimensions. In cases where resampling is used to generate part of a scene in a rendering process (the dashed arrow in figure 2.3) then depth effects may come into play.

These three processes cover the three ways of generating an image. Image processing in general (with the exception of image resampling) does not involve the creation of an intermediate intensity surface. Virtually all image processing operations carry a direct correspondence between input and

output pixels and can work by a discrete convolution process [see for example, Fang, Li and Ni, 1989, for a discussion of discrete and continuous convolution]. Image resampling, by comparison, does not have this direct correspondence and some process is required so that output pixels can be positioned anywhere, in relation to the input pixels. In our three-part model this process is provided by reconstructing an intensity surface, transforming this, and sampling the transformed version to produce a new image.

We have seen that sampling is a very similar process for the three distinct operations of image capture, image rendering, and image resampling. It is thus important for its part in image resampling and for its part in creating the images that are resampled. We now go on to discuss this sampling process.

2.4 The sampling process

The aim of sampling is to generate pixel values so that they "best represent" the two-dimensional intensity surface. [Foley *et al*, 1990, p.619]. This is a good concept but what is meant by 'best represent'? To some it may mean that the samples obey classical sampling theory. To others it may mean that the resulting image, when displayed on a certain device, is visually as similar as possible to the two-dimensional intensity surface. These two ideas are not necessarily the same thing. In the subsequent sections we discuss both of these ideas and the tension between them.

2.4.1 Classical sampling theory

The roots of sampling theory go back to 1915, with Whittaker's work on interpolation of a set of equispaced samples. However, most people attribute the sampling theorem to Shannon [1949], who acknowledges a debt to many others in its development. Attribution of the theorem has been jointly given to Whittaker and Shannon [Gonzalez and Wintz, 1977, p.72] Shannon and Nyquist [Turkowski, 1986], and to Shannon, Kotel'nikof and Whittaker [Petersen and Middleton, 1962, p.279]. Shannon's statement of the sampling theorem is[1]:

> If a function $f(t)$ contains no frequencies higher that W cps it is completely determined by giving its ordinates at a series of points spaced $\frac{1}{2W}$ seconds apart.
> [Shannon, 1949, Theorem 1] [2].

Mathematically, the sampling process is described as the product of $f(t)$ with the comb function:

$$\text{comb}(t) = \sum_{n=-\infty}^{\infty} \delta(t - nT)$$

where $\delta(t)$ is the Dirac delta-function[3]. This gives the sampled function:

$$\hat{f}(t) \quad = \quad \left(\sum_{n=-\infty}^{\infty} \delta(t - nT) \right) f(t)$$

[1] The theory laid out by Shannon [1949] and others is for one dimensional sampling only. Petersen and Middleton [1962] extended Shannon's work to many dimensions.

[2] cps = cycles per seconds ≡ Hertz

[3] The Dirac delta function is zero everywhere except at $t = 0$. The area under the function is unity, that is $\int_{-\infty}^{\infty} \delta(t)\, dt = 1$. One definition of the Dirac delta function is:

$$\delta(t) = \lim_{a \to \infty} \sqrt{a}\, e^{-a\pi x^2}$$

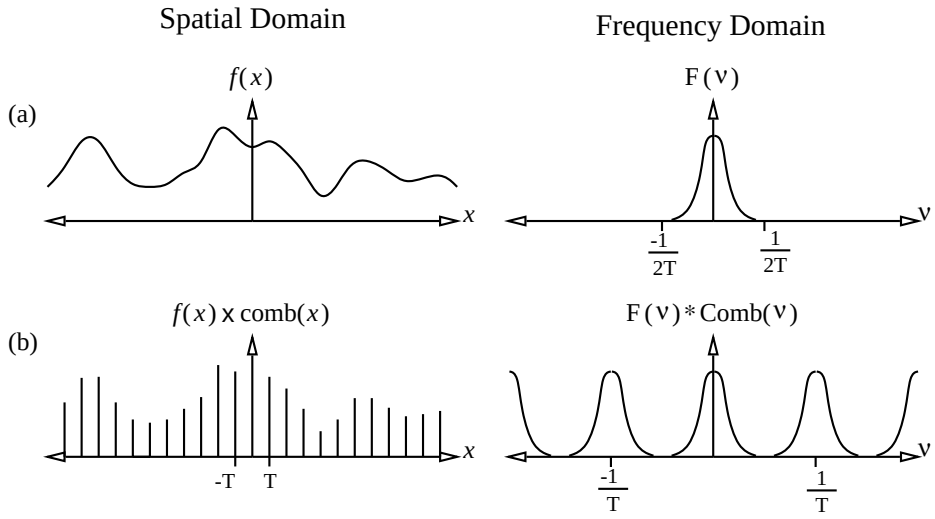

Figure 2.5: The sampling process: (a) the continuous spatial domain function, $f(x)$, has a Fourier transform, $F(\nu)$, bandlimited to below half the sampling frequency, $\frac{1}{2T}$; (b) when it is sampled $(f(x) \times \text{comb}(x))$ its Fourier transform is convolved with $\text{Comb}(\nu)$ producing replicas of the original Fourier transform at a spacing of $\frac{1}{T}$.

$$= \sum_{n=-\infty}^{\infty} (\delta(t - nT) f(t - nT)) \tag{2.1}$$

This is not the same as:

$$\hat{f}_n = f(nT) \tag{2.2}$$

Equation 2.1 is a continuous function which consists of an infinite sum of weighted, shifted Dirac delta functions and is zero everywhere except at $t = nT, n \in \mathcal{Z}$. Equation 2.2 is a discrete function which is defined on the set $n \in \mathcal{Z}$. The values of the discrete function are the weights on the delta functions that make up the continuous function, that is:

$$\hat{f}(t) = \sum_{n=-\infty}^{\infty} \hat{f}_n \, \delta(t - nT)$$

In a computer we, of course, store the discrete version; but mathematically and theoretically we deal with the continuous one. The sampling theorem can be justified by considering the function in the frequency domain.

The continuous spatial domain function, $f(t)$, is bandlimited. That is it contains no frequencies higher than ν_b (W in the statement of Shannon's theorem above). Its Fourier transform, $F(\nu)$ is thus zero outside the range $(-\nu_b, \nu_b)$. Sampling involves multiplying $f(t)$ by $\text{comb}(t)$. The equivalent operation in the frequency domain is to convolve $F(\nu)$ by $\text{Comb}(\nu)$, the Fourier transform of $\text{comb}(t)$. $\text{Comb}(\nu)$ is composed of Dirac delta-functions at a spacing of $\frac{1}{T}$ (for a proof of this see Marion [1991, pp.31–32]). Convolving this with $F(\nu)$ produces replicas of $F(\nu)$ at a spacing of $\frac{1}{T}$. Figure 2.5 illustrates this process.

If $T < \frac{1}{2\nu_b}$ then the copies of $F(\nu)$ will not overlap and the original $F(\nu)$ can be retrieved by multiplying $\hat{F}(\nu)$ by a box function:

$$\text{Box}(\nu) = \begin{cases} 1, & |\nu| < \nu_b \\ 0, & \text{otherwise} \end{cases}$$

This removes all the copies of the original except for the copy centred at $\nu = 0$. As this is the original frequency domain function, $F(\nu)$, the spatial domain function will also be perfectly reconstructed.

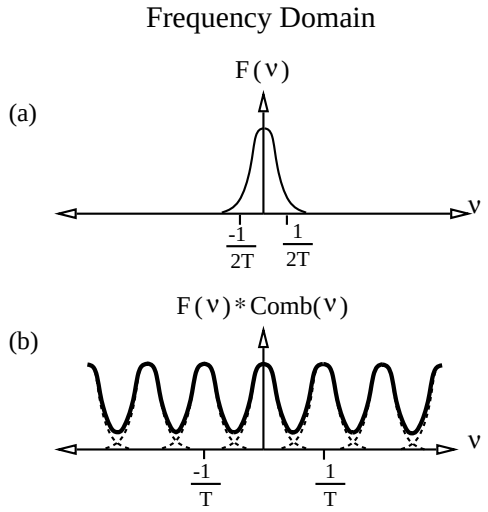

Figure 2.6: An example of sampling at too low a frequency. Here we see the frequency domain representations of the functions. The original function, (a), is not bandlimited to within half the sampling frequency and so when it is sampled, (b), the copies overlap and add up producing the function shown by the dark line. It is impossible to recover the original function from this aliased version.

Multiplying by a box function in the frequency domain is equivalent to convolving in the spatial domain by the box's inverse Fourier transform, $s(x)$. This can be shown to be $s(x) = 2\nu_b \text{sinc}(2\nu_b x)$, where $\text{sinc}(x) = \frac{sin(\pi x)}{\pi x}$ (a proof of this can be found in appendix B.1). The sinc function is discussed in sections 3.3 and 4.3.

If $T \geq \frac{1}{2\nu_b}$ then the copies of $F(\nu)$ will overlap (figure 2.6). The overlapping parts sum to produce $\hat{F}(\nu)$. There is no way that this process can be reversed to retrieve $F(\nu)$ and so $f(t)$ cannot be perfectly reconstructed. If $\hat{F}(\nu)$ is multiplied by the box function (the perfect reconstructor) then the resulting function is as if $F(\nu)$ had been folded about the frequency $\frac{1}{2T}$ and summed (figure 2.7). For this reason $\nu = \frac{1}{2T}$ is known as the folding frequency. The effect of this folding is that the high frequencies in $F(\nu)$ alias into low frequencies. This causes artifacts in the reconstructed image which are collectively known as 'aliasing'. In computer graphics the term aliasing is usually incorrectly used to refer to both aliasing and rastering artifacts [Pavlidis, 1990]. This point is picked up in section 2.7. Figure 2.8 gives an example of aliasing. It normally manifests as unsightly ripples, especially near sharp changes in intensity.

To avoid aliasing we must ensure that the sampled intensity surface is bandlimited to below the folding frequency. If it is not then it can be prefiltered to remove all information above this frequency. The procedure here is to multiply the intensity surface's Fourier transform by a box function, a process known as *bandlimiting* the intensity surface. Foley *et al* [1990, fig. 14.29] give an example of this procedure. This prefiltering followed by point sampling is equivalent to an area sampling process, as is explained later.

These procedures are mathematically correct and produce an image free of aliasing. However they have their drawbacks. Firstly, if an intensity surface has to be prefiltered then the image does not represent the original intensity surface but rather the filtered one. For certain applications this may be undesirable. To represent a flat or linearly sloped intensity surface, infinite frequencies *are* required. Bandlimiting prevents such surfaces from being perfectly represented, and so any 'flat' part of a bandlimited image will be ripply. An example of this effect is that any discontinuity in a band-unlimited intensity surface will have a 9% overshoot either side if it is bandlimited, no matter what the bandlimit is [Lynn and Fuerst, 1989, p.145]; ripples will also propagate out from the discontinuity, reducing in magnitude as they get farther away. Thus a bandlimited intensity

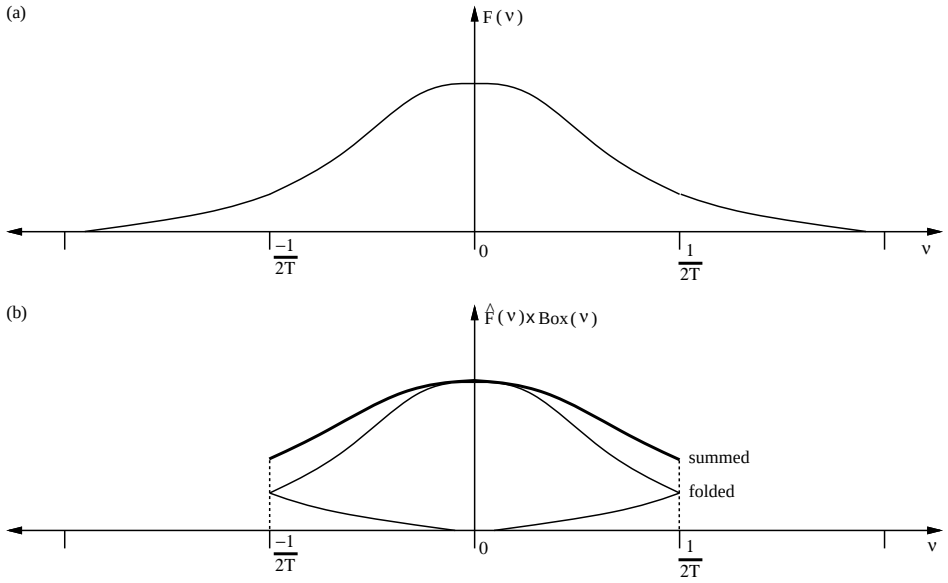

Figure 2.7: An example of aliasing. (a) is the frequency spectrum of the original image. If the original image is sampled and then reconstructed by multiplying its frequency spectrum by a box function then (b) is the result. The copies of the spectrum overlap and add up, as if $F(\nu)$ in (a) had been folded back about $\frac{1}{2T}$ and summed.

Figure 2.8: An example of a reconstructed intensity surface which contains aliases. These manifest themselves as ripples around the sharp edges in the image. The small image of the letter 'P' is the original. The large is an intensity surface reconstructed from this small original using an approximation to sinc reconstruction.

surface is, by its very nature, ripply. This can be seen in figure 2.12(a); there is no aliasing in this figure, the intensity surface is inherently ripply due to being bandlimited. The human visual system abhors ripples, they seriously degrade an image. If however, the ripples in the reconstructed intensity surface are undetectable by the human eye then the surface looks very good. These points are picked up in chapter 7.

More importantly, it is practically impossible to achieve perfect prefiltering and so some aliasing will creep in. In an image capture device, some (imperfect) prefiltering will occur; that is: the image capture device does not perform perfect prefiltering. Fraser [1987] asserts that most people depend on this prefiltering to bandlimit the intensity surface enough that little aliasing occurs. In the digital operations of rendering and resampling, perfect prefiltering is simply impossible, ensuring that some aliasing always occurs. This is because perfect prefiltering involves either continuous convolution by an *infinite* sinc function or multiplication of the *continuous* Fourier transform by a bandlimiting function. Both of these operations are impossible in a discrete computer.

Finally, perfect reconstruction is also practically impossible because it requires an infinite image. Thus, whilst it would be theoretically possible to exactly recreate a bandlimited intensity surface from its samples, in practice it is impossible. In fact, most display devices reconstruct so badly that correct sampling can be a liability. Sampling which takes into account the reconstruction method is the topic of section 2.8.

Before discussing this, however, we need to examine the various types of sampling. These fall into two broad categories: area samplers and point samplers.

2.5 Area *vs* point sampling

Any sampling method will fall into one of these two categories. Area sampling produces a sample value by taking into account the values of the intensity surface over an area. These values are weighted somehow to produce a single sample value. Point sampling takes into account the values of the intensity surface only at a finite set of distinct points[4]. If the set contains more than one point then these values must be combined in some way to produce a single sample value. This is not the usual description of point sampling, because 'point sampling' is usually used in its narrow sense: to refer to single point sampling. Fiume [1989, section 3.2.4] studied the various sampling techniques, the following sections draw partly on his work.

2.5.1 Area sampling

Exact-area sampling

The assumptions behind exact-area sampling are that each pixel has a certain area, that every part of the intensity surface within that area should contribute equally to the pixel's sample value, and that any part of the intensity surface outside that area should contribute nothing. Hence, if we make the common assumption that pixels are abutting squares then for a given pixel the sample value produced by the exact area sampler will be the average intensity of the intensity surface within that pixel's square (figure 2.9(a)) Alternately, we could assume that pixels are abutting circles [Durand, 1989] or overlapping circles [Crow, 1978] and produce the average value of the intensity surface over the relevant circular area (figure 2.9(b) and (c)). Obviously other assumptions about pixel shape are possible.

Exact-area sampling is very common, and is discussed again when we look at sampling methods which take into account how the image will be reconstructed (section 2.8).

[4]Fiume [1989, p.82] states that the set of point samples should be countable, or more generally, a set of measure zero.

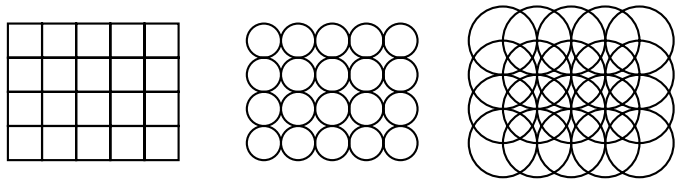

Figure 2.9: Three common assumptions about pixel shape: (a) abutting squares, (b) abutting circles, and (c) overlapping circles.

General area sampling

The general case for area sampling is that some area is chosen, inside which intensity surface values will contribute to the pixel's sample value. This area is usually centred on the pixel's centre. Some weighting function is applied to this area and the pixel's value is the weighted average over the area. Exact-area sampling is obviously a special case of this.

Equivalence to prefiltering

Area sampling is equivalent to prefiltering followed by single point sampling. In area sampling, a weighted average is taken over an area of the intensity surface. With prefiltering a filter is convolved with the intensity surface and a single point sample is taken for each pixel off this filtered intensity surface. To be equivalent the prefilter will be the same function as the area sample weighting function. The two concepts are different ways of thinking about the same process. Looking back to chapter 1, Heckbert [1989] proposed that the sampling sub-process be decomposed into prefiltering and single point sampling. Whilst this is entirely appropriate for all area samplers, not all point samplers can be represented in this way, because some point samplers cannot be represented by filters. Specific examples are adaptive super-samplers and stochastic point samplers, discussed below.

2.5.2 Point sampling

Unlike an area-sampling process, a point-sampler ignores all but a countable set of discrete points to define the intensity value of a pixel. Point sampling comes in two flavours: regular and irregular (or stochastic) point sampling. Wolberg [1990, sections 6.2 and 6.3] summarises the various types of point sampling; here we only outline them.

Single point sampling

In single point sampling, the samples are regularly spaced and each pixel's sample value is produced by a single point. In fact this is exactly the method of sampling described in classical sampling theory (section 2.4.1). All other point sampling methods are attempts to approximate area sampling methods or attempts to reduce artifacts in the reconstructed intensity surface (often they attempt to be both).

Super-sampling

As in single point sampling, the samples are arranged in a regular fashion, but more that one sample is used per pixel. The pixel's intensity value is produced by taking a weighted average of the sample values taken for that pixel. This can be seen as a direct approximation to area sampling.

Fiume [1989, p.96, theorem 6] proves that, given a weighting function, a super-sampling method using this weighting function for its samples converges, as the number of samples increases, toward an area sampling method using the same weighting function.

Such a super-sampling technique can be represented as a prefilter followed by single point sampling; on the other hand, the adaptive super-sampling method cannot.

Adaptive super-sampling

Adaptive super-sampling is an attempt to reduce the amount of work required to produce the samples. In order to produce a good quality image, many super-samples need to be taken in areas of high intensity variance but a few samples would give good results in areas of low intensity variance. Ordinary super-sampling would need to take many samples in all areas to produce a good quality image, because it applies the same sampling process for every pixel. Adaptive super-sampling takes a small number of point samples for a pixel and, from these sample values, ascertains whether more samples need to be taken to produce a good intensity value for that pixel. In this way fewer samples need to be taken in areas of lower intensity variance and so less work needs to be done.

Stochastic sampling

Stochastic, or irregular, sampling produces a sample value for each pixel based on one or more randomly placed samples. There are obviously some bounds within which each randomly placed sample can lie. For example it may be constrained to lie somewhere within the pixel's area, or within a third of a pixel width from the pixel's centre. The possible locations may also be constrained by some probability distribution so that, say, a sample point has a greater chance of lying near the pixel centre than near its edge. Stochastic methods cannot be represented as a prefilter followed by single point sampling, because of this random nature of the sample location.

Stochastic sampling is in favour amongst the rendering community because it replaces the regular artifacts which result from regular sampling with irregular artifacts. The human visual system finds these irregular artifacts far less objectionable than the regular ones and so an image of equal quality can be achieved with fewer stochastic samples than with regularly spaced samples (see Cook [1986] but also see Pavlidis' [1990] comments on Cook's work).

Fiume [1989, p.98, theorem 7] proves that the choice of point-samples stochastically distributed according to a given probability distribution will converge to the analagous area-sampling process as the number of points taken increases, a result similar to that for super-sampling.

2.5.3 Summary

Area sampling yields mathematically precise results, if we are attempting to implement some prefilter (section 2.4.1). However, in digital computations it may be impossible, or difficult to perform area sampling because it involves continuous convolution. In resampling it is possible to implement some area samplers, at least approximately, but a general area sampler is practically impossible. The point sampling techniques have been shown to be capable of approximating the area sampling methods. Such approximations are necessary in cases where area sampling is impracticable [Fiume, 1989, p.102].

Figure 2.10: Two very similar images: (a) on the left, was generated by summing the first twenty-nine terms of the Fourier series representation of the appropriate square wave; (b) on the right, was generated by super-sampling a perfect representation of the stripes.

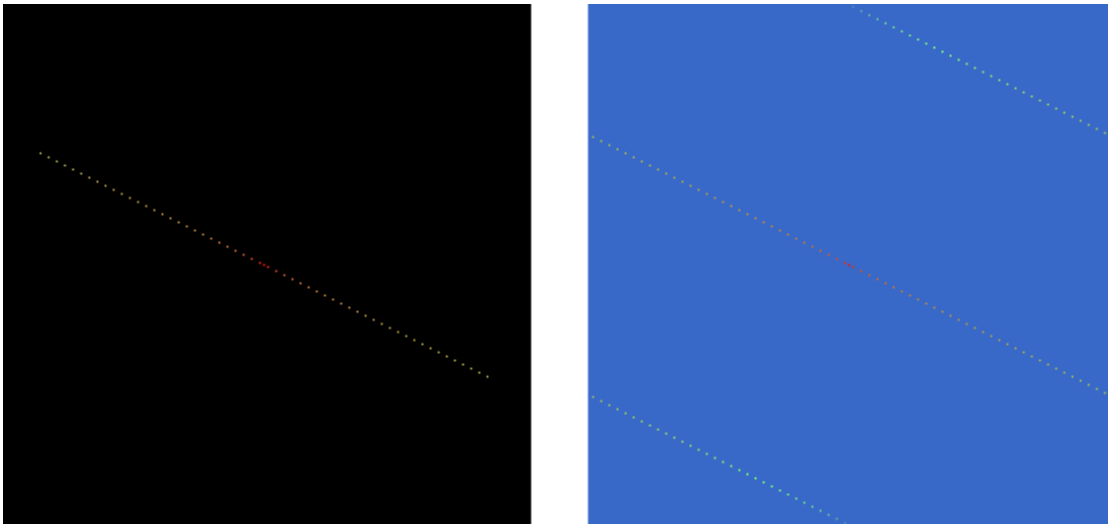

Figure 2.11: The Fourier transforms of the images in figure 2.10. (a) on the left and (b) on the right. The Fourier transforms are shown on a logarithmic scale. Note that the background is black (zero) in (a) but has non-zero, but small, magnitude in (b).

2.6 Practical considerations

An image capture device always implements some area sampling process. There is usually some small change that can be made in the area sampler by, for example, changing the focus of the lenses or inserting a mask. Major changes involve the expensive process of designing a new device.

Rendering and resampling occur in a digital computer and, for rendering, most area sampling techniques are analytically impossible and/or computationally intractable [Fiume, 1989, p.102]. Thus they cannot be implemented. The complexity of scenes in image rendering means that area sampling, where possible, can be extremely expensive to compute. Image rendering therefore makes almost exclusive use of point-sampling techniques.

Figure 2.12: The two images of figure 2.10 reconstructed using as near perfect reconstruction as possible. (a) on the left and (b) on the right. This figure shows part of the reconstructed intensity surface. Aliasing artifacts occur in (b) only

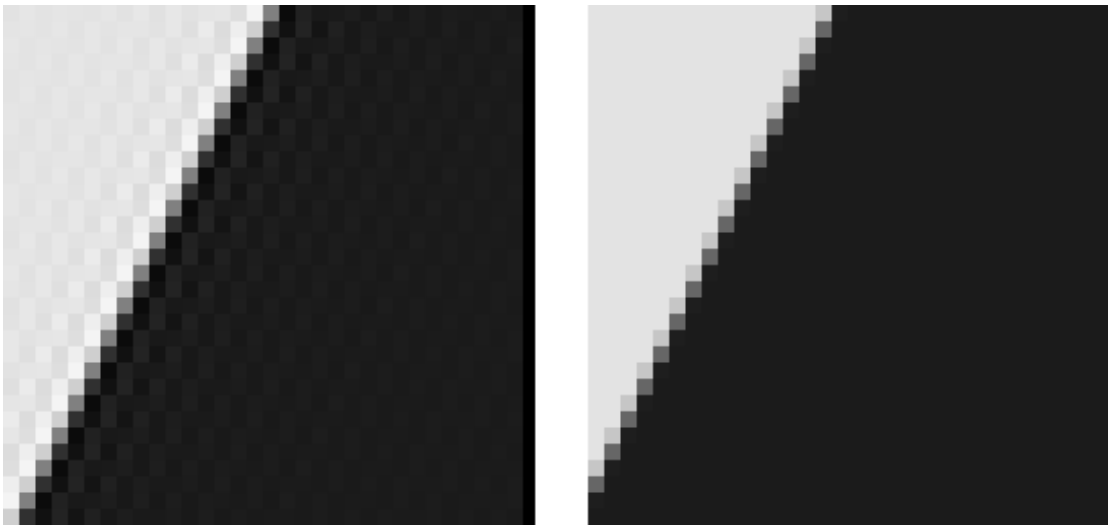

Figure 2.13: The two images of figure 2.10 reconstructed using as nearest-neighbour reconstruction. (a) on the left and (b) on the right. This figure shows part of the reconstructed intensity surface. (a) contains only rastering atifacts, while (b) contains a combination of rastering and aliasing artifacts.

Image resampling involves a simpler 'scene' and so both the computationally possible area samplers and the point samplers can be used. Heckbert [1989, sec. 3.5.1] dismisses point sampling techniques on the grounds that they do not eliminate aliasing. A super-sampling method shifts the folding frequency higher, but band-unlimited signals are common in texture mapping [*ibid.*, p.47], and so, while super-sampling will reduce aliasing, it will not eliminate all aliases, no matter how many super-samples are taken. Heckbert thus considers only area sampling techniques.

This argument is certainly valid for the surface texture mapping application discussed by Heckbert. However stochastic point sampling methods have done much to eliminate aliasing artifacts (by replacing them with less-objectionable noise artifacts) and many people *do* use point sampling methods in preference to area sampling methods simply because they are easier to implement. Further, in rendering work, it is often expedient to treat all samples identically and so, if texture mapping (a form of resampling) occurs in the scene, the samples will be taken in the same way as samples are taken in the rest of the scene: almost invariably by some point sampling technique. Wolberg [1990] covers the stochastic sampling methods, drawing on the rendering literature. However, Heckbert [1991a] found this material out of place in Wolberg's book. We think that it is necessary because such methods *are* used for resampling work.

Finally it is useful to realise that many practitioners in resampling use single point sampling. It appears to be the default method. We believe that this is because single point sampling is (a) simple to implement; (b) the obvious sampling method; and (c) all that is required if the image need only undergo a mild transformation.

This latter point draws on the fact that the aliasing (and other) artifacts, which more sophisticated sampling methods suppress, do not manifest themselves very much under a mild transformation (that is, scale changes of $\pm 20\%$ at most). Some applications of resampling only require such mild transformations, (for example the medical image registration system developed by Venot *et al* [1988] and Herbin *et al* [1989]) while others require more violent transforms (for example texture mapping) and thus require more advanced sampling, especially in cases of image shrinking where the sampling method dominates the resampler (see chapter 7).

2.7 Anti-aliasing

The purpose of all sampling, other than single-point sampling, is ostensibly to prevent any artifacts from occuring in the image. In fact it is usually used to prevent any artifacts from occuring in the intensity surface reconstructed from the image by the display device. This prevention is generally known in computer graphics as anti-aliasing. This is something of a misnomer as many of the artifacts do not arise from aliases. The perpetuation of the incorrect terminology is possibly due to the fact that the common solution to cure aliasing also alleviates rastering, the other main source of artifacts in images [Pavlidis, 1990, p.234].

Crow [1977] was the first to show that aliasing (sampling a signal at too low a rate) was the cause of some of the artifacts in digital imagery. He also notes [*ibid.*, p.800] that some artifacts are due to failing to reconstruct the signal properly. This latter problem he termed 'rastering'. 'Aliasing', however, became the common term for both of these effects, with some subsequent confusion, and it is only recently that the term 'rastering' has reappeared [Foley *et al*, 1990, p.641]. Mitchell and Netravali [1988] do discuss the two types of artifact as distinct effects but perpetuate the terminology by naming aliasing and rastering, pre-aliasing and post-aliasing respectively.

Sampling has thus been used to alleviate both types of artifact. This has an inbuilt problem that, to correct for reconstruction artifacts (rastering), one needs to know the type of reconstruction that will be performed on the image. Most images are displayed on a CRT, and all CRTs have a similar reconstruction method, so this is not too big a problem. However, when displayed on a different device (for example a film recorder) artifacts may appear which were not visible on the CRT because the reconstruction method is different. Further, an image used for resampling which

has been 'anti-aliased' for use on a CRT may not be particularly amenable to the reconstruction method used in the resampling algorithm.

Figures 2.10 through 2.13 illustrate the distinction between aliasing artifacts and reconstruction artifacts. Two images are shown of alternate dark and bright stripes. These images were specially designed so that no spurious information due to edge effects would appear in their discrete Fourier transforms (that is: the Fourier transforms shown here are those of these simple patterns copied off to infinity so as to fill the whole plane).

Figure 2.10(a) was generated by summing the first twenty-nine terms of the Fourier series representation of the appropriate square wave as can be seen by its Fourier transform (figure 2.11(a)). Figure 2.10(b) was generated by one of the common anti-aliasing techniques. It was rendered using a 16×16 super-sampling grid on each pixel with the average value of all 256 super-samples being assigned to the pixel. Figure 2.11(b) shows its Fourier transform. It is similar in form to figure 2.11(a) but the aliasing can be clearly seen in the wrap around effect of the line of major components, and also in that the other components are not zero, as they are in the unaliased case.

When these are reconstructed using as near-perfect reconstruction as possible we get the intensity surfaces shown in figure 2.12. The ripples in figure 2.12(a) are not an aliasing artifact but the correct reconstruction of the function; it is, after all, a sum of sine waves. The ripply effect in figure 2.12(b) *is* due to aliasing. The intensity surface that was sampled had constant shaded stripes with infinitely sharp transitions between the dark and light stripes. The perfectly reconstructed intensity surface shown here perfectly reconstructs all of the aliases caused by sampling the original intensity surface.

By contrast, figure 2.13 shows the intensity surfaces which result from an imperfect reconstructor: the nearest-neighbour interpolant. The artifacts in figure 2.13(a) are entirely due to *rastering* (the image contains no aliasing). This is the familiar blocky artifact so often attributed, incorrectly, to aliasing. The artifacts in figure 2.13(b) are due to a combination of aliasing and rastering. Oddly, it is this latter intensity surface which we tend to find intuitively preferable. This is probably due to the areas perceived as having constant intensity in figure 2.10(b) retaining this constant intensity in figure 2.13(b).

How these intensity surfaces are perceived does depend on the scale to which they are reconstructed. The 'images' in figure 2.10 are of course intensity surfaces but are reconstructed to one eighth the scale of those in figure 2.12 and figure 2.13. If one stands far enough back from these larger-scale figures then they all look identical.

It is fascinating that the intensity surface with both types of artifact in it appears to be the prefered one. This is possibly due to the facts that (a) the human visual system is good at detecting intensity changes, hence rippling is extremely obvious; and (b) most scenes consist of areas of constant intensity or slowly varying intensity separated by fairly sharp edges, hence representing them as a bandlimited sum of sinusoids will produce what we perceive as an incorrect result: most visual scenes simply do not contain areas of sinsoidally varying intensity.

Thus there is a tension between the sampling theory and the visual effect of the physical reconstruction on the display device. Indeed many researchers, instead of turning to the perfect sampling theory method of sampling, turn instead to methods which take the reconstruction process into account.

2.8 Sampling which considers the reconstruction method

In such sampling the reconstruction is usually onto a display device, rather than to any theoretical intensity surface. Several models of the display device have been used in the design of sampling methods.

The common assumption is that each pixel represents a finite area on the screen and therefore

should be area sampled from that area. This leads to the exact area sampling method given in section 2.5.1. Such an assumption can be found in many papers on resampling, for example Weiman [1980], Paeth [1986], Fant [1986], and Durand and Faguy [1990] all assume square (or rectangular) abutting pixels. Paeth [1990, pp.194-5] later revised his earlier work to allow for more sophisticated sampling methods. Durand [1989] used abutting circular pixels, which seems a less obvious choice, particularly as parts of the sampled intensity surface are not included in the sum for any pixel. His reasoning was to reduce the number of calculations in his resampling method (compared with abutting rectangular pixels). This assumption can also be found in Kiryati and Bruckstein [1991] but they are modelling a physical sampling device, not a physical reconstruction.

Foley *et al* [1990, pp.621-3] show that this exact area sampling method is inadequate for sequences of images. They suggest weighted area sampling functions which cover a larger area than the pixel (for example: a circularly symmetric tent function centred at the pixel centre).

Finally, it is well known that a CRT display reconstructs an image by first convolving it with a nearest-neighbour function (the effect of the digital to analogue converter) and then with a Gaussian (the effect of the spot in the CRT tube) [Blinn, 1989b]. Crow [1978] used this type of model in his sampling method. He says that: "A properly adjusted digital raster display consists of regularly spaced dots which overlap by about one-half." His conclusion was that a pixel sampled over such an area with a weighting function that peaked in the centre and fell off to the edges gave reasonable results.

We thus find that these methods are motivated by the reconstruction method rather than any sampling theory. Fortunately, they fit neatly into the sampling theory concept of prefiltering (that is: area sampling). A final important class of samplers are those which take into account the very limited range of intensity levels of a particular image format or display device. Examples of such samplers are those which perform half-toning (for example: the PostScript half-toning algorithm, illustrated in figure 1.2) and those which use dithering to reduce quantisation error effects. These methods are catering for devices with a small number of intensity levels and so do not produce images for which the assumption made in section 2.2 will hold. Reconstructing an intensity surface from such an image can produce bizarre results unless intelligence is built into the reconstruction algorithm, but they are useful where the target of the resampling is a device with a limited range of intensity levels. The PostScript image command [Adobe, 1985a, p.170, pp.72-83] essentially implements an image resampling process which uses a nearest-neighbour reconstruction technique and a half-toning sampling technique to decide which pixels are white and which are black in the image in the printer's memory. This resampled image is then reconstructed by the printer when it produces the picture on paper.

2.9 Summary

Sampling is the process of converting a continuous intensity surface into a discrete image. Sampling is used in all three processes (capturing, rendering, and resampling) which generate a discrete image, and is fundamentally the same in all three cases. Quantisation of intensity does not pose a problem, provided enough quantisation levels are available.

There are two basic types of sampling: area, where a sample's value is determined from the intensity surface's values over some non-zero area; and point, where a sample's value is determined from the intensity surface's values at only a finite set of points.

The main artifact caused by sampling is aliasing, not to be confused with the rastering artifact caused by reconstruction.

Chapter 3

Reconstruction

Reconstruction is the process of producing a continuous intensity surface from a discrete image. The produced intensity surface should follow the implied shape of the discrete data.

In this chapter we first present several ways of classifying reconstructors, introducing several concepts which are used in later work. From there we look at skeleton, super-skeleton and Dirac delta function reconstruction methods before turning our attention to more conventional reconstructors. The first of these is the 'perfect' interpolant: the sinc function. A brief glimpse at the theory of perfect interpolation is given here as a precursor to the discussion on piecewise local polynomials which takes up the remainder of this chapter. We return to perfect interpolation in chapter 4.

The piecewise local polynomial reconstructors are widely used, simple, and easy to implement. The sections in this chapter cover the first four orders of piecewise local polynomial (up to cubic) and briefly consider the extension to higher orders. There is also a substantial discussion of the criteria involved in designing a particular piecewise local polynomial, which has application to all reconstructors.

Beyond this chapter lie three more on reconstruction. The first considers edge effects, infinite extent reconstructors, and local approximations to these; the second examines the fast Fourier transform reconstructors; and the third develops some issues in *a priori* knowledge reconstruction.

We begin by presenting some classifications for reconstructors and introduce much of the terminology which is used throughout these four chapters.

3.1 Classification

There are several ways of classifying reconstructors. The following are some of the main distinctions which can be drawn between reconstruction methods.

3.1.1 *A priori* knowledge

The reconstruction process is influenced by the sampling method which generated the discrete image. How we assume the samples were created affects how we create our reconstruction method. How the samples were actually created, in collusion with our reconstruction method, affects the result. If these two sampling methods are not the same then the reconstructed intensity surface may not be what we intended.

In many cases the sampling method is unknown, or we may choose to ignore what we do know about it. In such a situation, where all that is known about the image are the image sample

values (and their relative positions), we must use a reconstructor which only takes those values into consideration. We call such a reconstructor a 'no *a priori* knowledge' (NAPK) reconstructor. That is, no knowledge is utilised except for the image sample values. Such a reconstructor can thus be applied to any image.

If we have some *a priori* knowledge about the image (that is knowledge that is separate from the image data itself) then we can potentially produce a better reconstructed intensity surface than a NAPK reconstructor could. Such *a priori* knowledge could be about the sampling method used, the content of the image, or both. A reconstructor which uses such knowledge we call an '*a priori* knowledge' (APK) reconstructor. APK reconstruction is discussed in chapter 6.

3.1.2 Reconstruction filters

Reconstruction methods can be classified as to whether or not they can be represented by a filter. Many reconstruction methods *can* be expressed as filters. A filter is some continuous function which is convolved with the sample values to produce the continuous intensity surface.

In dealing with images it is important to remember that there are two ways of thinking about them. The first is to think of an image as it is stored in the computer: as a finite array of intensity values, $f_{i,j}$, where (i, j) is the co-ordinate of the pixel with value $f_{i,j}$. The second way is to consider the image to be a continuous function consisting of an infinite sum of equispaced, weighted Dirac delta functions. For a square pixel array, for example:

$$\iota(x, y) = \sum_{i=-\infty}^{\infty} \sum_{j=-\infty}^{\infty} f_{i,j}\, \delta(x - i, y - j)$$

$\iota(x, y)$ is a continuous function which is non-zero only at integer locations[1]. It is this latter, continuous, function with which the reconstruction filter, $h(x, y)$, is convolved to produce the continuous intensity surface:

$$f(x, y) = h(x, y) * \iota(x, y)$$

$h(x, y)$ is referred to as the filter's impulse response, the filter's kernel, or sometimes simply as the filter itself.

A problem with this is that the mathematical image function, $\iota(x, y)$, is infinite in extent whilst the discrete function, $f_{i,j}$, is finite in extent. This means that all of the weights in $\iota(x, y)$ which lie beyond the edges of the discrete image have an indeterminate value. The solutions to this *edge effect* problem, how to determine these unknown values, are discussed in chapter 4.

Throughout the following chapters two different functions will be used in analysing reconstruction filters: the filter itself, $h(x, y)$, and the intensity surface produced by that filter, $f(x, y)$. In the case of a reconstruction method that cannot be represented by a filter, only the intensity surface, $f(x, y)$, can be used.

3.1.3 Skeleton *vs* continuous reconstruction

The skeleton reconstructors do not generate a continuous intensity surface, instead they generate a surface which only has a defined value at certain points and is elsewhere undefined. Such a surface cannot be represented by a filter. However, a similar idea can be, that is: a surface which is non-zero and finite at certain points and is elsewhere zero. A related idea to this is the Dirac

[1] It is a simplification to assume that the samples occur at integer locations in the real plane. But here we can make this simplification without loss of generality, because any rectangular sampling grid can be converted to one where the samples occur at integer locations. For example, if the samples are at $(x, y) = (x_0 + i\Delta x, y_0 + j\Delta y)$, then they can be put at integer locations by changing the coordinate system: $x' = \frac{x - x_0}{\Delta x}$ and $y' = \frac{y - y_0}{\Delta y}$

delta function surface, described above, which consists of an infinite sum of weighted, shifted Dirac delta functions.

Both the skeleton and Dirac delta function reconstructors are discussed under the general heading of 'skeleton reconstruction' (section 3.2) although a Dirac delta function surface can be considered continuous for area sampling processes. All other reconstructors produce a continuous intensity surface. As this is the norm, no special section is required to discuss continuous reconstruction.

3.1.4 Interpolating or approximating

There are two broad categories of reconstructor: the interpolants and the approximants. The interpolants (interpolating reconstructors) generate intensity surfaces which pass through all of the sample data points; the approximants (approximating reconstructors) generate surfaces which do not have to do this, but an approximant may generate an intensity surface which may pass through any number of the points.

If we have no *a priori* knowledge, then we are best advised to use an interpolant. This is because we know nothing about how the image was captured, so we must make an assumption. The simplest, and generally accepted, assumption is that the samples are single point samples of an original intensity surface and thus the original surface interpolates the sample points. Lacking any further information we assume that it is this intensity surface that we ideally wish to reconstruct, and thus the reconstructed intensity surface should interpolate the points. The concept of interpolating rather than the more general reconstruction is so strong that many authors assume that a reconstructor is an interpolant (Mitchell and Netravali [1988], for example, discuss approximants but use the word 'interpolation' to describe all reconstructors).

If, however, we have some *a priori* knowledge, or some such knowledge can be extracted from the image then we will probably find that our reconstructor is an approximant, as it is well known that no captured images are produced by single point sampling owing to limited resolution and bandwidth in the sampling process. Few rendered images are produced by single point sampling either, because more sophisticated sampling methods are used to prevent artifacts occurring in the images. Thus the samples do not necessarily lie on the original intensity surface, and so interpolating through them will not produce the original intensity surface.

3.1.5 Finite or infinite; local or non-local

Some reconstructors are formally infinite; they depend on an infinite number of sample points. Put another way, they have reconstruction filters of infinite support (assuming they have filters). Other reconstructors are finite; they depend on only a finite number of sample points to produce the value at any given point on the intensity surface.

A finite reconstructor may be local or non-local. This is a less sharp division. Local reconstructors base the value of the intensity surface at any point on only local data points. Typically this means data points no more than a few pixel widths away from the point being calculated. Non-local reconstructors depend on data farther away (as well as the local data). An infinite-extent reconstructor could be considered the limiting case of non-local reconstructors.

Most practical reconstructors are finite. Some infinite reconstructors *can* be implemented so that the calculation take finite time, but the vast majority cannot. Infinite-extent reconstructors and the finite-extent approximations to them are discussed in chapter 4.

Localness is an important consideration when implementing a reconstructor. In general, the more local a reconstructor, the faster the value of the intensity surface can be calculated at an arbitrary point. Localness is also an important consideration in stream processing: the fewer points needed at any one time, the better. It is discussed in more detail in section 3.5.5.

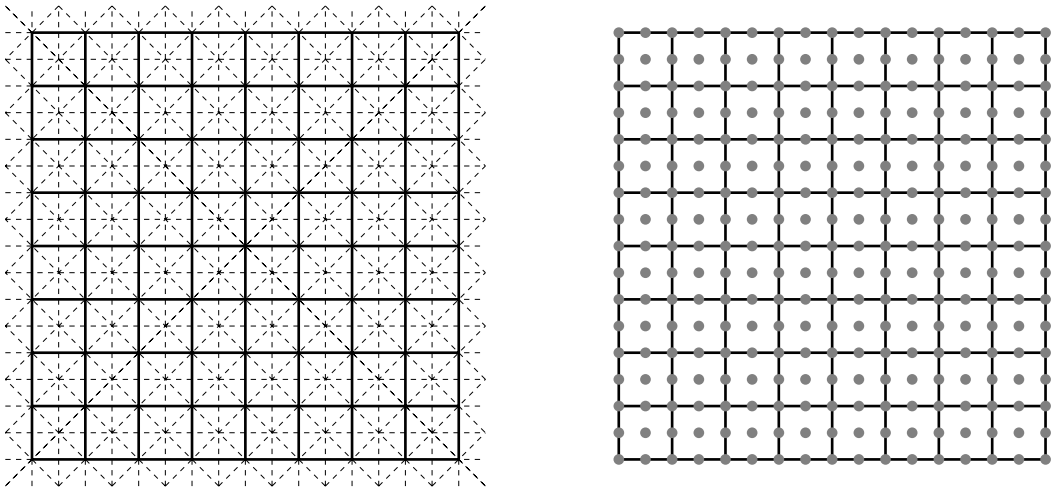

Figure 3.1: Each grid (solid lines) represents part of an infinite array of square pixels. On the left are the reflection lines (dashed lines) for those reflections which exactly map pixel centres into pixel centres. On the right are the rotation centres (dotted circles) for the $180n^\circ$ and $90n^\circ$ rotations which map pixel centres to pixel centres.

3.1.6 Other classifications

There are other ways of classifying reconstructors:

- is it a polynomial or not?
- does it have a strictly positive kernel or not? (see section 3.5.7)
- does it approximate some other function? If so, which? For example, approximations to the sinc function or to a Gaussian function are common.

In this dissertation several families of reconstructors are discussed. They are certainly not mutually exclusive. The family of piecewise local polynomials are examined later in this chapter. There, many of the criteria used in the design of reconstructors are evaluated. These criteria can also be used to classify reconstructors. Whilst the discussion there is focussed on piecewise local polynomials, it is applicable to all reconstructors. Thus, we leave discussion of these other classifications until then (section 3.5).

We now turn to the slightly odd families of skeleton and Dirac delta function reconstructors.

3.2 Skeleton reconstruction

The question arises as to whether a continuous intensity surface is actually required. In some circumstances it is only necessary to have the value of the intensity surface at the sample points themselves. Elsewhere the intensity surface is undefined (some may prefer to say that it is zero, which is not the same thing). Such a bare bones reconstruction is called *skeleton* reconstruction.

Skeleton reconstruction is only useful with a limited set of transformations and samplers. For example, with single point sampling, the set of transformations is that where the transformations exactly map pixel centres to pixel centres. This set includes (for a square pixel grid) rotation by $90n^\circ$ ($n \in \mathcal{Z}$); mirroring about certain horizontal, vertical and 45° diagonal lines; and translations by an integral number of pixels in the horizontal and vertical directions (see figure 3.1 and also Kornfeld [1985, 1987]). For one bit per pixel images, Fiume [1989, section 4.6] proves that these

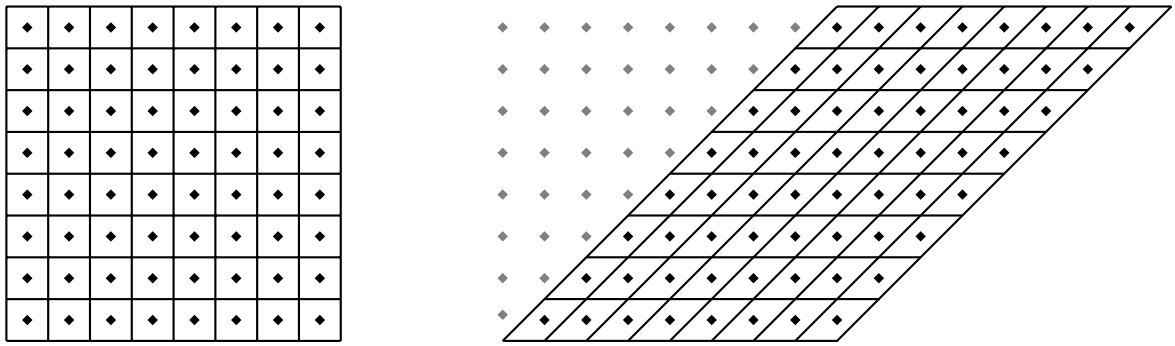

Figure 3.2: Shear distortion — the image on the left is sheared to produce that on the right. The pixel centres in the right hand image are still in the same square grid orientation. However the pixels themselves are distorted. This leads to distortions in the output image if only pixel centres are considered in the resampling from one image to the other.

transformations are the only ones which can be performed on a square pixel grid without degrading the image. For many bit per pixel images the questions of whether there are other transformations that lose no information is an open one.

As well as these, there are lossy transformations which map pixel centres to pixel centres. These include scaling by a factor of $\frac{1}{N}, N \in \mathcal{Z}, N \neq 0$, about certain points (generally pixel centres). This maps some pixel centres to pixel centres and is a digital sub-sampling operation. Guibas and Stolfi [1982] propose this form of image shrinking in their bitmap calculus. It gives the least pleasing result of all shrinking methods and is only applicable to shrinking by integral factors $(\frac{1}{N}, N \in \mathcal{Z}, N \neq 0)$[2].

A further set of transformations which map pixel centres to pixel centres is the set of shears, by an integral number of pixels. However, these transformations produce distortions if done in this simplistic way. These distortions occur because, while pixel centres do map to pixel centres, the pixel areas do not map onto pixel areas. Figure 3.2 shows the distortion for square pixels sheared by one pixel distance [3].

Skeleton reconstruction does not produce a continuous intensity surface because the value of the 'intensity surface' is undefined except at the sample points. But a surface can be designed which produces similar results to those described. The method described above has an intensity surface which takes the sample values at the sample points and is undefined at all other points. 'Undefined' is a difficult concept to express mathematically, so to generate a filter kernel which describes this skeleton reconstruction we replace 'undefined' with 'zero' and get the kernel:

$$h(x,y) = \begin{cases} 1, & x = 0 \text{ and } y = 0 \\ 0, & \text{otherwise} \end{cases}$$

The properties of an intensity surface reconstructed by this kernel are:

- it has non-zero values only at the sample points;
- it will produce a sensible result only if it is point sampled at only these points;

[2]For shrinking by a factor of $\frac{1}{R}, R \in \mathcal{R}, |R| \geq 1$, you need at least some form of reconstruction or a more sophisticated sampling method. Heckbert [1989] says that for $R \gg 1$ it is only necessary to reconstruct using a Dirac delta function reconstructor, but that a good area sampler *is* required.

[3]Interestingly enough, many other reconstruction methods will produce as bad a result in this case unless a more sophisticated sampling method is employed. This is because the value of the intensity surface at the pixel centres under interpolation methods is exactly the sample value at that pixel centre before interpolation and so point sampling at these points produces exactly the same value as if we had used skeleton reconstruction.

- a point sample anywhere else will produce the value zero;
- an area sampling method will not work at all.

This last point is due to the fact that any area sampler's prefilter applied to this surface will produce the filtered surface $g(x, y) = 0,\ \forall x, y \in \mathcal{R}$. Thus all the sample values from the area sampler will be zero.

This reconstructor is different to the Dirac delta function reconstructor discussed by Heckbert [1989, p.51], and it produces different results. The Dirac delta function produces a very different kind of intensity surface. Its filter is defined as:

$$h(x, y) = \delta(x, y)$$

and it has the following properties:

- it is the identity function, that is: it has the following effect on the continuous image function:

$$\begin{aligned} f(x, y) &= \delta(x, y) * \iota(x, y) \\ &= \iota(x, y) \end{aligned}$$

- it is zero everywhere except at pixel centres where it tends to infinity;
- for some small ϵ, less than the distance between pixels:

$$\int_{i-\epsilon}^{i+\epsilon} \int_{j-\epsilon}^{j+\epsilon} f(x, y)\, dy\, dx = f_{i,j}$$

- it only works with area sampling methods because using a point sampling method could result in the product of two Dirac delta functions, the value of such a product is undefined;
- not all area samplers produce a good result, only those for which a large number of delta functions fall within the area of the sampler for each sample taken.

The notable difference is that the Dirac delta function works with area samplers, but not point samplers, whilst the skeleton reconstructor works with point samplers but not area ones.

There are other reconstructors which produce a similar effect to skeleton reconstruction, the difference being that their set of defined points is not limited to the sample points. They are able to produce a finite number of new points between the existing data points. However they cannot be practically used to find the value of the surface at an *arbitrary* point. Such a reconstructor can be dubbed 'super-skeleton' by analogy to 'sampling' and 'super-sampling'.

The best example of a super-skeleton method is the fast Fourier transform (FFT) scaling method [Fraser, 1987, 1989a, 1989b; Watson, 1986] (section 5.1). This method produces a finite number of equispaced samples between existing samples but cannot be used to produce samples at arbitrary points. Fraser's implementation allows for $x \times 2^n, n \in \mathcal{Z}$ points from x original sample points. Watson's method allows us to produce an arbitrary number of points in place of our original x (these figures are quoted for one-dimensional signals, they need to be squared for two dimensions). To produce a continuous surface would require an infinite number of points and hence infinite time; so whilst theoretically possible it is hardly practicable. In this method, all the points have to be generated before you can use them for further processing, they cannot be generated one at a time.

This FFT method reconstructs a surface, which, as before, has non-zero values only at a set of points and is elsewhere undefined (alternatively, zero). There is no way of stating the method as a reconstruction *filter*. It is however, a perfectly valid reconstruction *method*. Again, on its own, it is only useful for a limited number of applications, most notably for scaling the image.

However, as part of a more powerful reconstruction method it has great utility, as we shall see later (section 5.3).

A super-skeletal intensity surface, like a skeletal surface, has defined values only at certain points, and is undefined elsewhere. The values at these points are finite. An analagous procedure could be followed to produce a 'super-delta function' reconstructor with extra delta functions occurring between the ones at the pixel centres. Which is chosen depends on the use that is being made of the intensity surface. The former is useful for point sampling; the latter for area sampling. Again only a limited set of transformations and samplers can be used with these reconstruction methods.

We now turn our attention to those reconstruction processes which do produce a continuous intensity surface in the more usual sense. We begin by looking at the theory of perfect interpolation.

3.3 Perfect interpolation

For any set of finitely spaced sample points there exist an infinite number of interpolating functions. Which of these functions is the one that we want? Whittaker posed this question in 1915 and produced the possibly unexpected result that through any set of finite-value, finite-spaced points there exists a single interpolating function which is everywhere finite valued and has no spatial frequencies greater than one half the sample frequency[4]. This function Whittaker called the *cardinal function* of the infinite set of functions through these sample points.

This result was also discovered empirically in signal processing work. Shannon [1949] states that both Nyquist (in 1928) and Gabor (in 1946) had pointed out that "approximately $2TW$ numbers are sufficient" to represent a one-dimensional function limited to the bandwidth W and the time interval T. Mitchell and Netravali [1988] note that Mertz and Gray (in 1934) had established the same principle as a rule of thumb for processing images (two-dimensional signals).

However, it was in 1949 that Shannon first formalised what we now call 'the sampling theorem' described in section 2.4.1. His contribution was to prove it as an exact relation, not just an approximate one. Shannon's theorem can be seen as a restatement of Whittaker's result, in different language. Given a set of samples of some function, one can reconstruct this cardinal function by convolving the samples with a sinc function (see section 2.4.1). The theory behind this can be found in both Whittaker [1915] and Shannon [1949] but perhaps more understandably in Wolberg [1990] or Foley *et al* [1990, section 14.10]. The sinc function has also been called the 'cardinal function', [Petersen and Middleton, 1962, p.292], the 'cardinal sine' [Marion, 1991, p.24], and some call it the 'cardinal spline' [Maeland, 1988 p.213]. However the term 'cardinal spline interpolation' is often used in a wider sense to mean *any* interpolation. Schoenberg [1973] uses the term to describe interpolants which fall between the sinc interpolant and linear interpolation in complexity.

Other perfect interpolation reconstructors exist for other classes of signal, but, for a square pixel grid, a two-dimensional sinc function perfectly reconstructs all signals band-limited to $|\nu_x|, |\nu_y| < \frac{1}{2T}$.

To use this 'perfect interpolation' one of the following two methods must be used: either (a) convolve the original image samples with the appropriate sinc function, or (b) do the appropriate processing in the continuous frequency domain. The latter method, being continuous, is impossible in a digital computer; the FFT method discussed in chapter 5 is, however, a digital approximation to it. The former method has drawbacks which will be discussed in more detail in section 4.3. At this point all we need know is that the 'perfect' interpolation method does have drawbacks; notably it is painfully slow, and for non-bandlimited images it reconstructs aliases (manifesting mainly as ripples in the intensity surface).

Because of these drawbacks other interpolating and approximating reconstruction methods have been used over the years. We begin our discussion of these with one very important family of reconstruction methods: the piecewise local polynomials.

[4]Equivalently "no periodic constituents of period less than twice the sampling period" [Whittaker, 1915, p.187].

3.4 Piecewise local polynomials

The piecewise local polynomials are a very useful and commonly used family of reconstructors. Before looking at them in detail we discuss the general form in one dimension and its extension to two or more dimensions. This is followed by a section on each order from the first to the third; the third being used as a case study of the design of such reconstructors. The case study leads us into a discussion of the factors involved in the design of piecewise local polynomial (and, more generally, all) reconstructors. In the final major part of this section we discuss the fourth order, finishing with a brief look at higher orders. At this juncture we need to point out that the order of a polynomial is one more than its highest degree term. Thus a quadratic is a second *degree* polynomial, but a third *order* one.

3.4.1 The general case in one dimension

The piecewise local polynomial curve consists of polynomial pieces, each one sample width wide. Every piece of the curve depends on the m nearest sample points. Thus, if m is even, each piece starts and ends at adjacent sample points; if m is odd, each piece starts and ends halfway between adjacent data points. This is important and is elaborated on in section 3.4.6.

The general form of the piecewise local polynomial is:

$$f(x) = \sum_{i=-a}^{b} c_i(x)\, f_{\alpha+i}$$

a and b depend on m:

$$\begin{aligned} a &= \left\lfloor \frac{m-1}{2} \right\rfloor \\ b &= \left\lfloor \frac{m}{2} \right\rfloor \end{aligned}$$

They can be shown to obey the property $a + b = m - 1$. Thus there are m terms in the sum.

α is an integer dependent on x:

$$\alpha = \begin{cases} \left\lfloor \dfrac{x - x_0}{\Delta x} \right\rfloor, & m \text{ even} \\ \left\langle \dfrac{x - x_0}{\Delta x} \right\rangle, & m \text{ odd} \end{cases}$$

The samples are assumed to be equispaced at a spacing of Δx. Sample zero has value f_0 and is at location x_0 (figure 3.3).

$c_i(x)$ is a polynomial function of order n. Its general form is:

$$\begin{aligned} c_i(x) &= \sum_{j=0}^{n-1} k_{i,j}\, t^j \\ \text{where: } t &= \frac{x - x_\alpha}{\Delta x} \end{aligned}$$

For m even: $0 \le t < 1$. For m odd: $-\frac{1}{2} \le t < \frac{1}{2}$.

x is thus split into two parameters: an integer part, α, and a fractional part, t. The relationship between them is:

$$\begin{aligned} x &= x_0 + (\alpha + t)\Delta x \\ &= x_\alpha + t\,\Delta x \end{aligned}$$

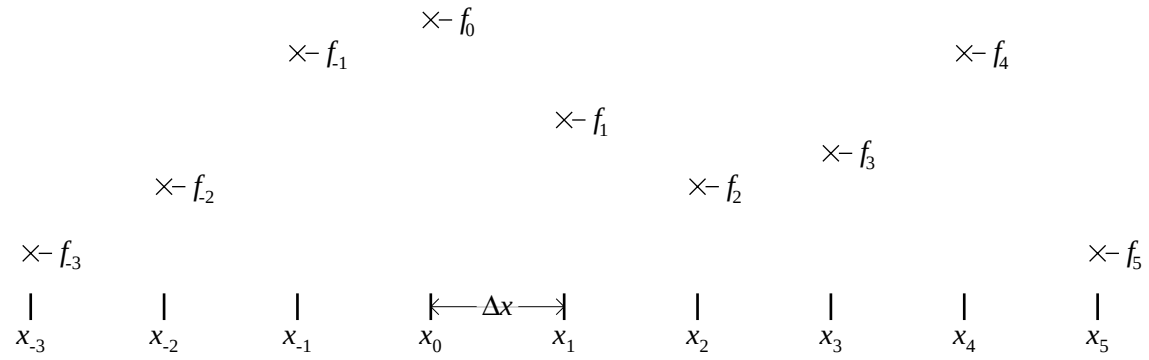

Figure 3.3: The relationship between x_i, f_i and Δx. The x_i are equispaced along the x-axis with a spacing of Δx. The value of the sample at x_i is f_i.

The whole general form can be represented as the single equation:

$$f(x) = \sum_{i=-a}^{b} \left(\sum_{j=0}^{n-1} k_{i,j} t^j \right) f_{\alpha+i} \tag{3.1}$$

where:

$$a = \left\lfloor \frac{m-1}{2} \right\rfloor \qquad \alpha = \begin{cases} \left\lfloor \dfrac{x - x_0}{\Delta x} \right\rfloor, & m \text{ even} \\ \left\langle \dfrac{x - x_0}{\Delta x} \right\rangle, & m \text{ odd} \end{cases}$$

$$b = \left\lfloor \frac{m}{2} \right\rfloor \qquad t = \frac{x - x_\alpha}{\Delta x}$$

Note that the formula has $m \times n$ degrees of freedom ($k_{i,j}$ values). The larger $m \times n$, the more computation is required. The smaller $m \times n$, the less the reconstructor can achieve. A balance must be found, choosing m and n to give the best result. In normal use $m = n$; the reasons for this are given in section 3.5.5. Figure 3.4 gives some examples of piecewise local polynomial reconstructors.

3.4.2 Extending to two dimensions

The standard way of extending this to more than one dimension is to use the same one-dimensional polynomial along each axis of the co-ordinate system (assuming the usual rectangular co-ordinate system). In two dimensions this thus gives:

$$\begin{aligned} f(x,y) &= \sum_{i=-a}^{b} \left(\sum_{j=0}^{n-1} k_{i,j} t^j \right) \sum_{p=-a}^{b} \left(\sum_{q=0}^{n-1} k_{p,q} s^q \right) f_{\alpha+i,\beta+p} \\ &= \sum_{i=-a}^{b} \sum_{p=-a}^{b} \sum_{j=0}^{n-1} \sum_{q=0}^{n-1} K_{i,j,p,q} t^j s^q f_{\alpha+i,\beta+p} \end{aligned} \tag{3.2}$$

where:

$$K_{i,j,p,q} = k_{i,j} \times k_{p,q}$$

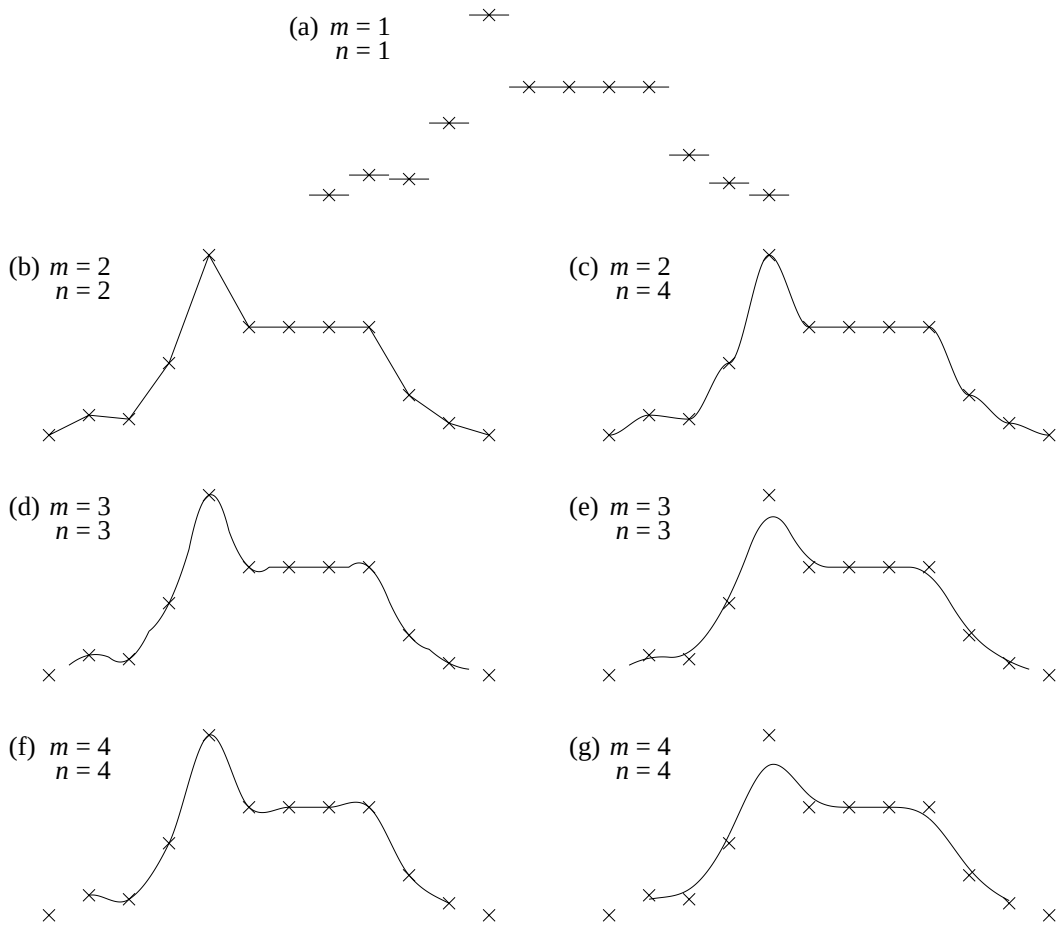

Figure 3.4: Some piecewise local polynomial reconstructed curves, showing the number of points each segment is based on (m) and the order of the piecewise curve (n). (a) Nearest-neighbour; (b) linear; (c) two point cubic; (d) interpolating quadratic; (e) approximating quadratic; (f) Catmull-Rom cubic; and (g) approximating cubic B-spline.

$$a = \left\lfloor \frac{m-1}{2} \right\rfloor \qquad b = \left\lfloor \frac{m}{2} \right\rfloor$$

$$\alpha = \begin{cases} \left\lfloor \frac{x-x_0}{\Delta x} \right\rfloor, & m \text{ even} \\ \left\langle \frac{x-x_0}{\Delta x} \right\rangle, & m \text{ odd} \end{cases} \qquad \beta = \begin{cases} \left\lfloor \frac{y-y_0}{\Delta y} \right\rfloor, & m \text{ even} \\ \left\langle \frac{y-y_0}{\Delta y} \right\rangle, & m \text{ odd} \end{cases}$$

$$t = \frac{x-x_\alpha}{\Delta x} \qquad s = \frac{y-y_\beta}{\Delta y}$$

Whilst this is only the product of two functions of the form of equation 3.1 it appears considerably more complex. Because the two-dimensional form is unwieldy we use the one-dimensional form in our work. We keep in mind that, in real image resampling, the equivalent two-dimensional form is used. The extension is similar for three or more dimensions.

It is possible to extend from one to many dimensions in a different way. This is very seldom done but one such extension method is discussed in section 3.4.5.

It is also possible to use different m and n values in each dimension, although it is difficult to conceive of a situation that would warrant it. Perhaps a spatio-temporal resampling would require a different reconstructor in the temporal dimension to that used in the spatial dimensions.

3.4.3 Why are they so useful?

The piecewise local polynomials are easy to understand, simple to implement, and quick to evaluate. The localness is especially useful in stream processing applications. The family contains many reconstructors which have been studied over the years: some in their own right and some as approximations to more complex functions.

Having examined the general form of the family we now move on to discuss the first, second, and third order sub-families.

3.4.4 Nearest-neighbour

The simplest reconstruction method of all is the nearest-neighbour method which assigns to each point the intensity of the sample at the sample point nearest to that point. It is the first order piecewise linear polynomial. The parameters, m and n, are set to $m = n = 1$. The single degree of freedom is given the value 1 so that the function interpolates the sample points. The function is:

$$f(x) = f_\alpha$$

where:

$$\alpha = \left\langle \frac{x - x_0}{\Delta x} \right\rangle$$

and its kernel is the box function:

$$h(s) = \begin{cases} 1, & |s| < \frac{1}{2} \\ 0, & \text{otherwise} \end{cases} \tag{3.3}$$

Thus the value of $f(x)$ at any point is based on just a single sample value. An example of nearest-neighbour reconstruction is shown in figure 3.4(a).

This reconstructor produces an intensity surface which is, in general, discontinuous. It is the worst of the common methods, but it has been widely used because of the speed with which it can be implemented and its sheer simplicity. Improvements in computer power have meant that it has been replaced in many applications although it is still the dominant method in one area: frame buffer hardware zoom functions [Wolberg, 1990, p.127]. It is only recently that hardware has become available for real-time hardware magnification using more sophisticated algorithms [TRW, 1988, chip TMC2301].

This reconstructor is the first order member of the family of B-splines. Each member of this family is generated by convolving a number of box functions to produce the filter kernel [Andrews and Patterson, 1976]. The first order member's filter (equation 3.3) is a single box function. Convolving two of these together produces the second order member: linear interpolation.

3.4.5 Linear interpolation

This is, perhaps, the most used reconstruction method. In one dimension it involves the two closest sample points to each point. The general form of a second-order piecewise linear polynomial with $m = n = 2$ is (from equation 3.1):

$$\begin{aligned} f(x) = & \quad (at+b)f_\alpha \\ & + \quad (ct+d)f_{\alpha+1} \end{aligned}$$

where:

$$\begin{aligned} \alpha &= \left\lfloor \frac{x - x_0}{\Delta x} \right\rfloor \\ t &= \frac{x - x_\alpha}{\Delta x} \end{aligned}$$

If we wish this to be an interpolating method then the four degrees of freedom are completely specified to give:

$$f(x) = (1-t)f_\alpha + tf_{\alpha+1}$$

It is basically a 'join the dots with straight lines' method and it is hard to think of any other useful values for the degrees of freedom. The filter kernel for this function is the convolution of two box functions (equation 3.3), producing a 'tent' function:

$$h(s) = \begin{cases} 1+s, & -1 < s < 0 \\ 1-s, & 0 \le s < 1 \\ 0, & \text{otherwise} \end{cases}$$

An example of this type of reconstruction is shown in figure 3.4(b).

There are two ways of extending this to two dimensions. The first is as described in section 3.4.2 and produces possibly non-planar, bilinear patches bounded by four sample points. The other divides each square bound by four adjacent sample points into two triangles and produces a planar patch in each triangle (figure 3.5) [Pratt, 1978, pp.114–116]. The two methods generally do not produce the same result and the latter method can produce different results depending on how the square is split into triangles. We will consider only the former as it is better, is more amenable to mathematical analysis, and is by far the most used.

Linear interpolation produces an intensity surface which is guaranteed continuous; however, it is discontinuous in its first derivative. It is one of the most widely used reconstruction algorithm and is recommended by Andrews and Patterson [1976] in their study of interpolating B-splines, of which it is the second order member. It produces reasonable, but blurry, results at a moderate cost [Wolberg 1990, p.128]. However, often a higher fidelity is required and so we go on to higher orders of polynomials.

3.4.6 Quadratic functions

The quadratic functions have $m = n = 3$; each section is thus a quadratic curve based on three points. This family of reconstructors does not appear to have been studied. Hence we make the quadratics a case study in the design of reconstructors. We begin with the general case, adding more and more criteria to the function until we have used all of the degrees of freedom to produce the best possible quadratic reconstructor.

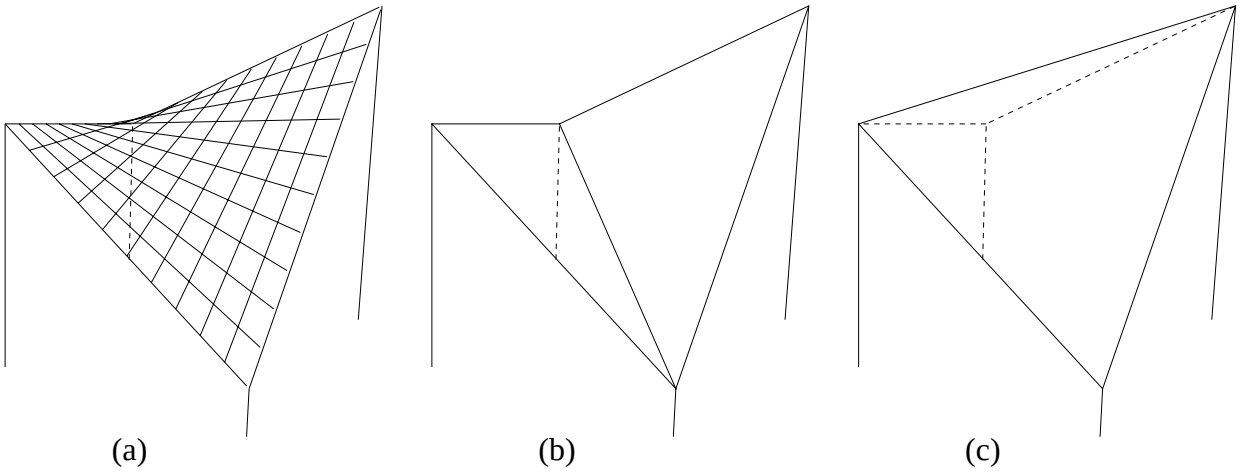

Figure 3.5: Two ways of extending linear interpolation to two dimensions. (a) shows the bilinear approach, which we recommend. (b) and (c) show the subdivision into two planar triangles approach. Notice that this can lead to different results depending on how the square is split into triangles (after Pratt [1978] fig. 4.3–6).

Before doing so, however, we must clear up a misunderstanding in the literature. Wolberg [1990] says that third order polynomials are inappropriate because it has been shown that their filters are space-variant with phase-distortions and, further, that these problems are shared by all polynomial reconstructors of odd order. This result is attributed to the fact that the number of sampling points on each side of the reconstructed point always differs by one. Wolberg thus does not consider any polynomials of odd order.

He bases his conclusion on the work of Schafer and Rabiner [1973] who show this result given certain assumptions (perhaps their work explains why no-one has considered quadratic reconstruction). However, as will be shown, if we replace one of Schafer and Rabiner's initial assumptions with another we can produce quadratic polynomials whose filters *are* space-invariant and which produce no phase-distortion.

It should also be noted that nearest-neighbour (first order) reconstruction is an odd order method and that Wolberg (and many others) do consider this without considering the fact that the number of sampling points on each side of the reconstructed point always differs by one (zero on one side and one on the other). This lack of consistency seems to be because nearest-neighbour is so simple that it has linear phase anyway, and so produces no phase distortions.

Parker *et al* [1983], who also consider the nearest-neighbour interpolant, say that using three points for reconstruction (that is: quadratic reconstruction) would result in two points on one side of the reconstructed point and only one point on the other side. They believe that this is a bad thing and therefore conclude that the next logical reconstruction function (after linear reconstruction) would use the two nearest points in each direction, that is: cubic reconstruction.

It is true that quadratic reconstruction requires that there be two points on one side of the reconstructed point and only one on the other but our assertion is that if these three points are the three points *closest* to the reconstructed point then a space-invariant, non-phase-distorted, perhaps even useful, reconstruction method can be created.

It is this assumption that the three points used for quadratic reconstruction are the three *closest* to the reconstructed point that distinguishes our work from that of Schafer and Rabiner [1973]. They assume that each piecewise segment of the curve must start and end at sample points. This leads to an unbalanced situation (figure 3.6). In half of each piecewise segment there is a fourth sample point that is closer to the reconstructed point than one of the sample points that is

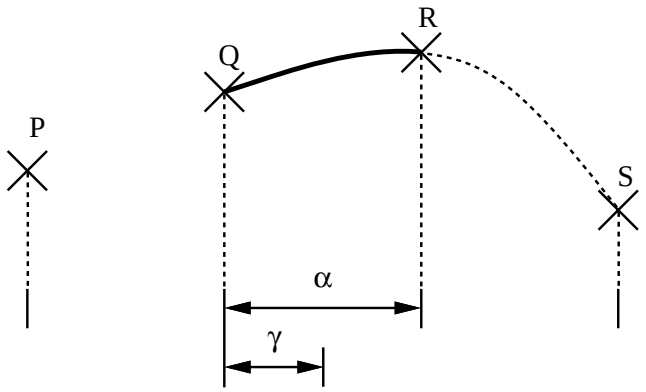

Figure 3.6: An unbalanced situation with a quadratic piece starting and ending at sample locations. The piece depends on three points: Q, R, and S. It is defined over the range α, to start and end at points Q and R. Thus for half the range, that is for range γ, point P is closer to the points on the reconstructed curve than point S, although it is point S which is used to calculate values.

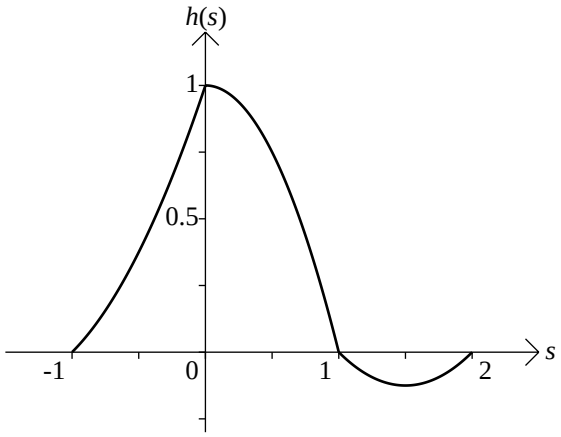

Figure 3.7: The kernel of one of Schafer and Rabiner's quadratic interpolants. This kernel does not have linear phase, as can be readily seen from the fact that the kernel has no vertical line of symmetry.

used to calculate the reconstructed value. Schafer and Rabiner prove that a quadratic Lagrange interpolating function based on this assumption does not have linear phase (that is: it produces phase distortion in the reconstructed intensity surface) and, hence, is useless as a reconstructor. It can be shown that *any* quadratic reconstructor based on this assumption will not have linear phase (see section 3.5.1 for a discussion of linear phase).

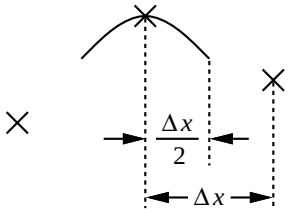

Figure 3.8: Each piece of a quadratic local polynomial starts and ends halfway between sample points.

The filter kernel for the continuous version of one of Schafer and Rabiner's quadratic Lagrange interpolants is shown in figure 3.7. It is defined as:

$$h(s) = \begin{cases} \frac{1}{2}s^2 + \frac{3}{2}s + 1, & -1 < s \leq 0 \\ -s^2 + 1, & 0 < s \leq 1 \\ \frac{1}{2}s^2 - \frac{3}{2}s + 1, & 1 < s \leq 2 \\ 0, & \text{otherwise} \end{cases} \tag{3.4}$$

The other possible Lagrange interpolant's kernel is this mirrored in the line $s = 0$.

It is obvious from this that the interpolant does not have linear phase. A reconstructor with linear phase obeys the rule that $h(s - s') = h(-(s - s'))$ for some constant s'. That is to say the function is symmetric about the line $s = s'$. For zero phase $s' = 0$ and $h(s) = h(-s)$.

The effect of linear phase is to translate the zero phase intensity surface in the spatial domain. Thus we can, without loss of generality, concentrate on the zero phase situation. The idea of linear, rather than zero phase comes from work in the time domain where a reconstructed point can only be output *after* all of the sample points which affect its value have been input. In a real-time system there must thus be some delay between points going into and points coming out of the system when data occurring after the time of the required output point affects that output point's value. Linear phase is necessary in such cases. In our case we have all of the data points available at once and so need only concern ourselves with the zero phase case. Should we need to shift the spatial domain filter later then we can be assured that it will have linear phase if we simply let $h'(s) = h(s - s')$ for some constant s'.

We will start by looking at the general quadratic reconstructor in the spatial domain. Its intensity surface will be made up of a piecewise quadratic curve. Every point on the curve will depend on the three sample points closest to that point. Thus each quadratic piece will start and end halfway between samples (figure 3.8). The equation is

$$\begin{aligned} f(x) = \quad & (at^2 + bt + c)\, f_{\alpha-1} \\ + \quad & (dt^2 + et + f)\, f_{\alpha} \\ + \quad & (gt^2 + ht + i)\, f_{\alpha+1} \end{aligned} \tag{3.5}$$

$$\text{where } \alpha = \left\langle \frac{x - x_0}{\Delta x} \right\rangle \text{ and } t = \frac{x - x_\alpha}{\Delta x}$$

We want this function to have zero phase. This applies the restriction that the function's filter kernel, $h(s)$, is real and even. For $f(x)$ above, the kernel is:

$$h(s) = \begin{cases} gs^2 + (h + 2g)s + (i + h + g), & -\frac{3}{2} \leq s \leq -\frac{1}{2} \\ ds^2 + es + f, & -\frac{1}{2} \leq s \leq \frac{1}{2} \\ as^2 + (b - 2a)s + (c - b + a), & \frac{1}{2} \leq s \leq \frac{3}{2} \\ 0, & \text{otherwise} \end{cases}$$

For this to be real and even, we require $h(s) = h(-s)$. This gives us the values of four parameters, say e, g, h, and i, in terms of the other five:

$$e = 0,\ g = a,\ h = -b,\ i = c$$

Thus reducing equation 3.5 to:

$$\begin{array}{rcl} f(x) = & (at^2 + bt + c)\, f_{\alpha-1} \\ + & (dt^2 + f)\, f_{\alpha} \\ + & (at^2 - bt + c)\, f_{\alpha+1} \end{array} \tag{3.6}$$

We now have a system with five degrees of freedom, compared to the original nine. What we use these degrees of freedom for depends on what features we would like our function to have.

Looking back we can see that nearest-neighbour interpolation does not produce a continuous curve, whilst linear interpolation does. So the first 'desirable feature' (after zero phase) is to constrain the curve to be continuous (this is called C0-continuity: continuity of the function itself). We do this by making sure that all the pieces join up at the 'knots'. If $f(x) = f(\alpha, t)$ (that is: $f(x) = f(x_\alpha + t\Delta x)$), then we want $f(\alpha, \frac{1}{2}) = f(\alpha + 1, -\frac{1}{2})$:

$$\begin{array}{rccccccc} & (\frac{1}{4}a + \frac{1}{2}b + c)f_{\alpha-1} & + & (\frac{1}{4}d + f)f_{\alpha} & + & (\frac{1}{4}a - \frac{1}{2}b + c)f_{\alpha+1} & & \\ = & & & (\frac{1}{4}a - \frac{1}{2}b + c)f_{\alpha} & + & (\frac{1}{4}d + f)f_{\alpha+1} & + & (\frac{1}{4}a + \frac{1}{2}b + c)f_{\alpha+2} \end{array}$$

Which gives us two parameters in terms of the other three (say, $c = -\frac{1}{2}b - \frac{1}{4}a$ and $d = -4(b + f)$). This reduces equation 3.6 to:

$$\begin{array}{rcl} f(x) = & (at^2 + bt + (-\frac{1}{2}b - \frac{1}{4}a))\, f_{\alpha-1} \\ + & (-4(b + f)t^2 + f)\, f_{\alpha} \\ + & (at^2 - bt + (-\frac{1}{2}b - \frac{1}{4}a))\, f_{\alpha+1} \end{array} \tag{3.7}$$

Leaving us with the three degrees of freedom: a, b and f.

We can use these in an attempt to make the piecewise quadratic interpolate the points. This requires that $f(x_\alpha) = f_\alpha$:

$$\begin{array}{rcl} f_\alpha = f(x_\alpha) = & (-\frac{1}{2}b - \frac{1}{4}a))\, f_{\alpha-1} \\ + & (f)\, f_{\alpha} \\ + & (-\frac{1}{2}b - \frac{1}{4}a))\, f_{\alpha+1} \end{array}$$

Giving us a and f, say, in terms of the one remaining parameter: $a = -2b$ and $f = 1$.

We are thus left with one degree of freedom: b. Equation 3.7 can now be rewritten as:

$$\begin{array}{rcl} f(x) = & (-2bt^2 + bt)\, f_{\alpha-1} \\ + & (-4(b + 1)t^2 + 1)\, f_{\alpha} \\ + & (-2bt^2 - bt)\, f_{\alpha+1} \end{array} \tag{3.8}$$

Thus far our function is doing no more than linear interpolation; it is: zero phase, C0-continuous and interpolating.

Let us add to this list: continuous in the first derivative (that is C1-continuous). This requires:

$$f'\left(\alpha, \tfrac{1}{2}\right) = f'\left(\alpha + 1, -\tfrac{1}{2}\right) \tag{3.9}$$

Substituting this into equation 3.8 we get:

$$\begin{array}{rccccccc} & (-b)f_{\alpha-1} & + & (-4b - 4)f_{\alpha} & + & (-3b)f_{\alpha+1} & & \\ = & & & (3b)f_{\alpha} & + & (4b + 4)f_{\alpha+1} & + & (b)f_{\alpha+2} \end{array}$$

Giving us the two conditions that:

$$b = 0 \text{ and } b = -\tfrac{4}{7}$$

This is an inconsistency and so we cannot have a zero-phase, C1-continuous, interpolating, piecewise quadratic reconstructed surface.

If we now remove the criterion that the curve be interpolating and enforce the criterion that it be C1-continuous we can apply equation 3.9 to equation 3.7 giving, say, b and f in terms of the one remaining parameter: $b = -a$ and $f = \frac{3}{2}a$. Again we can rewrite equation 3.7:

$$\begin{aligned} f(x) = & \quad (at^2 - at + \tfrac{1}{4}a)\, f_{\alpha-1} \\ + & \quad (-2at^2 + \tfrac{3}{2}a)\, f_{\alpha} \\ + & \quad (at^2 + at + \tfrac{1}{4}a)\, f_{\alpha+1} \end{aligned}$$

Factoring a out of this we get:

$$\begin{aligned} f(x) = \; a[& \quad (t^2 - t + \tfrac{1}{4})\, f_{\alpha-1} \\ + & \quad (-2t^2 + \tfrac{3}{2})\, f_{\alpha} \\ + & \quad (t^2 + t + \tfrac{1}{4})\, f_{\alpha+1}] \end{aligned} \tag{3.10}$$

So we now have two families of curves: zero-phase, C0-continuous and interpolating, as given in equation 3.8; and: zero-phase, C1-continuous and approximating as given in equation 3.10. These two families are plotted in figures 3.9 and 3.10, respectively, acting on a sample data set designed to illustrates some of their properties.

Given these families, what criterion can we use to pick the best reconstructor? Chu [1990], in a paper on the use of splines in CAD, uses the criteria that, if several of the points lie in a straight line then the interpolating function should give a straight line. This makes sense in an image, in as much as if several adjacent sample points have the same intensity then the intensity surface between those points should be that constant intensity (except possibly near the end of the run of constant intensity sample points). Look at it this way: we are producing a quadratic segment based on the nearest three sample points. If these three points lie in a straight line then the only sensible shape for that quadratic segment is to lie on that straight line. The *only* information available for the segment is those three points: if they lie in a straight line then the segment must too; there is no more available information for it to do anything else.

Applying this criteria to our two families, we find that, for the C0-continuous interpolant: $b = -\frac{1}{2}$. For the C1-continuous approximant: $a = \frac{1}{2}$. Examining figures 3.9 and 3.10, we see that these two curves are the ones which appear to most nearly match the implied shape of the data. These final two curves are shown in figure 3.11. Their equations are:

C0-continuous, interpolating quadratic:

$$\begin{aligned} f(x) = & \quad (t^2 - \tfrac{1}{2}t)\, f_{\alpha-1} \\ + & \quad (-2t^2 + 1)\, f_{\alpha} \\ + & \quad (t^2 + \tfrac{1}{2}t)\, f_{\alpha+1} \end{aligned} \tag{3.11}$$

C1-continuous, approximating quadratic

$$\begin{aligned} f(x) = & \quad (\tfrac{1}{2}t^2 - \tfrac{1}{2}t + \tfrac{1}{8})\, f_{\alpha-1} \\ + & \quad (-t^2 + \tfrac{3}{4})\, f_{\alpha} \\ + & \quad (\tfrac{1}{2}t^2 + \tfrac{1}{2}t + \tfrac{1}{8})\, f_{\alpha+1} \end{aligned} \tag{3.12}$$

Perhaps the most important thing to notice about both functions is that they are constrained to pass through the midpoints of the segments joining each pair of adjacent data points; that is they must pass through the points :

$$\left(\frac{x_\alpha + x_{\alpha+1}}{2}, \frac{f_\alpha + f_{\alpha+1}}{2} \right)$$

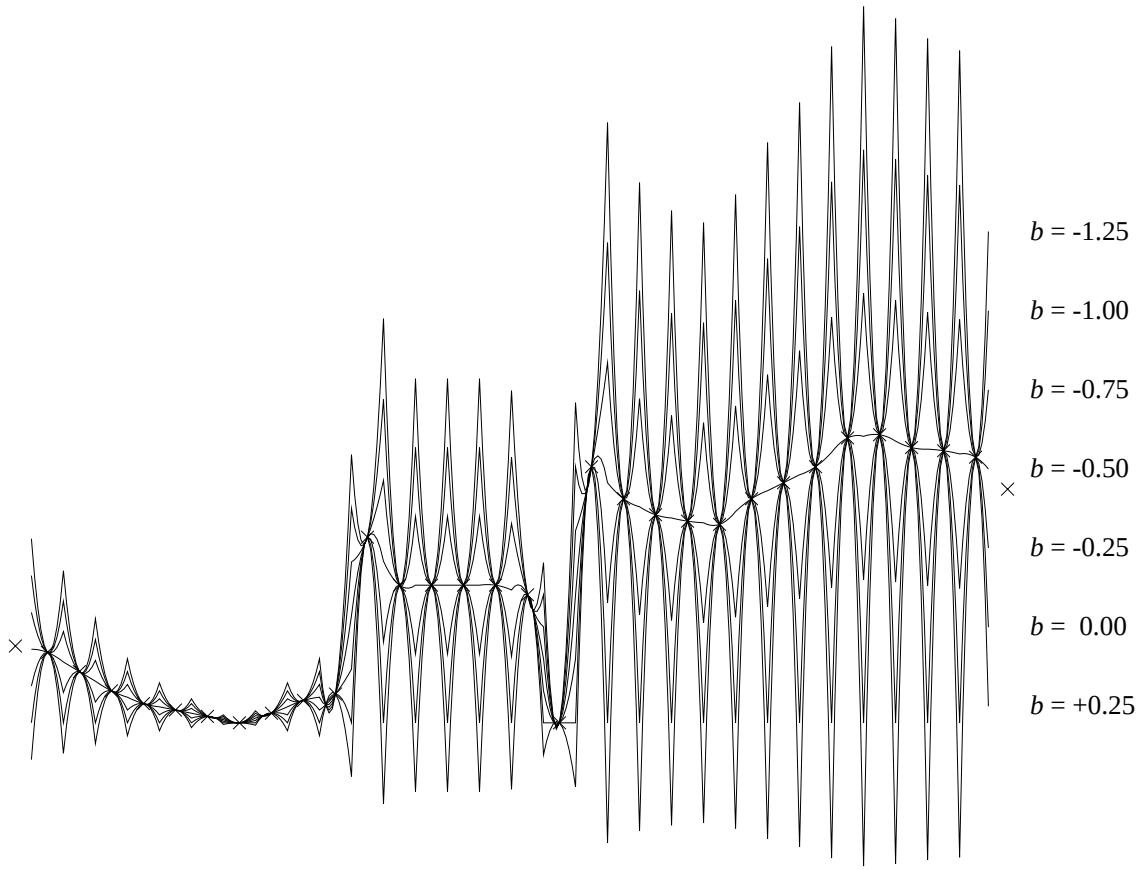

Figure 3.9: The one parameter family of C0-continuous interpolating quadratics (equation 3.8) acting on a one-dimensional image.

Formally this constraint is a direct result of imposing the C0-continuity and straightness criteria on $f(x)$. Intuitively the reasoning is that any two adjacent parabolic segments must meet at a point midway between the two sample points (that is: at $x = \frac{x_\alpha + x_{\alpha+1}}{2}$) and that, at this point, the value of $f(x)$ can only depend on the two sample points common to both segment definitions. Thus, the only sensible value of $f(x)$ lies on the line segment connecting those two points; and therefore $f(x)$ is constrained to pass through the midpoint of this line segment.

This problem will occur, in some form, for all odd order, piecewise polynomials, because, in each case, the segments meet midway between sample points rather than at sample points (which is where they meet in even order, piecewise polynomials).

The C0-continuous interpolant (equation 3.11) does no more than the linear interpolant (section 3.4.5). They have the same features (zero-phase, C0-continuity, interpolating and straightness); they achieve the same thing in different ways. With linear interpolation each segment is the single *straight line segment* between two adjacent data points; while with the quadratic interpolant each segment is the single *parabolic segment* through a data point and the two adjacent midpoints. In both cases the piecewise curve is exactly defined by the only possible pieces that can pass through the controlling points.

The C0-continuous interpolant can be shown to be a linear blend of two linear functions, as illustrated in figure 3.12. This is analagous to Brewer and Anderson's [1977] Overhauser cubic function which they derived as a linear blend of two interpolating parabolas. This fourth order function is better known as the Catmull-Rom cubic [Catmull and Rom, 1974]. Our third order

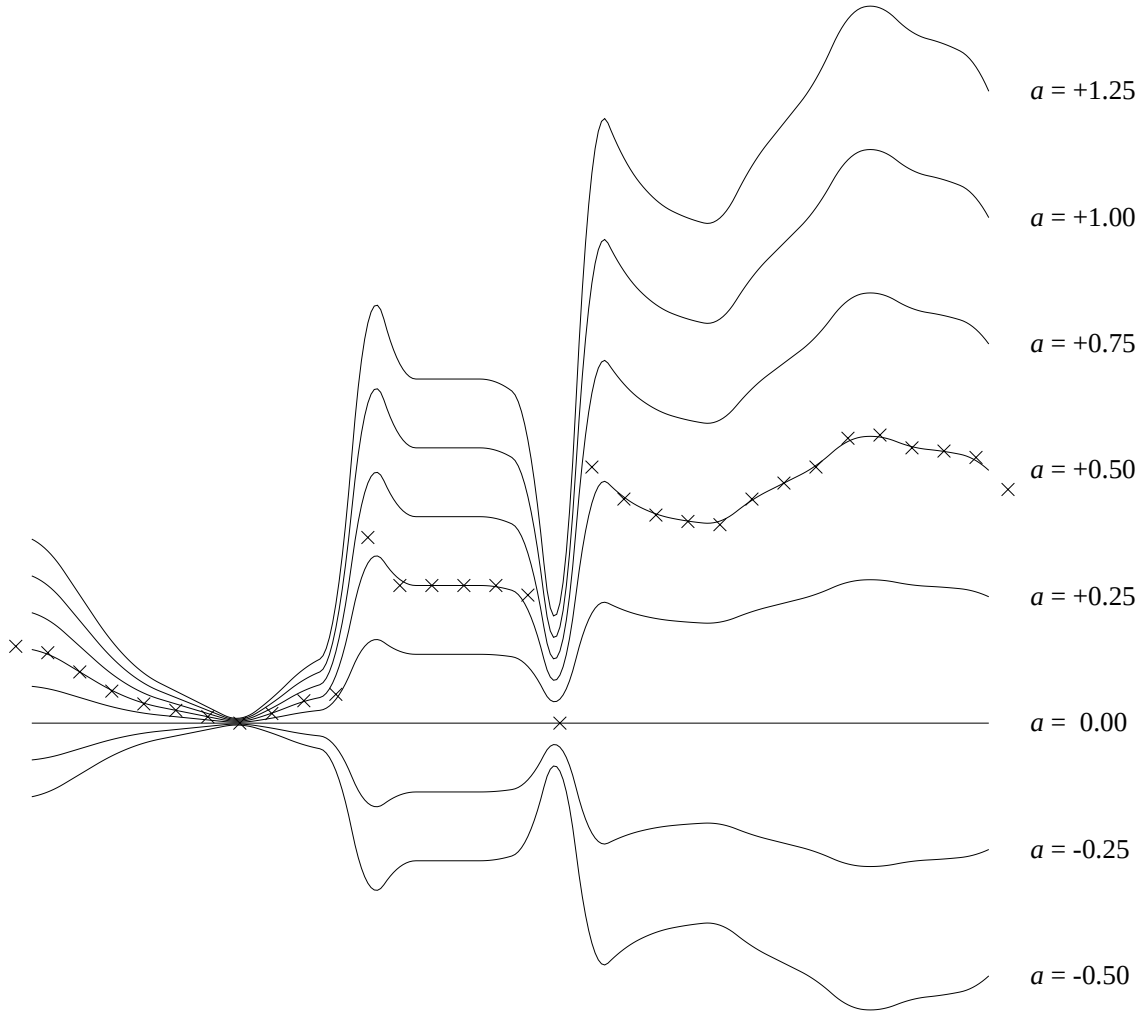

Figure 3.10: The one parameter family of C1-continuous approximating quadratics (equation 3.10) acting on a one-dimensional image.

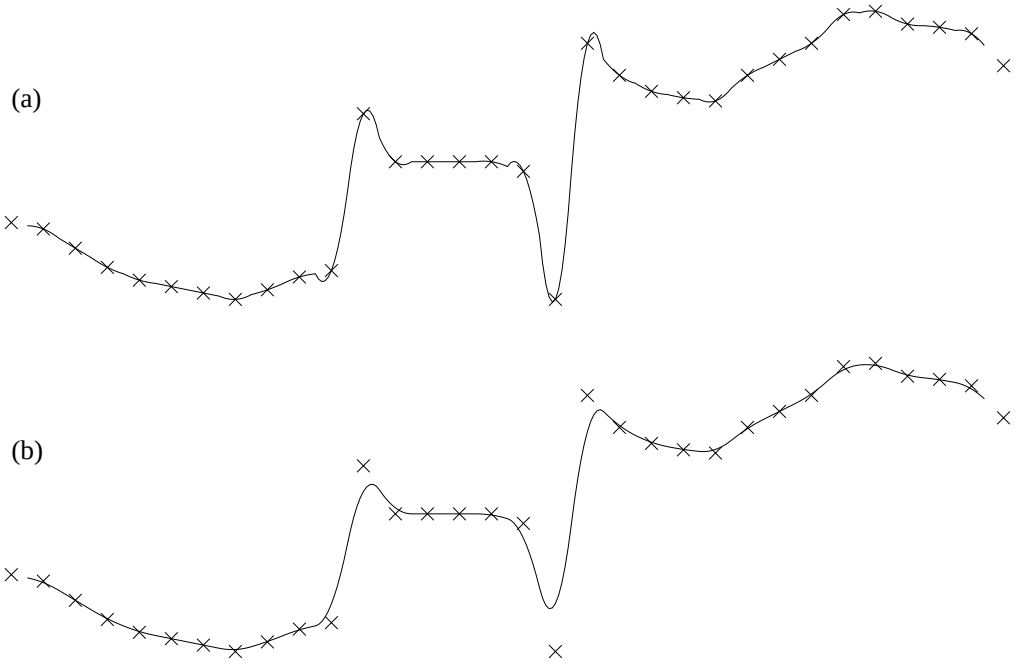

Figure 3.11: The two piecewise local quadratic reconstructors acting on a one-dimensional image: (a) the C0-continuous interpolant (equation 3.11), (b) the C1-continuous approximant (equation 3.12).

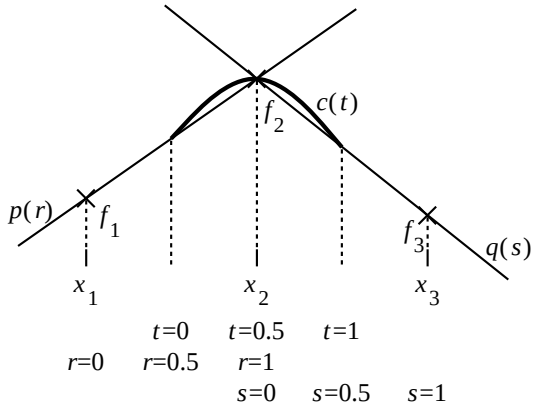

Figure 3.12: The C0-continuous quadratic interpolant as a linear blend of two linear functions. $p(r)$ and $q(s)$ are straight lines passing through the data points as shown. $c(t)$ is a linear blend of these, producing a quadratic function which passes through the central data point, and the midpoints of the two lines. $c(t)$ is calculated from $p(r)$ and $q(s)$ as: $c(t) = (1-t)p(t+\frac{1}{2}) + (t)q(t-\frac{1}{2})$

function is one of the general set of Catmull-Rom curves described in section 3.6.2.

The C1-continuous approximant (equation 3.12) is also constrained to pass through the midpoints but not through the sample points. It seems counter-intuitive to have a function which is constrained to pass through non-sample points and yet does not, in general, pass through the sample points themselves. However, this function is of good lineage, being the third order B-spline. It can be generated by convolving three box functions (equation 3.3).

Having looked at these two quadratic reconstruction methods, we can see that both have detractions. The C0-continuous interpolant can be said to do little more than linear interpolation (in fact, it can be viewed as adding a small 'correction' to linear interpolation, [Press *et al*, 1988, chapter 3]), whilst the C1-continuous approximant is constrained to interpolate a set of points that are not the sample points (but are derived from them).

3.4.7 Visual evaluation

While the above comments are valid from an inspection of the equations, an important test of the quality of any reconstructor is a visual inspection of the intensity surface that it produces. We said in section 3.4.5 that the linear interpolant produces a blurry intensity surface. Comparing the two quadratic reconstructors to linear interpolation we find that the approximant generates a blurrier surface than linear, and the interpolant generates a less blurry surface.

If we now compare these quadratics to similar cubic reconstructors, we find that the quadratic approximant is almost as blurry as the approximating cubic B-spline. The surprising result is that the intensity surface reconstructed by the quadratic interpolant is practically indistinguishable from that generated by the Catmull-Rom cubic interpolant, which is the best of the cubic interpolants (section 3.6.2).

As the quadratic can be evaluated in approximately 60% of the time of the cubic, this quadratic would appear to offer a faster way of achieving similar visual quality to the Catmull-Rom cubic.

3.4.8 Summary

We have shown that third order, zero-phase reconstructors exist. We have not disproved Schafer and Rabiner's [1973] proof that such a reconstructor does not exist, given certain initial assumptions; rather we have changed one of the initial assumptions and thus been able to consider a different family of functions.

From the family of third order, zero-phase reconstructors we have found two interesting members by progressively applying fruitful criteria to the general third order, zero-phase reconstructor. Both of these bear the straightness and C0-continuity criteria. One is also C1-continuous and can be shown to be the third order B-spline. The other is interpolating and only C0-continuous. It can be shown to be a linear blend of two linear functions, and gives similar visual quality to the Catmull-Rom cubic discussed in section 3.6.

The derivation of these third order reconstructors has brought out the important issue of *what* criteria a reconstruction method should include. The next section considers the various criteria which could be incorporated in a reconstructor.

3.5 What should we look for in a NAPK reconstructor?

There are many factors which could be taken into consideration when designing a 'no *a priori* knowledge' reconstructor. In this section we will discuss these factors, with specific reference to piecewise local polynomials.

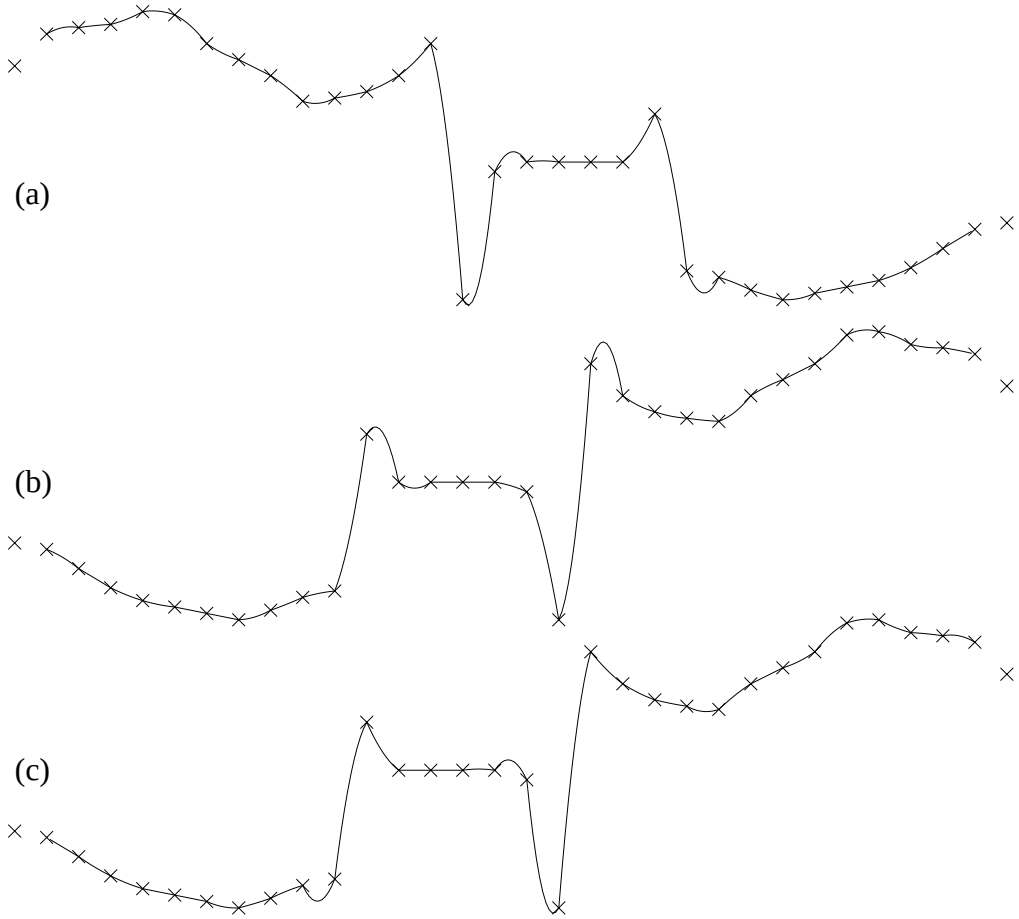

Figure 3.13: The effects of a non-linear phase reconstructor. (a) and (b) are the same data set, one the reverse of the other. They have both been reconstructed by the same non-linear phase reconstructor (equation 3.4 was used). (c) is (a) reversed so as to allow easy comparison with (b). The two curves are obviously different.

3.5.1 No phase distortion

The first need is for linear phase. This idea was introduced in section 3.4.6. It basically ensures that the signal will not be distorted by its frequency components having their phases shifted by non-linear amounts (shifting them by linear amounts is equivalent to moving the entire signal in the spatial domain [see page 66]; shifting them by non-linear amounts produces distortion in the spatial domain). Practically, linear phase implies that the reconstruction filter's kernel is real and evenly symmetric about some point. In filter design we can, without loss of generality, use the zero phase situation. With zero-phase the kernel is real and even (symmetric about the origin). In general, it would seem that a spatial filter can always have zero phase, while a temporal filter needs linear phase in the cases where a zero phase filter would be non-causal.

A very basic reason behind the need for zero or, at most, linear phase is for the intensity surface to be the same whether the data is presented forward or backward. With a non-linear phase reconstructor the orientation of the data affects the shape of the intensity surface, while with a linear phase reconstructor the orientation of the data has no bearing on the shape of the intensity surface. An example of this is given in figure 3.13.

The practical outworking of having linear phase is that, if there are an odd number of *points* controlling each section then the sections will start and end *midway between* sample points. If

there are an even number of points then the sections will start and end *at* sample points.

Other factors

While a linear phase reconstructor ensures that we will get no spatial distortion due to phase shifts in the frequency domain, our reconstructor still needs many more constraints in order that the spatial domain intensity surface is a good approximation to the original intensity surface. What is meant by 'good approximation' tends to depend on who you ask: are we trying to approximate the cardinal function through the sample points?, a Gaussian reconstructed surface?, or the real original function? Are we trying to make the intensity surface mathematically nice? (that is: obey some predefined mathematical criteria of goodness) or visually nice? (that is: look right). In this entire section we consider both mathematical and visual criteria for correctness.

Whatever the effect we are trying to achieve, from now on we can only affect *magnitudes* in the frequency domain, because we have already constrained our reconstructor to have zero (or at most linear) phase. Thus, if ever we need to look at the frequency response of a linear phase filter we know that we need only consider the magnitude of the frequency response.

3.5.2 Continuity

Continuity is arguably the most important criterion for our intensity surfaces, after linear phase. There are several grades of continuity. We met the first two in section 3.4.6. C0-continuity is simply continuity of the intensity surface. C1-continuity is C0-continuity plus continuity of the first derivative of the intensity surface. In general, Cn-continuity is C0-continuity plus continuity of all derivatives of the intensity surface up to and including the n^{th}.

The degree of continuity required depends on the application. In Computer-Aided Design (CAD), where design curves are being 'reconstructed' from control points, a minimum of C2-continuity is generally desirable [Chu, 1990, p.283].

For our application (reconstructing intensity surfaces) we have seen that a reconstructor with no continuity (the nearest-neighbour interpolant) is in frequent use and that the most common reconstructor (linear) has only C0-continuity. Thus the stringent requirements of CAD are not *essential* here.

How much continuity is required for intensity surface reconstruction? Nearest-neighbour interpolation is not good enough for many purposes and has been replaced by linear and other methods. The human eye is very sensitive to intensity differences [Pratt, 1977] and so C0-continuity is desirable.

It is true that the original intensity surface may have had C0-discontinuities (that is: edges[5]), but it is extremely unlikely that the nearest-neighbour reconstructed intensity surface has C0-discontinuities in the same place. The human eye is so sensitive to discontinuities that adding incorrect ones produces very visible rastering artifacts (for example: the familiar blocky effect due to nearest-neighbour interpolation; see figure 2.13).

C0-continuity is thus highly desirable because of the human eye's ease of picking out C0-discontinuities. Can we stop at C0-continuity? In the design of our quadratic reconstructors we attempted to enforce C1-continuity. How much continuity *is* required?

Keys [1981] in his development of a cubic interpolant constrains it to be zero-phase, interpolating, and C1-continuous, but gives no reason for doing so [Keys, 1981, p.1154] except to say that C1-discontinuities are not normally desirable [*ibid.*, p.1159]. Mitchell and Netravali [1988, p.223], in their study of cubic filters, insist that the filter should be smooth in the sense that its value and first derivative are continuous everywhere (that is: C1-continuous). Their reason is that discontinuities

[5] 'C0-discontinuity' is not a term defined in the literature. We define 'Cn-discontinuity' to mean "discontinuous in the n^{th} derivative but continuous in all derivatives from $0 \ldots n-1$".

in the function lead to high-frequency leakage in the frequency response of the filter which can allow aliasing. Chu [1990, p.283] states that, for CAD applications, the curves should have C2-continuity (that is: continuity of curvature). Foley, van Dam, Feiner and Hughes [1990, p.479] say that there are applications, such as the aerodynamic design of cars and aeroplanes, where it is important to control higher-derivatives than the second; so we can assume that C3- or even C4-continuity is required here. However, we are dealing with an intensity surface rather than with a curve that will be seen as a wiggly line. A gradient, or a discontinuity in intensity is perceived differently to a gradient or a discontinuity in a line, for example in a CAD curve. For this reason the criteria used for continuity in CAD applications are probably irrelevant.

The visual evidence favours C0-continuity — even though this intensity surface will never be seen (it must go through at least one sample-and-reconstruct cycle before it is consumed visually); lack of C0-continuity can cause visual problems which propagate through this cycle.

Unfortunately, it is not true that C0-continuity is desirable in all cases. If a C0-discontinuity in the intensity surface matches a C0-discontinuity in the original surface then the result is what we want (assuming that the sampling method is chosen intelligently). A good example of this is using nearest-neighbour interpolation to reconstruct a certain type of checkerboard image. The edges in the original image fell along pixel edges and so the nearest-neighbour interpolated image is an exact reconstruction of the original (figure 7.9). Such cases are, however, rare. All we can say from visual evidence is that introducing C0-discontinuities in the reconstructed intensity surface in places where they did not exist in the original intensity surface is a bad idea. With no *a priori* knowledge we cannot know where any C0-discontinuities could have been in the original image and so C0-continuity is a good criterion to use if there is no *a priori* knowledge about the placement of C0-discontinuities.

The visual evidence favouring C1-continuity is much weaker than that for C0-continuity because the visual response to a C1-discontinuity is much weaker than the response to a C0-discontinuity. There is evidence that the human visual system *cannot* detect C2-, or higher, discontinuities in intensity, and there exists little contrary evidence in favour of human ability to detect these higher order discontinuities. Mach [1865] does suggest that the Mach band effect is related to the value of the second derivative of intensity and hence the visual system is slightly sensitive to C2-discontinuities. It seems unlikely that we are affected by C2-discontinuities in the reconstructed intensity surface, especially as there is at least one cycle of sampling and reconstruction between this intensity surface and the intensity surface that is displayed and, hence, viewed by a human. On the other hand, if humans could be slightly sensitive to it, we should take this into consideration.

Turning to the mathematical evidence for requiring continuity we find much stronger arguments. Any discontinuity in a spatial function requires high, up to infinite, frequencies in the frequency domain. To minimise aliasing artifacts, high frequencies must be minimised, thus discontinuities should be avoided.

The biggest problems in reconstructed intensity surfaces arise from C0-discontinuities; however, C1-discontinuities are enough of a problem that Mitchell and Netravali [1988, p.223] cite this as the reason for requiring C1-continuity. C2-discontinuities seem to cause few problems and C2-continuity can be considered an optional extra: it is nice to have but not at the expense of other, more important criteria. Above C2-continuity, other problems start to creep in because of the number of degrees of freedom required to produce higher orders of continuity. The intensity surface may oscillate wildly to allow for Cn-continuity ($n > 2$) and this is a visually undesirable effect.

The recommendations for continuity are:

- C0-continuity is a very high priority;
- C1-continuity is a medium priority (it makes for smooth changes and there is evidence that humans detect C1-discontinuities);
- C2-continuity is a low priority, it need only be pursued when more important criteria have

been met;

- any higher continuity is a very low priority, it may actually be counter-productive to insist on higher continuity in a piecewise local polynomial as a lot of degrees of freedom, and hence a high order, are required to allow for it. Forcing a higher order of continuity may cause undesirable rippling artifacts in the reconstructed intensity surface. However, from a frequency domain point of view, the higher n in the Cn-continuity, the better the frequency response should be, all other things being equal.

Having decided, for a given reconstructor, that Cn-continuity is desired, it is enforced by ensuring that the piecewise function is Cn-continuous across the joins, or knots, between the pieces. Each piece is infinitely differentiable along its length by its very nature; it is only the ends that need to be matched up.

3.5.3 Straightness

This property can be interpreted in two ways, one of which includes the other. The first is that, for a piecewise function where each piece depends on the m nearest points; if, for a given piece, the sample value at all m points is the same, then the piece should have that value along its entire length. In other words, if the samples controlling a piece have a constant value then the reconstruction for that piece is a flat constant signal, producing a visually correct result.

Mitchell and Netravali [1988, p.223] explain the need for this criterion in a different way: it removes any sample frequency ripple. If you look back to figure 3.9 you will see that, for every reconstructed function except the one which meets this criterion ($b = -\frac{1}{2}$) there is a periodic ripple at the sample frequency. By insisting on this straightness criterion, this ripple is designed out of the reconstruction. Mitchell and Netravali [1988] illustrate this in their figure 8 using an unnormalised Gaussian filter. They say that sample frequency ripple can be shown to be aliasing of the image's DC ('direct current' or 'zero frequency') component in the frequency domain. Designing sample frequency ripple out of the filter ensures that its frequency response will be zero at all integer multiples of the sampling frequency (except zero), thus eliminating all extraneous replicas of the DC component. Parker, Kenyon and Troxel [1983, p.36] say that the straightness criterion also forces the reconstructor to have a DC amplification of one. This means that the average intensity of the intensity surface is the same as that of the image.

The mathematical expression of this constraint is that:

$$\sum_{m=-\infty}^{\infty} h(s-m) = 1, \ \forall s \in \mathcal{R}$$

Looking at it another way, for any order of reconstructor as given in equation 3.1, for the case where all the points affecting the piece have the same value ($f_i = f_\alpha$, $i \in [\alpha - a, \alpha + b]$) we have:

$$f(x) = f_\alpha \sum_{i=-a}^{b} \sum_{j=0}^{n-1} k_{i,j} t^j$$

We would like:

$$\begin{aligned} f_\alpha &= f_\alpha \sum_{i=-a}^{b} \sum_{j=0}^{n-1} k_{i,j} t^j, \ \forall t \in \mathcal{T} \\ \mathcal{T} &= \begin{cases} [0,1), & m \text{ even} \\ [-\frac{1}{2}, \frac{1}{2}), & m \text{ odd} \end{cases} \end{aligned}$$

which implies that:

$$\begin{aligned} \sum_{i=-a}^{b} k_{i,j} &= 0,\ \forall j \in \{1, 2, \ldots, n-1\} \\ \sum_{i=-a}^{b} k_{i,0} &= 1 \end{aligned} \tag{3.13}$$

These two conditions enforce the straightness criterion.

The second interpretation of straightness goes farther than this and insists that, for any set of m sample points in a straight line, the reconstructor produces that straight line for the appropriate polynomial piece. It is easy to show that, to ensure this, two constraints must be added to the two in equation 3.13 (the derivation of these equations is given in appendix B.4):

$$\begin{aligned} \sum_{i=-a}^{b} i k_{i,j} &= 0,\ \forall j \in \{0, 2, 3, \ldots, n-1\} \\ \sum_{i=-a}^{b} i k_{i,1} &= 1 \end{aligned} \tag{3.14}$$

The first two constraints (equation 3.13) ensure that, for sample points lying on a first order curve (that is: a horizontal straight line) the reconstructed function also lies on that first order curve. The second pair of constraints (equation 3.14) ensure that, for sample points, lying on a second order curve (that is: on an arbitrary straight line) the reconstructed function also lies on that second order curve. It is also possible to extend this criterion to third order curves, in which case the points lie not on a straight line but on a parabola.

The first order constraint allows us to select functions with no sample frequency ripple (as in figure 3.9) and also with the correct multiplicative constant (as in figure 3.10) because it constrains the function to be both flat (no sample frequency ripple [Mitchell and Netravali, 1988, p.223]) and interpolative (correct multiplicative constant [Parker *et al*, 1983, p.36]) when the m points all have the same sample value.

For both interpolants and approximants this constraint ensures that, given m sample points with the same sample value, the piece controlled by those points will be flat, constant and interpolating. This is obviously desirable for an interpolant. A few moments thought and a glance at figure 3.10 will show that it is also the only sensible choice for an approximant; basically the m data points reduce to a single piece of information (the common sample value) and so the approximant can do no better than be flat, constant and interpolating.

Obviously, the criterion can be extended to higher orders but it is the first order that is important. Only the first order constraints (equation 3.13) are required to enforce the straightness criterion as it is needed for reconstructing intensity surfaces.

3.5.4 Interpolating or approximating

If we assume that our sample points are perfect point samples then we should use an interpolating function, because the sample points are constrained to lie on the original intensity surface.

In an ideal world that would be the end of the matter, however, it is well known that the intensity samples in captured imagery cannot be perfect point samples and often do not approximate point samples at all well. In rendered imagery, perfect point samples are possible, but they are not common in good quality rendered images. Given this, an approximant is a valid reconstructor.

In order to produce a useful approximant, however, some *a priori* knowledge is required about how the samples are produced and/or about the type of image sampled. In the discussion in this section we are restricting ourselves to the case where we have no *a priori* knowledge. In this

case we assume, as mentioned earlier (section 3.1.4), that the samples are perfect point samples, and reconstruct the surface represented by those samples as best we can. It can be argued that, because we know that we have not got perfect point samples, it is better to make some assumption of non-perfection. The problem is that we do not know what assumption to make. It would be possible to make a guess as to how the samples were formed, or it may be possible to derive such information from the image. Here we make the guess that they are single point samples, which is the commonest assumption. Other assumptions could throw us into the world of APK reconstructors, considered in chapter 6, where reconstruction is done on the basis of knowledge about the sampling process.

Given the assumption of single point sampling, is there a use for any approximant? The answer is *yes*. In order to make a piecewise curve of a certain order interpolate, we have to use some of its degrees of freedom. If we remove the interpolation constraint then we release these degrees of freedom. They can then be used to constrain the piecewise polynomial to meet other criteria. This is exactly what was done in the case of the quadratic in section 3.4.6; the interpolation criterion was dropped, releasing two degrees of freedom which were used to meet the C1-continuity criterion. Thus an approximant is useful where criteria other than interpolation are considered more desirable than interpolation.

3.5.5 Localisation

This is not a criterion applied to our general form (equation 3.1) but is more fundamental, relating to how that formula was derived. The question is: which sample points are used to calculate the intensity at any given point? In our examples so far we have used the rule that, for a piecewise reconstructor of order n, the function value at any point is based solely on the n nearest sample points to that point.

This leads to several questions:

- Why use the sample points directly?
- Why n points?
- Why the nearest points?

The first question is profound. Our general formula for a piecewise polynomial reconstructor is given in equation 3.1. This is, however, a specific form of the more general:

$$f(x) = \sum_{i=-a}^{b} \left(\sum_{j=0}^{n-1} k_{i,j} t^j \right) g_{\alpha+i} \tag{3.15}$$

where:

$$\begin{aligned} a &= \left\lfloor \frac{m-1}{2} \right\rfloor & \alpha &= \begin{cases} \left\lfloor \frac{x-x_0}{\Delta x} \right\rfloor, & m \text{ even} \\ \left\langle \frac{x-x_0}{\Delta x} \right\rangle, & m \text{ odd} \end{cases} \\ b &= \left\lfloor \frac{m}{2} \right\rfloor & t &= \frac{x - x_\alpha}{\Delta x} \end{aligned}$$

The difference here is that $g_{\alpha+i}$ is used in place of $f_{\alpha+i}$ The g_α are coefficients *calculated from* the f_α plus, in some cases, other fixed conditions. Equation 3.1 is a special case of equation 3.15 with $g_\alpha = f_\alpha$.

A well known example of equation 3.15 is the interpolating cubic B-spline. Wolberg [1990, pp.136-137] gives an example of this showing that one method of calculating the g_α from the f_α is by the

following matrix equation (assuming N sample points):

$$\begin{bmatrix} f_0 \\ f_1 \\ f_2 \\ \vdots \\ f_{N-2} \\ f_{N-1} \end{bmatrix} = \begin{bmatrix} 4 & 1 & & & & \\ 1 & 4 & 1 & & \mathbf{0} & \\ & 1 & 4 & 1 & & \\ & & 1 & \ddots & 1 & \\ & & & 1 & 4 & 1 \\ & \mathbf{0} & & & 1 & 4 \end{bmatrix} \times \begin{bmatrix} g_0 \\ g_1 \\ g_2 \\ \vdots \\ g_{N-2} \\ g_{N-1} \end{bmatrix}$$

That is, $F = KG$.

Inverting the tridiagonal matrix, K, gives its inverse, K^{-1}, giving us $G = K^{-1}F$. We thus get a function for each g_α:

$$g_\alpha = \sum_{l=0}^{N-1} K^{-1}_{\alpha,l} f_l$$

where $K^{-1}_{i,j}$ is the element in the i^{th} row and j^{th} column of the matrix K^{-1}. The nature of K^{-1} (it contains no zeros) means that every g_α depends on every f_α. Thus every point, $f(x)$, on the intensity surface depends on all the f_α sample values. In general, for almost all such methods, each g_α value is a function of all of the f_α values, and so the conclusions from this specific interpolating B-spline example can be generalised.

Thus, from equation 3.15:

$$\begin{aligned} f(x) &= \sum_{i=-a}^{b} \left(\sum_{j=0}^{n-1} k_{i,j}\, t^j \right) \sum_{l=0}^{N-1} K^{-1}_{\alpha+i,l}\, f_l \\ &= \sum_{l=0}^{N-1} \left(\sum_{i=-a}^{b} \sum_{j=0}^{n-1} k_{i,j}\, K^{-1}_{\alpha+i,l}\, t^j \right) f_l \\ &= \sum_{l=0}^{N-1} \left(\sum_{j=0}^{n-1} \kappa_{\alpha,j,l}\, t^j \right) f_l \end{aligned} \tag{3.16}$$

where:

$$\kappa_{\alpha,j,l} = \sum_{i=-a}^{b} k_{i,j} K^{-1}_{\alpha+i,l}$$

The $\kappa_{\alpha,j,l}$ values can be precalculated in the same way that the $k_{i,j}$ values are for equation 3.1. Indeed equation 3.16 is almost equation 3.1 with $m = N$, but note that here κ depends on α while, in equation 3.16, the equivalent k is independent of α.

By using such a method every point on the intensity surface will, in general, depend on all the sample points. Finding the intensity value, $f(x)$, for any point will thus involve a lot of calculation. The great advantage of using only the local sample points (the n nearest) is that the calculation is fast. If, as in many resampling situations, there is a need for quick computation or for fast arbitrary sampling off the intensity surface, localisation is a good idea and therefore equation 3.1 is preferable to equation 3.16.

It is feasible to precalculate all of the g_α coefficients for use in equation 3.15; and this is generally what is done in any real system. This gives the same speed advantage in the actual resampling as using equation 3.1. Instead of calculating intensity values from local sample values they are calculated from *local*, pre-computed, g_α coefficients.

The disadvantage here is that the precomputation still has to be done and is different for each image[6]. If we want a quick reconstructor we may not be willing to pay the price of the precompu-

[6] whilst the $k_{i,j}$ values are the same for all images, and the $\kappa_{\alpha,j,l}$ for all images of the same size.

tation. Further, if the data is being processed as a stream, as in scan-line algorithms, it may be impractical to read and store a whole scanline, calculate the coefficients and produce the output samples. In this case an algorithm requiring this precomputation of coefficients will be impractical.

The advantage of using precomputed coefficients is that they allow all of the data to be taken into account at each sample point rather than just the local data. This should, arguably, make possible a more accurate reconstructor.

In chapter 4 we look at such non-local reconstructors and their advantages. For now we will concentrate on the simplicity of local reconstructors. That is reconstructors where $g_\alpha = f_\alpha$. It is possible to conceive a way of calculating the g_α values which makes $f(x)$ dependent only on local f_α values. For example, $g_\alpha = \frac{1}{4}f_{\alpha-1} + \frac{1}{2}f_\alpha + \frac{1}{4}f_{\alpha+1}$. Such a reconstructor can, however, be easily recast in the terms of equation 3.1 by changing the $k_{i,j}$ values. Another local possibility is a non-linear manipulation of the f_α values, for example $g_\alpha = \log(f_\alpha)$. We do not consider such functions here because non-linear manipulations of the intensity values are not useful in resampling work, section 2.2 points out the necessity of the intensity surface being a linear function of the input image data.

This still leaves two questions:

- Why n points?
- Why the nearest points?

Why do we use n points when reconstructing with an n^{th} order piecewise polynomial?

A polynomial of order n can be expressed as

$$f(x) = \sum_{i=0}^{n-1} c_i x^i$$

That is, it has n coefficients. These n coefficients can be uniquely determined from n data values. For example, in a piecewise polynomial function each piece is a function of the form:

$$f(t) = \sum_{j=0}^{n-1} c_j t^j$$

where $c_j = \sum_{i=-a}^{b} k_{i,j} f_{\alpha+i}$ (this is simply a reformulation of equation 3.1).

Note that $a + b = n - 1$, thus there are n $f_{\alpha+i}$ values involved in calculating the c_i co-efficients.

But why use exactly n data points when wanting an order n function? Approaching the problem from the other end: given m data points why limit ourselves to a function of order m? There are two alternatives: either use a function with order less than m or use a function with order greater than m.

A function of order less than m has fewer than m coefficients and thus cannot take all the available data into account. With an order n function ($n < m$) the effective result will be that $m - n$ data points will be irrelevant in calculating the function values, that is: m independent variables are used to calculate n values therefore the potential of $m - n$ values are 'lost'. Given that m points have the expressive power to produce m independent coefficients [Foley *et al*, pp.478–479] it seems ludicrous to limit the function to any order less than m. The counter to this observation is that a good reconstructor, the interpolating cubic B-spline, has $m \gg n$. The m data values are combined to give n coefficients for each segment of the curve, producing a better result than can be obtained from just n data values. Another example of $m > n$ is given by Keys [1981, pp.1159-60]. He presents a cubic function based on six data points which has an $O(h^4)$ convergence rate

to the Taylor series expansion of the function being interpolated, as compared to $O(h^3)$ for the Catmull-Rom spline.

The use of a function of order n greater than m, is very tempting. While the data can only determine m independent coefficients the extra $n - m$ coefficients give more degrees of freedom with which to satisfy more criteria (note that with a function of order n, and m data points you get $m \times n$ degrees of freedom).

Unfortunately, the problem here is that the coefficients are underconstrained and have to create data items to define themselves on. There is simply not enough data available to fully define the function and so the extra criteria that are imposed (using the extra degrees of freedom) force 'default data values' to be accepted — for example a quintic function ($n = 6$) based on $m = 4$ data points has a potential for two extra data values. As these are not supplied the criteria force these extra data values to some value, which may be constant for all pieces. For example, in this case, it may be that the value of the second derivative at each end of the segment is zero. Thus we now have six data values to base the six coefficients on, the $m = 4$ real data points plus the two constant data values that $f''(\alpha, 0) = 0$ and $f''(\alpha, 0) = 0$.

The following example will help to clarify this.

Previously we produced the standard linear interpolant ($m = n = 2$) when deriving a reconstructor for the two point case. Now let $m = 2$ and $n = 4$. Thus we will produce a piecewise cubic function where each piece depends on two data points:

$$f(x) = (at^3 + bt^2 + ct + d)f_\alpha + (et^3 + ft^2 + gt + h)f_{\alpha+1}$$

If we now impose the criteria met by the piecewise linear function in section 3.4.5 and use the extra freedom given by the cubic function to also enforce C1-continuity we get:

$$f(x) = f(\alpha, t) = (2t^3 - 3t^2 + 1)f_\alpha + (-2t^3 + 3t^2)f_{\alpha+1} \tag{3.17}$$

Thus function's kernel is:

$$h(s) = \begin{cases} -2s^3 - 3s^2 + 1, & -1 \le s \le 0 \\ 2s^3 - 3s^2 + 1, & 0 \le s \le 1 \\ 0, & \text{otherwise} \end{cases}$$

This is a member of the one parameter family of cubics described by Wolberg [1990, pp.129-131] and many others (equation 3.20). To produce this particular member the parameter, a, is set to zero.

Analysis of this function in the spatial domain shows that, for any α: $f'(\alpha, 0) = 0$ and $f'(\alpha, 1) = 0$[7]. Thus the two extra data points required by the cubic are provided by these two 'default data points'; the first derivatives of the function at x_α and $x_{\alpha+1}$ default to zero. This gives the interpolated function the form shown in figure 3.14.

The extra C1-continuity provided by the cubic function means that its frequency response is smoother; it does, however, produce a rather odd looking interpolant.

Maeland [1988] claims, from frequency domain evidence, that this piecewise cubic interpolant produces a much better quality of interpolation than the simple linear interpolation. In contrast, Fraser [1989b, p.272–3] claims that it produces much the same quality. Our visual evaluation shows that it is less blurry than linear interpolation but has a blocky (anisotropic) artifact, similar to nearest-neighbour, but not as obvious[8].

[7] $f'(\alpha, t) = f'(x_\alpha + t\Delta x)$

[8] Mitchell and Netravali's [1988] subjective evaluation also shows that the dominant artifact in this reconstructor is anisotropy.

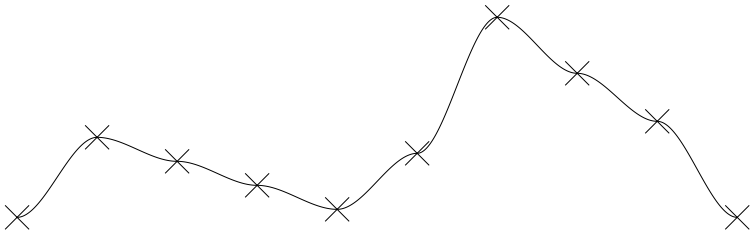

Figure 3.14: The two point cubic operating on an image. Notice that the slope of the curve at each data point is zero.

Using a function of order higher than m allows more constraints to be met by the reconstructor at the expense of every piece being partly controlled by these 'default data values'.

Given that a piecewise function of order n can be used to meet up to n independent data items the most sensible course of action is to take those n items to be n real data points from the set of data available, rather than force $n - m$ $(m < n)$ of these items to be default data values, most likely the same value for every piece. We conclude that $m = n$ is the ideal case but that both $m < n$ and $m > n$ are useful.

Why the nearest points?

The simple answer is that, to find the value of the function at a given point, the data points which are most relevant are those nearest to the point. The farther apart two points are, the weaker the relation between their function values. Thus if you are going to use m data points to calculate the value at some point, then it is logical to use the m nearest data points.

Thus we should use the nearest sample points to define the pieces of a local polynomial piecewise function. This gives us simplicity and localisation of data references in implementations. No data point beyond the local neighbourhood of the point we are interested in is used in the calculation of the function value at that point; unlike methods with precalculation where every data point tends to be involved in calculating the function value at every point.

3.5.6 Approximating sinc, approximating Gaussian, or neither

One measure of the quality of a reconstructor is how closely it approximates some other, more desirable, reconstructor. The reasons for not implementing this more desirable reconstructor could be many; most often we are looking for a good local approximation to a non-local reconstructor.

Mathematically the sinc reconstructor is the most desirable. Much effort can be expended in designing a local filter to match the sinc function as closely as possible [Schafer and Rabiner 1973]. This work is usually undertaken in the frequency domain where the frequency response is designed to be as close to a box function as possible. For example, Reichenbach and Park [1989] analyse the two parameter family of cubics (equation 3.19) in the frequency domain to find the best approximation to sinc reconstruction. Another example is Wolberg's [1990, sec.5.4.7] tanh filter which has an approximate box function frequency response composed of the product of two tanh functions.

Visually, the sinc function may not necessarily be the best function to use (figures 2.10–2.13). The Catmull-Rom function is considered to be a local approximation to the sinc function [Wolberg 1990, sec.5.4.3] yet both Mitchell and Netravali [1988], and Ward and Cok [1989] claim that visually the Catmull-Rom cubic produces a better reconstructed intensity surface than the sinc function. What reasons can be put forward to explain this apparent inconsistency?

Ward and Cok [1989] suggest that this is due to the original signal not being bandlimited and

thus sinc reconstruction causing ripples near edges because of the aliased high spatial frequencies. However, we saw in section 2.7 that even a perfectly bandlimited image can display objectionable ripples in its sinc reconstructed intensity surface. The sinc reconstructed intensity surface of any image will contain ripples, although, if the image is bandlimited to *well* below the Nyquist limit, then the ripples will almost certainly be visually acceptable.

Ward and Cok's theory is that the sharp cutoff in the frequency domain of the sinc reconstruction (infinitely sharp, it is a box function) causes the rippling and that passing some frequency information above the Nyquist limit is beneficial, producing visually nicer results, especially near edges. They believe that linear interpolation makes the picture too blurry (and thus must pass too much information above Nyquist and too little below) whilst the Catmull-Rom cubic interpolant gives about the right balance.

Taking their argument and developing it further we postulate the following frequency domain explanation for the perceived differences in intensity surface quality arising from sinc and Catmull-Rom reconstructions:

Almost any image of interest will have a frequency spectrum which is not bandlimited; this spectrum will usually peak near zero and fall off rapidly at higher intensities, as shown in figure 3.15(a). When sampled without perfect prefiltering, as is usual, the resulting spectrum contains aliases, as illustrated in figure 3.15(b). Reconstructing this using sinc perfectly reproduces these aliases (figure 3.15(c)). Comparing figure 3.15(c) with figure 3.15(a) shows what is wrong with the reconstructed intensity surface: the frequencies just below the Nyquist frequency have too large a magnitude, whilst those just above have too small. Catmull-Rom cubic reconstruction, on the other hand, produces a reconstructed surface closer to the original. Figure 3.15(d) shows that the frequency domain representations of the original and the reconstructed surfaces match much better than with sinc reconstruction. Those extra high frequencies prevent the offensive rippling artifacts.

These diagrams, look quite convincing but how realistic are they? Firstly, many images do exhibit this distribution of frequencies: a high peak near zero and a long tail off to infinity. Certainly the images we looked at had frequency responses that dropped as they approached the Nyquist frequency, but they did not fall all the way to zero, which indicates the presence of aliases. The effect of sampling such a signal will be as illustrated in figure 3.15(b): the frequencies near zero undergoing little change whilst the frequencies near Nyquist exhibit large changes.

However, these diagrams show only the effect on magnitudes. The effect of phase in all this has not been mentioned. The phases of the frequency components of the reconstructed intensity surfaces near and above Nyquist will bear little relationship to those in the original intensity surface, because the phases of the correct component and the aliased component will be added together, producing an incorrect result. The aliased component has a large magnitude relative to the correct component around the Nyquist frequency, so causing the largest errors in phase around this frequency. This may turn out to be unimportant, but it throws doubt on this explanation of why we observe that the Catmull-Rom cubic is better that the sinc function at image reconstruction.

The ripples caused by sinc reconstruction are certainly caused by the limited frequency domain spectrum; that is there are no spatial frequencies greater than the Nyquist frequency. The outworking of this is that no change can occur in the intensity surface faster than a distance of $\frac{1}{2\nu_N}$ (the sampling spacing) and that any change is accompanied by subsidiary ripples on either side.

To explain the good results from Catmull-Rom interpolation we can consider the results in the spatial domain. Here we note several features of this reconstruction:

- like sinc, no changes can occur faster than $\frac{1}{2\nu_N}$ (the sample spacing);
- the side lobe sharpening effect (one ripple either side of an edge) is used to make edges appear sharper, and is thus not perceived as a ripple but as a sharper edge;
- unlike sinc, no distracting extra ripples are produced;

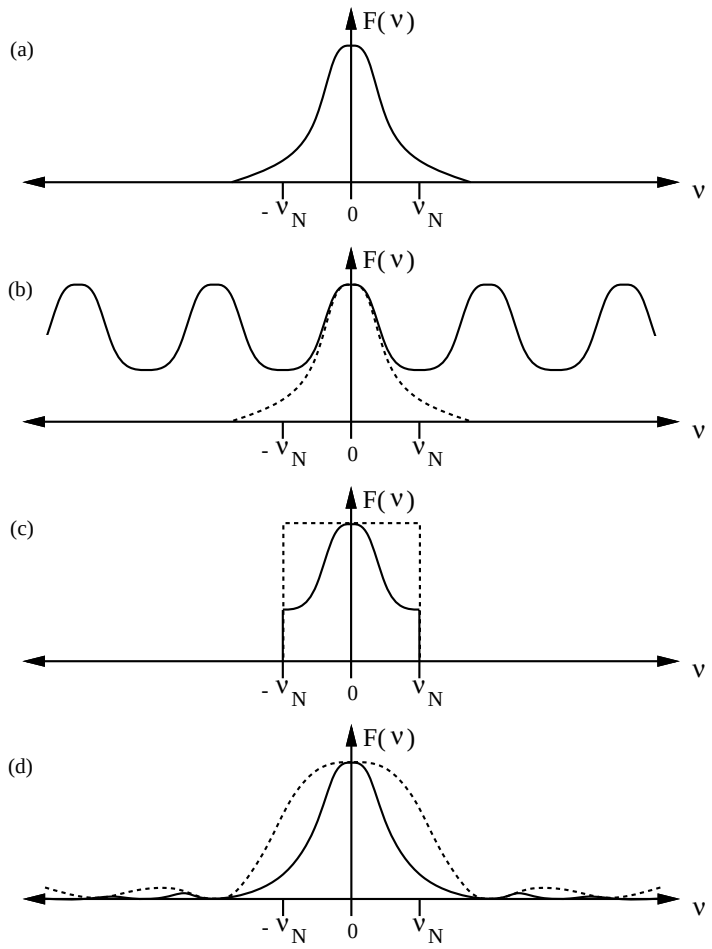

Figure 3.15: The effects, in the frequency domain, of sampling and subsequent reconstruction by sinc and Catmull-Rom reconstructors: (a) the original intensity surface's Fourier transform, note that it has frequencies higher than the sampling frequency ν_N; (b) the sampled image's Fourier transform after sampling at frequency ν_N, the dotted line is the curve from (a), aliasing has occurred (c) the Fourier transform of the sinc reconstructed image; the Fourier transform of the sinc reconstructor is shown by the dotted line; (d) the Fourier transform of the Catmull-Rom reconstructed image; the Fourier transform of the Catmull-Rom reconstructor is shown by the dotted line.

- large, near constant, areas can be reproduced with no visible internal rippling.

Basically the Catmull-Rom cubic panders to our visual system's predilections, whilst the sinc function panders to our desire for mathematical correctness. We are good at recognising sharp edges; the Catmull-Rom cubic sharpens edges. We object to extra ripples in 'flat shaded' areas, which sinc reconstruction produces in abundance; the Catmull-Rom cubic produces none.

Other approximations

The other function to which a good local approximation is frequently sought is the Gaussian. The Gaussian is infinite in extent, like sinc, and it falls off to zero as it goes to infinity, also like sinc. There the similarities stop. Sinc is an oscillatory function whilst a Gaussian is strictly positive. The Gaussian is the limit of the B-spline family. It can be generated by convolving an infinite number of boxes together. All members of the B-spline family are approximations to the Gaussian.

The Gaussian tends to produce a blurry intensity surface (as do most B-splines) but is prized because it is strictly positive and has other nice analytical properties [Turkowski, 1990, p.150]. These other properties are irrelevant when designing an approximation as they will not be present in the approximation. The strict positiveness is an important property which is discussed in the next section.

The sinc and Gaussian are by far the most approximated functions. There appears to be no work on approximating other functions. Keys [1981] chooses his cubic function by finding the member of the family of cubics which produces an intensity surface which matches the Taylor series expansion for the original intensity surface to as many terms as possible . This criterion is not making the reconstruction filter approximate some other filter, but is making the reconstructed intensity surface approximate the original intensity surface in a well defined mathematical way.

The final option is to approximate no particular function at all. This means that the reconstructor is designed based on the other criteria discussed in this chapter and judged on its own merits, not on its closeness to some more 'desirable' reconstructor. Any resulting resemblance to some other reconstructor is thus purely coincidental.

3.5.7 Negative lobes *vs* strictly positive

These terms refer to the shape of the reconstruction filter. All reconstruction filters are mostly positive (to ensure that the average intensity of the intensity surface is the same as that of the image from which it is reconstructed, the integrated area under the whole reconstruction filter must be unity). The debate is over whether the filter should be all positive or whether negative lobes are permissable. The problem with negative lobes is that they introduce the possibility that some parts of the intensity surface may have intensity values brighter than the brightest white in the image, or, worse still, darker than black. The former can be dealt with, as it is always (theoretically) possible to produce a brighter white. The latter is a major problem, there is no such thing as negative light, there is no intensity 'blacker than black' and so such intensities cannot be displayed[9]. Blinn [1989b] says that clamping these values to zero (black) is about the best you can do, but is not ideal. This issue is taken up in section 4.5.2.

Because of this problem of negative light some have advocated using only a strictly positive kernel. Unfortunately, such reconstructors tend to produce blurry intensity surfaces. Further this makes it difficult to produce a good interpolating reconstruction. Blinn [1989b, p.87] asserts that any decent approximation to a low-pass filter, for either sampling or reconstruction, has negative lobes.

[9]Negative light is an interesting concept. A negative light bulb, for example, would be very useful: if you are working nights and have to sleep during the day, just turn on your negative light bulb, flooding the room with negative light and there you have it, a darkened room. It can't do anything about traffic noise though.

It is the negative lobes in the Catmull-Rom cubic, for example, that generate the desirable edge sharpening effect.

Thus we are faced with a simple choice: either allow negative lobes and cope with any negative intensities which arise; or reject negative lobes and accept a certain amount of blurriness in the intensity surfaces.

3.5.8 Computational considerations

In all this we have given little consideration to the length of time required to generate actual values of the intensity at arbitrary points. Keys [1981, p.1153] remarks "Because of the [large] amount of data associated with digital images, an efficient interpolation algorithm is essential." Obviously some housekeeping calculations are common to all piecewise local polynomials (for example, finding α and t) but there is part of the calculation which depends on m and n. To calculate a single value using equation 3.1 (the one-dimensional version) requires $m(n+1)$ multiplications (plus $(n-2)$ to find all the t^j values for $t \in \{2, 3, \ldots, n-1\}$) and $(mn-1)$ additions. Thus it is an $O(mn)$ process. For computational efficiency we therefore need to keep $m \times n$ as small as possible.

Small m also means that there need to be less of the image in memory at once, an important point for stream processing: the fewer input points that need to be operated on for each output point, the better. Speed of computation, which is a function of $m \times n$, not just m, is also very important in stream processing.

So we find a tension here: on the one hand the larger $m \times n$ the more criteria the reconstruction can meet; on the other hand the smaller $m \times n$, the faster the resampling can be performed.

This generalises to other reconstructors; computational cost is related to 'M', the number of input points used to produce one output point, and 'N', the amount of processing required for each of the 'M' input points.

In general, the more criteria a reconstructor has, and the more input points required to generate one output point, the longer it takes to evaluate.

3.5.9 No extra knowledge

Finally it should be noted that there is no knowledge about the image besides the data points and thus any reconstruction method must be based solely on information in the data points. Indeed, this is what is meant by 'no *a priori* knowledge'.

Later we will look at what can be achieved when more knowledge is available. For example, Mitchell and Netravali [1988] show that a much better cubic reconstruction can be produced if both intensity and first derivative of intensity values are available at each sample point.

3.5.10 Summary

Chu [1990] gives a list of the five features which a good interactive interpolation procedure for CAD should possess. While providing a good starting point for investigating features which a good reconstructor should possess, the use of the resulting curve dictates different priorities.

The features which a good NAPK reconstructor should possess are:

- Linear phase.
- C0-continuity, C1-continuity if possible, higher orders of continuity if desirable (a general rule is that the higher the order the better the frequency response, all other things being equal).

- First order straightness, so that the intensity surface does not exhibit sample frequency ripple.
- Maximum use of the available information — a practical outworking of this is if we restrict ourselves to an order n function then we should use the same number of data points (n) and the most relevant ones (the closest).
- Reasonable computational effort.

3.6 Cubic functions

We now turn back to considering specific functions. The cubic piecewise functions are amongst the most studied group of reconstructors. The general form is:

$$\begin{aligned} f(x) = \quad & (k_{-1,3}t^3 + k_{-1,2}t^2 + k_{-1,1}t + k_{-1,0})f_{\alpha-1} \\ + \quad & (k_{0,3}t^3 + k_{0,2}t^2 + k_{0,1}t + k_{0,0})f_{\alpha} \\ + \quad & (k_{1,3}t^3 + k_{1,2}t^2 + k_{1,1}t + k_{1,0})f_{\alpha+1} \\ + \quad & (k_{2,3}t^3 + k_{2,2}t^2 + k_{2,1}t + k_{2,0})f_{\alpha+2} \end{aligned}$$

or, more compactly:

$$f(x) = \sum_{i=-1}^{2} \left(\sum_{j=0}^{3} k_{i,j}t^j \right) f_{\alpha+i} \tag{3.18}$$

where

$$\alpha = \left\lfloor \frac{x - x_0}{\Delta x} \right\rfloor, \; t = \frac{x - x_\alpha}{\Delta x}$$

Given these 16 degrees of freedom ($k_{i,j}$) we agree with Mitchell and Netravali [1988] in imposing the following criteria:

- Linear phase (Mitchell and Netravali do not explicitly state this but it is implicit in their formulations of the function as a symmetric cubic filter with only eight degrees of freedom, the other eight are required to ensure linear phase).
- C0-continuity
- C1-continuity
- Straightness (which they call designing "the problem of sample-frequency ripple" out of the filter).

With these constraints, which, from our discussion in section 3.5, are not contentious, the degrees of freedom in equation 3.18 are reduced from sixteen to two[10].

The function is now as follows:

$$\begin{aligned} f(x) = \quad & \left(\left(-\tfrac{1}{6}B - C\right)t^3 + \left(\tfrac{1}{2}B + 2C\right)t^2 + \left(-\tfrac{1}{2}B - C\right)t + \left(\tfrac{1}{6}B\right) \right) f_{\alpha-1} \\ + \quad & \left(\left(2 - \tfrac{3}{2}B - C\right)t^3 + \left(-3 + 2B + C\right)t^2 + \left(1 - \tfrac{1}{3}B\right) \right) f_{\alpha} \\ + \quad & \left(\left(-2 + \tfrac{3}{2}B + C\right)t^3 + \left(3 - \tfrac{5}{2}B - 2C\right)t^2 + \left(\tfrac{1}{2}B + C\right)t + \left(\tfrac{1}{6}B\right) \right) f_{\alpha+1} \\ + \quad & \left(\left(\tfrac{1}{6}B + C\right)t^3 + \left(-C\right)t^2 \right) f_{\alpha+2} \end{aligned} \tag{3.19}$$

where B and C are the two remaining degrees of freedom as used by Mitchell and Netravali [1988, p.223].

[10] The only bone of contention here could be whether the C1-continuity is necessary. As we decided in section 3.5.2 that C1-continuity is desirable, if possible, and as there are quite enough degrees of freedom to allow C1-continuity then it is sensible to include it as a criterion here.

If we add the C2-continuity criterion then the equation above reduces to the case where $B = 1$ and $C = 0$. This C2-continuous cubic is the approximating cubic B-spline (which is not interpolating).

If we impose the interpolating criterion (and do not impose the C2-continuity criterion) then we get: $B = 0$ with C still a free parameter. This one-parameter family of interpolating cubic functions have been extensively studied [Keys, 1981; Park and Schowengerdt, 1983; to a lesser extent: Maeland, 1988 and Parker *et al.*, 1983].

Keys [1981] uses the parameter a ($a = -C$) while Park and Schowengerdt [1983] use the parameter α ($\alpha = a$). Whatever the name of the parameter, it is the same family of cubics. Its general form is:

$$\begin{array}{rccccccccc} f(x) = & & (& (a)t^3 & + & (-2a)t^2 & + & (a)t & &)f_{\alpha-1} \\ & + & (& (2+a)t^3 & + & (-3-a)t^2 & & & + \quad 1 &)f_{\alpha} \\ & + & (& (-2-a)t^3 & + & (3+2a)t^2 & + & (-a)t & &)f_{\alpha+1} \\ & + & (& (-a)t^3 & + & (a)t^2 & & & &)f_{\alpha+2} \end{array} \tag{3.20}$$

Various members of this family have been advanced as useful:

$-3 \leq a \leq 0$ because between these limits the parametric cubic is a local approximation to the sinc interpolant [Wolberg, 1990, p.130].

$a = -1$ because the slope of the kernel, $h(s)$ at $s = \pm 1$ is then equal to the slope of the sinc function kernel at $s = \pm 1$ [Parker *et al*, p.36].

$a = -\frac{3}{4}$ to make the function C2-continuous at $s = \pm 1$; it is still C2-discontinuous at $s = \pm 2$ [see Maeland, 1988].

$a = -\frac{1}{2}$ to make the interpolation function agree with the Taylor series expansion of the function being interpolated to as many terms as possible [Keys, 1981]. In this case this means that the interpolation function can exactly reproduce a quadratic (second-order) function. Park and Schowengerdt [1983] propose this value also, their argument being that $a = -\frac{1}{2}$ gives the best frequency response in that it provides the best low frequency approximation to the ideal reconstruction filter (sinc) and is also particularly effective at suppressing aliasing [*ibid.*, p.265]. Therefore, they state that it is the optimal value of a in the image-independent case.

$a = 0$ is recommended by Maeland [1988] as a strictly-positive two-point cubic reconstructor and is, in fact, the two-point cubic that we derived in section 3.5.5.

"a dependent on the image energy spectrum". This idea, from Park and Schowengerdt [1983], is that the value of a is tailored to the energy spectrum of the image that is to be resampled. They show that, in typical cases, this value should lie in the range $-\frac{3}{4} \leq a \leq -\frac{1}{2}$.

3.6.1 Other criteria

Mitchell and Netravali [1988] performed an experiment to find the combination of values for B and C which gave the best subjective results. They concluded that the reconstructor defined by $B = \frac{1}{3}, C = \frac{1}{3}$ in equation 3.19 is subjectively the best (based on nine experts' opinions). This is neither interpolating nor C2-continuous but a curious blend of two-thirds Catmull-Rom spline (see below) plus one-third approximating cubic B-spline. This reconstructor will exactly reproduce a first-order function as will any reconstructor for which $2C + B = 1$ [Mitchell and Netravali, 1988, p.244], reconstructors for which $2C + B \neq 1$ can only exactly reproduce zeroth-order functions and the reconstructor $C = \frac{1}{2}, B = 0$ (Catmull-Rom spline) can (as mentioned already) exactly reproduce a quadratic function.

Mitchell and Netravali [1988] propose a further reconstructor, $B = \frac{3}{2}, C = -\frac{1}{4}$ which very strongly suppresses rastering artifacts but also blurs the image.

3.6.2 The Catmull-Rom spline

The reconstructor for which $B = 0, C = \frac{1}{2}$ is commonly known as the Catmull-Rom spline. The name derives from a 1974 paper by Catmull and Rom in which they propose a large family of functions defined by the weighted blending of other (usually simpler) functions. Their general form, translated into our notation, is:

$$f(x) = \frac{\sum_i g_i(x) w_i(x)}{\sum_i w_i(x)} \tag{3.21}$$

where the $g_i(x)$ are the original functions, the $\frac{w_i(x)}{\sum_i w_i(x)}$ are the weighting or blending functions, and $f(x)$ is the resulting function. Note that in this model *functions* are blended together, rather than *sample values* as in our model (equation 3.1).

While there are many reconstructors that can be defined using Catmull and Rom's method, one specific example in their paper has become widely known as *the* Catmull-Rom spline. It is generated as follows:

The $g_i(x)$ are defined to be the set of straight lines passing through adjoining points:

$$g_i(x) = f_i \left(1 - \frac{x - x_i}{\Delta x}\right) + f_{i+1} \left(\frac{x - x_i}{\Delta x}\right)$$

The $w_i(x)$ are defined to be offset third order B-splines:

$$w_i(x) = B_3 \left(\frac{x - x_i}{\Delta x} - \frac{1}{2}\right)$$

where:

$$B_3(s) = \begin{cases} \frac{1}{2}s^2 - \frac{3}{2}s + \frac{9}{8}, & \frac{1}{2} \le s \le \frac{3}{2} \\ -s^2 + \frac{3}{4}, & -\frac{1}{2} \le s \le \frac{1}{2} \\ \frac{1}{2}s^2 + \frac{3}{2}s + \frac{9}{8}, & -\frac{3}{2} \le s \le -\frac{1}{2} \end{cases}$$

(Note that $B_3(s)$ is also the kernel of one of our quadratic reconstructors — see equation 3.12.)

This produces the Catmull-Rom spline, which was also chosen by Keys [1981] and Park and Schowengerdt [1983] as the best member of the family of parametric cubics which they were studying.

There is yet another way of deriving the Catmull-Rom reconstructor. It can be generated by taking a linear blend of two *parabolic* functions. This process is explained by Brewer and Anderson [1977] who base their derivation on earlier work by Overhauser [1968]. It is illustrated in figure 3.16.

The unique quadratic through the three points $(x_{\alpha-1}, f_{\alpha-1})$, (x_α, f_α) and $(x_{\alpha+1}, f_{\alpha+1})$ can be shown to be:

$$\begin{aligned} q_\alpha(s) = & \quad (\tfrac{1}{2}s^2 - \tfrac{1}{2}s) f_{\alpha-1} \\ & + \quad (-s^2 + 1) f_\alpha \\ & + \quad (\tfrac{1}{2}s^2 + \tfrac{1}{2}s) f_{\alpha+1} \end{aligned}$$

where $s = \frac{x - x_\alpha}{\Delta x}$. In figure 3.16, $p(r) = q_2(r)$ and $q(s) = q_3(s)$.

From this we can easily derive the cubic, $c_\alpha(t)$:

$$c_\alpha(t) \quad = \quad (1 - t) q_\alpha(t) + t q_{\alpha+1}(t - 1)$$

Which is the Catmull-Rom spline yet again (in figure 3.16, $c(t) = c_\alpha(t)$).

Brewer and Anderson [1977] call this spline the 'Overhauser Curve' after the original inventor of the parabolic blending method. However Overhauser's [1968] statement of the method (and Rogers

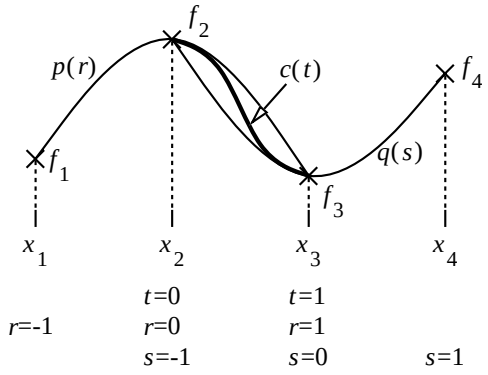

Figure 3.16: Brewer and Anderson's [1977] Overhauser cubic, defined as the linear blend, $c(t)$ of two interpolating parabolas, $p(r)$ and $q(s)$: c(t) = (1-t)p(r)+tq(s) = (1-t)p(t)+tq(t-1) .

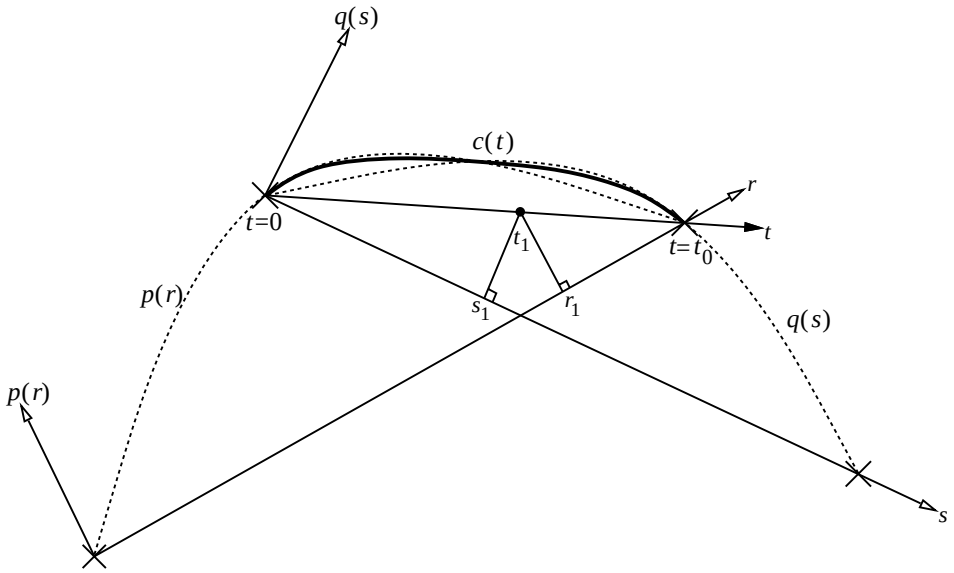

Figure 3.17: How Overhauser [1968] defined the Overhauser cubic (after Overhauser [1968] figure 1, p.1).

and Adams' [1975, pp.133–138] subsequent restatement) uses a slightly different derivation. His derivation uses a local coordinate system for each of the two parabolas, as illustrated in figure 3.17. c(t) is then linearly blended from the two functions, as before, by:

$$c(t) = \left(1 - \frac{t}{t_0}\right) p(r) + \left(\frac{t}{t_0}\right) q(s)$$

To make sense of this it is necessary to have r and s as functions of t. Overhauser chose to define these two functions by dropping a perpendicular from the point t, on the t-axis, to the r- or s-axis, as illustrated by the points t_1, s_1 and r_1 in figure 3.17. Unfortunately, this makes the resulting algebra extremely complex. So much so that it is not worth following for our use[11].

Thus, while Brewer and Anderson [1977] do produce a curve in the spirit of Overhauser, it is not the same curve as that developed by Overhauser [1968].

Brewer and Anderson's 'Overhauser Curve' can be fitted into Catmull and Rom's formalism by defining:

$$\begin{aligned} g_i(t) &= q_i(t) \\ w_i(x) &= B_2(x - i) \\ \text{where} \quad B_2(s) &= \begin{cases} 1 + s, & -1 \le s \le 0 \\ 1 - s, & 0 \le s \le 1 \\ 0, & \text{otherwise} \end{cases} \end{aligned}$$

$B_2(s)$ is a linear blending function. It is the same function as the linear interpolation kernel and the second order B-spline.

We have now seen that the same spline has been derived independently in four different ways. To Catmull and Rom [1974] it was the quadratic B-spline blend of three linear functions; to Brewer and Anderson [1977] it was the linear blend of two quadratics; to Keys [1981] it was the C1-continuous interpolating cubic which matched a Taylor's series expansion to the highest order and to Park and Schowengerdt [1983] it was the C1-continuous interpolating cubic with the best frequency response. As if this were not enough, there is a fifth derivation of the same cubic, which can be found in the next section. The fact that the same cubic has been independently put forward as somehow 'the best' cubic by two separate methods, and is also the end result of three other derivations would seem to be heavy evidence in favour of adopting the Catmull-Rom spline as the best all-round cubic *interpolant*. Mitchell and Netravali's [1988] subjective analysis backs this up; the Catmull-Rom spline falls near the middle of the region of 'satisfactory' subjective behaviour.

Whether the Catmull-Rom spline is the best all-round cubic *reconstructor* is another question. Mitchell and Netravali would say *no*, the reconstructor defined by $B = \frac{1}{3}, C = \frac{1}{3}$ in equation 3.19 is subjectively better, while Reichenbach and Park [1989] in their critique of Mitchell and Netravali's [1988] paper claim that, from a frequency domain analysis, *yes*, the Catmull-Rom spline is the best. Their criterion for 'best' is closeness of the reconstructor's frequency response to that of the perfect reconstructor: sinc. Wolberg [1990, p.132] points out that this disagreement brings into question whether Reichenbach and Parks' criterion for 'best' is useful, as it does not equate to the subjective 'best' and, for pictures for human consumption, it is subjective quality that is important. On the other hand Mitchell and Netravali's experiment involved scaling and sampling as part of the resampling process; so their results judge the subjective quality of the whole resampling, not just the reconstruction. This theme is picked up in chapter 7.

For a given application, it may be desirable to use a different interpolant. In particular, if a strictly positive interpolating kernel is required, then the cubic interpolant with parameter $a = 0$ can be used [Maeland, 1988, pp.215-216]. If an interpolant is required that perceptually sharpens the picture then the cubic interpolant with $a = -1$ can be used [Parker *et al.*, 1983, pp.36, 39].

[11] However, it should be noted that Overhauser's use (CAD) is very different in its requirements to ours.

However, Mitchell and Netravali [1988] claim that this interpolant introduces too much ringing into the reconstructed intensity surface. An interpolant with properties midway between this sharpening interpolant and the Catmull-Rom interpolant can be obtained by using $a = -\frac{3}{4}$ [Parker *et al.*, 1983, p.36].

3.6.3 Other cubic methods

There are many methods for generating cubic reconstructors in the literature. Some fit into our formalism and some do not. Cubic polynomials are the most often used polynomials because lower order polynomials give too little flexibility and higher order polynomials can introduce unwanted wiggles (and require more computation) [Foley *et al.*, 1990, p.478, sec. 11.2]. Their usefulness has lead to a large body of knowledge about them — mostly about their usefulness for describing surfaces in computer aided design (CAD) and its related fields.

It is useful to briefly scan through these methods to see if they shed any more light on useful methods for intensity surface reconstruction. Foley *et al.* [1990] give a summary of the most common of these. We will consider the utility of each one.

Hermite

The Hermite form of a cubic is determined from two endpoints and tangents (first derivatives) at those endpoints. The formula for a piecewise Hermite is: [Foley and van Dam, 1982, p.516]:

$$\begin{aligned} f(x) &= \begin{bmatrix} t^3 & t^2 & t & 1 \end{bmatrix} \begin{bmatrix} 2 & -2 & 1 & 1 \\ -3 & 3 & -2 & -1 \\ 0 & 0 & 1 & 0 \\ 1 & 0 & 0 & 0 \end{bmatrix} \begin{bmatrix} f_\alpha \\ f_{\alpha+1} \\ f'_\alpha \\ f'_{\alpha+1} \end{bmatrix} \\ &= (2t^3 - 3t^2 + 1)f_\alpha \\ &\quad + (-2t^3 + 3t^2)f_{\alpha+1} \\ &\quad + (t^3 - 2t^2 + t)f'_\alpha \\ &\quad + (t^3 - t^2)f'_{\alpha+1} \end{aligned}$$

where $\alpha = \left\lfloor \frac{x - x_0}{\Delta x} \right\rfloor$ and $t = \frac{x - x_\alpha}{\Delta x}$ as usual.

Here f_i are the sample values, as before, and f'_i are the tangents of the sampled function at the sample points[12].

We will not, in general, have these tangent values as we are dealing with NAPK reconstructors. However, Mitchell and Netravali [1988] show that, if these tangent values are available (as, for example, is possible with some artificially generated images), then the Hermite form produces a better result than the best cubic reconstruction based only on the sample values.

In the absence of explicit tangent information, it is common to approximate the tangent by the difference between adjacent sample values. That is:

$$f'_i \approx (\Delta x)\frac{\Delta f_i}{\Delta x} = \Delta f_i = f_{i+1} - f_i$$

[12] N.B. $f'_i = \frac{df}{dt}\Big|_{x=x_i}$ because the equation is in terms of t rather than x:

$$f'_i = \frac{df}{dt}\Big|_{x=x_i} = \frac{df}{dx}\frac{dx}{dt}\Big|_{x=x_i} = (\Delta x)\frac{dx}{dt}\Big|_{x=x_i}$$

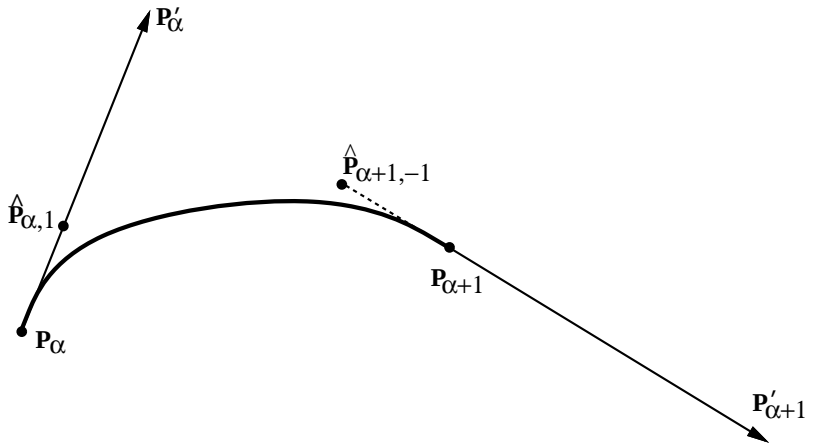

Figure 3.18: How the Bezier and Hermite cubics are related: the Hermite form of the curve is controlled by the two data points, $\mathbf{P}_\alpha$ and $\mathbf{P}_{\alpha+1}$ and by the two derivative vectors $\mathbf{P'}_\alpha$ and $\mathbf{P'}_{\alpha+1}$; the Bezier form is controlled by the two data points, $\mathbf{P}_\alpha$ and $\mathbf{P}_{\alpha+1}$ and by two other control points, $\hat{\mathbf{P}}_{\alpha,1}$ and $\hat{\mathbf{P}}_{\alpha+1,-1}$. The relationship between these is given in equations 3.22 and 3.23.

The approximation $f'_i \approx f_i - f_{i-1}$ is equally valid and it is the average of these two approximations that is generally taken:

$$f'_i \approx \frac{\Delta f_i + \Delta f_{i-1}}{2}$$

where $\Delta f_j = f_{j+1} - f_j$.

If this approximation is used in the Hermite cubic then resulting function is the Catmull-Rom spline. This is the fifth derivation of the Catmull-Rom spline (mentioned in section 3.6.2). Reichenbach and Park [1989] independently discovered this derivation of the spline.

Bezier

The Bezier form of the cubic is related to the Hermite. It uses four control points for each piece: two endpoints plus two other points to control the shape of the curve. If we take the two endpoints to be (x_α, f_α) and $(x_{\alpha+1}, f_{\alpha+1})$ and the two control points to be $(\hat{x}_{\alpha,1}, \hat{f}_{\alpha,1})$ and $(\hat{x}_{\alpha+1,-1}, \hat{f}_{\alpha+1,-1})$. The location of these two control points is linked to the Hermite form by the formula: [see Foley and van Dam, 1982, p.519].

$$\hat{\mathbf{P}}_{\alpha,1} = \mathbf{P}_\alpha + \frac{1}{3}\mathbf{P'}_\alpha \tag{3.22}$$

$$\hat{\mathbf{P}}_{\alpha+1,-1} = \mathbf{P}_{\alpha+1} - \frac{1}{3}\mathbf{P'}_{\alpha+1} \tag{3.23}$$

This relationship is illustrated in figure 3.18.

The Bezier form can be used in two ways: either by defining the control points in some way, or by using the existing data points as control points. The former method presents us with a situation similar to that with the Hermite: how do we define these extra points? If we have the derivative values then we can use equations 3.22 and 3.23 to calculate the positions of the control points and thus produce a Hermite cubic as before.

Rasala [1990] shows how the positions of the control points can be computed from all the available data[13], this is discussed in section 4.5.1. However, his first approximations to this globally con-

[13]Theoretically all of the available data should be used. In practice it is only necessary to use the 12 to 16 nearest points, still rather more than the four nearest points we are using here.

trolled piecewise cubic, which require four defining points are, in one case the Catmull-Rom spline (again!) and in the other case, the one-parameter cubic (equation 3.20) with $a = -\frac{3}{8}$.

The second way of using a Bezier is either to allow every third sample point be an endpoint (of two adjoining sections) with the intermediate points being the other control points, or to use the four nearest points as the control points. The former produces a curve which, in general is only C0-continuous and interpolates only one third of the points. The latter produces a curve which in general is discontinuous and not interpolating. For these reasons, neither is useful.

B-splines

The uniform non-rational cubic B-spline [Foley *et al*, 1990, pp.491-495] is the reconstructor defined by setting $B = 1$ and $C = 0$ in equation 3.19, otherwise known as the approximating cubic B-spline.

Non-uniform, non-rational B-splines [Foley *et al.*, 1990, pp.495-500] have advantages over the uniform rational B-spline, in that the knots do not have to be uniformly spaced in parameter space and knots can have a multiplicity which creates a Cn-discontinuity at the knot. Neither of these properties is useful for intensity surface reconstruction because the samples are uniformly spaced in parameter space ($\alpha = \frac{x-x_0}{\Delta x}$) and there is no need for multiple knots. Thus non-uniform, non-rational B-splines offer features that we do not need. They could be useful if we had an image that was not sampled uniformly.

Non-uniform rational B-splines (NURBS) [Foley *et al.*, 1990, pp.501- 504; Piegl, 1991], have many features which make them extremely useful in CAD/CAM and other graphics applications. However, for image reconstruction they are 'over the top' because, again, the extra features that they provide are unnecessary for reconstruction. These features are similar to those for non-uniform, non-rational B-splines, plus the fact that they can precisely define any conic section.

β-splines

β-splines [Foley *et al.*, 1990, pp.505-507] have two extra parameters: β_1, the bias parameter, and β_2, the tension parameter. These are used to further adjust the shape of the B-spline curve. They can be either local to each control point ('continuously shaped β-splines' or 'discretely shaped β-splines') in which case we are again faced with the problem of how to derive these two extra data for each point, or are global ('uniformly shaped β-splines') in which case we need to find acceptable values for β_1 and β_2. β_1 biases each segment more towards either its left-hand control points ($1 < \beta_1 \leq \infty$) or its right-hand control points ($0 \leq \beta_1 < 1$). This is undesirable in our case as there should be no global bias in either direction. Thus we must constrain $\beta_1 = 1$.

This makes the β-spline C1-continuous:

$$\begin{aligned} f(x) = \quad & \frac{1}{12+\beta_2}\big[(-2t^3+6t^2-6t+2)f_{\alpha-1} \\ & ((2\beta_2+6)t^3+(-3\beta_2-12)t^2+(\beta_2+8))f_\alpha \\ & ((-2\beta_2-6)t^3+(3\beta_2+6)t^2+6t+2)f_{\alpha+1} \\ & (2t^3)f_{\alpha+2}\big] \end{aligned}$$

where $\alpha = \left\lfloor \frac{x-x_0}{\Delta x} \right\rfloor$ and $t = \frac{x-x_\alpha}{\Delta x}$.

If $\beta_2 = 0$ then this is the ordinary cubic B-spline, which can be represented by the Mitchell and Netravali cubic (equation 3.19) with $B = 1$ and $C = 0$. However, if $\beta_2 \neq 0$ then this function cannot be represented by equation 3.19 and so it cannot be meeting all of the criteria met by equation 3.19. A little analysis shows that it does not have linear phase for $\beta_2 \neq 0$ and so we must reject it for this reason (see section 3.5.1).

The final cubic in Foley *et al*'s [1990, p.507] list is the Kochanek-Bartels function; a variant of

the Hermite cubic where each segment depends on the four nearest control points and three extra parameters specific to that segment. As with the Hermite curve the problem with using this function is that we have no way of generating these extra parameters.

This completes the list of cubics given by Foley *et al* [1990]. Others do exist and some families have been given names which have not been mentioned here, for example the Mitchell and Netravali cubics with $C = 0$ are Duff's tensioned B-splines [see Mitchell and Netravali, 1988, p.223]. Most of these functions have been primarily designed for CAD; few of them are applicable to reconstruction. The aims of the two fields are different, there tends to be more data available for describing the curve in CAD than in resampling (for example: derivative values), thus allowing these more complex forms, and CAD has greater need of weird and wonderful properties in its curves than resampling (for example: discontinuities at some sample points, and not at others). However, this section has, at least, considered the utility of these functions. The approximating cubic B-spline has already been met as a case of equation 3.19. The interpolating cubic B-spline and interpolating Bezier cubic are discussed in chapter 4.

3.6.4 Summary

It would appear that the all-round best cubic *interpolant* is the Catmull-Rom spline. There is less consensus on the all-round best cubic *reconstructor*, but Mitchell and Netravali's results would indicate that it is some linear blend of the Catmull-Rom spline and the cubic B-spline:

$$f(x) = (1 - \zeta)\text{CatRom}(x) + \zeta\text{BSpline}(x)$$

with ζ closer to zero than one. Mitchell and Netravali [1988] recommend $\zeta = \frac{1}{3}$, while Reichenbach and Park [1989] recommend $\zeta = 0$.

3.7 Higher orders

In section 3.5.10 we saw the multitude of conditions which it would be useful to get a reconstructor to obey. It would be almost impossible to meet all these conditions. If we look at the Catmull-Rom spline, it does meet most of the conditions but fails in that it is not C2-continuous and its frequency response, while the closest to the perfect frequency response of any cubic [Reichenbach and Park, 1989], is still not particularly close to it (Note that the approximating cubic B-spline is the only C2-continuous cubic, and it is not an interpolant. It produces a rather blurry intensity surface.) The solution to this problem could be to go to a higher-order.

Parker *et al* [1989, p.39] state that "although the length [cubic function, 4 data points] for interpolating functions is adequate for many tasks, additional improvement in performance could be made by including more points in the calculation. The same criteria used for selecting interpolating functions used in this paper — frequency responses, phase shift and gain — would also be useful in selecting between functions with a longer extent."

Keys [1981, pp.1159-60] six point cubic function has an $O(h^4)$ convergence rate to the Taylor series expansion of the function being interpolated. As cubics can give at most $O(h^4)$ accuracy, it immediately follows that higher order convergence rates require higher order piecewise polynomials.

However, Mitchell and Netravali [1988, p.225] believe that no simple filter (such as a piecewise local polynomial) will be found that will improve much on the cubic filters they have derived. They thus suggest that other avenues of research would be more fruitful. Further, Foley and van Dam [1982] note that higher order polynomials can introduce unwanted wiggles in the reconstructed function.

Quadratics and cubics allow a single lobe, or ripple, either side of an edge, which perceptually sharpens the edge (section 4.5.2). Quartics, and higher orders, allow more ripples either side, which can perceptually degrade the image. Hence it may be counter-productive to go to higher orders than cubic.

We have done little work on fifth, and higher, order piecewise polynomials and so cannot give evidence as to the validity of these arguments. It should be fairly simple, though, to extend our analysis to higher orders. We leave this for future work. However, there seems to be little room for significant improvement, and so, perhaps, the subject of piecewise local polynomials should be closed.

3.8 Summary

We have seen several ways of classifying reconstructors, including local *vs* non-local, and skeleton *vs* continuous. Skeleton reconstruction describes a situation where the intensity surface is defined only at specific points, and is undefined elsewhere. Delta function reconstruction is a similar idea.

The bulk of this chapter was devoted to piecewise local polynomials. There are, by far, the most studied group of local reconstructors. They are easily understood, quickly implemented, and fast to evaluate. We proved that zero-phase piecewise local quadratics do exist, and derived two new quadratic reconstructors. One of these provides similar visual quality to the Catmull-Rom cubic, with faster evaluation.

The study of quadratics led into an examination of the factors involved in the design of reconstructors. This in turn brought us to a discussion of piecewise local cubics. Here we saw that the evidence indicates that the Catmull-Rom cubic is the best all-round cubic interpolant, and that it, or some linear mix of it and the cubic B-spline, is the best all-round cubic reconstructor.

Chapter 4

Infinite Extent Reconstruction

In the previous chapter we discussed the most studied group of reconstructors, the piecewise local polynomials. We now turn our attention to other classes of reconstructor:

1. the infinite reconstructors
2. the local approximations to the infinite reconstructors
3. the *a priori* knowledge reconstructors.

The first two are discussed in this chapter. The final class we leave until chapter 6.

4.1 Introduction to infinite reconstruction

Into this class fall all the reconstructors which use all of the sample points in the image. We will concentrate on these four:

- sinc interpolant
- Gaussian approximant
- interpolating cubic B-spline
- interpolating Bezier cubic

All these methods are based on a theory of an infinite image; that is: the theory does not take the image's edges into account. In a practical situation the image has edges and these must be dealt with if we are to use an infinite reconstructor. Edge effects and the edge extension solutions are discussed in the next section.

4.2 Edge effects

While the finite size of real images is a readily apparent problem for infinite extent reconstructors, the problem exists to a lesser extent for finite-extent reconstructors, such as those discussed in the previous chapter. It is feasible that a certain transformation, reconstructor, and sampler may combine to produce a resampling which never needs to access data beyond the edge of the image, but in general, we have to answer the question: what is out there?

The simple answer is that nothing is out there, we know absolutely nothing about the intensity values beyond the edges of our finitely sized image. This is unfortunately of little use in cases where we need to know the value of a sample beyond the edge of the image.

There are at least eight ways of specifying the values of the pixels beyond the image's edge; thus producing an infinite image from a finite one. These are:

1. Undefined
2. Error Limits
3. Constant
4. Extrapolation
5. Replication
6. Reflection
7. Transparent
8. Special Cases

The last one requires special knowledge about the reconstructor involved and must be tailored to suit. The others are independent of the reconstructor.

There are *two* types of occurrence which require information about pixel values beyond the edge of the image: (a) when we require the value of the intensity surface at some point within the finite image's edges, but, to calculate the value at that point, the reconstructor needs pixel values from beyond the edge of the image; and (b) when we require the value of the intensity surface at some point outside the finite image's edges. Figure 4.1 gives an example of both these types of pixel. It is possible to use a different method to generate intensity surface values of type (a) from that used for type (b). For example, type (a) could be generated by some edge extension method while type (b) is given a constant value. In most situations, these two cases collapse nicely into the single case: 'when the reconstructor requires the value of a pixel beyond the image's edges'.

In figure 4.1 the shaded band shows the area near the edge of the image where the reconstructor needs values beyond the image's edge to produce intensity surface values. For an infinite extent reconstructor this shaded area extends over the whole image, but for finite extent reconstructors it is a band, usually a few pixels wide, around the edge of the image. It is non-existent only for nearest-neighbour, skeleton, and Delta-function reconstruction.

The necessity of edge extension depends on the reconstructor, transformer, and sampler used. If they form a resampling where the required portion of the intensity surface lies within the inner region in figure 4.2 (region A) then no image extension is required, and no edge effects will occur. An example is shown in figure 4.3(a). However, many resampling applications require values of the intensity surface in region B (the band) and often also in region C (the outer region). An example is shown in figure 4.3(b). In these cases we must decide how to perform edge extension and how to minimise the resulting edge effects.

There are two possible ways of defining edge extension. One is to assign values to the unknown pixels and use the reconstruction method on these assigned sample values to generate the intensity surface. The other method may give values to some, or all, of these unknown pixels but it also overrides the reconstruction method by explicitly defining part of the intensity surface, usually region C in figure 4.2.

Little work has been done on the edge extension problem. The usual assumption that is made is that any pixel outside the image has the intensity zero [Fiume, 1989, p.78, definition 16; Pratt, 1978, ch.9]. Two other common assumptions are that the image is repeated (that is: it tiles the plane), or that it is mirrored and repeated. These are illustrated later in the chapter. White and

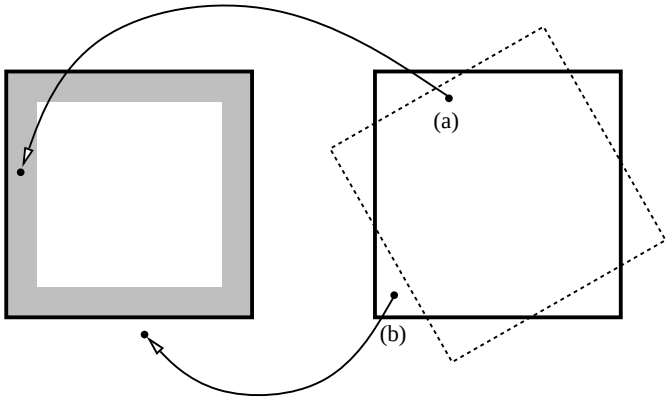

Figure 4.1: The two types of destination pixel for which edge effects are important. The image on the left is rotated (dashed line on right) to produce a new image (solid line on right). The shaded area in the left hand image represents that part of the reconstructed intensity surface whose values depend on samples outside the image's edges. Pixel (a) in the final image lies within the original image's edges but its value depends on sample values outside those edges. Pixel (b) lies within the final image's edges but outside the original image's edges.

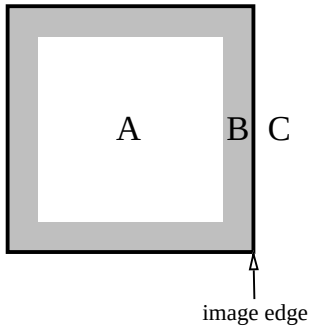

Figure 4.2: The three areas of an image: A: the intensity surface in this area depends only on pixel values within the image's edges. B: the intensity surface in this area depends on pixel values both inside and outside the image's edges. C: the intensity surface in this area lies outside the image's edges.

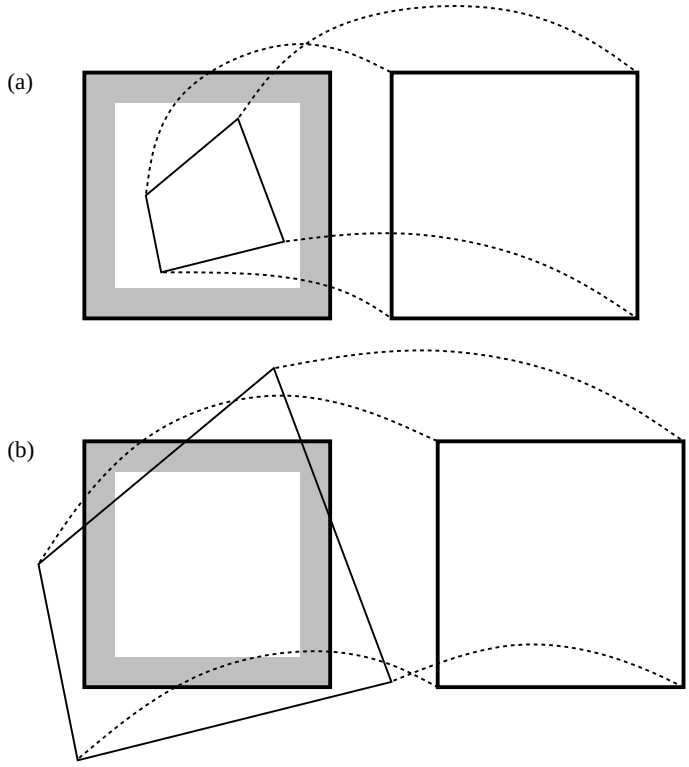

Figure 4.3: Two examples of transforms, one requiring edge extension and one not. (a) all intensity surface values in the final image (right) lie within region A (figure 4.2) in the original image, so no edge extension is required. (b) Intensity surface values in the final image lie in all three regions of the original image, so some edge extension is required.

Brzakovic [1990] present two novel methods of image extension but, otherwise, there appears to be little published on it. These, and other, methods of edge extension are discussed in detail below.

4.2.1 The methods of edge extension

Edge extension is fundamentally the process of producing pixel values outside the image's edges for the reconstructor to operate on, thus producing an intensity surface of infinite extent. It also includes those methods which explicitly define part of the intensity surface to have values independent of the reconstructor. The ensuing discussion covers the eight methods of edge extension.

(1) Undefined

Our opinion is that this is the philosophically correct value to give to those pixels which lie beyond the image's edges. We don't know what these values are and so they should remain undefined. Furthermore, if the value 'undefined' occurs in the definition of the intensity surface's value at any point then that intensity surface value is also undefined.

The practical upshot of this is that the only part of the intensity surface which is defined is that which lies within the inner boundary of the shaded area in figure 4.2 (region A). So, if we have an $N \times N$ image, and a reconstructor which requires an L pixel wide boundary, the resulting intensity surface will be defined over only $(N - 2L) \times (N - 2L)$ pixels. This assumption is often used in other image processing operations, where the loss of a few pixels is unimportant. For example, see Fang, Li and Ni's [1989] discussion of two dimensional convolution.

In resampling, however, this solution is unworkable. Firstly, if we use an infinite extent reconstructor, practically the entire intensity surface will be undefined[1]. Secondly, and more importantly: in most cases, some of the destination pixels will have an undefined value. It is impossible to display 'undefined' as it is not a real intensity value.

We could decide that a pixel with an undefined value is displayed with some constant intensity but, if we do this, undefined pixels cannot be distinguished from pixels which really have that intensity. Further, if undefined values are stored as this constant value then errors will occur if the destination image is the source for further processing unless we also keep note of which stored pixels are defined and which are not.

The problem has a simple solution in Fang, Li and Ni's case. Their destination image is simply smaller than the source, and there are no undefined pixels within the destination's edges. In our general resampling case we cannot guarantee this, and, if we do display an image which contains undefined pixels we must display them with some intensity other than 'undefined'. We cannot have undefined pixels and display them too!

This particular solution to the edge problem, while philosophically sound, is unsatisfactory for practical purposes. We must look to other solutions.

(2) Error bounds

In the previous case we assumed that we knew nothing about the value of the pixels beyond the image's edges. This is untrue, in that we will, in general, know the bounds within which these pixel values are constrained to lie. If we are dealing with an image representation which bounds all pixel values between two extrema, then we can assume that all the unknown pixel values must lie between them also.

Having defined bounds within which the unknown pixel values can lie, it is possible to calculate bounds within which the intensity surface must lie, as illustrated in figure 4.4. Thus, for every destination pixel, it is possible to give an upper and a lower bound to the pixel's value. For some destination pixels (under some reconstructors) these two bounds will be equal to one another and for some they will be equal to the extrema, or even beyond them, as in figure 4.4(Catmull-Rom cubic).

It may be thought that the error bounds of source pixels just beyond an image edge should be less separated than those well beyond the edge. That is: the error bounds should increase as one moves away from the edge until they reach the extrema (figure 4.5(b)). Unfortunately, this is not the case. Theorem 1 gives the lie to the scenario in figure 4.5(b) for a general image.

Theorem 1 *The first unknown pixel beyond an image's edge can take any value between the extrema.*

Proof: Whittaker [1915] proves that, for *any* set of equispaced samples,

$$F_\infty = \{(x_i, f_i) : i \in \mathcal{Z},\, x_i = x_0 + i\Delta x\}$$

there exists a unique function, $f(x)$, through those sample points such that $f(x)$ is bandlimited to below $\frac{1}{2\Delta x}$ (later named the folding frequency[2]).

[1] 'practically' because, for example, a sinc reconstructed intensity surface would be undefined everywhere except at the sample points, where it would be equal to the sample value at that point.

[2] note that the Nyquist frequency of $f(x)$ will be less than or equal to the folding frequency [see Lynn and Fuerst, 1989, p.11]

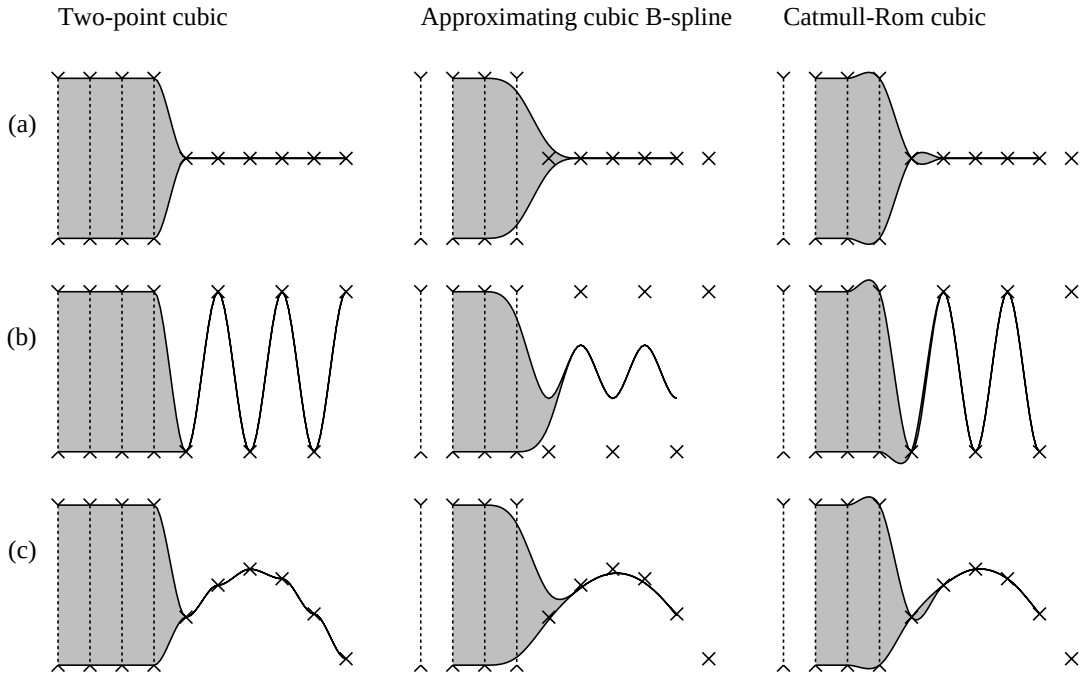

Figure 4.4: Error bounds on intensity surface values. The crosses mark known pixel values, the dotted vertical lines unknown pixel values, bounded above and below. The shaded area shows the range of values within which the intensity surface can lie. Here we show three local piecewise polynomial reconstructors operating on three situations: (a) constant intensity; (b) oscillating intensity; (c) slowly varying intensity.

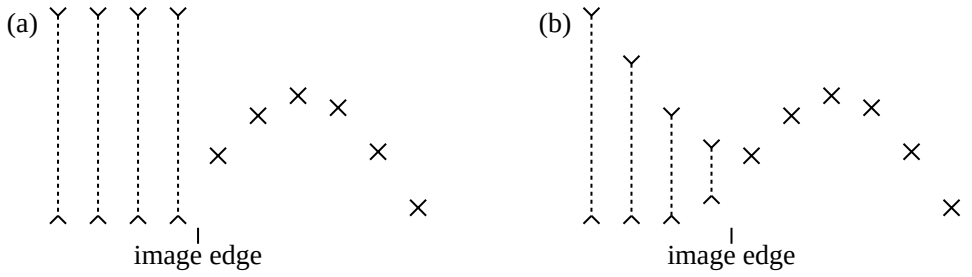

Figure 4.5: Two possible scenarios for error bounds on unknown pixels. (a) all unknown pixels can take any value between the extrema; (b) pixels close to the image edge are more tightly bounded than those farther away. Theorem 1 gives the lie to the scenario in (b).

Now, our image is of finite extent:

$$F_{a,b} = \{(x_i, f_i) : i \in [a, b],\, x_i = x_0 + i\Delta x\}$$

and we have assumed that we do not know the values f_i, $i \notin [a, b]$. By assigning values to these, an infinite number of infinite sets, F_∞, can be created; each containing the set $F_{a,b}$. Thus, from Whittaker's result, we see that there are an infinite number of bandlimited functions which pass through any finite set of sample points.

Therefore the first unknown pixel (f_{a-1} or f_{b+1}) can take any value and there will still be a bandlimited function through the set of samples. If all the samples are constrained to lie between two extrema then these first unknown pixels will be able to take any value between them. QED.

If we know that the image is bandlimited to below the folding frequency then we may be able to define tighter bounds than the extrema for unknown pixels close to the image's edge. In general, we do not have this *a priori* knowledge, therefore all unknown pixels are bounded between the extrema.

This solution to the edge problem has much the same drawbacks as the previous solution: (1) it is impossible to display a range of intensities for a single pixel; (2) an infinite extent reconstructor will contain some uncertainty at practically every point. For example, the sinc reconstructor would produce bounds at the extrema for all but the known sample points.

A solution to this problem would be to display the mean of all possible values at each point. However, calculating this mean is not a simple matter. An approximation to the mean could be obtained by setting all unknown values to the mean of the two extrema and calculating the intensity surface from these. This collapsing of the error bounds onto a single value takes us to a third solution: the constant value.

(3) Constant

The solution most often adopted is to set all unknown pixels to be a constant value. By common consent it appears that this value is invariably chosen to be zero, which nearly always represents black.

Zero, at first glance, is a sensible value. Any multiplications involving zero evaluate to zero and thus need not be performed. Thus, for any reconstructor that can be represented by a filter, no unknown values need to be taken into consideration when producing the intensity surface because they contribute nothing to the evaluation of the surface values.

However, the identification of zero with black[3] is unfortunate. Black is at one end of the spectrum of possible intensity values. We are thus setting all unknown pixels to one of the two extreme values. In other applications, for example sound and electrical current, zero is an average value. The signal can fluctuate to positive or negative. With intensity, zero is a minimum value — you cannot have negative light. While it is sensible to set zero intensity to be absence of light (in a similar way to zero mass being absence of mass) and setting unknown values to be zero can be justified (an identification of 'nothing' with 'nil'), the combination of the two produces a problem, in that it can cause excessive ringing artifacts, and negative intensities near the image's edges.

The previous edge extension method contains the seed of a better constant value: the value halfway between the two extrema; a mid-grey. Using mid-grey in place of any unknown value minimises the maximum discrepancy between the last known value and the first unknown value on either side of an edge (see figure 4.6).

Purists may balk at the idea of using any value but zero to replace the unknown values. A simple solution to this objection is to subtract the mid-grey value from all pixels in the image, set unknown pixels to zero, resample the image and then add back the mid-grey value. However, this only works

[3] or, in some rare cases, with the brightest white, for much the same effect.

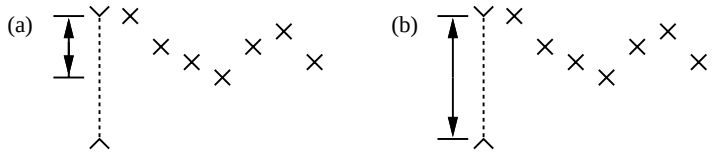

Figure 4.6: Minimising the maximum discrepancy between pixel values and the constant value. (a) using a mid-grey constant, the maximum discrepancy is half the full range; (b) using a black constant, the maximum discrepancy is the full range.

for resamplings in which the final pixel values are linear combinations of the original pixel values, which, fortunately, are the great majority of resamplings (see section 2.2).

Another candidate constant value is the average value of all the known image pixels. One motivation behind this choice is that it retains the DC component of the frequency spectrum: the DFT of the finite image and the FT of the infinite extended image have the same DC component. In most cases this average value would be close to the suggested mid-grey value. For the minority of cases in which the image is unusually dark or unusually light, this average value is a better choice than the mid-grey. For the rare situations with a dark centre and bright edge (or vice-versa) it is conceivable that this average would be a worse choice than the mid-grey.

Though, overall it would appear that the average value would be slightly preferable to the mid-grey value, this advantage must be offset against the need to calculate the average. Taking this into consideration, there is little to choose between the two values.

Use of a constant intensity beyond the edges of the image is simple and efficient. It requires little computational effort (except when the average intensity of the known image values needs to be calculated, but even that need only be done once per resampling). When a destination pixel falls well outside the edge of the transformed source image it will, in general, be given a value close to the constant value. However, just inside and just outside the source image edge, the reconstructed surface will display 'edge effects'. The severity of these effects depends partly on the difference between the pixel values just inside the edge and the constant value assigned to the unknown pixels just outside the edge. It also depends on the reconstructor used. The sinc interpolant produces many obvious artifacts, while a very local reconstructor, such as linear interpolation, displays virtually no artifacts at all (see figure 4.7).

We can attempt to reduce this edge effect problem by extrapolating more 'sensible' values off the edge of the image rather than simply setting all the unknown pixels to a constant.

(4) Extrapolation

Extrapolation out from the edge of the image is an attempt to make what is beyond the edge bear some relation to what is inside the edge. It cannot create any extra information, but the hope is that the available information can be used to produce sensible values for the unknown pixels.

Extrapolation is considerably more hazardous than interpolation [Press *et al*, 1988, p.85]. A typical interpolating function (which is perforce an extrapolating function) will tend to go berserk at a distance beyond the image edge greater than the inter-pixel spacing [*ibid.*, p.88]. We must be careful how we extrapolate.

One advantage we have over general extrapolation is our knowledge of the bounds within which the values must lie. These can be used to prevent the values from going berserk and reaching values way beyond the bounds.

The simplest extrapolation method is to copy the final row of pixels to infinity. This is illustrated in figure 4.9 which shows the images in figure 4.8 extrapolated by this method. White and Brzakovic [1990] modify this idea by assigning a virtually constant intensity to each unknown

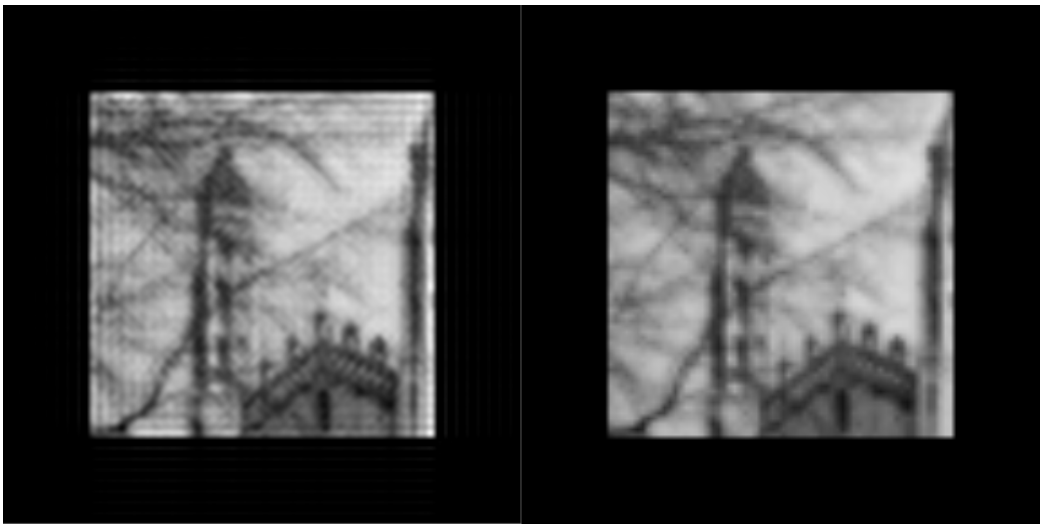

Figure 4.7: The effect of a constant zero edge extension on two reconstructors. On the left is the intensity surface reconstructed by sinc interpolation, notice the ripples near the image edges (both inside and outside of the edges), caused by the sharp fall off to zero. On the right is the intensity surface reconstructed by linear interpolation. The only edge effect is a slight fading off at the very edge of the image. The right hand image is quite blurry, but this is a property of the reconstructor, not an edge effect.

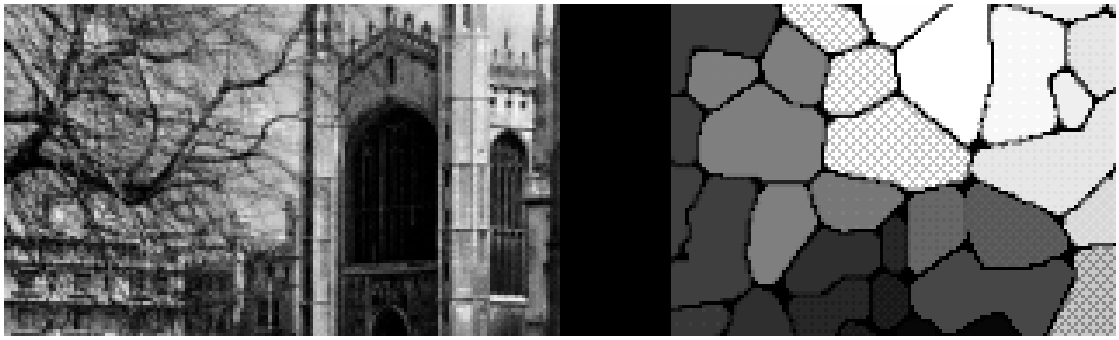

Figure 4.8: The original images used in the extrapolation examples.

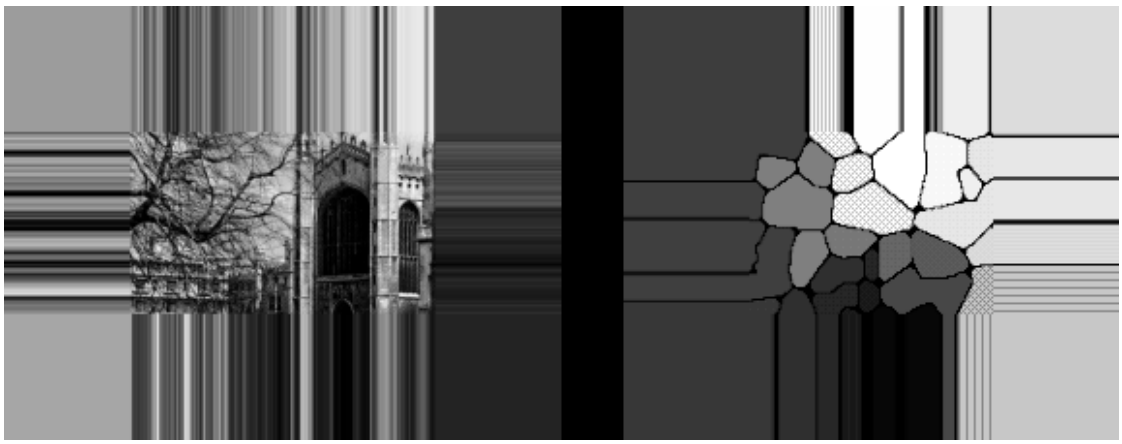

Figure 4.9: Extrapolation by copying the final row of pixels off to infinity. This process is applied to the two images in figure 4.8

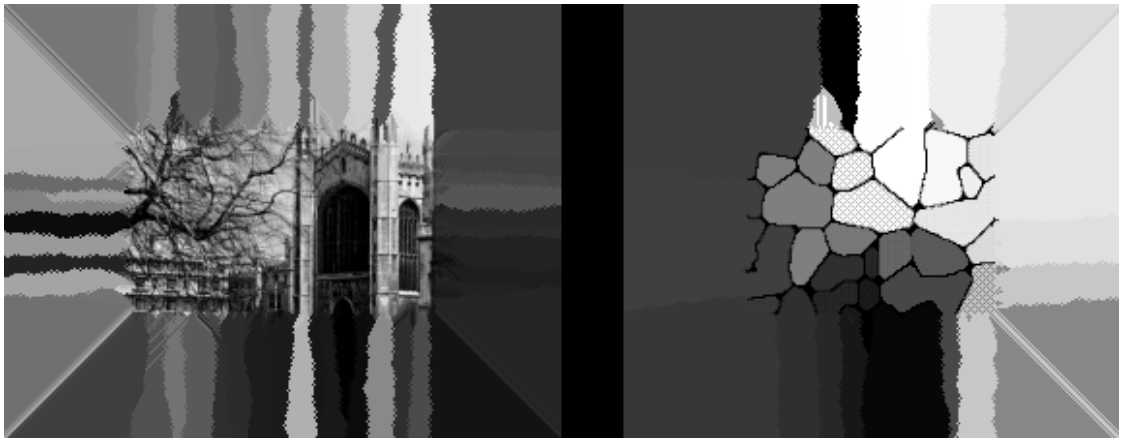

Figure 4.10: Extrapolation by White and Brzakovic's [1990] derivative method, which resolves ties (equal derivative values in two or three directions) by using a random number generator. This process is applied to the two images in figure 4.8

half-row or half-column[4]. These values are based on a set of known pixels in that row or column. This, their 'random sequence' method, uses the n pixels on the row (or column) just within the image edge to calculate the values using linear extrapolation under the assumption that the image intensities form a random field. The values assigned to an unknown half-row or half-column are not quite constant, they are very slowly varying, but the effect looks much the same as a constant [see White and Brzakovic, 1990, figs. 3(b) and 3(c), 4(b), and 4(c) and 5(b) and 5(c)].

White and Brzakovic point out that, while this method generates pixels whose statistical properties are close to those of true pixel within a few pixels of the image edge, this closeness deteriorates farther from the edge. For our purposes, this method gives little advantage over simple pixel replication. It requires much more calculation and this outweighs the slightly better estimate of the unknown pixel values just beyond the edge.

White and Brzakovic's [1990] second image extension method holds more promise. This 'derivative' method attempts to preserve the directionality of the pattern lying along the image border. It is more successful than the other methods in generating natural looking images for a small extension, but it deteriorates at greater distances from the image's edges. The images in figure 4.10 were generated using generalised Sobel operators of size 3×3 [Rosenfeld and Kak, 1982, vol. 2, pp.96, 99–100] to calculate the derivative values[5]. A modification of their method which resolves ties by taking the average intensity of the tied pixels produces very similar results (figure 4.11). The

[4]A half-row is all of the pixels in a row of pixels to the right (left) of a given pixel. An unknown half-row is all of the unknown pixels to the right (left) of the image edge. A similar definition holds for 'half-column' and 'unknown half-column'.

[5]Note that there are two errors in White and Brzakovic's paper:
(1) Equation 6 (page 348) should read:

$$D(j,i) = \sum_{m=1}^{k} \sum_{n=1}^{k} M_\phi(m,n) I\left(j-(k+1)+m, i+n-\lambda-\frac{k+1}{2}\right)$$

where $\lambda = \frac{k+1}{2}\tan\phi$ and $m, n \in \{1, 2, \ldots, k\}$.
Alternatively and equivalently:

$$D(j,i) = \sum_{m=0}^{k-1} \sum_{n=0}^{k-1} M_\phi(m,n) I\left(j-k+m, i+n-\lambda-\frac{k-1}{2}\right)$$

where $\lambda = \frac{k+1}{2}\tan\phi$ (as before) and $m, n \in \{0, 1, \ldots, k-1\}$.
And (2) using this formula, pixels A, B and C in figure 2 (page 344) are the centre pixels for estimating derivatives for 5×5 derivative masks but not for any other size.

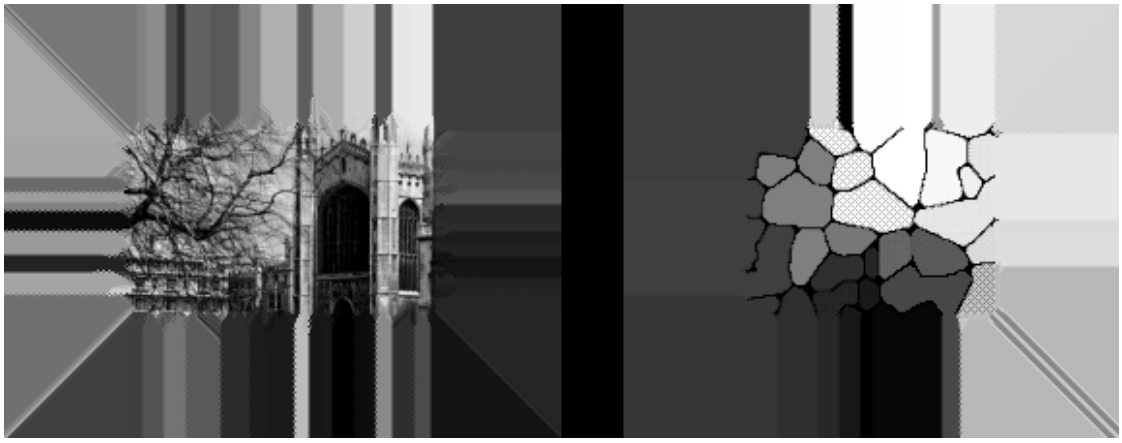

Figure 4.11: Extrapolation by a modification of White and Brzakovic's [1990] derivative method. This modification resolves ties by taking the average of the intensities in the tied directions. This process is applied to the two images in figure 4.8

original method resolves ties in two or three directions by the use of a random number generator.

Extrapolation is a risky business. Even these moderately sophisticated methods only succeed for a small distance out from the image edge. This is good for small kernel operators, those which only need information up to a few pixels out (for example: a local reconstructor calculating values just inside the image's edges and needing some pixel values from just outside). But they are not useful for infinite operators nor for large kernel operators (although White and Brzakovic [1990] imply that they need to use kernels up to size 47×47, an edge extension of 23 pixels). Nor are they particularly useful for finding a pixel value when the destination pixel maps to a source pixel well outside the image's edge (case (b) in figure 4.1). Because extrapolation is inaccurate at large distances from the pixel edge we propose the following 'hybrid' solution:

> For any pixel farther outside the image edge than a given distance, the pixel's value is a given constant. Between this region's boundary and the image edge the pixels are given extrapolated values such that they match up neatly with both the image and the constant at the respective edges.

Figure 4.12 illustrates this concept.

There are still questions to be answered: what constant to use, how wide the extrapolated region should be, how to perform the extrapolation. However, this solution holds promise in that: (a) it has not got the sharp changes in intensity at the image edge that the constant solution has, and (b) it does not tend to produce bad results at great distances from the image edge, as straightforward extrapolation can do.

Our discussion in the previous section gives us guidance as to which constant value to use. The three useful possibilities are:

- zero (usually black), because of the simplification this can make to the calculation of intensity surface values;
- half-way between the minimum and maximum intensities (a mid-grey), because this minimises the maximum possible difference between the intensity of an edge pixel and the constant intensity[6];

[6] an 'edge pixel' is the last known pixel, on a row or column, just within the image's edge.

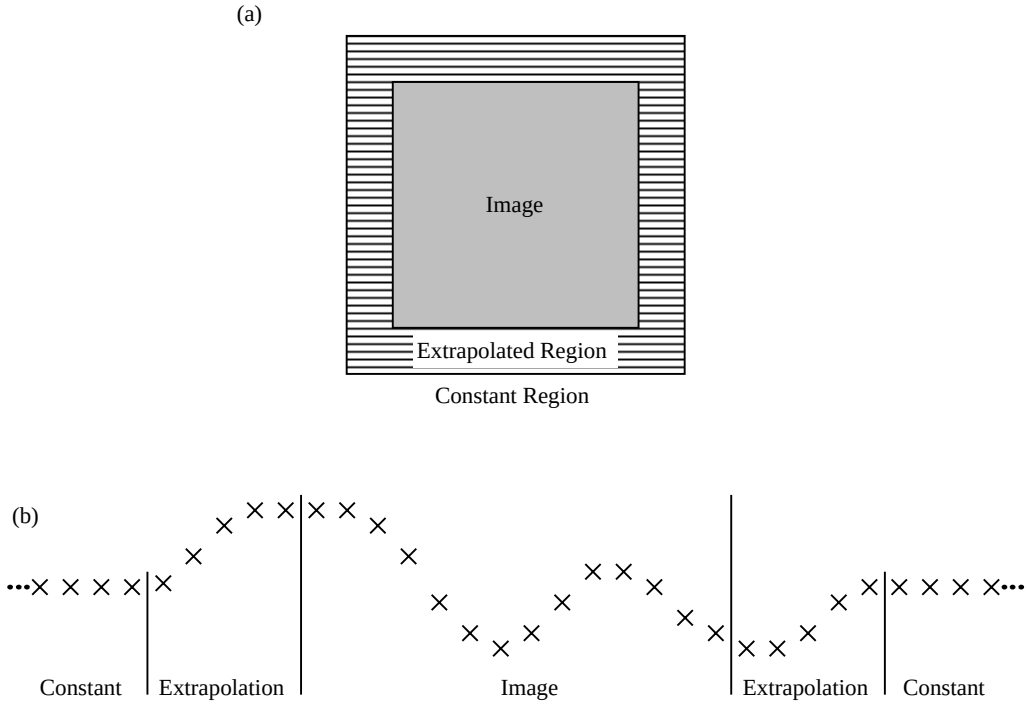

Figure 4.12: Extrapolation to a constant. (a) shows the basic idea: the image is surrounded by an area that is extrapolated, beyond this area the pixel values are set to a constant; (b) shows the idea for a single scanline.

- the average intensity of the known pixels in the image (usually a mid-grey[7]), because this keeps the average intensity of the infinite image the same as that of the finite image.

Once a constant value is chosen, the other problems remain to be tackled. How wide should the extrapolated region be? It must be wide enough that we do not get any untoward effects in the intensity surface near the image edges. A zero width gives the equivalent of the constant solution in the previous section. This is obviously too small a width as it is the edge effects caused by that solution which led us to consider other solutions. The minimum acceptable width of the extrapolated region is a subjective judgement, depending partly on the type of image and the constant value chosen.

On the other hand, the extrapolated region cannot be too wide. If it *is* allowed to be too wide then the problem of the extrapolation being inaccurate rears its head once more. A width of eight or sixteen pixels would seem to be practical. A width of four pixels may be acceptable.

Given this band of unknown values, how do we extrapolate sensible values? There are some obvious simple methods of interpolating between the edge pixels and the constant pixels. For example, simple linear interpolation between the edge pixel and the first constant pixel (figure 4.13) or cubic interpolation through two edge pixels and the first constant pixel, ensuring that the first derivative of the interpolated curve is zero at the first constant pixel (figure 4.14). Such methods, and the like, produce results similar to that shown in figure 4.15. More complex methods, which take into account more of the context of each extrapolated pixel, could be employed.

However, there is a simple method of ensuring that the extrapolated values fade off to the correct value. That is to extrapolate using any of the existing methods and then window the resulting data. Figure 4.16 illustrates this idea. Windowing allows such methods as the windowed, derivative method illustrated in figure 4.17. Compare this with figure 4.10 (the unwindowed derivative

[7] not exactly half-intensity grey like the previous value, but usually close to this.

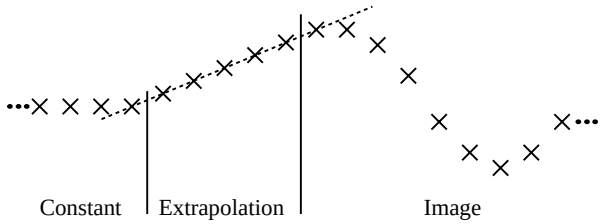

Figure 4.13: Extrapolation between the image edge and the constant region by simple linear interpolation between the edge pixel and the first constant pixel.

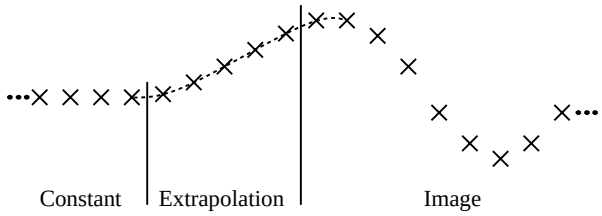

Figure 4.14: Extrapolation between the image edge and the constant region by cubic interpolation between the edge pixel, its neighbour (the pixel second from the edge), and the first constant pixel, setting the slope of the curve to zero at the first constant pixel.

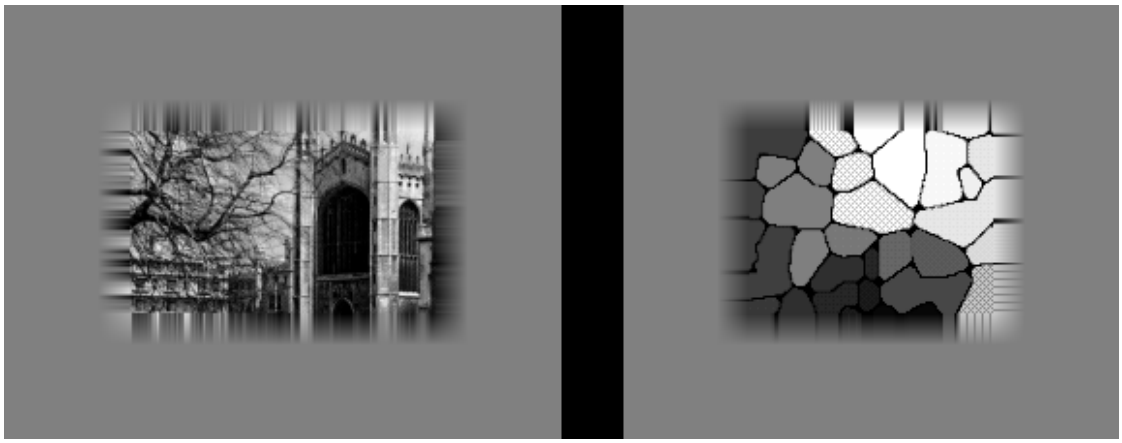

Figure 4.15: Extrapolation by linear interpolation between the edge pixel and the first constant pixel over a band of pixels around the image edge. All pixels beyond this band are set to a constant (mid-grey) value. This process is applied to the two images in figure 4.8

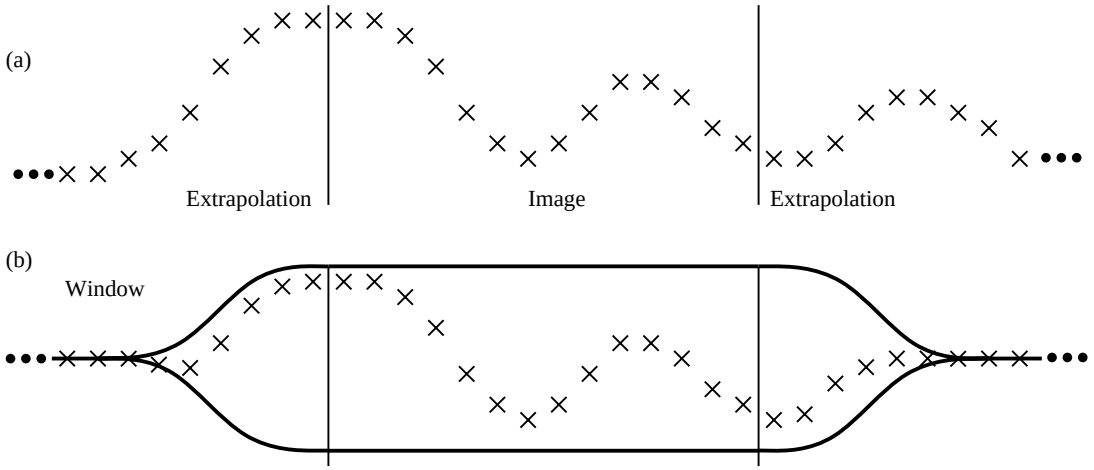

Figure 4.16: Windowed extrapolation. (a) shows the image extrapolated, (b) shows this windowed so that the pixels outside the window are constant, the image pixels are unchanged, and the pixels in between are smoothly windowed off to the constant value.

Figure 4.17: Extrapolation by derivative method (as in figure 4.10) windowed using a piecewise linear window. This process is applied to the two images in figure 4.8

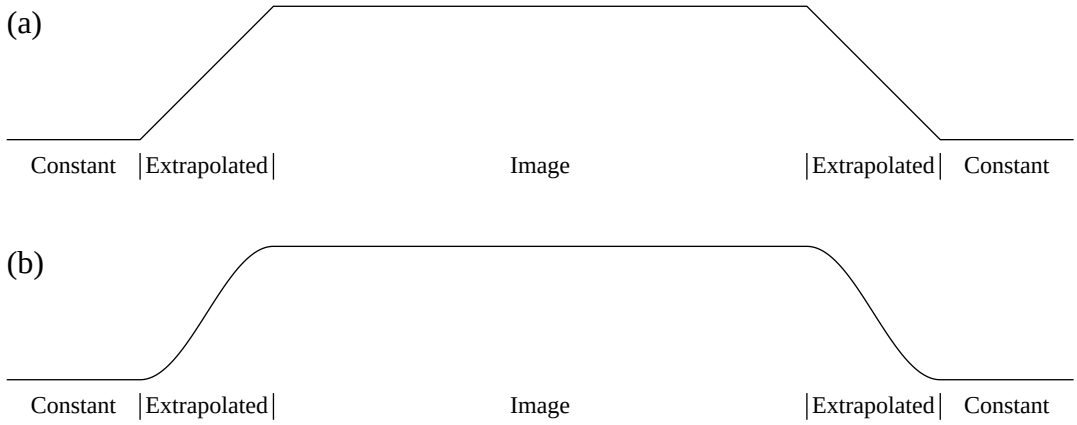

Figure 4.18: Two simple windows: (a) piecewise linear; (b) cosine half-bells in the extrapolated region. Both windows have value one inside the image and zero in the constant region.

method) and figure 4.15 (linear extrapolation to a constant).

Windowing, in this context, has some non-standard features. Firstly, the window does not necessarily fade the function to zero, but to the constant intensity. This can be achieved by using the formula:

$$i'(x) = W(x) \times (i(x) - c) + c$$

where $i(x)$ and $i'(x)$ are the unwindowed and windowed intensity functions respectively, $W(x)$ is the windowing function in the range zero to one, and c is the constant intensity to which $i'(x)$ fades. Secondly, the window function should be unity for all pixels within the finite image. This restriction is to prevent corruption of the existing, and presumably correct, intensity values.

The shape of the window is probably of little importance, given that the extrapolated values are themselves approximations. A piecewise linear function, as in figure 4.18(a); or cosine half-bell (figure 4.18(b)) are two simple windows. The cosine half-bell is the better of these two, as it is C1-continuous.

An extension of this idea is to window the known pixel values and thus remove the need for any extrapolation. All unknown pixels are set to the constant value. Pixels just within the image edge are windowed, while the central portion of the image remains unaffected. Fraser [1989b] uses such a method to fade the image to zero at the edges. However, he is quick to point out that such windowing, while a good technique for other signal types (for example, sound), causes an undesirable effect, vignetting, when applied to images. Figure 4.19 gives an example of vignetting.

(5) Replication

This is a simple method, often used in texture mapping applications. The image is simply replicated an infinite number of times to completely tile the plane. Glassner [1990b] uses this as the simplest way of generating an infinite texture from a finite 'texture cell'. When using the fast Fourier transform (FFT), (section 5.4.1), this is the method of edge extension implicit in the algorithm. This property of the FFT has important ramifications, as we shall see in chapter 5.

Hall [1989] used this method in his pipelined binary image processor, where he dealt with black text on a white background. His assumption was that the image would be all white near the edges and so there would be no untoward edge effects (as the edges, being all white, would exactly match up). In his later work, Hall [1991] rejected this assumption and altered his algorithm (to a constant edge extension) in order to avoid the errors it could conceivably cause.

Figure 4.19: An example of vignetting. The image on the left is the original, on the right it is vignetted: it fades off towards its edges. This is almost always an undesirable effect.

Replicating the image in this way is a valid image extension method, and works well for certain texture mapping applications (for example, generating wallpaper). However, in other areas it has a major flaw. Except in fortuitous cases, the intensity values at one edge of the image bear no relation to those at the opposite edge. Yet, in replication, these unrelated pixels are placed next to one another. This causes edge effects similar to those caused by the constant extension method, as illustrated in figure 4.20. In general, this method is not recommended except for specialist applications such as the texture mapping operation mentioned above.

Along with simple copying, Glassner [1990b] explains that many different textures can be generated by rotating, reflecting and/or offsetting the texture cell before copying. This is basically using the texture cell as the unit cell for one of the wallpaper groups [Martin, 1982]. Some of these are illustrated in figure 4.21.

While this is extremely useful for generating repetitive textures (so long as the textures are carefully chosen), it is not generally useful for edge extension. The one wallpaper group that is useful is that illustrated in figure 4.21 (W_2^2 (`pmm`)) where the image is reflected about its edges.

(6) Reflection

This, as well as being one of the methods of generating a wallpaper pattern, has been widely used as an inexpensive method of image extension [White and Brzakovic, 1990, p.343]. It is inexpensive because there is no need to generate any additional values, the only overhead is the simple one of evaluating which of the existing image values to use. It is widely used because of the expectation that, by reflecting, the pixels just outside the edge will bear a good relation to those just inside, hence minimising edge effects. This method is implicit in the discrete cosine transform (DCT) variation of the FFT method described in section 5.4.1, greatly improving the edge effect performance over the FFT's implicit replication method.

White and Brzakovic [1990] use this method as the standard against which they compare their new methods. They conclude that this method leads to good results only in cases of highly textured regions or regions of uniform intensity. However, this method is certainly better than either copying or using a constant and is certainly cheaper than explicitly extrapolating. One of White and Brzakovic's complaints is that this method fails dismally for highly directional images. Figure 4.22 illustrates how the various other methods cope with such a situation. Note that

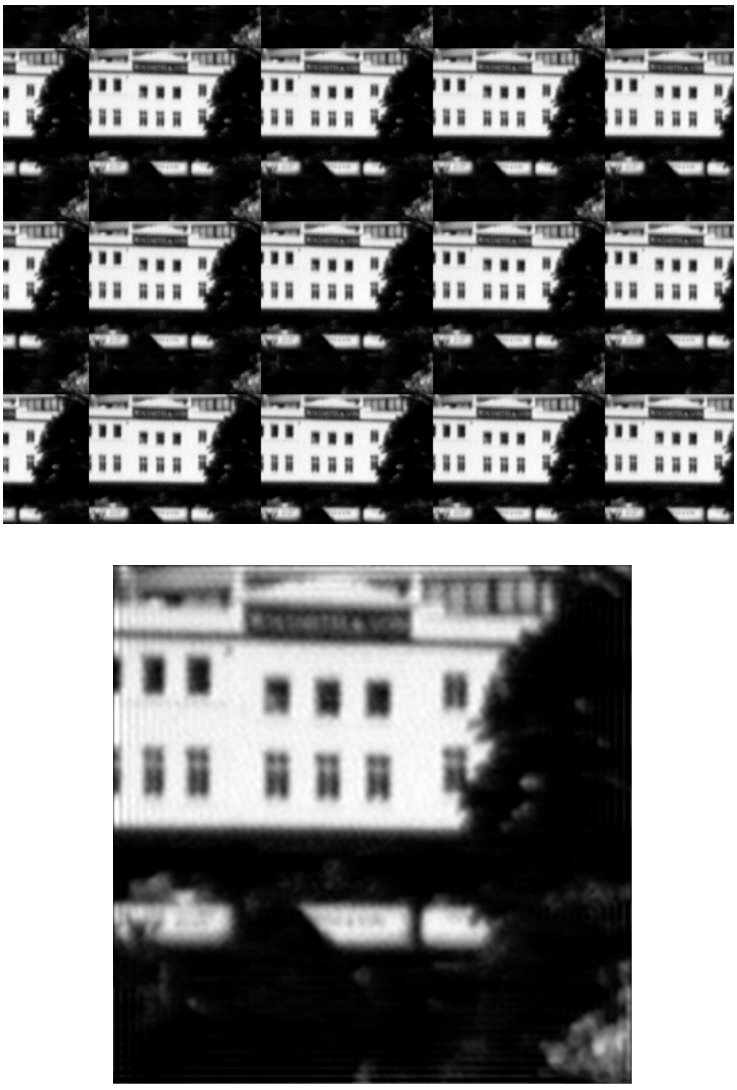

Figure 4.20: An example of edge effects caused by the replication edge extension method. The top photograph shows an image replicated, notice how the edges of the image do not match up, causing a large intensity difference where the replicas meet. The bottom photograph shows an intensity surface reconstructed from this image by sinc reconstruction. Notice the ripples in the image near the edges, similar to those in figure 4.7(left) for a constant edge extension method.

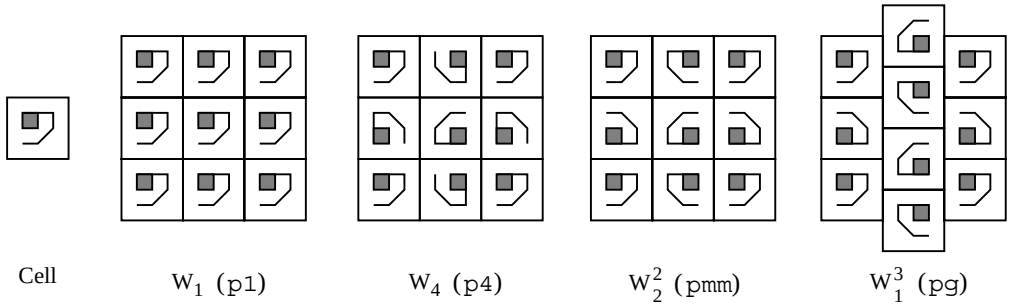

Figure 4.21: Some of the possible textures that can be generated by replicating a square texture cell with no rotational or reflectional symmetry of its own. On the left is the texture cell, the four wallpaper groups shown here are: W_1, simple replication of the cell; W_4, a replication that has centres of four-fold rotation; W_2^2, replication by reflection in both horizontal and vertical reflection lines; and W_1^3 replication with glide reflections. All except W_4 could also be used with a rectangular texture cell. The notation used here is that used by Martin [1982]. That in brackets is the common abbreviated form of the International Union of Crystallography.

Figure 4.22: How the edge extension methods cope with a pathological case. At top left is the original which consists of diagonal lines at 22.5° (left half) and 45° (right half). Bottom left is extrapolated by copying, this fails for either case as it extrapolates horizontally or vertically. Top right is White and Brzakovic's [1990] derivative method (figure 4.10), and bottom right is our modification of that method (figure 4.11). Both of these perform excellent extrapolation of the 45° features, but fail for the 22.5° features, extending them horizontally, vertically, or at 45°.

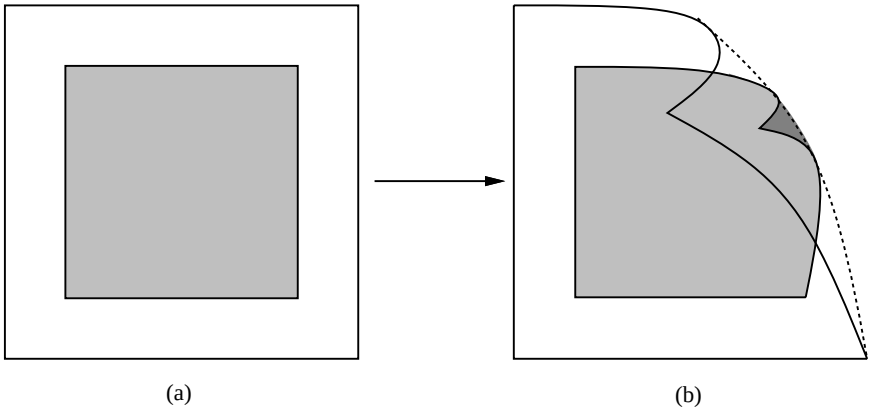

Figure 4.23: An example of an image folding back on itself. The shaded region represents the finite sized image, and the clear region around it part of the infinite plane on which the image sits. (a) shows the original image, (b) the transformed image. If edge extension is done by any method other than transparent then the image will be obscured by the area around it, which is undesirable.

White and Brzakovic's derivative method copes splendidly with features aligned at angles of zero, forty-five and ninety degrees, but not with a feature at twenty-three degrees. Thus, whilst giving better results in some cases, it fails in other cases and so it has little or no advantage over reflection.

The final two edge extension methods are special cases.

(7) Transparent

In this solution, the intensity surface beyond the image's edge is defined to be transparent. That is, whatever existed in destination image space before the resampling can still be seen in these regions. In many cases this will simply be equivalent to setting the intensity surface to a constant outside the image edges. This is because the original content of the destination image will have been that constant intensity.

However, in some situations it is vital that we make the assumption that the intensity surface beyond the image's edges is transparent. If the transform is such that the image folds back on itself, then the source image must be transparent beyond its edges (and, also, it needs to have the same intensity values on the 'back' as on the 'front'). Intuitively, it is as if the opaque image is printed on a transparent medium (such as an overhead projector acetate) which is then manipulated (see figure 4.23). Were this transparent medium to be replaced by an opaque one (for example: of constant intensity) then the image itself would be obscured.

Transforms of this nature have the further problem that a point in the destination intensity surface can map to two or more points on the source intensity surface and arbitrating between them, to determine which is visible, or how to mix the values, can be a difficult problem.

Compounding the difficulty of the transparent solution is the problem of defining the intensity surface just within the image edge (region B in figure 4.2). The intensity values in this area are evaluated using pixel values both inside and outside the image edges. Therefore, even though the intensity surface is defined as being transparent outside the image edge, it is still necessary to extend the image in order to calculate the values of the intensity surface just inside the image edge. Thus one of the other methods of image extension must be used to produce these values, and so there still exists the potential for edge effects just within the image edge.

One advantage of this method is that extrapolation need only be performed out as far as the reconstructor needs values. For an infinite extent reconstructor, obviously all values still need to

be available. But, for a piecewise cubic reconstructor, a band two pixels wide outside the image edge is all that need be generated by extension.

Such situations as these lead to the final solution to the edge extension problem.

(8) Special cases

In situations where the *intensity surface* beyond the edge of the image is defined to be a constant, or transparent, or some other case that does not depend on the reconstructor, then a small-kernel reconstructor can use a special case extension method to produce the necessary pixel values beyond the image edge. These methods are not the general extension methods discussed earlier but methods specific to particular reconstructors which may only be valid for an extension of one or two pixels beyond the image edge.

For local piecewise polynomials (chapter 3) the only documented extension method of this nature is Keys' [1981] single pixel extension method for the Catmull-Rom interpolant. Keys derives the interpolant by insisting that the cubic agree with the Taylor's series expansion of the original function to as many terms as possible. He then [*ibid.*, p.1155] develops a formula to approximate one pixel value beyond the image edge in order to maintain this agreement. This extension can be used for pixels farther out from the edge but it was developed specifically for the first pixel out and specifically for the Catmull-Rom reconstructor.

The cubic B-spline interpolant, discussed later in this chapter (section 4.5) is theoretically of infinite extent. In order to use this in a practical (finite) situation, end conditions have to be specified. In this instance we do not require the values of pixels beyond the image edge, but other edge conditions. For example, the 'natural cubic spline' criterion requires that the second derivative of the intensity surface at the edge points is zero [Press *et al*, 1988, p.96]. Wolberg [1990, p.136], on the other hand, implicitly assumes that the pixels just outside the image edge have intensity zero when he uses the cubic B-spline interpolant.

A final category of special case extension methods includes the *a priori* method described in section 6.4. The analysis done by this method can be used to generate an infinite image by extending the edges found to infinity. Alternatively the pixels outside the image edge can be left undefined and the final image have an implicit extra edge around the outside. The intensity surface beyond the image edge can then be undefined, constant or transparent as required.

Summary

All these methods fail in certain cases. The best option for general image extension would appear to be either reflection for quick processing, or a good extrapolation windowed to a constant. Such an extrapolation would need to give good results out to the extent of the window[8]. If extremely fast processing is required, a constant value may be used. For resampling work, it is usually desirable to use these methods of edge extension when generating pixel values of type (a) in figure 4.1, and to use a constant value (for example: zero, mid-grey, transparent) for pixels of type (b).

4.3 Sinc and other perfect interpolants

The theory of perfect interpolation is straightforward. If the original intensity surface is band-limited and the sampling rate is high enough then the samples in the image contain all the information necessary to exactly reconstruct the original intensity surface. The reconstructors that can perform this exact reconstruction are the 'perfect interpolants'. When we introduced perfect

[8] In fact it need not be good quite all the way as any strange effects at the limits would be rendered practically negligible by the windowing.

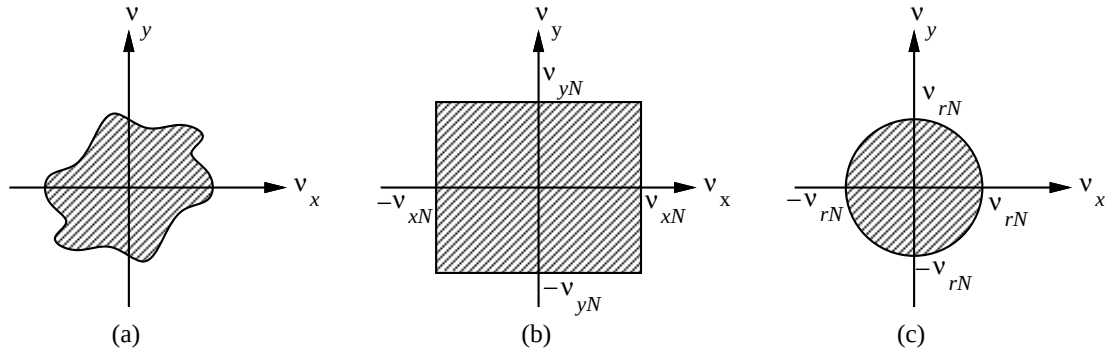

Figure 4.24: Examples of the ranges over which an image's Fourier transform can be non-zero. (a) an example of the non-zero area of a bandlimited image's Fourier transform, (b) a rectangular passband, with Nyquist frequencies: ν_{xN} and ν_{yN}, (c) a circular passband, with Nyquist frequency: ν_{rN}.

interpolation, in section 3.3, we only looked at the sinc function, but other perfect interpolants exist.

An infinite extent intensity surface, $s(x, y)$, in the spatial domain can be represented equally well in the frequency domain by its Fourier transform:

$$S(\nu_x, \nu_y) = \int_{-\infty}^{\infty} \int_{-\infty}^{\infty} s(x, y) e^{-i2\pi(x\nu_x + y\nu_y)} \, dy \, dx$$

This frequency domain function, if bandlimited, will have a certain range over which it is non-zero, shown in figure 4.24 (a).

Point sampling on a regular grid in the spatial domain equates to regularly replicating in the frequency domain (section 2.4.1) as illustrated in figure 4.25.

To reconstruct a continuous spatial function from this we need an interpolation filter with a frequency response which is unity for the original bandlimited area (shaded in figure 4.25) and zero for all the replicas. Obviously such a filter cannot exist if the replicas overlap the original in any way, so the samples need to be sufficiently close that the replicas are separated.

However, the filter does not need to take any specific value *between* the replicas because the Fourier transform of the sampled image is zero in these regions. So, if the replicas do not tile the plane, there are an infinite number of perfectly reconstructing filters for a given intensity surface.

If the bandlimited area can be bounded by a circle (figure 4.24 (c)) then a perfect interpolation filter is one which is unity within the circle and zero outside it. In the spatial domain this filter is a first order Bessel function [Pratt, 1978; Heckbert, 1989]. Mersereau's [1979] results allow us to derive the spatial domain equation for a perfect hexagonal filter, useful when processing hexagonally sampled images. However, except for a few experimental cases [Wüthrich, Stucki and Ghezal, 1989; Wüthrich and Stucki, 1991], all images are sampled on a rectangular grid.

For a given sampling rate there is a single function that can perfectly reconstruct *any* function that is bandlimited at or below half that rate. If we take the largest rectangular area in the frequency domain which can be replicated without overlap (figure 4.21(b)), then the perfect interpolation filter must be unity inside this area and zero outside it, because the replicas tile the plane. In the spatial domain this filter is a two dimensional sinc function. For bandlimits of ν_{xN} and ν_{yN} in the frequency domain, the spatial domain function is:

$$h(x, y) = 4\nu_{xN}\nu_{yN}\text{sinc}(2x\nu_{xN})\text{sinc}(2y\nu_{yN}) \tag{4.1}$$

This is the function which is generally used as the perfect interpolant, because it perfectly interpolates all rectangularly bandlimited images. This function's spatially separability is advantageous

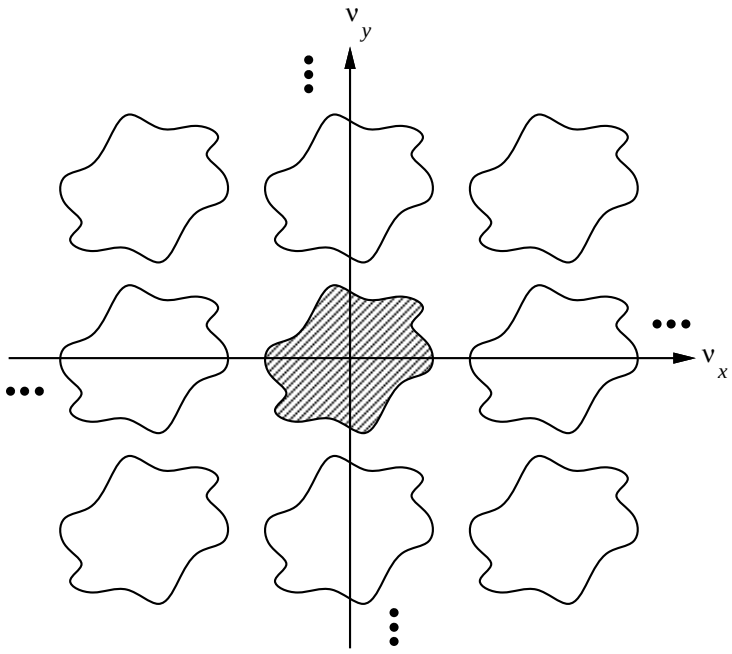

Figure 4.25: The example frequency spectrum of figure 4.24(a) replicated infinitely many times. This is caused by sampling in the spatial domain. The original copy is shown shaded, the others are left white.

when implementing it. If rotational invariance is more desirable then the first-order Bessel function may be used, though it is a more difficult function to evaluate.

The most common complaint levelled against the sinc function (and is equally valid against the other perfect interpolants) is that it produces unsightly ripples in the reconstructed intensity surface [Mitchell and Netravali, 1988; Ward and Cok, 1989]. Another commonly mentioned problem is that the sinc function can produce negative values in the intensity surface [Pratt, 1978; Blinn, 1989b] (section 3.5.7).

In answer to these two criticisms, it is necessary to point out that a perfect interpolant *perfectly* reconstructs a sufficiently bandlimited intensity surface. If the original intensity surface is sufficiently bandlimited then it will contain no negative values (negative light being impossible) and any ripples in it are supposed to be there. The sinc function cannot introduce any negative light or extra ripples because it *exactly* reconstructs the original surface.

These complaints about the sinc interpolator come from attempting to apply it to an image sampled from an intensity surface which is not bandlimited within the limits required. In such a case, aliasing will occur and the sinc interpolator will perfectly reconstruct an aliased version of the original intensity surface, possibly with negative values and unsightly ripples, rather than the original surface itself. Using the sinc function with an intensity surface that is not sufficiently bandlimited is fraught with difficulties.

Opinion is divided in the literature about how many real images are sampled from intensity surfaces which are bandlimited within tight enough limits to prevent aliasing. Any real world intensity surface will be bandlimited before sampling by the physical device used to capture the image, because no real-world device has an infinite bandwidth [Wolberg, 1990, p.99]. Fraser [1987] believes that people, often unwittingly, rely on the physical device to sufficiently bandlimit the signal so that either minimal or no aliasing occurs.

Artificially generated intensity surfaces can contain infinite frequencies due to discontinuities in the surfaces. Such surfaces are not bandlimited and will always generate images that contain aliases. If

such a surface is filtered before point sampling then it may, depending on the filter, be bandlimited sufficiently.

From the images we have seen, it would appear that most images are not bandlimited sufficiently to prevent the sinc interpolant from producing ripples around quick intensity changes; Wolberg [1990, p. 108] is of the same opinion.

This is not the end of the problems with the sinc interpolant. As discussed earlier, a practical image must be finite. When using sinc interpolation the only sensible edge extension methods are those which fall off to zero (including the constant method which sets all values outside the edges to zero). The following formula can be used to calculate the value of the interpolated surface at the point (x, y):

$$f(x,y) = \sum_{i=-\infty}^{\infty} \sum_{j=-\infty}^{\infty} \text{sinc}(x-i)\text{sinc}(y-j) f_{i,j} \tag{4.2}$$

where the sample points are located at integer locations in the xy-plane and $f_{i,j}$ is the sample located at (i, j). If the sample values, $f_{i,j}$, in the image are zero outside certain bounds then this infinite (and hence impossible to do) sum reduces to a finite (do-able) one. This is why defining all samples outside certain limits to be zero is the only sensible method of edge extension. Sinc reconstruction is a linear process, and so we could use the trick described in section 4.2.1 to allow any constant value, not just zero, and still require only a finite sum[9].

Unfortunately, by insisting that the image be zero outside a finite boundary, the sampled intensity surface cannot be bandlimited. While this result is not intuitive, we have found a proof of it, which is given in theorem 2.

Theorem 2 *An image that is only non-zero within finite bounds must contain aliases.*

Proof: an infinite bandlimited, intensity surface is sampled by an infinite extent comb function. The resulting function (a continuous representation of an image (section 2.4.1)), is clamped to zero outside finite limits. This is equivalent to multiplying the sampled function by a box function. Multiplication is commutative and so we could have got the same result by first multiplying by a box function and then multiplying by the comb sampling function. The function that is sampled is thus the product of the original intensity surface and a box function. It is thus of finite extent in the spatial domain. A function cannot be simultaneously of finite extent in both the spatial domain and the frequency domain (a detailed proof of this statement is given in appendix B.5), and so this function cannot be bandlimited, and therefore the sampled version must contain aliases QED.

The most obvious effect of this aliasing is rippling around the edges — this is the reason why we went from the constant edge solution in section 4.2.1 to the 'extrapolation to a constant' edge solutions in the following subsection. However, even this latter edge solution produces aliasing effects, although not as badly.

Pratt [1978] shows another way of looking at this finite-extent sampling process. This is that a finite extent sampling grid can be generated by multiplying the box and comb functions and applying the product to the continuous intensity surface. The product is simply a truncated (finite-extent) comb function. In the same way that sampling using an infinite extent comb is equivalent to convolving with the comb's Fourier transform in the frequency domain, sampling using this finite extent comb is equivalent to convolving with this function's Fourier transform in the frequency domain. This Fourier transform is fairly simple to evaluate. With limits $(\pm b_x \Delta x, \pm b_y \Delta y)$, for a

[9]The ensuing discussion applies equally to those cases as the effect of the trick in the frequency domain is to modify only the DC component, then to do the same processing as for the zero case (leaving the modified DC component unchanged) and finally to reset the DC component to its original value (leaving the rest of the components unchanged).

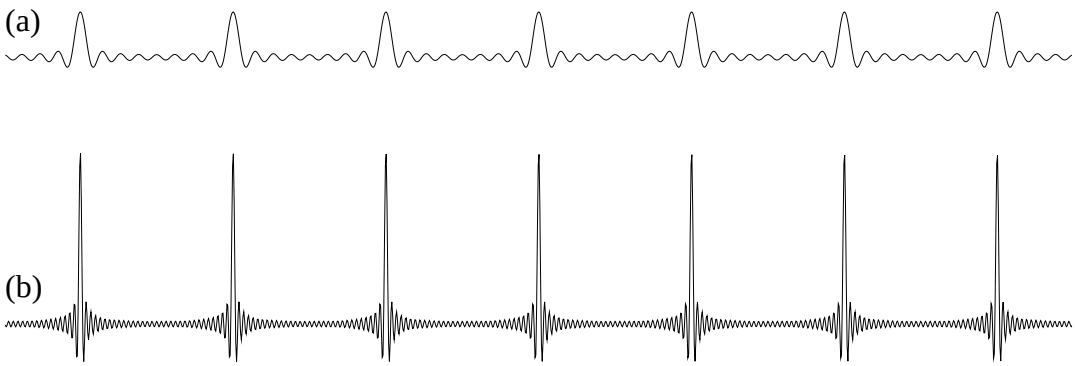

Figure 4.26: The Fourier transform of a finite extent comb function. (a) the Fourier transform of a comb function with 8 teeth, (b) the Fourier transform of a comb function with 32 teeth.

comb of spacing $(\Delta x, \Delta y)$, it can be shown to be:

$$D(\nu_x, \nu_y) = \frac{\sin(2\pi\nu_x(b_x - \frac{1}{2})\Delta x)}{\sin(\pi\nu_x\Delta x)} \times \frac{\sin(2\pi\nu_y(b_y - \frac{1}{2})\Delta y)}{\sin(\pi\nu_y\Delta y)} \tag{4.3}$$

The derivation of this can be found in appendix B.6. This function is illustrated in figure 4.26. It has a similar but nonetheless different effect to convolving with a comb, with the results described earlier.

4.3.1 Richards' positive perfect interpolant

Pratt [1978, p.98] points out that a sinc-reconstructed function can be considered to be the superposition of an infinite number of weighted translated sinc functions. Because each of the functions in the sum has negative lobes, it is impossible to optically create the image by superposition because negative light does not exist. Pratt then points to Richards' [1966] discovery of a family of perfect interpolants that are positive in regions in which their magnitude is large, and hence can be used for sequential optical interpolation. In resampling, we can add the intensities up inside a computer, and so negative addends are not a problem. Nevertheless, it is instructive to look at Richards' function.

Richards' interpolants are interesting in that he generates them in a similar way to the Bezier and B-spline interpolants discussed later (section 4.5). He effectively defines a set of coefficients:

$$h_n = f_n - \alpha \times (f_{n-1} + f_{n+1}) \tag{4.4}$$

which he convolves with a kernel, $g(x)$, such that:

$$h * g = f * \text{sinc}$$

$g(x)$ can be evaluated from this equation and shown to be [Richards, 1966, equation 4]:

$$g(x) = \frac{1}{\sqrt{1-4\alpha^2}} \frac{\sin \pi x}{\pi x} \left[1 - 2x^2 \sum_{n=1}^{\infty} \frac{(-\beta)^n}{n^2 - x^2}\right]$$

where $\beta = \frac{1-\sqrt{1-4\alpha^2}}{2\alpha}$. Figure 4.27 shows this kernel graphed for two different values of α.

While this kernel is indeed positive over a significant range, when combined with the kernel $\ldots, 0, 0, -\alpha, 1, -\alpha, 0, 0, \ldots$ operating on $h(x)$ (equation 4.4) it is exactly equivalent to the sinc function and so is simply another way of writing sinc convolution. This situation is analogous

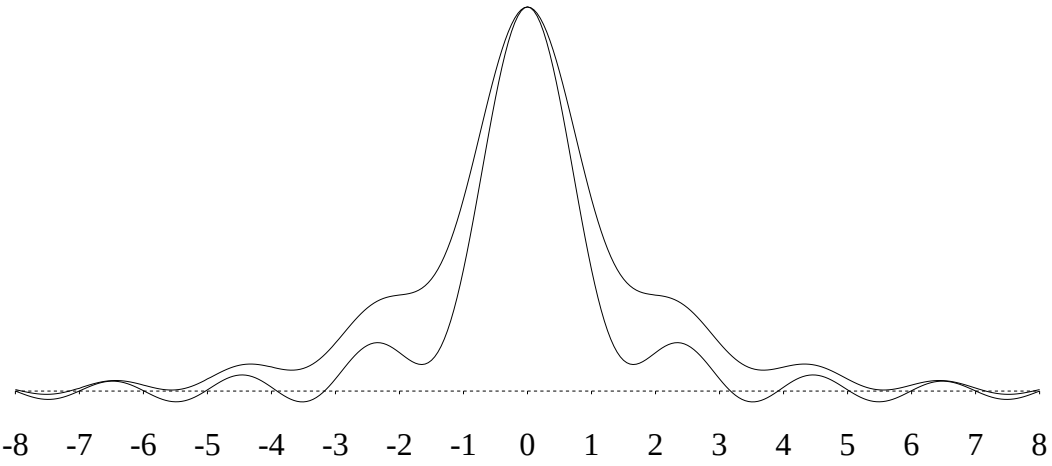

Figure 4.27: Richards' [1966] kernel, for $\alpha = 0.2875$ (lower curve) and $\alpha = 0.4$ (upper curve).

to that with the B-spline and Bezier interpolants discussed in section 4.5. In those cases, a local kernel operates on coefficients, g_n, derived from the data values, f_n. However, the overall kernel which operates on the f_n values is not local. In a similar manner, the Richards kernel is positive over its central region and operates on a set of coefficients, h_n, derived from the data values, f_n. However, the sinc kernel which operates directly on the f_n data values is not positive over such a wide region.

Pratt was attracted to Richards' kernel because it is positive in regions where its magnitude is large. This, he claimed, allows it to be employed for sequential optical interpolation. Unfortunately this claim is only true if all of the h_n coefficients are non-negative. It is true that all of the *data* values, f_n, must be non-negative, because negative light does not exist. So applying a Richards kernel to these values would have the effect desired by Pratt. However, the Richards kernel is applied to the h_n coefficients. Thus, sequentially generating an image using a Richards kernel can only be achieved if all the h_n are non-negative. A coefficient, h_i, is non-negative if, and only if:

$$f_i \geq \alpha \times (f_{i-1} + f_{i+1}) \tag{4.5}$$

For the Richards kernel to be positive in the region $|x| < 5$ (this is the significant range used by Richards [1966, fig. 1]) then we must have $\alpha \geq 0.34222888 \pm 5 \times 10^{-9}$ (rather than Richards' value of $\alpha > 0.2875$). This curve is shown in figure 4.28. With α in this range, many images will contain at least one location where equation 4.5 will not be satisfied. This unfortunately means that the Richard's kernel can not be used for sequential optical interpolation of these images. For an image that is bandlimited well below the folding frequency, equation 4.5 should be satisfied at all locations and, in these cases, it can be used for sequential optical interpolation.

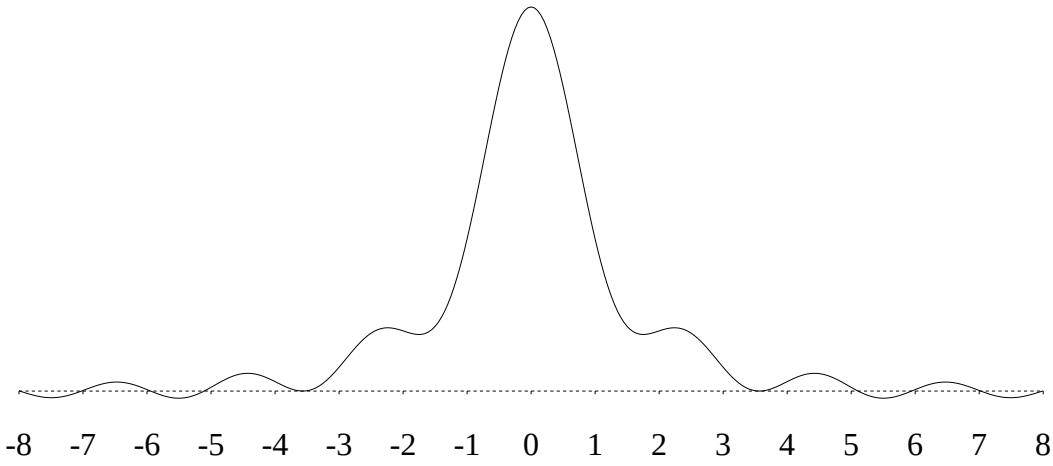

Figure 4.28: Richards' [1966] kernel, for $\alpha = 0.342229$. For α greater than this value the kernel is positive in the range $|x| < 5$.

4.4 Gaussian reconstructors

The Gaussian filter is of the form:

$$h(s) = \frac{1}{\sigma\sqrt{2\pi}} e^{-s^2/2\sigma^2} \tag{4.6}$$

for a standard deviation of σ with unit area under the curve.

The Gaussian has many interesting features:

- it will never produce negative values, unlike the sinc function.
- it falls to zero much faster than the sinc function and so can be truncated with little loss of quality, unlike the sinc function [Heckbert, 1989, p.41]. See section 4.6 for more details.
- it is both circularly symmetric and separable (the only function that is), properties that are useful in implementing the filter, for example: in Greene and Heckbert's [1986] elliptical weighted average filter [see also Heckbert, 1989, sec 3.5.8 and 3.5.9].
- it is an approximant, as opposed to sinc which is an interpolant.

Whilst its properties make it useful, it produces a blurrier intensity surface than, say, the Catmull-Rom spline.

When using a Gaussian we must decide what value of σ to use. For reconstruction of unit spaced samples, Heckbert [1989, p.41] recommends a standard deviation of about $\sigma = \frac{1}{2}$. Ratzel [1980], and subsequently Schreiber and Troxel [1985], use $\sigma = 0.52$ (see footnote 10 for details of where this value comes from, as it is not the value which they report). Turkowski [1990] uses two Gaussian functions, expressed in the form:

$$h(x) = 2^{-x^2/\tau^2}$$

where $\tau = \frac{1}{\sqrt{2}}$ or $\tau = \frac{1}{2}$. Some consider this form to be more convenient than equation 4.6 [Wolberg, 1990]. This form is not normalised, but when it is (by multiplying by the correct constant) these two values of τ correspond to $\sigma \approx 0.600561$ and $\sigma \approx 0.424661$ respectively.

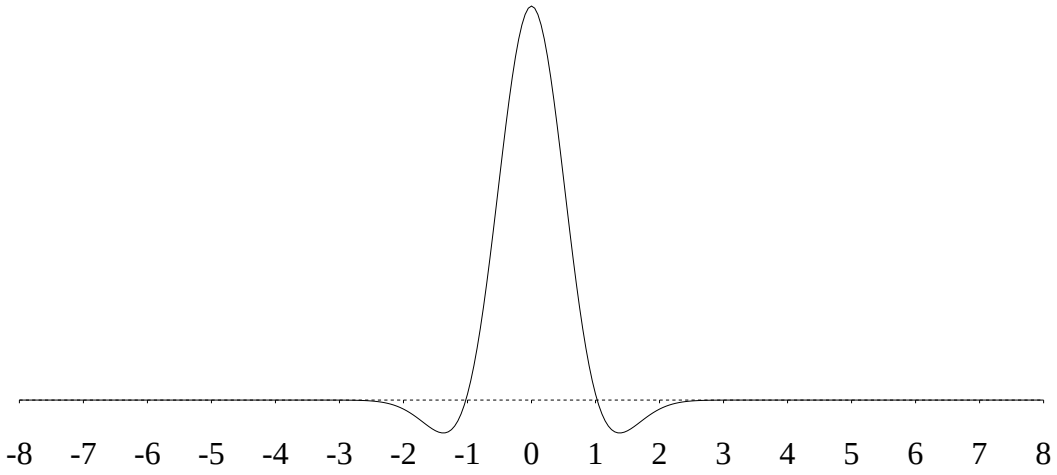

Figure 4.29: The sharpened Gaussian kernel.

4.4.1 The sharpened Gaussian

This was developed by Ratzel [1980] to improve on the sharpness of a Gaussian reconstructed intensity surface. The Gaussian's kernel is[10]:

$$h_g(s) = \frac{1}{0.52\sqrt{2\pi}} e^{-s^2/2(0.52)^2} \tag{4.9}$$

The sharpened Gaussian kernel is the weighted sum of three of these functions, two of them offset from the origin:

$$h_{sg}(s) = \frac{1}{5}\left(7h_g(s) - h_g(s-1) - h_g(s+1)\right) \tag{4.10}$$

This is graphed in figure 4.29. The single side-lobe each side of the central lobe perceptually sharpens the picture, as discussed in section 4.5.2.

The sharpened Gaussian can be considered to be the convolution of two simpler functions:

$$h_{sg}(s) = h_g(s) * m$$

where m is a discrete function: $m_0 = \frac{7}{5}$; $m_1 = -\frac{1}{5}$; $m_n = 0$, $n \geq 2$; and $m_{-n} = m_n$.

Thus, a sharpened Gaussian intensity surface can be generated by precomputing a set of coefficients, $g = m * f$, and then applying the simple Gaussian (equation 4.9) to these coefficients:

$$f(x) = h_g(s) * g$$

This is computationally more efficient than the straightforward $f(x) = h_{sg}(s) * f$, especially for the two-dimensional version of the reconstructor [Schreiber and Troxel, 1985].

---

[10] Ratzel claims to have used this Gaussian [Ratzel, 1980, p.68]:

$$h_g(s) = \frac{1}{2.6\sqrt{2\pi}} e^{-n^2/2(2.6)^2} \tag{4.7}$$

where n is an integer and $s = \frac{n}{5}$. This is equation 4.6 with $\sigma = 2.6$. However, converting this to normal co-ordinates gives:

$$h_g(s) = \frac{1}{2.6\sqrt{2\pi}} e^{-s^2/2(0.52)^2} \tag{4.8}$$

which is not normalised; to normalise it requires us to use equation 4.6 with $\sigma = 0.52$, which is equation 4.9. If one examines Ratzel's hand-tuned approximation this is, in fact, the function that he used, rather than the virtually identical one (equation 4.7) he claims to have used. The only difference is the normalising coefficient. This is a minor correction, but it makes a difference to the results in table 4.5 (section 4.6).

	j			
i	3	2	1	0
-1	$-\frac{1}{6}$	$\frac{1}{2}$	$-\frac{1}{2}$	$\frac{1}{6}$
0	$\frac{1}{2}$	-1	0	$\frac{2}{3}$
1	$-\frac{1}{2}$	$\frac{1}{2}$	$\frac{1}{2}$	$\frac{1}{6}$
2	$\frac{1}{6}$	0	0	0

Table 4.1: The coefficients $k_{i,j}$ in equation 4.11.

Ratzel's [1980, p.97] results indicate that the sharpened Gaussian is a perceptual improvement over the ordinary Gaussian[11].

4.5 Interpolating cubic B-spline

In chapter 3 we met the approximating cubic B-spline (equation 3.19 with $B = 1$ and $C = 0$). It does not produce an interpolating intensity surface. To make an interpolating cubic B-spline we apply the B-spline filter to a different set of sample values, g_i, derived from the image's sample values, f_i, in such a way that the resulting curve interpolates the image's sample points. This process was briefly described in section 3.5.5.

The interpolating cubic B-spline intensity surface is defined as:

$$f(x) = \sum_{i=-1}^{2} \left(\sum_{j=0}^{3} k_{i,j}\, t^j \right) g_{\alpha+i} \tag{4.11}$$

where $\alpha = \left\lfloor \frac{x-x_0}{\Delta x} \right\rfloor$ and $t = \frac{x-x_\alpha}{\Delta x}$. The $k_{i,j}$ are listed in table 4.1 [Foley and van Dam, 1982]. In order that equation 4.11 interpolates all the sample points, we must ensure that:

$$f_i = \frac{1}{6}(g_{i-1} + 4g_i + g_{i+1}) \tag{4.12}$$

which gives us an infinite set of equations to solve.

In a practical situation, only a finite number, say n, of the f_i will be known. Say these values are $f_0, f_1, \ldots, f_{n-1}$, then to define the entire curve between x_0 and x_{n-1}, $n+2$ values, $g_{-1}, g_0, g_1, \ldots, g_{n-1}, g_n$, are required. These can be partially evaluated by solving the n equations in $n+2$ unknowns:

$$\begin{bmatrix} 1 & 4 & 1 & & & & & \\ & 1 & 4 & 1 & & & 0 & \\ & & 1 & 4 & 1 & & & \\ & & & 1 & \cdots & 1 & & \\ & & & & 1 & 4 & 1 & \\ & & 0 & & & 1 & 4 & 1 \end{bmatrix} \begin{bmatrix} g_{-1} \\ g_0 \\ g_1 \\ \vdots \\ g_{n-1} \\ g_n \end{bmatrix} = 6 \begin{bmatrix} f_0 \\ f_1 \\ f_2 \\ \vdots \\ f_{n-2} \\ f_{n-1} \end{bmatrix}$$

This leaves us with two edge effects problems: (1) how to define the last two equations required to find the g_i values; and (2) how to define the intensity surface outside the range x_0 to x_{n-1}.

Three common solutions to the first problem are the free-end, cyclic, and not-a-knot boundary conditions [Wolberg, 1990, p.289].

[11] Ratzel actually used a truncated version of this Gaussian, setting $h_g(s) = 0$, $|s| > 1.2$. Such approximations are discussed in the section 4.6.

The *free-end*, or natural, end condition involves setting the second derivative of the intensity function equal to zero at the end points. That is, $f_0'' = 0$ and $f_{n-1}'' = 0$. This is equivalent to setting:

$$\begin{aligned} g_{-1} &= 2g_0 - g_1 \\ g_n &= 2g_{n-1} - g_{n-2} \end{aligned}$$

and from equation 4.12 we can show that this implies that $g_0 = 3f_0$ and $g_{n-1} = 3f_{n-1}$, giving us a system of $n+2$ equations in $n+2$ variables:

$$\begin{bmatrix} 0 & 2 & & & & & & \\ 1 & 4 & 1 & & & 0 & & \\ & 1 & 4 & 1 & & & & \\ & & 1 & 4 & 1 & & & \\ & & & 1 & \cdots & 1 & & \\ & & & & 1 & 4 & 1 & \\ & & & & & 1 & 4 & 1 \\ & & 0 & & & & 2 & 0 \end{bmatrix} \begin{bmatrix} g_{-1} \\ g_0 \\ g_1 \\ g_2 \\ \vdots \\ g_{n-2} \\ g_{n-1} \\ g_n \end{bmatrix} = 6 \begin{bmatrix} f_0 \\ f_0 \\ f_1 \\ f_2 \\ \vdots \\ f_{n-2} \\ f_{n-1} \\ f_{n-1} \end{bmatrix} \tag{4.13}$$

The *cyclic* end condition puts $g_i = g_{i+n}$, which means that $g_{-1} = g_{n-1}$ and $g_n = g_0$. This gives n equations in n variables:

$$\begin{bmatrix} 4 & 1 & & & & & & 1 \\ 1 & 4 & 1 & & & & & \\ & 1 & 4 & 1 & & 0 & & \\ & & 1 & 4 & 1 & & & \\ & & & 1 & \cdots & 1 & & \\ & & & & 1 & 4 & 1 & \\ & & 0 & & & 1 & 4 & 1 \\ 1 & & & & & & 1 & 4 \end{bmatrix} \begin{bmatrix} g_0 \\ g_1 \\ g_2 \\ \vdots \\ g_{n-2} \\ g_{n-1} \end{bmatrix} = 6 \begin{bmatrix} f_0 \\ f_1 \\ f_2 \\ \vdots \\ f_{n-2} \\ f_{n-1} \end{bmatrix} \tag{4.14}$$

The third end condition, that favoured by Wolberg, is the not-a-knot boundary condition. This condition requires $f'''(x)$ to be continuous at x_1 and x_{n-2} [Wolberg, 1990, p.289]. This is equivalent to $g_{-1} = 4g_0 - 6g_1 + 4g_2 - g_3$ and $g_n = 4g_{n-1} - 6g_{n-2} + 4g_{n-3} - g_{n-4}$. These, combined with equation 4.12, give (see appendix B.7): $g_1 = \frac{1}{6}(8f_1 - f_0 - f_2)$, $g_{n-2} = \frac{1}{6}(8f_{n-2} - f_{n-1} - f_{n-3})$ and:

$$\begin{bmatrix} 0 & 0 & 36 & & & & & \\ 1 & 4 & 1 & & & & & \\ & 1 & 4 & 1 & & 0 & & \\ & & 1 & 4 & 1 & & & \\ & & & 1 & \cdots & 1 & & \\ & & & & 1 & 4 & 1 & \\ & & 0 & & & 1 & 4 & 1 \\ & & & & & 36 & 0 & 0 \end{bmatrix} \begin{bmatrix} g_0 \\ g_1 \\ g_2 \\ \vdots \\ g_{n-2} \\ g_{n-1} \end{bmatrix} = 6 \begin{bmatrix} 8f_1 - f_0 - f_1 \\ f_0 \\ f_1 \\ \vdots \\ f_{n-1} \\ 8f_{n-2} - f_{n-1} - f_{n-3} \end{bmatrix} \tag{4.15}$$

Note that equation 4.13 is a tridiagonal system of equations and can be solved in $O(n)$ time [Press *et al*, 1988, sec 2.6]. Equation 4.14 is virtually tridiagonal and so should be solvable in similar time [*ibid.*, sec 2.10]. A similar comment applies to equation 4.15.

The second question, (what exists beyond the edges), is a little more tricky. Note that by defining the values of $n+2$ coefficients, $g_{-1}, g_0, g_1, \ldots, g_{n-1}, g_n$, the intensity curve described by equation 4.11 is defined over the range $x \in [x_0, x_{n-1})$. If we only define the values of $g_0, g_1, \ldots, g_{n-1}$, (as Wolberg [1990, p.136] does) then equation 4.11 describes an intensity curve defined over the smaller range $x \in [x_1, x_{n-2})$.

Outside these ranges, the intensity curve is undefined, because the necessary g_i coefficients are undefined. One solution is to set the intensity curve to a constant value outside this range, thus making it unnecessary to specify any of these unknown coefficient values.

The cyclic boundary condition automatically defines all the coefficients by the formula $g_i = g_{i+n}$. This gives a result identical to the 'replication' solution in section 4.2.1.

For the other boundary conditions we could specify the unknown f_i values, the unknown g_i values, or the value of the intensity curve outside the defined area, as described above. Specifying the unknown f_i values would allow us to find the g_i values by the impossible task of solving an infinite system of equations. It would be possible to specify the unknown f_i values only in the region which will actually be seen in the output, making it possible to calculate all the necessary g_i values.

Specifying the unknown g_i values directly is perhaps a more tempting solution, and certainly requires far less computation. This extrapolation can be achieved by any of the edge solutions in section 4.2.1, although we are no longer working with the image samples but with equation 4.11's coefficients. Wolberg [1990, p.136] seems to assume that $g_i = 0, i \notin \{0, 1, 2, \ldots, n-1\}$.

The interpolating cubic B-spline has been praised as being of higher quality than the Catmull-Rom cubic spline [Keys, 1981]. It has also been recommended as being a strictly positive interpolant, which it certainly is not. This confusion arises from the fact that the cubic B-spline function, which is applied to the g_i coefficients, is a strictly positive function. However, the function that is applied to the f_i values is not strictly positive [Maeland, 1988]. The kernel of the interpolating cubic B-spline actually oscillates in a manner similar to the sinc interpolant's kernel.

The interpolating cubic B-spline's kernel

The kernel of the interpolating cubic B-spline can be analytically derived if we ignore boundary conditions . Equation 4.11 can now be written as a discrete convolution:

$$f = h * g \tag{4.16}$$

where $f = \ldots, f_{-2}, f_{-1}, f_0, f_1, f_2, \ldots$, likewise for h and g. Further, h is defined as: $h_{-1} = \frac{1}{6}$; $h_0 = \frac{4}{6}$; $h_1 = \frac{1}{6}$; $h_n = 0, n \notin \{-1, 0, 1\}$.

In the frequency domain equation 4.16 is equivalent to:

$$F = H \times G \tag{4.17}$$

where, for unit spaced samples, H can be shown to be:

$$H(\nu) = \frac{4}{6} + \frac{2}{6}\cos 2\pi\nu$$

To find g in terms of f, we invert equation 4.17:

$$\begin{aligned} G &= \frac{1}{H} \times F \\ &= L \times F \end{aligned}$$

where L is:

$$L(\nu) = \frac{1}{H(\nu)} = \frac{3}{2 + \cos 2\pi\nu}$$

and by judicious use of Dwight [417.2] we get:

$$L(\nu) = \frac{3}{2} \times \frac{1 + a^2}{1 - a^2} \left(1 + \sum_{j=1}^{\infty} 2a^j \cos 2j\pi\nu \right) \tag{4.18}$$

where $a = -2 + \sqrt{3}$. A little algebra shows that $\frac{3}{2} \times \frac{1+a^2}{1-a^2} = \sqrt{3}$.

Transferring this back to the discrete spatial domain we get:

$$g = l * f$$

where l is the inverse Fourier transform of L:

$$\left.\begin{array}{rcl} l_n & = & \sqrt{3}a^n \\ l_{-n} & = & l_n \end{array}\right\} n \geq 0 \tag{4.19}$$

Thus each g_i is dependent on all of the f_i values.

Numerical verification of the values of l_i can be achieved by running a modified version of Sedgewick's [1988, p.549] algorithm for finding interpolating B-spline coefficients. On a dataset of 32 samples, this gave values (for the middle region of the data, where edge effects are minimised) for the l_i to three significant figures of:

$$\begin{array}{rrcrl} & l_0 & = & 1.732 & \pm 0.001 \\ & l_{-1} = l_1 & = & -0.464 & \pm 0.001 \\ & l_{-2} = l_2 & = & 0.124 & \pm 0.001 \\ & l_{-3} = l_3 & = & -0.033 & \pm 0.001 \\ & l_{-4} = l_4 & = & 0.009 & \pm 0.001 \\ & l_{-5} = l_5 & = & -0.002 & \pm 0.001 \\ n \geq 5: & l_{-n} = l_n & = & 0.000 & \pm 0.001 \end{array}$$

In agreement with the theoretically derived formula.

The creation of an intensity curve can be written as:

$$i = b * g$$

where b is the approximating cubic B-spline kernel. This is equivalent to:

$$\begin{array}{rcl} i & = & b * (l * f) \\ & = & (b * l) * f \end{array}$$

The approximating B-spline kernel, b, is graphed in figure 4.30, and the interpolating B-spline kernel, $b * l$, is graphed in figure 4.31. Note that $b * l$ has negative lobes.

This derivation roughly parallels that given by Maeland [1988]. Maeland's formula for the cubic B-spline kernel [p.214, equation 8] is, however, wrong. It is:

$$B_{\text{Maeland}}(s) = \begin{cases} \frac{3}{4}|s|^3 - \frac{3}{2}|s|^2 + 1, & 0 \leq |s| < 1 \\ -\frac{1}{4}|s|^3 + \frac{1}{2}, & 1 \leq |s| < 2 \\ 0, & \text{otherwise} \end{cases}$$

Compare this with the correct version (equation 4.21) provided by Parker *et al* [1983, p.35] and Wolberg [1990, p.135, equation 5.4.18]. Maeland's conclusions are still valid, but the details are slightly incorrect.

The interpolating cubic B-spline is often cited as being better than the Catmull-Rom spline (or other cubics which fit Mitchell and Netravali's [1988] formula (equation 3.19)) [Keys, 1981; Maeland, 1988]. This is due to the fact that this interpolant considers a wider range of data than these other cubics. Further it is sinc-like in form; with the advantages that negative lobes bring (section 3.5.7). However, it has an advantage over the sinc function in that, while the sinc kernel only has a $\frac{1}{x}$ decay, the interpolating B-spline exhibits an exponential decay (see section 4.6).

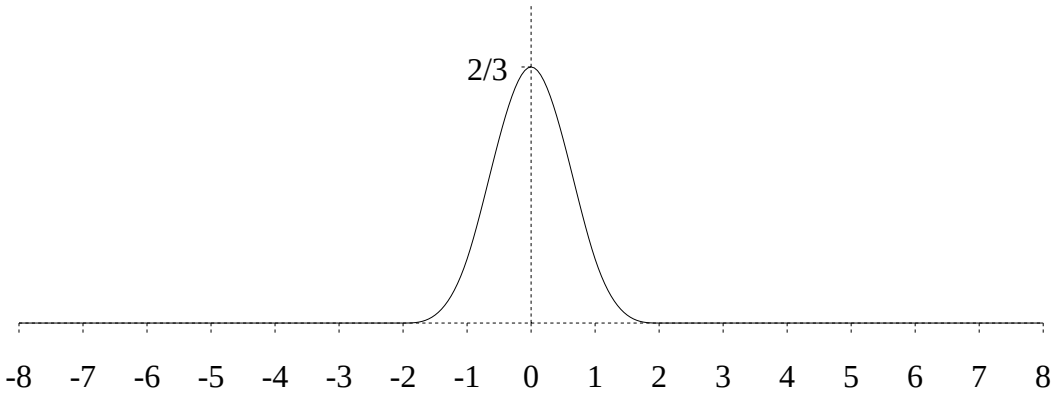

Figure 4.30: The approximating cubic B-spline kernel, b.

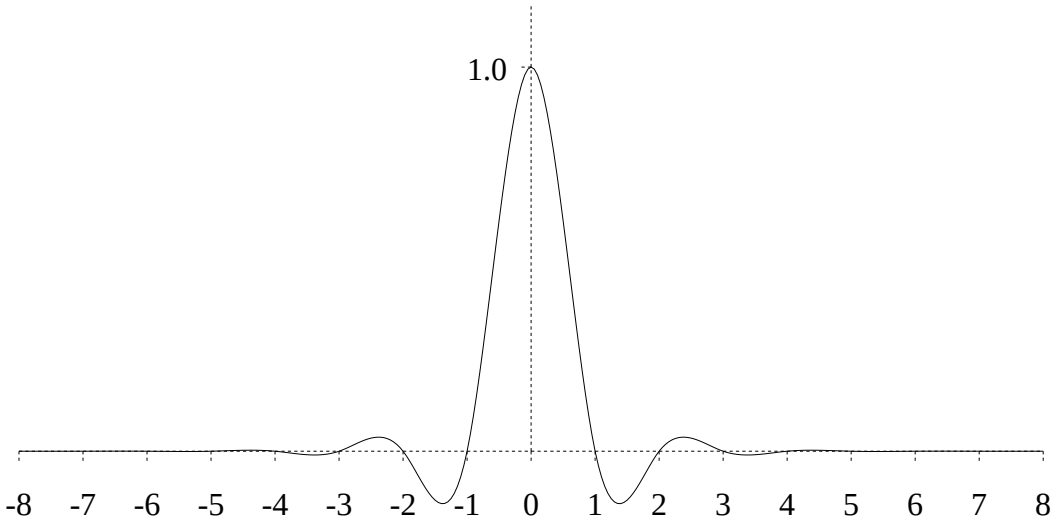

Figure 4.31: The interpolating cubic B-spline kernel, $b * l$.

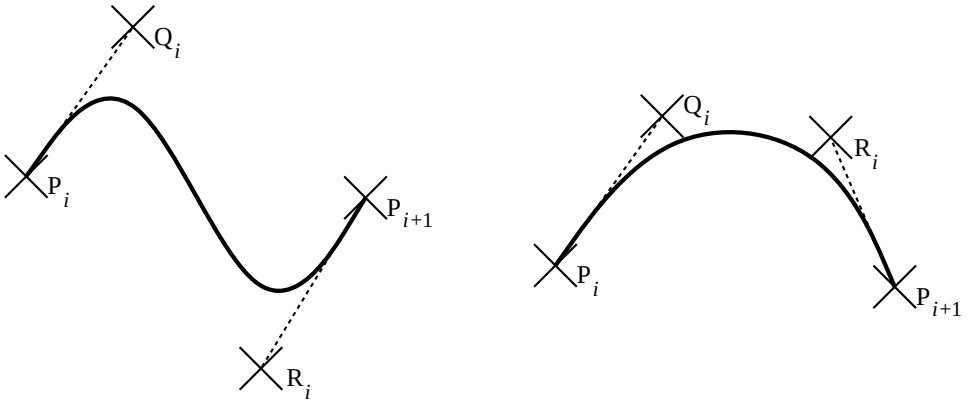

Figure 4.32: A Bezier cubic curve is defined by four points: its two endpoints, P_i and P_{i+1}, and two control points, Q_i and R_i.

The interpolating B-spline kernel can be used directly on the image data values, f_i. In this case boundary effects would be handled by one of the methods in section 4.2.1. The interpolating B-spline kernel is analytically defined as:

$$h(s) = \sum_{j=-\infty}^{\infty} B_4(j-s)\sqrt{3}a^{|j|},\ a = -2+\sqrt{3} \tag{4.20}$$

where $B_4(s)$ is the approximating B-spline kernel:

$$B_4(s) = \begin{cases} \frac{1}{2}|s|^3 - |s|^2 + \frac{2}{3}, & 0 \le |s| < 1 \\ -\frac{1}{6}|s|^3 + |s|^2 - 2|s| + \frac{4}{3}, & 1 \le |s| < 2 \\ 0, & \text{otherwise} \end{cases} \tag{4.21}$$

This equation looks as if it is uncomputable because of the infinite sum. However, for any given value of s, only four of the terms in the sum will be non-zero: those for which $j \in \{\lfloor s \rfloor - 1, \lfloor s \rfloor, \lfloor s \rfloor + 1, \lfloor s \rfloor + 2\}$.

4.5.1 Bezier cubic interpolation

Bezier cubic interpolation is related to cubic B-spline interpolation in that a particular cubic function is applied to a set of coefficients derived from the data points. We briefly discussed the Bezier cubic in section 3.6.3. The Bezier cubic form is described by Foley and van Dam [1982, sec. 13.5.2] and the Bezier cubic interpolation formula is presented by Rasala [1990]. The cubic form is:

$$P(x) = [t^3\, t^2\, t\, 1] \begin{bmatrix} -1 & 3 & -3 & 1 \\ 3 & -6 & 3 & 0 \\ -3 & 3 & 0 & 0 \\ 1 & 0 & 0 & 0 \end{bmatrix} \begin{bmatrix} P_\alpha \\ Q_\alpha \\ R_\alpha \\ P_{\alpha+1} \end{bmatrix} \tag{4.22}$$

Where $\alpha = \left\lfloor \frac{x-x_0}{\Delta x} \right\rfloor$, $t = \frac{x-x_\alpha}{\Delta x}$, and $P(x) = (x_\alpha, f_\alpha)$ is a point in space rather than simply a function value. This equation produces a cubic curve which passes through its end points (P_α and $P_{\alpha+1}$) and whose shape is controlled by the endpoints and by the control points as shown in figure 4.32.

Given a set of points, $\{P_i : i \in \mathcal{Z}\}$, we can generate a set of control points, $\{(Q_i, R_i) : i \in \mathcal{Z}\}$, such that the piecewise Bezier cubic defined by the points is C2-continuous. Rasala [1990] gives the conditions required to generate the control points as:

$$P_i - R_{i-1} = Q_i - P_i \tag{4.23}$$

$$P_i - 2R_{i-1} + Q_{i-1} = R_i - 2Q_i + P_i \tag{4.24}$$

Given equation 4.23, a difference vector can be defined:

$$\begin{aligned} D_i &= P_i - R_{i-1} && (4.25)\\ &= Q_i - P_i && (4.26)\end{aligned}$$

Equations 4.24, 4.25, and 4.26 can be combined to produce a recurrence relation between the D_i and the P_i:

$$D_{i+1} + 4D_i + D_{i-1} = P_{i+1} - P_{i-1}$$

Rasala produces the following result for a closed loop of n points (that is: $P_i = P_{i-n}$):

$$D_i = \sum_{k=1}^{m} a_k (P_{i+k} - P_{i-k}) \tag{4.27}$$

where:

$$\begin{aligned} a_k &= -\tfrac{f_{m-k}}{f_m} \\ f_j &= -4f_{j-1} - f_{j-2},\ j \geq 2 \\ \text{for } n \text{ even} \quad m &= \tfrac{n-2}{2},\ f_0 = 1, f_1 = -3 \\ \text{for } n \text{ odd} \quad m &= \tfrac{n-1}{2},\ f_0 = 1, f_1 = -4 \end{aligned}$$

For the infinite case (that is: a non-repeating infinite set of points) it can be shown that:

$$a_n = -(a)^n$$

where $a = -2 + \sqrt{3}$ (see appendix B.3 for details).

This is the same constant as that used in the B-spline case (equation 4.20) and, indeed, the same sequence of coefficients (a_n). This is unsurprising as both situations involve the 1–4–1 kernel. Note, however, that these values are used in different ways.

If we let $D_i = \begin{bmatrix} \epsilon_i \\ \delta_i \end{bmatrix}$ then $Q_i = (x_i + \epsilon_i, f_i + \delta_i)$, $R_i = (x_{i+1} - \epsilon_{i+1}, f_{i+1} - \delta_{i+1})$.

Taking equation 4.27 for the infinite case, and splitting it into two parts we get:

$$\epsilon_i = \sum_{k=1}^{\infty} a_k (x_{i+k} - x_{i-k}) \tag{4.28}$$

$$\delta_i = \sum_{k=1}^{\infty} a_k (f_{i+k} - f_{i-k}) \tag{4.29}$$

With the sample points equispaced ($x_{i+1} = x_i + \Delta x$) equation 4.28 becomes:

$$\begin{aligned} \epsilon_i &= -\sum_{k=1}^{\infty} (a)^k \times 2k\,\Delta x \\ &= -2\,\Delta x \sum_{k=1}^{\infty} k(a)^k \\ &= -2\,\Delta x\, a \frac{1}{(1-a)^2} \qquad \text{[Dwight 9.06]} \\ &= \frac{1}{3}\,\Delta x \end{aligned}$$

Thus the four control points are equispaced over the unit distance, at x_i, $x_i + \frac{1}{3}\Delta x$, $x_i + \frac{2}{3}\Delta x$, and x_{i+1}. Further, δ_i (equation 4.29) can be expressed as:

$$\delta_i = -\sum_{k=1}^{k=\infty} (a)^k \, (f_{i+k} - f_{i-k})$$

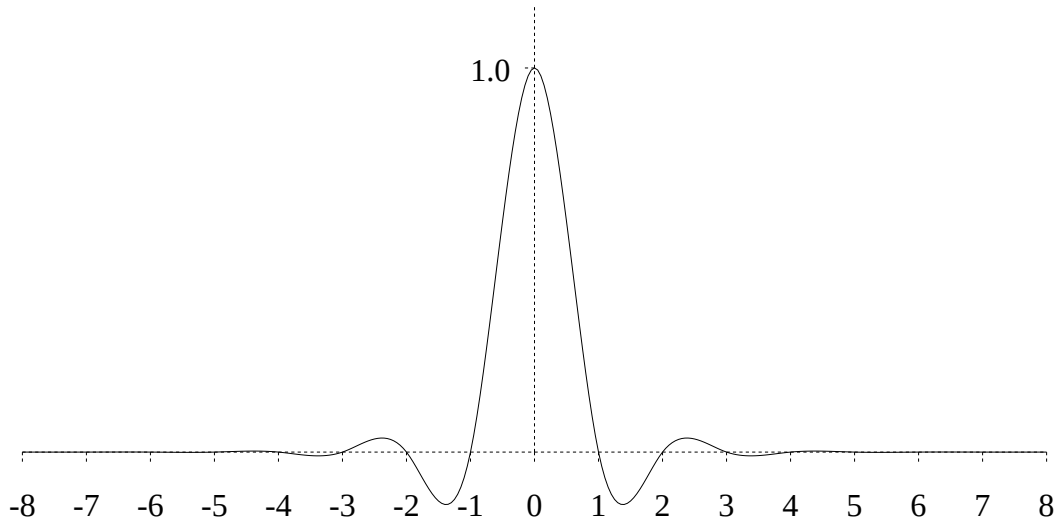

Figure 4.33: The Bezier interpolating cubic's filter kernel.

Substituting this into equation 4.22 we get:

$$\begin{array}{rcl} f(x) = & & (-t^3+3t^2-3t+1)f_\alpha \\ & + & (3t^3-6t^2+3t)\left(f_\alpha - \sum_{k=1}^{\infty} a^k(f_{\alpha+k}-f_{\alpha-k})\right) \\ & + & (-3t^3+3t^2)\left(f_{\alpha+1} - \sum_{k=1}^{\infty} a^k(f_{\alpha+1+k}-f_{\alpha+1-k})\right) \\ & + & (t^3)f_{\alpha+1} \end{array} \tag{4.30}$$

From this we can evaluate this interpolant's kernel:

$$h(s) = \begin{cases} a^{i+1}(3x^3+(-9i-3)x^2 & \\ \quad +(9i^2+6i)x+(-3i^3-3i^2)) & \\ +\,a^i(3x^3+(-9i-6)x^2 & \\ \quad +(9i^2+12i+3)x+(-3i^3-6i^2-3i)), & i \geq 1, i = \lfloor x \rfloor \\ & i \leq x < i+1 \\ a(3x^3-3x^2) & \\ +\,2x^3-3x^2+1, & 0 \leq x < 1 \\ & \\ a(-3x^3-3x^2) & \\ -\,2x^3-3x^2+1, & -1 \leq x < 0 \\ & \\ a^{i-1}(-3x^3+(-9i+3)x^2 & \\ \quad +(-9i^2+6i)x+(-3i^3+3i^2)) & \\ +\,a^i(-3x^3+(-9i+6)x^2 & \\ \quad +(-9i^2+12i-3)x+(-3i^3+6i^2-3i)), & i \geq 2, i = -\lfloor x \rfloor \\ & -i \leq x < -i+1 \end{cases} \tag{4.31}$$

This kernel is shown in figure 4.33. Comparing figures 4.33 and 4.31 it may be suspected that this Bezier kernel may be identical to the interpolating cubic B-spline kernel (equation 4.20) in the same way that several paths led to the Catmull-Rom. This suspicion is in fact true: a goodly amount of algebra will show that equations 4.31 and 4.20 are identical.

An image to which Bezier/B-spline reconstruction is to be applied can be edge extended in any of the usual ways (section 4.2.1). Rasala's [1990] paper, rather than discussing the general method presented here, gives the exact Bezier reconstruction for two special cases: the case of a 'closed loop', that is the replication edge extension method, where the image edges, in effect, wrap round

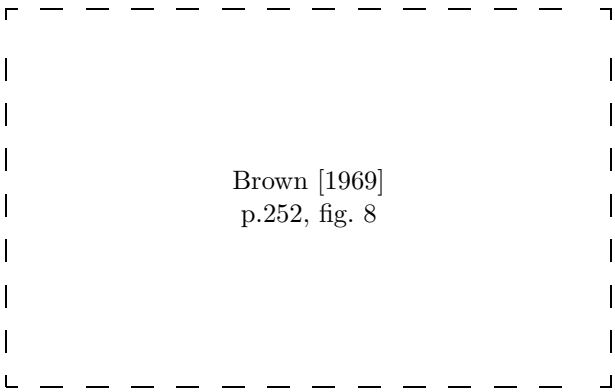

Figure 4.34: Brown's [1969] figure 8. Images were reconstructed using a filter with first and second side lobes. The second side lobe height was set at 2% of the central lobe's height. This graph shows the subjective score for two images, one live and one still, against the height of the first side lobe as a percentage of the height of the central lobe. The best subjective quality occurs at a height of around 12%.

to meet one another; and the case of an 'open curve'. In this latter case, one specifies the tangent values of the curve at the end points and reflects the curve about its endpoints. This is a special case edge extension, similar, but not equal to, the reflection edge extension method.

The B-spline/Bezier kernel has the properties of oscillating about zero and of decaying exponentially to zero. It thus has negative lobes. The first negative lobe is by far the biggest, and hence contributes most to any sub-black or supra-white value, the second and subsequent negative lobes contribute a negligible amount to the final intensity surface values.

The Catmull-Rom spline has these properties also. It has been suggested that the interpolating cubic B-spline is a good interpolant because it is continuous in its second derivative, while the Catmull-Rom spline, which is not as good [Keys, 1981] has only first derivative continuity. However, the discussion in section 3.5.2 indicates that the presence or absence of C2-continuity has little effect on the visual fidelity of the interpolation. It appears that it is the sharpening effect caused by the negative lobes is the important factor here.

4.5.2 The sharpening effect of negative lobes

A reconstruction filter which has a negative side lobe, such as the Catmull-Rom or B-spline/Bezier, produces a visually sharper intensity surface than reconstructors without such lobes. Schreiber and Troxel [1985] noted this effect in their sharpened Gaussian filter. They point out that the overshoot caused by the negative lobes appears to be a defect but actually is the feature responsible for the better tradeoff between sharpness and sampling structure.

However, ringing, when there is more than one lobe either side of the central lobe, is perceived to be a bad effect. Brown [1969] carried out a test to discover the subjective effects of these side lobes. Brown's results show that the presence of the first side lobe increases subjective picture quality, provided the second lobe is non-existent or at least small. The subjective quality was measured on a scale of 0–4 by seven observers and the average value plotted in figure 4.34. A value of 1 indicates no improvement; less than 1 is degradation. A value of 3 indicates that the image is subjectively as good as an image of twice the test bandwidth. The best improvements occur for a lobe of height 10–14% of the height of the intensity change (in our filters this means a first side lobe of height 10–14% of the central lobe height). Brown's results for the second lobe show that it

Reconstructor	Sinc	Catmull-Rom	B-Spline/Bezier	Sharpened Gaussian
First side lobe	22%	7.4%	14%	8.4%
Second side lobe	13%	0%	3.7%	0%

Table 4.2: The heights of the side lobes of four reconstructor's filters, given as a percentage of the height of the central lobe.

causes subjective degradation of the image but that, for a height of 4% or less this degradation is not significant compared to the enhancing attributes of the first lobe.

Table 4.2 contains the size of the first two side lobes of each of the reconstructors with a negative first side lobe. The figures are given as percentages of the height of the central lobe. This table indicates that sinc will produce a visually degraded intensity surface. This result is well known from simply viewing sinc reconstructed and enlarged images [Mitchell and Netravali, 1988; Ward and Cok, 1989]; see figures 2.8, 2.12, and 4.20 for examples of this degradation.

The B-spline/Bezier interpolant should produce a result which is about right, whilst both the Catmull-Rom and sharpened Gaussian, appear to have a first side lobe that is slightly small for best effect.

Brown states [p.252] that, for moving pictures, with a signal to noise ratio of 40dB, the best height for the first side lobes is reduced. He found that moving the ideal value from 12% (noiseless) to 6% (noisy) gave the best results. Thus the Bezier/B-spline reconstructor would be expected to do badly with noisy images while the other two would be better.

This effect does not account for all subjective quality, as it only improves the sharpness of the image. However it does give an important pointer to why some reconstructors appear better than others. Other factors, though also come into play.

The sinc and Bezier/B-spline kernels are both oscillatory. The reason the sinc kernel causes ringing artifacts while the B-spline tends not to is that sinc has a much slower fall off to zero than the B-spline. Thus sinc has much more prominent side lobes than the B-spline. This is picked up in section 4.6.

The Mach band effect

One possible explanation of this sharpening is that it is due to the Mach band effect. This physiological effect was first described by Mach [1865] and is described in detail by Ratliff [1965] (Ratliff's book also includes translations of Mach's papers on this and related effects). The basic effect, as it concerns our work, is that the bright side of an edge appears brighter than its surrounds and the dark side appears darker. The stimulus presented to the eye by a sharp edge, and the sensation passed by the eye to the brain, are illustrated in figure 4.35.

The sharper the edge, the more pronounced the effect [Ratliff, 1965, p.89]. The importance of this effect is that, if the eye is presented with a different intensity distribution which produces a sensation similar to the sensation curve in figure 4.35 then the visual system will interpret it as the stimulus curve in the same figure. Thus, to give the appearance of a sharp edge, it is not necessary to present the eye with an actual sharp edge. It is sufficient to present a sloping edge with a lobe at either end, producing a very similar sensation curve to that given by a sharp edge. Cornsweet [1970] presents an interesting illustration of two different stimuli producing the same sensation. This is shown in appendix D.

The response function of the human visual system is known to be shaped something like that shown in figure 4.36 [Ratliff, 1965]. This shape, with a single prominent negative side lobe is very like that of the Catmull-Rom, sharpened Gaussian, and B-spline/Bezier kernels. Thus these kernels will produce an intensity curve, around an edge in the image, similar to the eye's response to a sharp edge. This may fool the eye into seeing a sharp edge at that point. This phenomenon

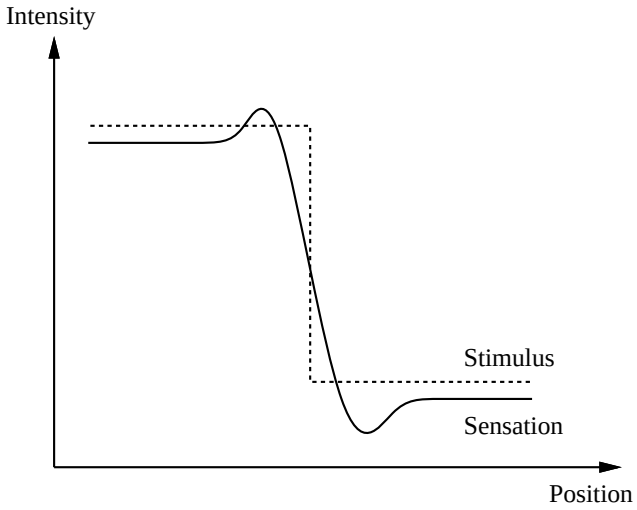

Figure 4.35: The Mach band effect, showing the stimulus presented to the eye and the sensation passed by the eye to the brain. The sensation curve has bumps either side of the edge which make the intensity appear slightly darker on the dark side and slightly lighter on the light side.

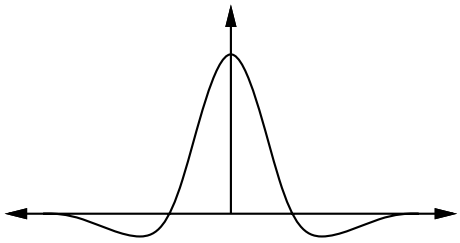

Figure 4.36: The response function of the human visual system, similar in shape to the kernels of the Catmull-Rom, sharpened Gaussian, and B-spline/Bezier reconstructors.

could account in part for the success of these kernels as reconstructors, that is: they are perceived to be good because they take advantage of a physiological effect of the eye.

The problem of negative intensities

A final note here is that there is some debate as to whether negative lobes are desirable (section 3.5.7). The main argument against negative lobes is that they can produce negative pixel values. Blinn [1989b] states "there is no such thing as negative light and clamping these negative values to zero is about all you can do, but it is not ideal". Clamping will, in fact, destroy the lobes we are using to sharpen the edge.

An alternative to clamping is to rescale the values so that the lowest and highest intensities are physically realisable [Wolberg, 1990, p.131]. This maintains the intensity changes required to produce the desired effect. However, the unfortunate consequence is that the image's contrast is reduced, which is undesirable.

If we consider Blinn's [1989b, p.87] statement that clamping negative values to zero is about all you can do, it appears that something could be achieved when we examine the visual phenomena shown in appendix D. There, Cornsweet's [1970] figures indicate that a third solution, that of locally rescaling intensity values, could produce desirable results. Cornsweet shows that two different

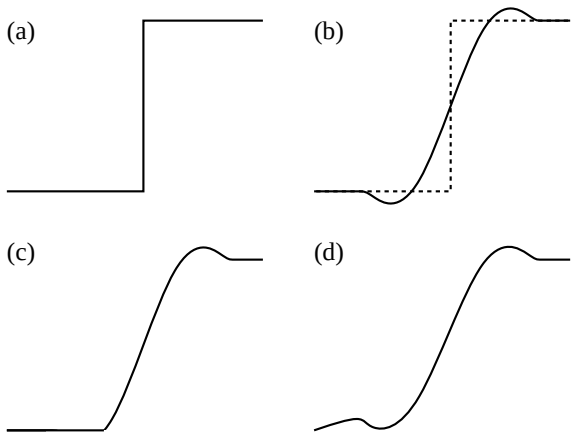

Figure 4.37: A possible solution to the problem of generating negative intensity values. (a) shows the curve we would like to simulate: a sharp edge. (b) shows the stimulus we would like to present to the eye to fool the brain into seeing the sharp edge. (c) shows this stimulus clamped to zero, thus destroying the illusion of a sharp edge. (d) shows a possible solution: locally modifying the intensities so that the stimulus is still there at the dark side of the edge, and gently blending this into the dark area to the left.

intensity distributions produce identical visual response for two different cases.

This, and other, evidence indicate that local intensity changes are far more important than slow (non-local) changes and absolute intensity values. Thus, if we could 'raise' a region of negative light into positive values and gently blend this raised region in with the surrounding areas then the resulting visual response should be closer to the desired response than simply clamping negative values to zero, and it would not have the undesirable characteristics of globally reducing image contrast. The basic idea is shown in figure 4.37.

Some way of implementing a function of this nature needs to be found. This is not a simple process as the correction applied at any one point can depend on a large neighbourhood around that point, on the distance to the 'centre' of the nearest negative trough, and on the depth of that trough. It is difficult to decide if such a 'correction' can be performed. If it can, then a decision must be made as to whether it is worth the effort. Further work on this solution is required.

4.5.3 The two-dimensional interpolating cubic B-spline

The B-spline interpolant has been presented in a one-dimensional form. When using filters, such as the sinc or Gaussian, it is simple to extrapolate from the one- to the two-dimensional filter kernel by convolving two one-dimensional filter kernels, perpendicular to one another. This is illustrated in figures 4.38, 4.39, and 4.40.

This two dimensional kernel can be directly convolved with the sample points. The B-spline kernel could also be treated like this. However, the usual way of producing a B-spline curve is to evaluate the coefficients, g_i and then use a simple, local B-spline kernel on these. The standard way of extending this to two dimensions is to evaluate the coefficients for each scan-line in one direction, then, for each point for which a value is required, the coefficients must be evaluated for the line, passing through the point, perpendicular to those scan lines; and hence the value at that point calculated (see figure 4.41). This is a very time consuming process.

In practice, this limits the B-spline interpolant's usefulness to scan-line algorithms rather than 2-D algorithms. However, if we treat the B-spline as a filter (equation 4.20), rather than as a calculation

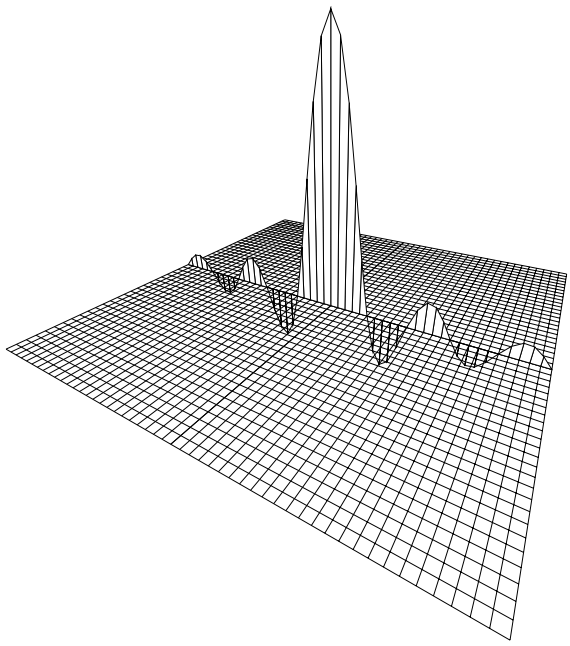

Figure 4.38: The sinc kernel aligned along the x-axis.

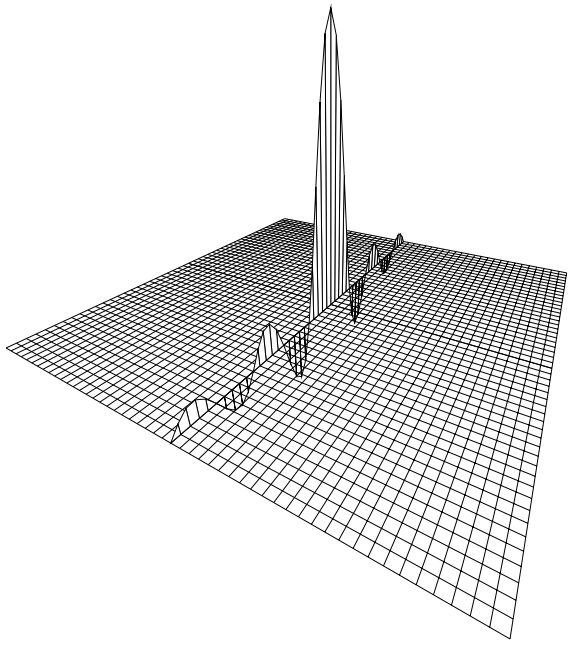

Figure 4.39: The sinc kernel aligned along the y-axis.

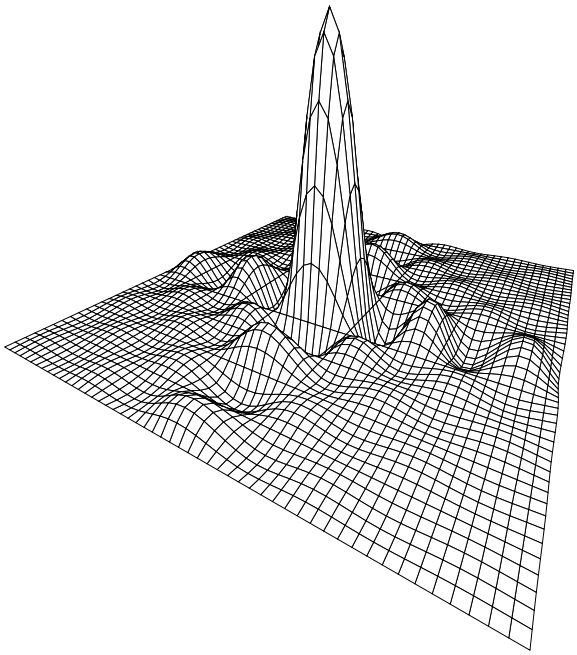

Figure 4.40: The two-dimensional sinc kernel, generated by convolving the two one-dimensional kernels shown in figures 4.38 and 4.39.

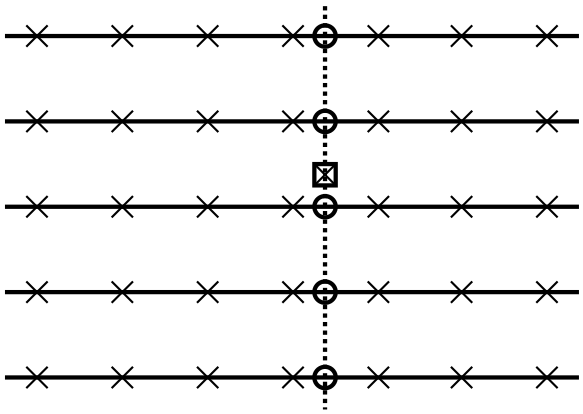

Figure 4.41: The traditional extension of the one-dimensional interpolating cubic B-spline to two-dimensional interpolation. Coefficients are calculated for each scan-line in the horizontal direction, then to find the value at any one point we need to calculate a complete set of coefficients in the vertical direction — a time-consuming process, because in general, the required points can be anywhere in the plane, and so these vertical coefficients will not be used for more than one point.

of coefficients, followed by a simpler filter, the two dimensional version is easy to construct from two one-dimensional versions, as in figures 4.38 through 4.40:

$$h(x,y) = h(x) \times h(y)$$

where $h(x,y)$ is the two-dimensional kernel and $h(s)$ is the one-dimensional kernel.

The question now arises, is it possible to generate a two-dimensional set of coefficients and apply a simple local kernel (for example: the two-dimensional approximating cubic B-spline) to them to produce the same result as applying the complicated non-local kernel to the image sample values?

If we assume an image of infinite extent, then equation 4.20 is the one-dimensional filter kernel for the interpolating B-spline:

$$h(s) = b(s) * \check{l}(s)$$

where $b(s)$ is the cubic B-spline kernel and $\check{l}(s)$ is the discrete kernel which is convolved with the data-values, f_i, to produce the coefficients, g_i.

The two one-dimensional versions of $h(s)$ are:

$$\begin{aligned} h_x(x,y) &= \begin{cases} h(x), & y = 0 \\ 0, & \text{otherwise} \end{cases} \\ h_y(x,y) &= \begin{cases} h(y), & x = 0 \\ 0, & \text{otherwise} \end{cases} \end{aligned}$$

These can be convolved to produce the two-dimensional interpolating cubic B-spline kernel:

$$h(x,y) = h_x(x,y) * h_y(x,y)$$

Expanding this out and rearranging terms we get:

$$\begin{aligned} h(x,y) &= b_x(x,y) * \check{l}_x(x,y) * b_y(x,y) * \check{l}_y(x,y) \\ &= b_x(x,y) * b_y(x,y) * \check{l}_x(x,y) * \check{l}_y(x,y) \\ &= b(x,y) * \check{l}(x,y) \end{aligned}$$

where $b(x,y)$ is the two-dimensional approximating cubic B-spline kernel and $\check{l}(x,y)$ can be shown to be a discrete function with values: $l_{x,y} = l_x \times l_y,\ x,y \in \mathcal{Z}$ (l_n is defined in equation 4.19). Thus:

$$l_{x,y} = 3a^{|x|+|y|},\ x,y \in \mathcal{Z}$$

Now if we perform the discrete convolution:

$$g_{x,y} = l_{x,y} * f_{x,y}$$

then the two-dimensional B-spline kernel, $b(x,y)$ applied to the $g_{x,y}$ coefficients will produce an intensity surface which interpolates the $f_{x,y}$ data values.

$l_{x,y}$ is an infinitely wide filter. Its values, however, decrease exponentially as $|x| + |y|$ increases (this rapid decrease is noted by Rasala [1990, p.584] in his discussion of the Bezier interpolant). This means that an excellent approximation to $l_{x,y}$ can be obtained by only considering values of x and y for which $|l_{x,y}|$ is greater than some constant. For example, if we consider all values such that $|l_{x,y}| \geq 10^{-4}$ (an adequate lower bound for our purposes) then we need only consider values of x and y for which $|x| + |y| \leq 7$. This gives a diamond of $l_{x,y}$ coefficients to consider, with a diagonal length of 15 coefficients (total, 113 coefficients). This can be used to calculate all the $g_{x,y}$ coefficients. There are the usual edge effect problems near the image edges but these can be solved by any of the standard edge solutions in section 4.2.1.

This method of producing the coefficients differs from the standard method. The standard method involves the solution of a one-dimensional system of equations for each scan-line. This system has

special end conditions (because scan-lines are finite in length) and thus cannot be represented as a digital filter[12]. The special end-conditions cause a problem in that they mean that a solution cannot easily be found to a two-dimensional system of equations, and so we must resort to the time-consuming method shown in figure 4.41. A two-dimensional system of equations could be generated based on the fact that:

$$f_{x,y} = \frac{1}{36}(g_{x-1,y-1} + 4g_{x-1,y} + g_{x-1,y+1} + 4[g_{x,y-1} + 4g_{x,y} + g_{x,y+1}] + g_{x+1,y-1} + 4g_{x+1,y} + g_{x+1,y+1})$$

End conditions could be imposed for the edge values. This would produce a system of $(N+2)^2$ equations in $(N+2)^2$ unknowns. This two-dimensional system does not have the tridiagonal property of its one-dimensional counterpart and so would take $O(N^6)$ time to solve [Press *et al*, 1988]. It may be possible to reduce this order with a specially designed algorithm [*ibid.*, sec. 2.10], but this possibility has yet to be investigated.

The coefficients resulting from the method of figure 4.41 are virtually identical to those generated by the filter method except near the image edges. Near the edges, the different results are due to the different edge solutions employed by the two methods.

4.5.4 Using the two-dimensional interpolating B-spline

We have developed three different ways of producing an intensity surface using the interpolating cubic B-spline. To evaluate the usefulness of each method, assume that the original image contains $N \times N$ sample values and that we need to evaluate the intensity surface at $M \times M$ points. That is: the reconstructor forms part of a resampler which also includes some sort of point sampler.

The first of the three methods is to convolve the two dimensional interpolating B-spline kernel, $h(x, y)$, directly with the $f_{x,y}$ data values. Given these assumptions, resampling using this first method is an $O(M^2)$ process.

The second method is to precalculate the $g_{x,y}$ coordinates using the $l_{x,y}$ filter on the $f_{x,y}$ data values. The local B-spline kernel, $b(x, y)$, can then be applied to these. The precalculation is an $O(N^2)$ process and the intensity surface evaluation is an $O(M^2)$ process. Thus, overall this is an $O(M^2)$ process (N is of order $O(M)$).

The third method is that illustrated in figure 4.41. It involves precalculating one-dimensional coefficients for each scan-line and then, for each point evaluated, calculating a perpendicular set of one-dimensional coefficients and then using these to evaluate the value of the intensity surface at the point. The precalculation here is $O(N^2)$, but the evaluation of the intensity surface values is $O(NM^2)$, except in certain special cases where it can be reduced to only $O(M^2)$. This makes the overall process $O(M^3)$ (except in those special cases).

Thus, either of the first two cases reduces the time from $O(M^3)$ (for the third, traditional, method) to $O(M^2)$. Which of these two is faster depends on the actual timings of the two, and on the values of N and M.

As a rough guide, let us say that the execution time of the two methods can be written as follows:

$$\begin{aligned} T_1 &\approx k_1 M^2 \\ T_2 &\approx cN^2 + k_2 M^2 \end{aligned}$$

Now, for each intensity surface value evaluated by the first method, 113 numbers have to be computed and summed (assuming we adopt the diamond-shaped kernel of page 139); while the total for the second method is only 16. Thus $k_1 \approx 7k_2$. For the second method to be faster than

[12] Remember that we originally produced the filter version by assuming an infinitely long scan-line, and therefore no end conditions.

Method	Precalculation	Calculation
1. Direction convolution	—	$O(M)$
2. Filter precalculation	$O(N)$	$O(M)$
3. Traditional method	$O(N)$	$O(M)$

Table 4.3: The orders of the operations involved in each of the three ways of calculating the one-dimensional, interpolating cubic B-spline.

Operation	k_1	k_2	k_3	c_2	c_3
Multiplies	62	18	18	15	1
Divides	—	—	—	—	3
Adds	74	15	15	14	5
Table lookups	60	16	16	15	—
Function value lookups	15	—	—	15	3

Table 4.4: The operations involved in calculating a value for each constant in timing equations for each of the three ways of calculating the one-dimensional, interpolating cubic B-spline.

the first thus requires:

$$cN^2 < \frac{6}{7}k_1M^2$$

It can be shown that k_1 is between 2 and 3 times c (see appendix B.8) and thus, for $T_2 > T_1$, we require:

$$N^2 < 2M^2$$

Therefore, so long as the destination image has the same or a greater number of pixels as the source image, the second method should be noticeably faster. On the other hand if the destination has significantly less pixels than the source (say $M^2 \leq \frac{1}{4}N^2$), then the first method will be noticeably faster. The third method, being $O(M^3)$ will be slower than both, except, perhaps, for very small M.

4.5.5 Using the one-dimensional interpolating B-spline

While this $O(M^3)$ behaviour makes the traditional method unsuitable for two-dimensional reconstruction, it suffers no such problem in one-dimension. Do these new methods of evaluating the interpolating B-spline offer any advantages in one-dimensional reconstruction?

Again, assume that the one-dimensional source 'image' contains N sample values and the destination, M sample values. Table 4.3 gives the time complexities of the three methods. They are all of the same order. To get some idea of how they compare, we will again produce some approximate timings.

Assume:

$$\begin{aligned} T_1 &\approx k_1M \\ T_2 &\approx c_2N + k_2M \\ T_3 &\approx c_3N + k_3M \end{aligned}$$

The number of operations involved in each of these constants is shown in table 4.4. This shows that $k_2 = k_3$ (the process is identical for both methods), $k_1 \approx 4k_2$, and $c_2 \approx k_2$. Thus, for the second method to be faster than the first requires $N < 3M$, that is the source image is at most three times the length of the destination. The second and third methods are identical for calculating the destination image values. Comparing their times for precalculating the coefficients depends on how long a divide operation takes compared to a multiply. If a divide is about five times the

length of a multiply the two methods take about the same time; if less then the third is faster; if more then the second is faster.

Tests on one particular machine (a DEC Decstation 5400 running Ultrix 3.1 and X11R4) indicated that a divide was about five times the length of a multiply. This indicates that both methods are as fast as each other, although the second method uses less storage than the third.

Thus, for shrinking a one-dimensional image by a factor smaller than a third, the first method is fastest. For other cases there is little to choose between the second and the third (traditional) method. However, as we have seen, for two-dimensional images the third method is considerably slower than either of the two new methods.

4.6 Local approximations to infinite reconstructors

The infinite extent reconstructors are good theoretical devices. With appropriate edge solutions they can be used in a real situation, operating on an entire image. In practice, however, resampling is a faster operation if a smaller local reconstructor is used. Thus we seek local approximations to these non-local reconstructors.

These are two basic types of approximation: either a windowed version of the infinite reconstructor, or a local polynomial approximation, matching the shape of the infinite reconstructor. We have already discussed several members of this latter class. In particular, the one-parameter family of cubics (equation 3.20) was originally developed by Rifman [Keys, 1981, p.1153] as an efficient approximation to the sinc reconstructor [Park and Schowengerdt, 1983, p.260; Wolberg 1990, p.129]. As such, Rifman set the parameter $a = -1$ in order to match the slope of the sinc function at $s = \pm 1$. Since then, Keys [1981] and Park and Schowengerdt [1983] have shown that $a = -\frac{1}{2}$ (the Catmull-Rom spline) is a better choice. It is still, of course, a valid approximation to a sinc function. The local B-splines, on the other hand, are local approximations to the Gaussian [Heckbert, 1989, p.41]. The approximating cubic B-spline is the most used member of this family.

The other form of approximation to an infinite function is a windowed version of that infinite function. Windowing is a simple process where the infinite function's kernel is multiplied by an even, finite-extent window kernel. The simplest window function is a box, which has the value one within certain bounds and zero outside. Windowing by a box function is commonly called truncation.

Truncation's effectiveness depends on the nature of the infinite function being truncated. If the infinite function's values are negligible outside the truncation bounds then the effect of truncation on the function will also be negligible. However, if the function's values outside these bounds are not negligible then truncation will have a noticeable, usually deleterious, effect on the reconstructor.

Table 4.5 gives the bounds beyond which the listed functions' magnitudes remain below each of the listed limit values. Note that all the functions are normalised so that the area under the curve is one. This especially relates to the the two 2^{-kx^2} Gaussians, which are usually presented in their unnormalised form. (Note that the Gaussians chosen by the different researchers are all similar in value with standard deviations, ranging between $\sigma = 0.42$ and $\sigma = 0.61$.)

All of the tabulated functions, except for the sinc function, decay exponentially. All of the exponential methods' kernel values become negligible within at most ten sample spaces. The fact that these reconstructor kernels become negligible so quickly means that they can be truncated locally with negligible loss of quality [Heckbert, 1989 p.41; Wolberg, 1990, pp.143–146].

Examples of such truncation include Ratzel's [1980, p.68] truncation of his Gaussian to $|x| < 1.3$ and of the sharpened Gaussian to $|x| < 2.3$ [*ibid.*, p.69]. This truncation limit on the Gaussian would appear to be a little low.

Turkowski [1990, pp.153–154] truncates his 2^{-2x^2} filter to $|x| < 2$ and his 2^{-4x^2} filter to $|x| < 1.5$.

Function	Limits ±0.01	±0.001	±0.0001	Source
$\sqrt{\frac{8\ln 2}{2\pi}}2^{-4x^2}$	1.280	1.571	1.816	Gaussian; Turkowski [1990], Wolberg [1990]
$\frac{1}{0.5\times\sqrt{2\pi}}e^{-\frac{1}{2}\frac{x^2}{(0.5)^2}}$	1.480	1.828	2.119	Gaussian; Heckbert [1989, p.41]
$\frac{1}{0.52\times\sqrt{2\pi}}e^{-\frac{1}{2}\frac{x^2}{(0.52)^2}}$	1.532	1.895	2.199	Gaussian; Ratzel [1980], Schreiber and Troxel [1985]
$\sqrt{\frac{4\ln 2}{2\pi}}2^{-2x^2}$	1.740	2.165	2.520	Gaussian; Turkowski [1990], Wolberg [1990]
Sharpened Gaussian	2.212	2.650	2.992	Ratzel [1980], Schreiber and Troxel [1985]
tanh, $k = 4$	1.81	2.79	3.76	Wolberg [1990, pp.145–146]
Interpolating B-spline	2.855	4.804	6.735	section 4.5
tanh, $k = 10$	3.77	6.52	8.68	Wolberg [1990, pp.145–146]
$\mathrm{sinc}(x)$	≈ 31.5	≈ 318.5	≈ 3183.0	section 4.3

Table 4.5: The functions on the left are all normalised. The table shows the minimum value of x above which the functions value never goes outside the listed limits. All values are given to 3 or 4 significant digits. On the right are the sources for each function.

His basic assumption appears to be that three decimal places are sufficient accuracy for his purposes [see *ibid.*, figures 9, 10, 13, and 14]. These limits are close approximations to the 0.001 limits in table 4.5.

Wolberg [1990, p.146] reports that the tanh filter yields excellent results when truncated to $|s| \leq 3$. The numbers in table 4.5 confirm this for the $k = 4$ filter, truncated to the 0.001 limit, but throw doubt on it for the $k = 10$ filter. Wolberg does not make it clear which of the two filters this truncation limit is applied to, presumably it is the $k = 4$ version.

In section 4.5.3 we truncated the interpolating B-spline to $|s| \leq 7$, that is to the 0.0001 level. Judging from the other results, this is a little conservative. Limiting at the 0.001 level, say $|s| \leq 5$, seems to be adequate, and agrees with Rasala's [1990, p. 584] estimation of the truncation limit. (Rasala estimates that for practical purposes a point is affected by values up to seven samples away on either side. However, he comments that this estimate is pessimistic and that given certain limits [met by our application] only values up to five samples away need be considered).

4.6.1 Sinc

The sinc function decays as $\frac{1}{x}$. Table 4.5 shows that the practical outworking of this is that sinc cannot be truncated locally without severely affecting its quality. Here, 'locally' means within at most a dozen sample spaces.

Ratzel [1980, p. 69] used a sinc truncated to $|x| \leq 10$. He found that it performed poorly. While for a Gaussian this truncation limit is adequate, even excessive, for a sinc it is nowhere near big enough to make the truncation errors negligible.

A solution to this problem is to multiply the sinc function by a better window function, one which falls off smoothly to zero. Wolberg [1990, pp. 137-143] and Smith [1981, 1982] describe the common windowing functions used with the sinc interpolant. These windows were all originally derived for use in one-dimensional signal processing such as sound or radar signals. Visual signals tend to be a little different (see section 2.7) and so we should not expect the results from these types of signal to necessarily hold for images [Blinn, 1989a].

Unfortunately, any window, except a very local one, will leave the resulting reconstructor with

large side lobes beyond the first. These will produce ringing artifacts in the reconstructed intensity surface. Of the very local reconstructors, the best appears to be the Lanczos-3 window [Turkowski, 1990; Wolberg, 1990; Blinn, 1989b], which is:

$$\text{Lanczos3}(s) = \begin{cases} \text{sinc}(\frac{s}{3}), & |s| < 3 \\ 0, & \text{otherwise} \end{cases}$$

This gives a windowed function:

$$S(s) = \begin{cases} \text{sinc}(s)\,\text{sinc}(\frac{s}{3}), & |s| < 3 \\ 0, & \text{otherwise} \end{cases}$$

However, a window this local produces a function which is quite different to the original sinc function. Hence, neither type of windowing is ideal for the sinc function.

4.7 Summary

We have discussed the problem of edge effects and the methods of edge extension. The best edge extension solutions are windowed extrapolation, and reflection. Constant edge extension is the fastest to evaluate.

Several of the infinite extent reconstructors have been examined. Sinc and Gaussian are well-known reconstructors, and we briefly examined these and some of their variants.

We have derived the kernels of the interpolating cubic B-spline and the interpolating Bezier cubic. These have been shown to be identical, and the kernel has allowed us to implement an efficient two-dimensional version of the interpolating cubic B-spline.

Finally, we save that all of the common infinite reconstructors can be locally truncated with practically no loss of quality, except for the sinc reconstructor. Any non-local windowing of sinc will not remove the problem of ripply artifacts, where as a local windowing will. However, the local windowing will also significantly change the reconstructor.

We now go on to consider a way of implementing an approximation to sinc reconstruction which implicitly uses the replication edge extension method.

Chapter 5

Fast Fourier Transform Reconstruction

The theoretically perfect reconstructed intensity surface is generated by convolving the image with a sinc function. Whatever the advantages and disadvantages of this reconstruction method, it is sometimes necessary to implement it. Sinc reconstruction is, however, extremely expensive to implement. We saw in section 4.6.1 that the sinc function cannot be truncated to produce a local reconstructor without severe artifacts; windowing gives better results but is still not ideal. To implement ideal sinc reconstruction for use with point sampling and constant edge extension will be an $O(N^2)$ process for every sample point for an $N \times N$ image. Thus resampling an $N \times N$ image to another $N \times N$ image with single point sampling will be an $O(N^4)$ process.

Fraser [1987, 1989a, 1989b] presents a method which uses the fast Fourier transform (FFT) to produce practically identical results to sinc reconstruction in $O(N^2 \log N)$ time. This chapter discusses his method and presents two variations on it: one to improve its accuracy near image edges; the other to increase its speed and reduce its memory requirements.

5.1 The reconstructed intensity surface

The fast Fourier transform techniques are fast ways of implementing the discrete Fourier transform (DFT). The DFT transforms a finite-length discrete image into a finite-length discrete frequency spectrum. The intensity surface generated by DFT reconstruction is the periodic function described by a Fourier series consisting of the DFT coefficients below the Nyquist frequency and zeros above it [Fraser, 1987]. No doubt this statement requires some explanation.

Given a one-dimensional sequence of N samples, f_j, the DFT produces N frequency values, F_k [Lynn and Fuerst, 1989, p.212]:

$$F_k = \sum_{j=0}^{N-1} f_j \, e^{-i2\pi jk/N}, \; k \in \{0, 1, \ldots, N-1\}$$

These two discrete series, f_j and F_k, each form the weights of periodic weighted comb functions:

$$\begin{aligned} \iota(x) &= \sum_{j=-\infty}^{\infty} f_j \, \delta(x - \frac{j}{N}), \; f_j = f_{j-N} \\ I(\nu) &= \sum_{k=-\infty}^{\infty} F_k \, \delta(\nu - k), \; F_k = F_{k-N} \end{aligned}$$

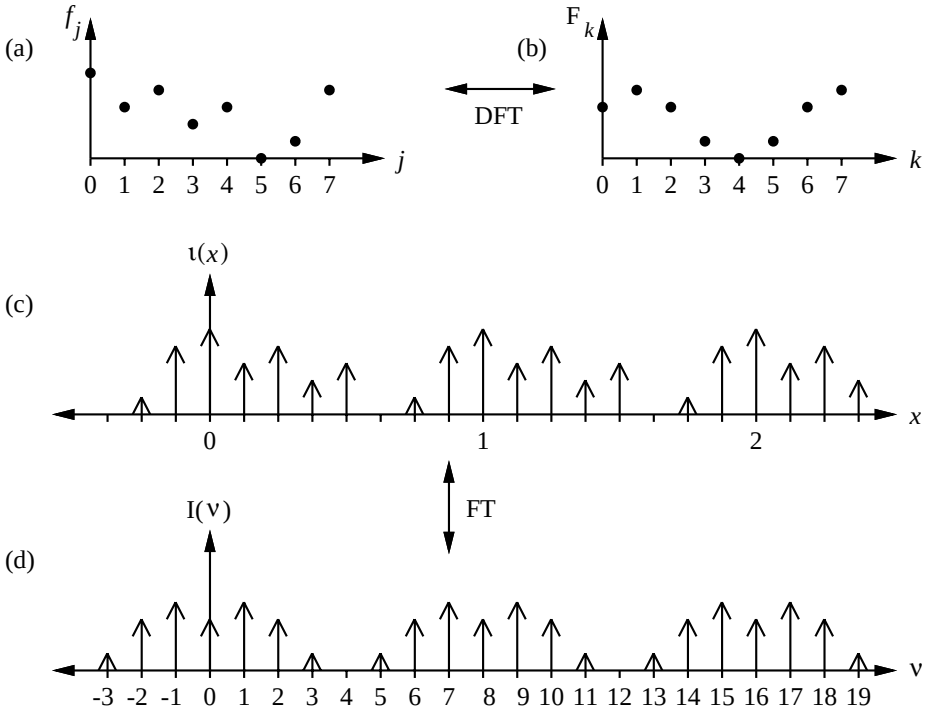

Figure 5.1: The relationship between the discrete and continuous representations of a sampled function. (a) shows the discrete samples, which can be discrete Fourier transformed to give (b) the DFT of (a). (c) shows $\iota(x)$, the continuous version of (a), it consists of an infinite periodic set of Dirac delta functions. Its Fourier transform, (d), is also an infinite periodic set of Dirac delta functions and is the continuous representation of (b).

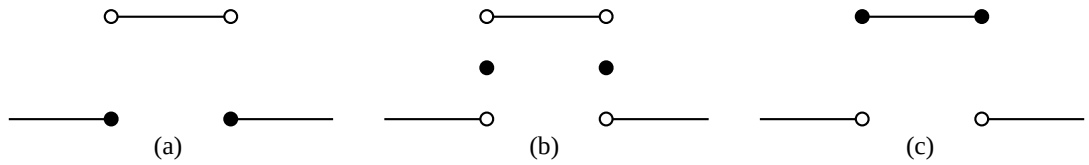

Figure 5.2: The three possible forms of the box function:

(a) $b_1(x) = \begin{cases} 1, & |x| < \frac{m}{2} \\ 0, & |x| \geq \frac{m}{2} \end{cases}$ (b) $b_2(x) = \begin{cases} 1, & |x| < \frac{m}{2} \\ \frac{1}{2}, & |x| = \frac{m}{2} \\ 0, & |x| > \frac{m}{2} \end{cases}$ (c) $b_3(x) = \begin{cases} 1, & |x| \leq \frac{m}{2} \\ 0, & |x| > \frac{m}{2} \end{cases}$

Watson [1986] shows that these two comb functions are Fourier transforms of one another. The relationship is illustrated in figure 5.1.

Now, to perfectly reconstruct $f(x)$ from $\iota(x)$ we convolve it with $N\text{sinc}(Nx)$. This is equivalent to multiplying $I(\nu)$ in the frequency domain by a box function, suppressing all periods except the central one between $\nu = -N/2$ and $\nu = N/2$.

An important question here is what happens at the discontinuities of the box function? Figure 5.2 gives the three plausible answers to this: the value at the discontinuity can be zero, a half, or one. In continuous work it does not matter particularly which version is used. Here, however, we are dealing with a weighted comb function. If this comb has a tooth at the same place as the box function's discontinuity then it makes a good deal of difference which version of the box function is used. Fraser [1987, p.122] suggests that the central version be used (where $b_2(\frac{N}{2}) = \frac{1}{2}$). His reasoning is that all components of the Fourier sequence appear once in the box windowed function

but the component at the Nyquist frequency occurs twice (once at each end) and so must be given a weight of one half relative to the other components.

A more rigorous reason can be found from taking the Fourier transform of the spatial domain sinc function:

$$B(\nu) = \int_{-\infty}^{\infty} N\text{sinc}(Nx)e^{-i2\pi\nu x}\,dx,\ N > 0$$

This can be shown (appendix B.2) to be:

$$B(\nu) = \begin{cases} 1, & |\nu| < \frac{N}{2} \\ \frac{1}{2}, & |\nu| = \frac{N}{2} \\ 0, & |\nu| > \frac{N}{2} \end{cases} \tag{5.1}$$

Thus we see that the middle version of the box function is the mathematically correct one to use[1].

Applying the box function (equation 5.1) to the function $I(\nu)$ gives a non-periodic weighted comb function, $V(\nu)$:

$$\begin{aligned} V(\nu) &= I(\nu) * B(\nu) \\ &= \sum_{k=-\infty}^{\infty} V_k\,\delta(\nu - k) \end{aligned}$$

$$V_k = \begin{cases} F_k, & 0 \le k < \frac{N}{2} \\ F_{N-k}, & -\frac{N}{2} < k < 0 \\ \frac{1}{2}F_{N/2}, & |k| = \frac{N}{2} \\ 0, & |k| > \frac{N}{2} \end{cases}$$

Note that there will only be coefficients at $|k| = \frac{N}{2}$ when N is even.

The coefficients of $V(\nu)$ form a Fourier series which describes a continuous function in the spatial domain [Lynn and Fuerst, 1989, p.338]:

$$f(x) = \sum_{k=-\infty}^{\infty} V_k\,e^{i2\pi kx} \tag{5.2}$$

This is the intensity surface reconstructed by DFT reconstruction. The whole process is illustrated in figures 5.3 and 5.4.

This same sequence of events can be seen in Watson [1986, figs 2 and 4] except that Watson uses the third version of the box function ($b_3(\frac{N}{2}) = 1$) rather than the second.

The reconstructed intensity surface is thus perfectly reconstructed from the samples by theoretically convolving it with a sinc function and, in practice, using the DFT method. The significant fact about this surface is that it is periodic. Edge extension has been done by replication and thus the infinite convolution of $\iota(x)$ by $N\text{sinc}(Nx)$ can be performed in finite time: the value at any point on the surface can be found by evaluating the sum of N or $N + 1$ terms in equation 5.2, although this method of evaluation is as expensive as sinc convolution of the spatial domain samples.

The edge extension implicit in the DFT method is different from that which must be used for sinc interpolation (section 4.3). There we saw that all pixels beyond the image edges must be given the value zero (or somehow be faded off to zero). Here edge extension is by copying, which means that edge effects will be visible in the intensity surface unless we get a fortuitous case where the edges match [Fraser, 1989a, pp.667–668] (section 4.2.1).

[1] Any of the versions, when Fourier transformed, gives the sinc function, but the inverse transform gives the middle version of the box function.

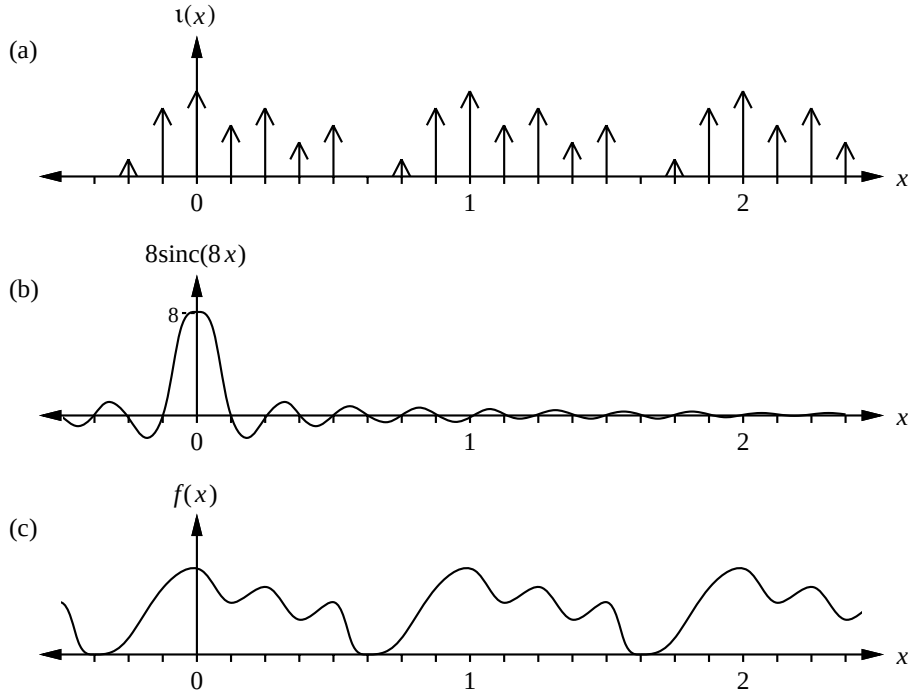

Figure 5.3: The spatial domain representation of FFT reconstruction. The sampled function, $\iota(x)$ is shown in (a). It is Fourier transformed to give figure 5.4(a). This Fourier transform is multiplied by a box function (figure 5.4(b)) to give a finite extent function (figure 5.4(c)) in the frequency domain. This is inverse Fourier transformed to give the continuous function (c) here. Multiplication by a box in the frequency domain is equivalent to convolving by a sinc function, (b), in the spatial domain.

5.2 DFT sample rate changing

The DFT can be used to change the sample rate of the image, that is: to scale the image. The seed of this idea can be found in Schafer and Rabiner [1973]. The idea itself was developed by Prasad and Satyanarayana [1986] and modified slightly by Fraser [1989a] to use the correct box function. Their implementation only allows for magnification by an integer power of two. Watson [1986] independently developed the idea, though he does not use the correct box function in part of his implementation. His algorithm allows for scaling by a rational factor such that, if the original sequence is N samples and the final L samples, then scaling is by a factor L/N. Watsons' algorithm can thus be used to scale from any whole number of samples to any other whole number of samples whilst Fraser's can only scale from N to $2^n N$, $n \in \mathcal{N}$.

5.2.1 How it works

The following explanation is based on Watson's [1986] work, with the modification that the correct box function is used in the first multiplication (Watson already uses it in the second stage so it is surprising that he is inconsistent). We first present the algorithm in the continuous domain, then explain how it can be implemented digitally. Again the one-dimensional case is used for clarity.

The continuous version of the DFT sample rate changing process is illustrated in figure 5.6 (minification) and figure 5.7 (magnification). Our image sample values represent the weights on one period of a periodic, weighted comb function (figure 5.6(a)). This is Fourier transformed to give another periodic weighted comb function (figure 5.6(b)). The Fourier transform is then correctly

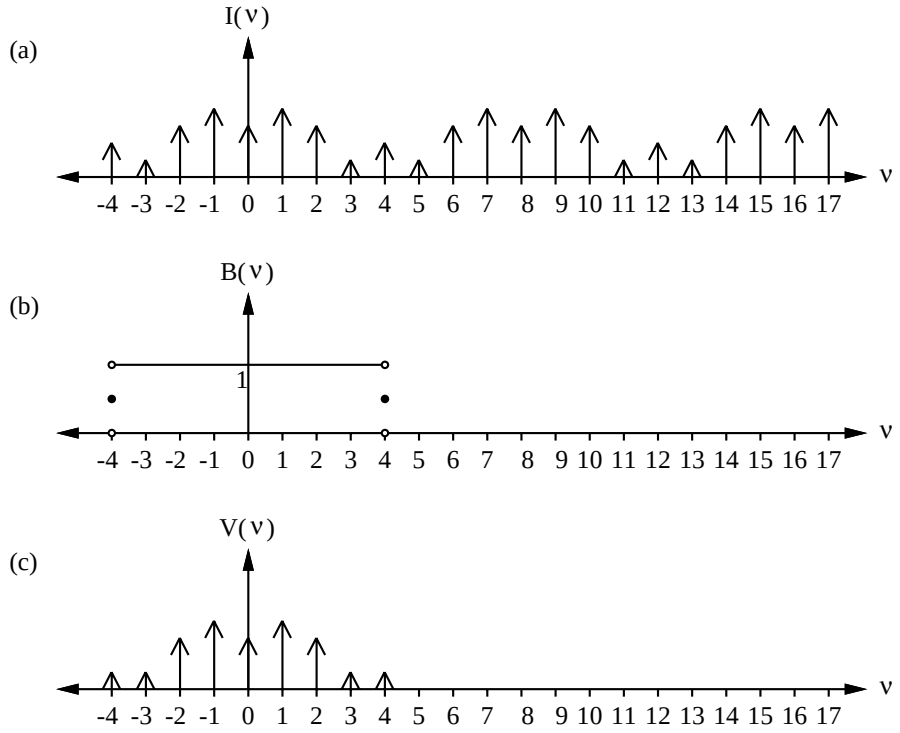

Figure 5.4: The frequency domain representation of FFT reconstruction. See the caption of figure 5.3.

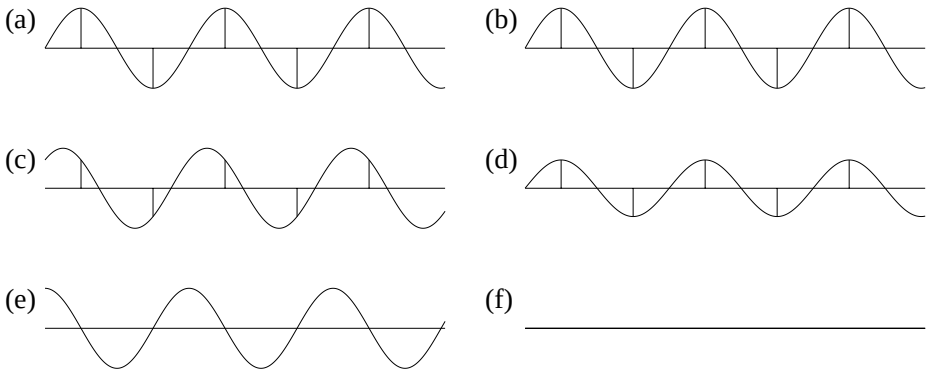

Figure 5.5: Critical sampling. The sine waves in (a), (c), and (e) are sampled at exactly twice their frequencies. The perfectly reconstructed versions are shown in (b), (d), and (f) respectively. The function is only correctly reconstructed when the samples are in exactly the right place.

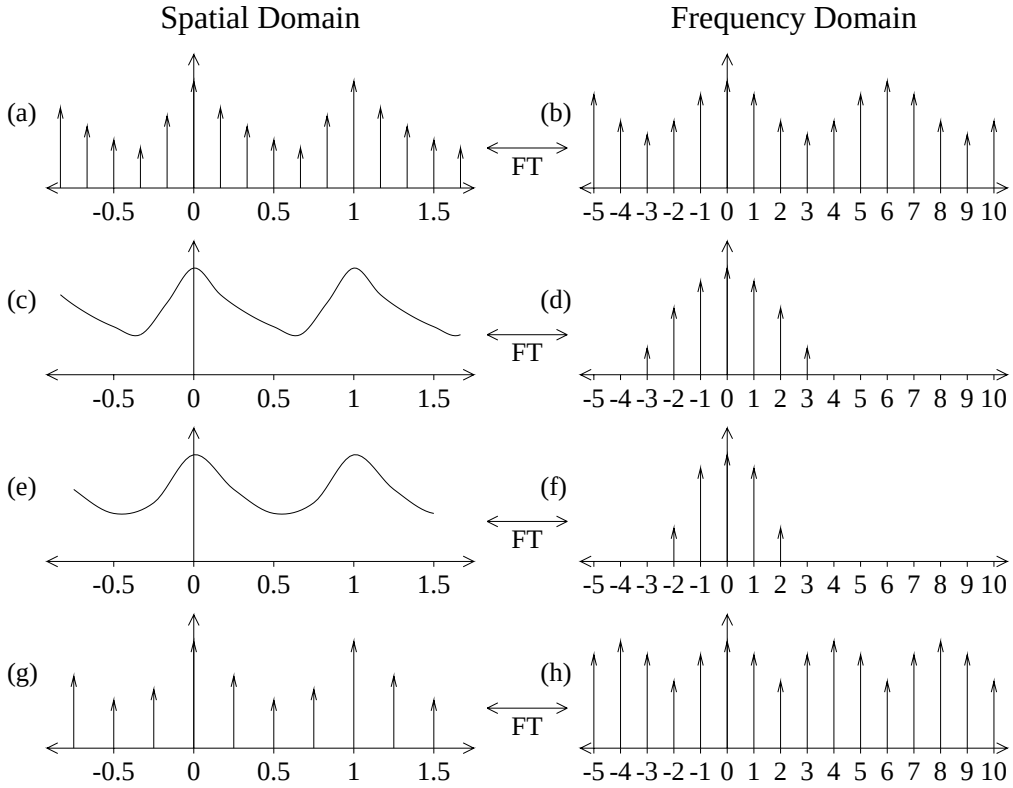

Figure 5.6: An example of 'perfect' minification. The sampled spatial function (a) is transformed to give (b), this is multiplied by a box function producing (d) [and thus generating a continuous function (c) in the spatial domain]. (d) is multiplied by another box function to band-limit it [filtering the spatial domain function (e)], and then sampling is performed to replicate the frequency spectrum (h) and produce a minified image in the spatial domain (g).

box filtered (figure 5.6(d)) which gives a continuous intensity surface in the spatial domain (figure 5.6(c)). To resample this intensity surface at a different frequency (equivalent to scaling it and then sampling it at the same frequency) we first perfectly prefilter it, using another correct box function in the frequency domain. If we are enlarging the image this makes no difference to the image (figure 5.7(f)), if reducing it then the higher frequency teeth in the comb function are set to zero and any component at the new Nyquist frequency is halved (figure 5.6(f)). We can then point sample at the new frequency, which produces periodic replication in the frequency domain. Figure 5.6(h) shows this for reduction and figure 5.7(h) for enlargement.

Notice that the first multiplication with a box is redundant for reduction and the second is redundant for enlargement. So, in either case only one multiplication by a box function is required. Note also that the periodic copies move farther apart in enlargement, as if they had been pushed apart at the Nyquist frequency (and its copies); and they have been pushed closer together in reduction, hence the need to prefilter to prevent overlap and thus aliasing. The overlap at the Nyquist frequency (and its copies at $(2N+1)\nu_N$, $N \in \mathcal{Z}$) appears to be acceptable [Watson, 1986]. Here the negative and positive Nyquist frequencies add together (hence, again, the need for the box function to have half values at the Nyquist frequencies). With a real spatial domain function this will mean that the even component at this frequency will be doubled and the odd component will cancel itself. So, if the original spectrum is non-zero at the Nyquist frequency then samples at the sampling frequency preserve only the even portion of this component. This is known as critical sampling [Watson, 1986, p.4]. Figure 5.5 shows three sine waves sampled at twice their own frequency, and the perfectly reconstructed version of these: only the even component survives.

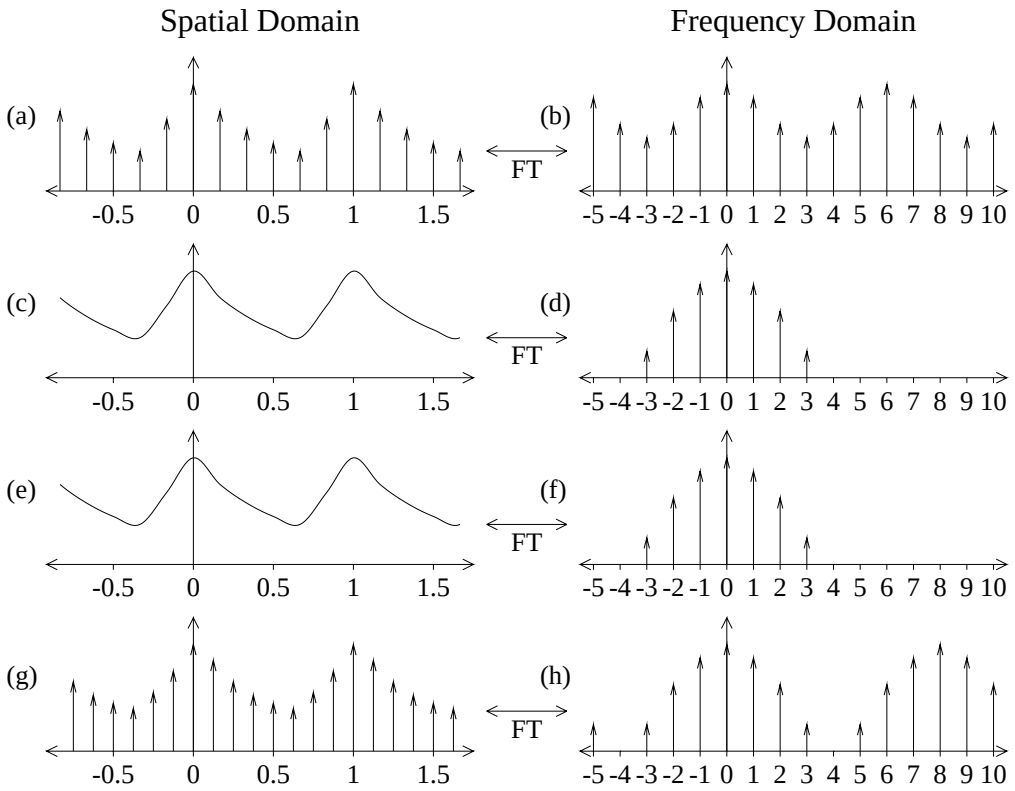

Figure 5.7: An example of 'perfect' magnification. See the caption of figure 5.6 for a description of the processes. Note that multiplying (d) by the appropriate box function to give (f) has no effect on the function in this magnification case.

Whilst this theoretical explanation clearly shows that a continuous intensity surface is generated and resampled, as a practical reconstruction method a super-skeleton surface is generated, because samples can only be produced at regularly spaced points, not at any arbitrary point. To be able to sample at any point there would need to be an infinite number of points generated in each period, and hence an infinite length of time to evaluate all the points (they must all be evaluated in a single operation using this method).

5.2.2 Practical implementation

This algorithm is implemented using the discrete Fourier transform (normally its fast version: the fast Fourier transform (section 5.2.4)). The process mirrors that shown in figure 5.6 and figure 5.7. In this section we consider first the case of discrete reduction and then that of enlargement. In both cases we use even length sequences in our examples. We consider the differences between even and odd length sequences in the next section.

For reduction, the image (figure 5.8(a)) is discrete Fourier transformed (figure 5.8(b)). Notice that this transform has only one Nyquist component (here shown at the negative end of the spectrum). The periodic nature of the continuous equivalent means that the other Nyquist component, and all the other copies of this component, have the same value. The transformed data are then multiplied by a box function the same width as the new sample sequence. For an even length sequence, this creates a sequence of length one more that the new sample sequence, with a Nyquist frequency component at each end (figure 5.8(c)). These two components are added together to give a single Nyquist component, here shown at the negative end of the period (figure 5.8(d)). Compare this with figure 5.6(f) and (h) where sampling in the spatial domain causes the copies of the spectrum

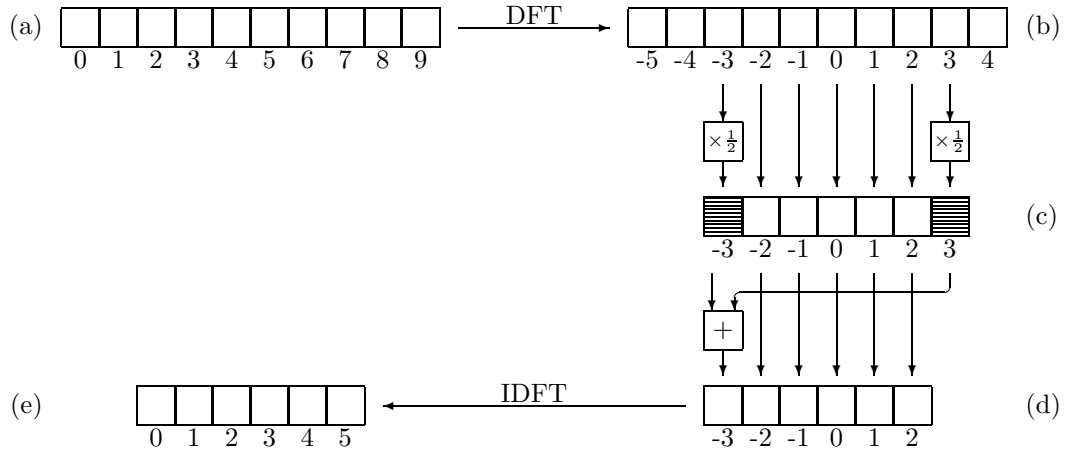

Figure 5.8: An example of DFT minification. The image, (a), is discrete Fourier transformed, giving (b), which is multiplied by a box function to give (c). The two Nyquist components are collapsed into one, producing (d), which is inverse discrete Fourier transformed, thus generating (e), a minified version of (a).

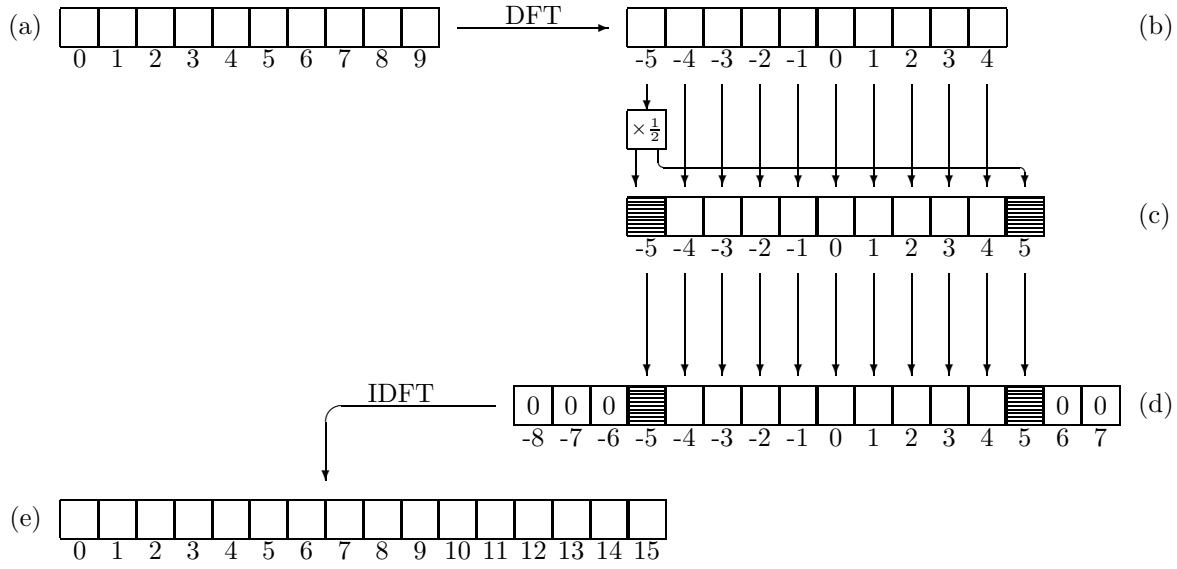

Figure 5.9: An example of DFT magnification. The image, (a), is discrete Fourier transformed, giving (b). The Nyquist component is split into two halves, producing (c). This is padded with zeros at either end to give (d), which is inverse discrete Fourier transformed, thus generating (e), a magnified version of (a).

to overlap at the Nyquist frequency and its copies, and hence add up at these points. The modified sequence can now be inverse transformed to give the resampled image (figure 5.8(e)).

Enlargement is a similar process. The image (figure 5.9(a)) is discrete Fourier transformed to give its frequency domain representation (figure 5.9(b)). The Nyquist frequency component is split into two halves, one at each end of the sequence (figure 5.9(c)). The sequence is now one sample longer. Compare this step with figure 5.7(b) and (d) where the positive and negative Nyquist components are both halved leaving a sequence with one tooth more in figure 5.7(d) that the number of teeth in each period in figure 5.7(b). The altered transformed sequence in figure 5.9(c) is now padded with zeroes at each end to give a sequence of the desired length (figure 5.9(d)). Note, in this example,

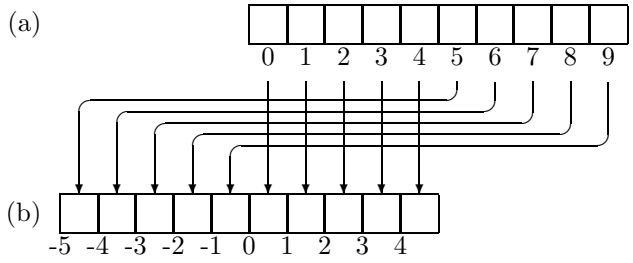

Figure 5.10: Comparison of the usual FFT output order and the DFT output order used in figure 5.8 and figure 5.9. At the top is the usual FFT output order. The Nyquist component is number 5. This can be easily converted to our DFT output order, shown at the bottom. The Nyquist component here is -5.

that one more zero is added at the negative end than at the positive end because we are assuming that the Nyquist component is at the negative end of the spectrum. The discrete spectrum is finally inverse discrete Fourier transformed to produce the desired enlarged image (figure 5.9(e)).

5.2.3 Odd *vs* even length sequences

All of the examples, up to this point, have used even length sequences. The processing required for an odd length sequence is slightly different and slightly easier. This is due to the fact that there is no frequency component at the Nyquist limit in an odd length sequence. Refer back to the continuous case in figure 5.6(a) and (b). In general, for a sequence of length L, there are L samples (teeth) in a unit distance in the spatial domain. Each period in the frequency domain is L units long, with the teeth of the comb function at integer locations. The Nyquist frequency is at $\pm\frac{L}{2}$. For an even length sequence there are components (teeth) at these frequencies; for an odd length sequence there are no components at these frequencies because they are not at integer locations. There are therefore no special case frequencies to consider when dealing with an odd-length sequence, because there is no Nyquist component.

5.2.4 Implementation using the FFT

Implementing this algorithm using a fast Fourier transform is straightforward. Two transforms are required, one of the original length and one of the final length. Provided an FFT algorithm can be implemented for both lengths the whole algorithm can be implemented. All FFT algorithms decompose the DFT into a number of successively shorter, and simpler DFTs [Lynn and Fuerst, 1989, p.221]. Thus an FFT of length $2^n,\ n \in \mathcal{N}$ is well known and widely used. Decomposition of other, non-prime length DFTs is less widely used. Finally, FFTs for prime length DFTs or lengths with large prime factors are most difficult, because the DFT has to be split into pieces of unequal length.

One important implementation issue is that most FFT algorithms produce N coefficients in the frequency domain ranging from $\nu = 0$ to $\nu = 2\nu_N - 1$. The examples shown here in figures 5.8 and 5.9 show them ranging from $\nu = -\lfloor \nu_N \rfloor$ to $\nu = \lfloor \nu_N - \frac{1}{2} \rfloor$. This is no great problem as the values generated are exactly the same because the sequence is periodic with period $2\nu_N$ (see figure 5.1). Figure 5.10 shows the equivalence. So long as this is borne in mind in implementation, no problems will arise.

5.3 Using the FFT to produce a continuous reconstructed intensity surface

As pointed out in section 3.2, the FFT method is a super-skeleton reconstruction method. As it stands it is only useful for scaling and a limited set of other transforms.

Fraser [1987, 1989a, 1989b] takes this FFT method and extends it to produce a continuous intensity surface, which is thus useful for any transform. Fraser's idea is to use the FFT method to generate several extra points between the existing sample points. If the FFT method is used to scale by a factor of M (an integer) then $M-1$ extra sample points will be generated between each adjacent pair of original sample points. A local interpolant is then used to interpolate between these points, which all lie on the theoretically perfect intensity surface (equation 5.2). The FFT enlargement eliminates the majority of the rastering artifacts that would arise from applying the local interpolant to the original samples.

In practice Fraser [1987, p.122] scales the image by a factor of four or eight using the FFT method and then employs the Catmull-Rom cubic interpolant to produce the intensity surface. It is profitable to compare interpolation by the sinc function, the Catmull-Rom cubic and the FFT/Catmull-Rom interpolant. Ignoring edge effects, figure 5.11 compares these three interpolants in the frequency domain. The sinc function preserves the central copy of the signal, as is required for perfect interpolation. The Catmull-Rom interpolant attenuates some frequencies below the Nyquist frequency and passes some above it, thus the reconstructed signal is a distorted version of the 'perfectly' reconstructed signal.

The FFT/Catmull-Rom method consists of two steps. The first, the FFT step, produces a spectrum which has copies of the original spectrum at four or eight times the spacing in the sampled signal, with gaps between them of three or seven times the sampling frequency respectively. In the second step, where the Catmull-Rom interpolant is convolved with the FFT scaled signal, the central copy is almost perfectly preserved and the other copies are almost completely suppressed. Thus the FFT/Catmull-Rom method produces a nearly perfect reconstructed surface.

5.3.1 Implementation

There are two distinct steps in this process, as illustrated in figure 5.12. First the image is 'enlarged' by a factor of, say, four and then this intermediate image is reconstructed using the Catmull-Rom cubic to give the continuous intensity surface.

The FFT process requires a large amount of extra storage for the intermediate image. The intermediate image is generated in its entirety by a single FFT and cannot be generated a piece at a time on demand (but see section 5.4.2). Further, storage must be provided for the frequency domain representation of the image. This can be stored in the same location as the images if an in-place FFT is used [Lynn and Fuerst, 1989]. However the image data is real while the frequency domain data is complex; hence the frequency domain data requires twice the storage space of the image data if a naive FFT algorithm is used.

Two features of the process enable it to be implemented more efficiently than a general FFT. Firstly, the image data is real, so the frequency domain data exhibits conjugate symmetry; that is: $F_k = F^*_{-k}$. This symmetry enables us to halve the number of operations required for both the forward and inverse fast Fourier transforms [Watson, 1989, p.15] and halve the storage required for the frequency domain data. Secondly, there are a large number of zero values in the frequency domain image that is to be inverse transformed. Operations on these zeros are unnecessary because the FFT consists of several multiply and add stages. Multiplying by zero and adding the product gives the same result as doing nothing. Some savings can be made by implementing a special version of the FFT which does not perform the unnecessary operations. Smit, Smith and Nichols [1990] discuss precisely this version of the FFT. They show that, for scaling an image of size N by

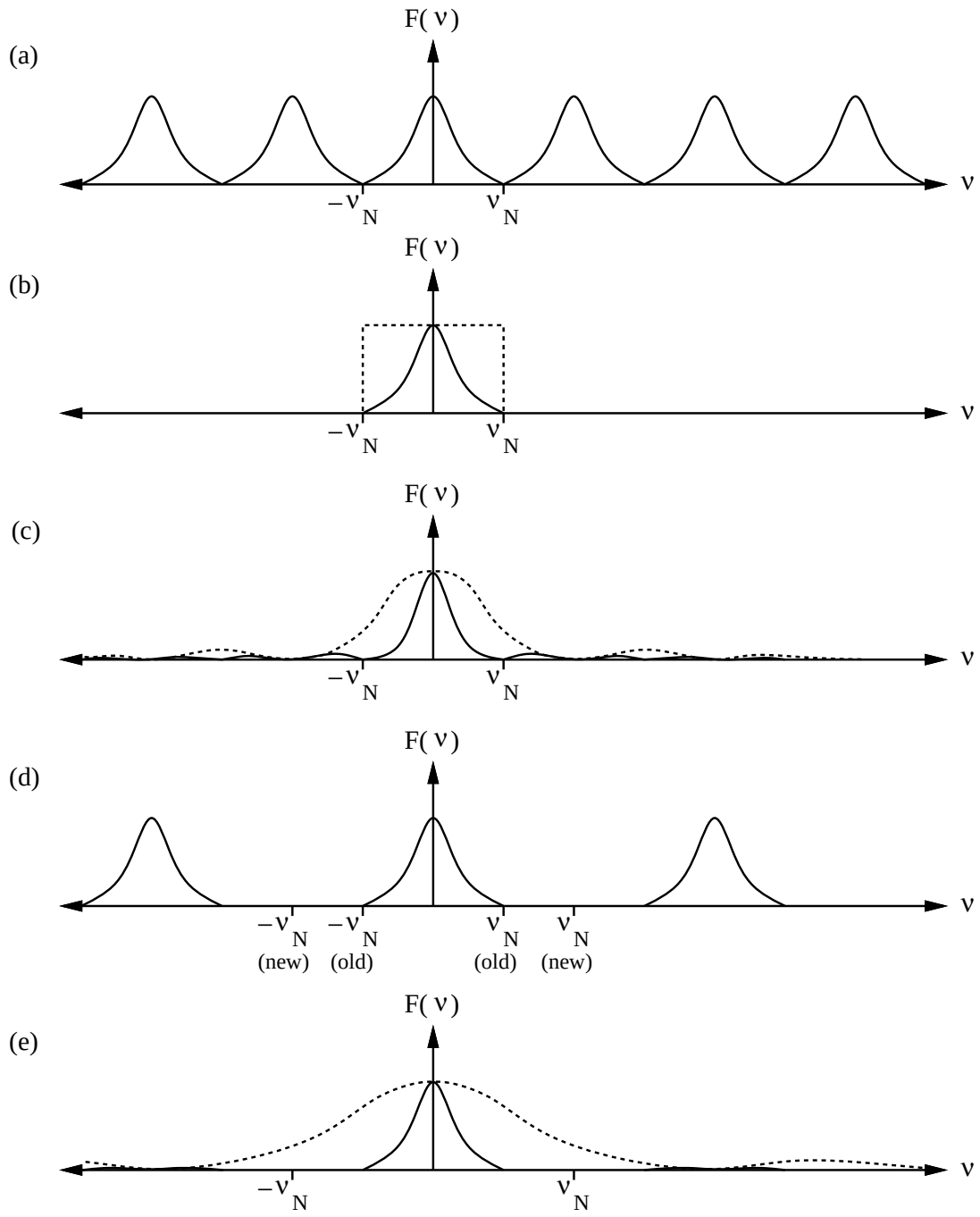

Figure 5.11: A comparison of sinc, Catmull-Rom, and FFT/Catmull-Rom reconstruction. (a) shows the Fourier transform of the sampled function; (b) is the sinc reconstructed function, there are no aliases in this function; (c) is the Catmull-Rom reconstructed function, it contains aliases. (d) is the FFT scaled function, which has the effect of pushing the components farther apart (in this figure they are moved twice as far apart). When (d) is reconstructed using a Catmull-Rom function, fewer aliases are produced (e). In a real situation the components will be moved farther apart than shown here, reducing the errors further.

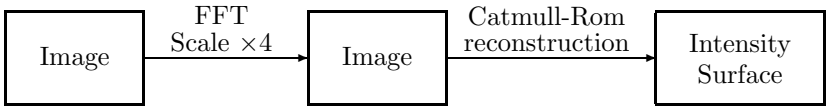

Figure 5.12: FFT/Catmull-Rom reconstruction is a two-stage process, requiring production of an intermediate (scaled) image. The scaling can be ×4 or ×8.

a factor of M, a reduction in time of around $\log_2 N / \log_2 MN$ can be achieved when M and N are both powers of two.

Combining both savings, a 512 sample one-dimensional sequence magnified by a factor of four takes just over 40% of the time that a naive FFT implementation would take. The saving for a 512×512 two-dimensional image is the same.

5.4 Problems with the FFT reconstructor

There are two major problems with the FFT reconstructor. Firstly, edge effects appear in the intensity surface to a considerable distance from the edges. Secondly, the process is both time and memory intensive. We tackle these two problems separately and draw them together at the end.

5.4.1 Edge effects

Inherent in the FFT reconstructor is the assumption that edge extension is done by replicating (copying) the image. Looking back to section 5.1 we can see this in the explanation of FFT scaling. Except in exceptional cases, there will be a sharp change in intensity along the edges of the image where the replicas join. Figure 4.20(top) gives an example of this.

From section 4.2.1 we know that perfect reconstruction causes unsightly ripples for some distance around such sharp changes. The FFT method implements perfect reconstruction and so there will be ripples visible around the 'edge' of the intensity surface. Figure 4.20(bottom) gives an example of these ripples.

Visual examination of images with large intensity differences at the edges indicates that these ripples can extend twelve to sixteen original sample spacings from the edge. This means that around twelve percent of a 512×512 image is degraded by this process. A larger proportion is degraded in smaller images.

Solving the edge effect problem

Fraser [1989a, p.668] noted the errors due to edge effects, and that low errors occur when there are "fortuitous end-around effects", that is: when the intensities at opposite edges are very close. We simply cannot depend on good fortune to always provide images with nice end-around effects. Indeed, most images do not fall into this category.

Fraser [1989a, p.669; figs. 3, 4; 1989b, p.269 & fig. 1] avoided the edge effects in his experimental measurements by considering only the central portion of the image, remote from the edges and any edge effects. In resampling work, however, it is usually necessary to use the entire image and so the edge effect problem cannot be avoided.

The solution is to produce a situation where the intensities at opposite edges of the image match before the image is transformed. There are several ways to do this:

1. window the image;
2. extend the image so that the edges match;
3. linearise the image;
4. use reflection in place of replication.

(1) Window the image

Fraser [1989a, pp.671–3] solves the edge effect problem by end-windowing the image. He applies cosine half-bells to each end of each row and column in the image to form a new image whose intensities fall off smoothly to zero at the edges. Fraser showed that only a small amount of windowing can significantly affect the result. A window covering only four sample spacings (two at each end) reduces the distance from the edge that errors are noticeable to around a sixth of the distance without windowing, in the cases where the ripples are most noticeable.

The problem with this method is that it causes a different visual artifact, known as vignetting. This effect is illustrated in figure 4.19. Windowing reduces the rippling artifact near the edges of the image at the expense of introducing the vignetting artifact. In places where the rippling was less noticeable, the vignetting may cause larger errors than the ripples would have. That is: it is possible for the vignetting to be more objectionable than the rippling.

(2) Extend the image so that the edges match

This is similar to the windowing idea. The image is left unchanged in this case and a few extra lines of pixels added around the outside to 'fade off' to some constant value. A more sophisticated algorithm than simple fading could be tried (section 4.2.1). Once the image has been enlarged by the FFT method the extra lines can be discarded.

A simple algorithm can be developed which fades each row and column to a constant value within a few pixels. A problem with this method is that many FFT algorithms are designed for sequences of length $2^n,\ n \in \mathcal{N}$, and many images have heights and widths which are also powers of two. Extending an image by a few pixels before transforming will be extremely inconvenient in these cases. Extending an image to twice its width and height (with mostly some constant value in the extension) would be more convenient (figure 5.13).

(3) Linearisation

The idea behind linearisation is to remove a linear trend from the data, so that the two ends match in intensity, then do the processing, and finally add the trend back in. This process, illustrated in figure 5.14, can be described for one dimension as follows:

Given a set of N data points, f_n, subtract a linear trend from the data to give a new sequence g_n:

$$g_n = f_n - sn$$

$$\text{where: } s = \frac{f_{N-1} - f_0}{N}$$

Expand g_n by a factor Z, using the FFT method, to give h_n. This can be converted back to an expansion of f_n by adding back the linear trend:

$$i_n = h_n + s\frac{n}{Z}$$

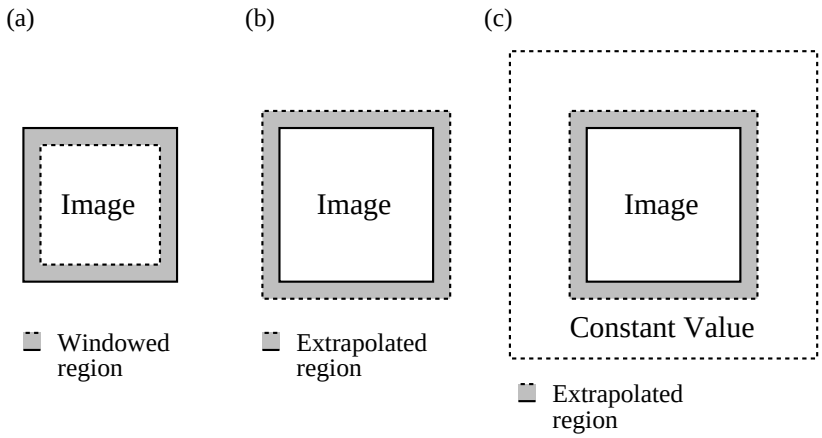

Figure 5.13: Three ways of coping with edge effects in FFT expansion of an image. (a) windowing the image, shaded area affected; (b) extending the image; and (c) extending the image to twice its size in both dimensions. In all three cases the resulting image (larger in (b) and (c)) is extended by replication by the FFT.

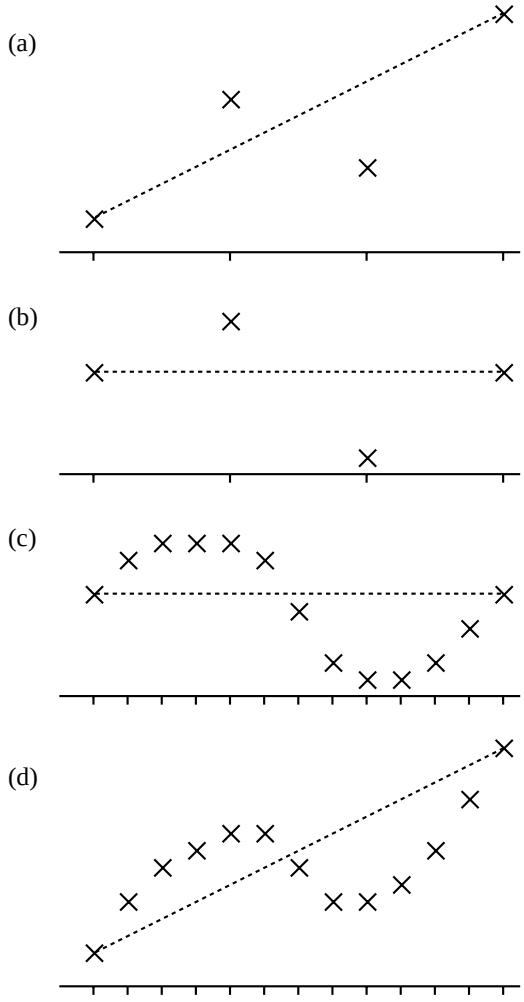

Figure 5.14: An example of linearisation. (a) shows the original samples and a linear trend through them; (b) shows the same samples with the linear trend removed; (c) is the FFT expanded version of (b); (d) is (c) with the linear trend added back in.

Analysing this method shows that it removes the edge ripples from the resulting image.

The transform of the original image, f, is F:

$$F_k = \sum_{n=0}^{N-1} f_n \, e^{-i2\pi kn/N}$$

This can be expanded by the FFT method to give J, the Fourier transform of the expanded image, j:

$$J_k = \sum_{n=0}^{ZN-1} j_n \, e^{-i2\pi kn/ZN}$$

In general j will contain edge ripples.

On the other hand, the transform of the linearised image, g, is G:

$$\begin{aligned} G_k &= \sum_{n=0}^{N-1} g_n \, e^{-i2\pi kn/N} \\ &= \sum_{n=0}^{N-1} f_n \, e^{-i2\pi kn/N} - s \sum_{n=0}^{N-1} n \, e^{-i2\pi kn/N} \\ &= F_k - sE_k \end{aligned}$$

This can be expanded to give H:

$$H_k = J_k - sE'_k$$

Inverse transforming H gives the image, h, which then has the linear trend added back in to give the final image, i:

$$i_n = j_n - se'_n + s\frac{n}{Z}$$

The difference between the latter two terms is an edge ripple which cancels out the edge ripple in j.

Extending to two dimensions

It is a simple matter to linearise a two dimensional image so that either the horizontal or the vertical edges match. This is achieved by linearising each column or row individually. It is possible to linearise every row and then linearise every column in the row-linearised image (this can be shown to leave every row and every column linearised). However, after FFT enlargement the image cannot be de-linearised because new rows and columns have been generated, between the existing rows and columns, for which no linearisation information exists.

It is impossible to linearise the image as a two dimensional whole so, if we wish to apply the linearisation process to a two-dimensional image we must think of some other way to perform the operation. To do this we alter the two-dimensional FFT expansion. A two dimensional FFT is performed by applying the FFT to every row in the image and then to every column in the row-transformed image. The FFT expansion expands the resulting frequency domain image and then two-dimensionally inverse transforms it. As noted above, this process is not amenable to linearisation. However, if the process is altered so that the rows are expanded first and the columns of the row-expanded image are expanded as a separate step, then linearisation is possible. The standard method and this new two-stage method are illustrated in figures 5.15 and 5.16. It is not immediately obvious that both methods should produce the same result (without linearisation). Experiments on several images have shown that they are equivalent (to within the numerical accuracy of the computer on which the operations were performed).

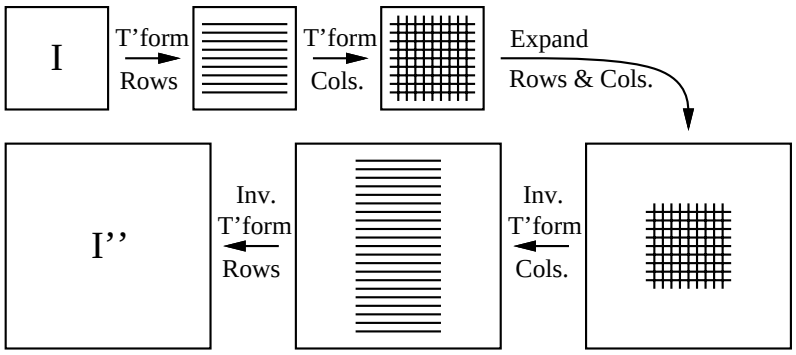

Figure 5.15: The standard way of performing two-dimensional FFT expansion of an image. This method is not amenable to linearisation.

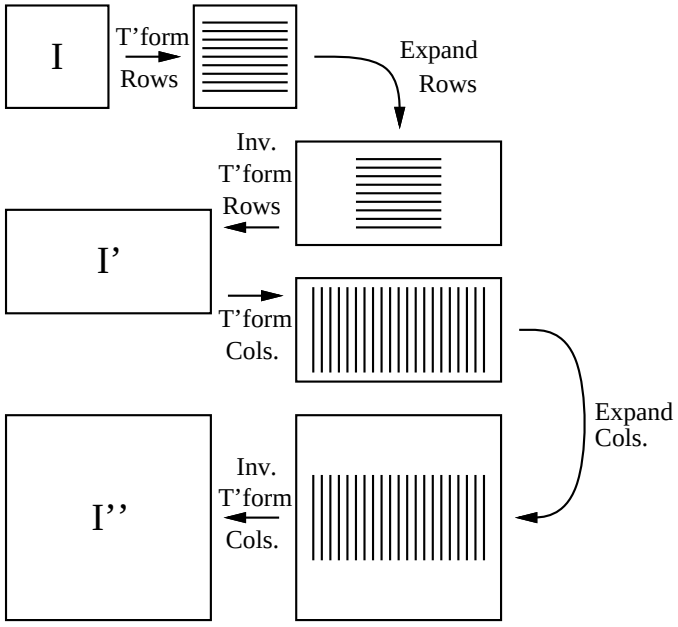

Figure 5.16: The two-stage method of performing two-dimensional FFT expansion of an image. This method is amenable to linearisation of each of the two stages.

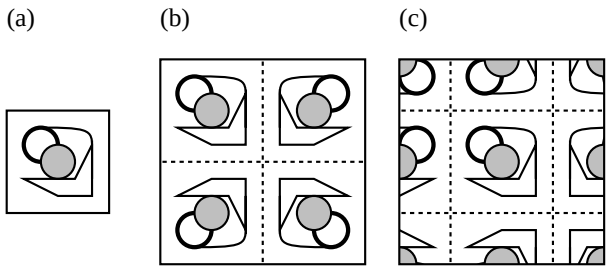

Figure 5.17: Two ways of reflecting an image to produce an image of twice the size in each dimension. (a) the original image; (b) reflected with the original in a corner; (c) reflected with the original in the centre.

Applying the linearisation to each of the two stages suppresses the edge ripples which would otherwise result. Obviously linearisation is applied to the rows in the row-expansion stage and to the columns in the column expansion stage[2].

(4) Using reflection in place of replication

In chapter 4 we saw that reflection is a better extension method than replication. Reflection ensures that the edges match. Reflection can be implemented in the FFT expansion stage by using an image twice the size in both dimensions and filling the extra three quarters with reflected versions of the image as illustrated in figure 5.17. Once this image is enlarged, using FFT expansion, only the appropriate quarter of the expanded image need be used in the ensuing Catmull-Rom reconstruction.

This method quadruples the computation required to perform the FFT expansion. Fortunately there is a way to compute the expansion in the same time as the basic FFT method; that is to use the discrete cosine transform (DCT), in place of the DFT.

Discrete cosine transform expansion

The discrete cosine transform of a sequence $f_n,\ n \in \{0, 1, \ldots, N-1\}$, is [Ahmed, Natarajan and Rao, 1974]:

$$\begin{aligned} F_0 &= \frac{\sqrt{2}}{N} \sum_{n=0}^{N-1} f_n \\ F_k &= \frac{2}{N} \sum_{n=0}^{N-1} f_n \cos \frac{(2n+1)k\pi}{2N},\ k \in \{1, 2, \ldots, N-1\} \end{aligned}$$

The special case for F_0 can be combined into the general form as illustrated in the two-dimensional DCT [Chen and Pratt, 1984]:

$$F_{k,l} = \frac{4C(k)C(l)}{MN} \sum_{m=0}^{M-1} \sum_{n=0}^{N-1} f_{m,n} \cos \frac{(2m+1)k\pi}{2M} \cos \frac{(2n+1)l\pi}{2N}$$

[2]Linearisation is a good word to play that game where you try to get as many words as possible from a single long word. For example: line, arise, ear, rise, is, at, on, in, ate, note, not, near, rest, least, sat, sate, nation, sir, sire, sit, sits, tin, tins, linear, salt, real, role, sole, aerial, nil, sale, rail, tail, tale, notion, elation, eat, eats, nit, trial, *etc.* [Gibbs, 1992]

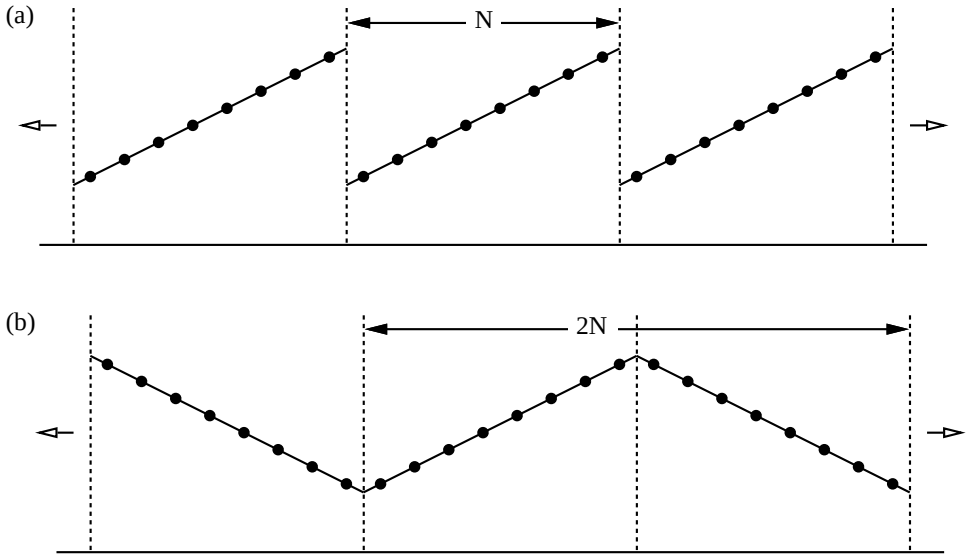

Figure 5.18: The implicit periodicity of (a) the discrete Fourier transform, and (b) the discrete cosine transform (after Rabbani and Jones [1991], figure 10.4).

$$\begin{aligned} & k \in \{0, 1, \ldots, M-1\} \\ & l \in \{0, 1, \ldots, N-1\} \\ C(j) \quad = \quad & \begin{cases} \frac{1}{\sqrt{2}}, & j = 0 \\ 1, & \text{otherwise} \end{cases} \end{aligned} \tag{5.3}$$

The DCT expresses the image as a sum of cosinusoidal terms [Chen and Pratt, 1984]:

$$f(m,n) = \sum_{k=0}^{M-1} \sum_{l=0}^{N-1} C(k)C(l)F_{k,l} \cos\frac{(2m+1)k\pi}{2M} \cos\frac{(2n+1)l\pi}{2N}$$

Compare this with the DFT decomposition into a sum of complex exponential terms (equation 5.2). The two transforms have different implicit periodicities (figure 5.18). As we have seen the DFT assumes a replicated periodic image whilst the DCT assumes a reflected periodic image [Rabbani and Jones, 1991, pp.108-111]. Expansion of the DCT can be performed in much the same way as for the DFT. But there turns out to be a slight catch to DCT expansion, which we now explain.

Working in one dimension for clarity, given an image $f_n,\ n \in \{0, 1, \ldots, N-1\}$, the DCT is defined as:

$$F_k = \frac{2C(k)}{MN} \sum_{n=0}^{N-1} f_n \cos\frac{(2n+1)k\pi}{2N},\ k \in \{0, 1, \ldots, N-1\} \tag{5.4}$$

where $C(k)$ is defined in equation 5.3.

This can be expanded by a factor Z to G_k:

$$G_k = \begin{cases} F_k, & k < N \\ 0, & \text{otherwise} \end{cases},\ k \in \{0, 1, \ldots, ZN-1\}$$

Note that, unlike the DFT expansion, there is no special (Nyquist) frequency component, nor are there any negative frequencies.

G can now be inverse transformed to give an expanded image, g:

$$g_n = \sum_{k=0}^{ZN-1} C(k)\, G_k \cos\frac{(2n+1)k\pi}{2ZN},\ n \in \{0, 1, \ldots, ZN-1\} \tag{5.5}$$

Here lies the catch: with the DFT every Z^{th} member of the expanded image would be in the original image, with $Z-1$ new image samples between every adjacent pair. That is: $g_{Zn} = f_n$. With the DCT, as it stands, this is not the case and a small correction must be made to equation 5.5 to make it the case. To explain what happens we see that:

$$f_n = \sum_{k=0}^{N-1} C(k)\, F_k \cos\frac{(2n+1)k\pi}{2N},\ n \in \{0,1,\ldots,N-1\} \tag{5.6}$$

this is simply the inverse of equation 5.4. Equation 5.5 can be rewritten as:

$$g_n = \sum_{k=0}^{N-1} C(k)\, F_k \cos\frac{(2n+1)k\pi}{2ZN},\ n \in \{0,1,\ldots,ZN-1\} \tag{5.7}$$

The differences between these two equations are the factor of $\frac{1}{Z}$ in the cosine's argument, and that there are Z times as many g_n as there are f_n. We require:

$$g_{Zn} = f_n,\ n \in \{0,1,\ldots,N-1\}$$

We can rewrite equation 5.7 for g_{Zn} as:

$$g_{Zn} = \sum_{k=0}^{N-1} C(k)\, F_k \cos\frac{(2n+\frac{1}{Z})k\pi}{2N},\ n \in \{0,1,\ldots,N-1\} \tag{5.8}$$

The only difference between equation 5.6 and equation 5.8 is that the $(2n+1)$ in equation 5.6 is replaced by $(2n+\frac{1}{Z})$ in equation 5.8. The net result is that there is a linear phase shift in the g_n with respect to the f_n.

This can be simply corrected by either:
(a) altering equation 5.5 to:

$$g_n = \sum_{k=0}^{ZN-1} C(k)\, G_k \cos\frac{(2n+Z)k\pi}{2ZN}$$

or:
(b) correcting for the linear phase shift in the subsequent small kernel interpolation. That is: instead of sample g_n being at location $x = x_0 + n\frac{\Delta x}{Z}$ it is shifted slightly to be at:

$$x = x_0 + \left(n - \left(\tfrac{1}{2} - \tfrac{1}{2Z}\right)\right)\frac{\Delta x}{Z}$$

Thus the DCT can be successfully used as an expansion method which does not produce edge ripple effects.

Expansion using other transforms

The DFT and DCT are only two of many types of image transform. We have seen that both of these can be used for image expansion. In general, any transform can be used for image expansion provided that N of the basis functions of the expanded version are identical to the N basis functions of the smaller version, except for a scale factor and possibly a linear phase shift, $n' = sn + c$. The DFT and DCT are examples of such transforms. For the DFT the basis functions are:

$$\{e^{-i2\pi kn/N},\ k \in \{-\tfrac{N}{2}, -\tfrac{N}{2}+1, \ldots, 0, 1, \ldots, \tfrac{N}{2}-1\},\ n \in \{0,1,2,\ldots,N-1\}\} \tag{5.9}$$

Expanding this by a factor Z we find the basis functions for $k \in \{-\frac{N}{2}, -\frac{N}{2}+1, \ldots, 0, 1, \ldots, \frac{N}{2}-1\}$ are:

$$\{e^{-i2\pi kn'/ZN}\} \tag{5.10}$$

Setting $n' = Zn$ gives N functions from equation 5.10 which are equal to the N in equation 5.9. Thus it is possible to expand an image using the DFT.

Likewise for the DCT the basis functions are:

$$\{\frac{1}{\sqrt{2}},\ \cos\frac{(2n+1)k\pi}{2N},\ k \in \{1, 2, \ldots, N-1\},\ n \in \{0, 1, 2, \ldots, N-1\}\} \tag{5.11}$$

Expanding by a factor of Z we find that the lowest N basis function of the new sequence are:

$$\{\frac{1}{\sqrt{2}},\ \cos\frac{(2n'+1)k\pi}{2ZN},\ k \in \{1, 2, \ldots, N-1\}\} \tag{5.12}$$

Setting $n' = Zn + (\frac{1}{2} - \frac{1}{2Z})$ makes N functions in equation 5.12 equal to those in equation 5.11 and so the DCT can also be used for image expansion.

Such an expansion is carried out by taking the coefficients of the basis functions in the original sequence and allocating them to the equivalent basis function in the expanded sequence. All other coefficients in the expanded sequence are set to zero. The DFT is a bit of a special case as the Nyquist component in the original sequence has two matching components in the expanded sequence with half its coefficient being given to each.

To illustrate this principle for other transforms take two square wave transforms: the Walsh-Hadamard transform and the Haar transform, both considered for $N, Z \in \{2^n, n \in \mathcal{N}\}$. The basis function for both transforms are square-like waves. The first sixteen Walsh-Hadamard basis function are shown in figure 5.19(a) and the first sixteen Haar basis function are shown in figure 5.19(b). Enlarging either by a factor of Z leaves the first N basis functions scaled but otherwise unchanged and thus either can be used for image expansion.

This can be implemented so that there is no phase shift or so that there is the same phase shift as in the DCT. For both transforms, this latter case produces identical results to nearest-neighbour expansion of the image, which would be considerably quicker to implement. The former produces a shifted version of this nearest-neighbour expansion. Therefore, while theoretically possible, neither of these transforms provide a particularly efficient way of achieving this type of expansion.

5.4.2 Speed and storage requirements

These image expansion methods are extremely time and memory intensive. Transform expansion for an $N \times N$ image is $O(N^2 \log N)$, thus increasing rapidly as image size increases. An $N \times N$ image expanded by a factor Z requires Z^2N^2 complex numbers to be stored for a straight forward FFT expansion, a quarter of this for an optimised FFT expansion, and Z^2N^2 real numbers for the other transforms discussed in the previous section. For example, a DCT expansion of a 256×256 image by a factor of four would typically require 4MB of storage. Experience on the Computer Laboratory's workstations has shown that they tend to fail when asked to allocate these huge quantities of memory to an image processing program. On occasion processes have required over 50MB of memory to expand a large image by a factor of eight, and such quantities seem well beyond the capability of the machines. Even where large quantities of memory are available most of it will tend to be in virtual memory, incurring an extra time cost as data is paged in and out of random access memory. In order to speed up the algorithm and reduce the need for large quantities of quickly accessible storage we can tile the image (figure 5.20). Tiling is used in image coding to reduce the time and memory cost of the coding algorithm and because image tend to be locally similar and globally dissimilar. The JPEG image compression method, for example, splits the image into 8×8 pixel non-overlapping tiles [Rabbani and Jones, 1991, p.114].

In image extension we will use relatively large tiles (32×32 pixels is a good size), and they will overlap. Processing is done on each tile separately and so, if they did not overlap, the edges of the tiles would be obvious. Overlapping the tiles places each tile in its local context. That is: a tile is expanded but only the central portion is used, as illustrated in figure 5.21.

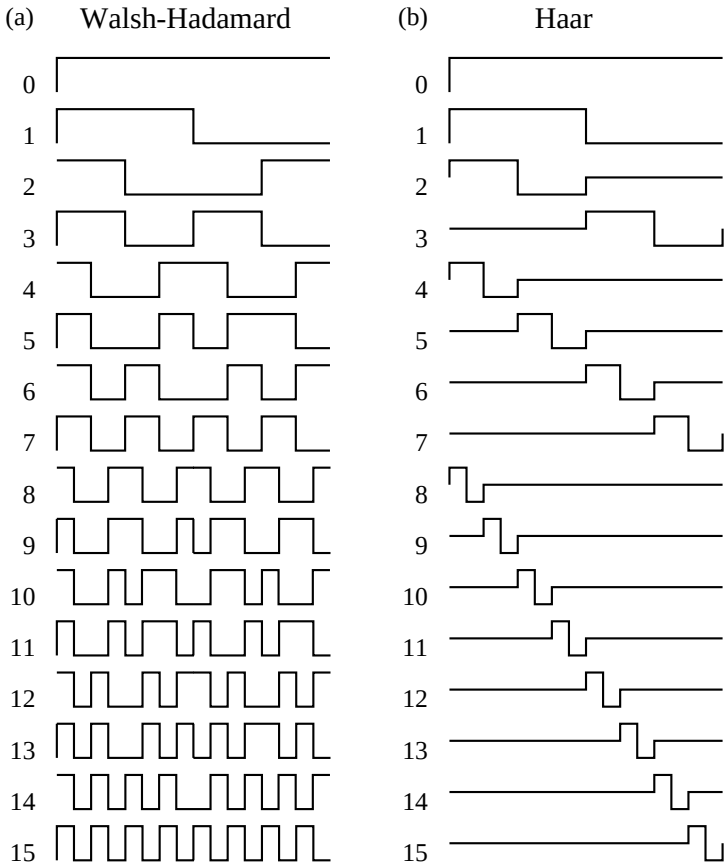

Figure 5.19: (a) the first sixteen Walsh-Hadamard basis functions; (b) the first sixteen Haar basis functions (after Hall [1979, pp.138–145]), these remain the same, no matter how many more coefficients there are.

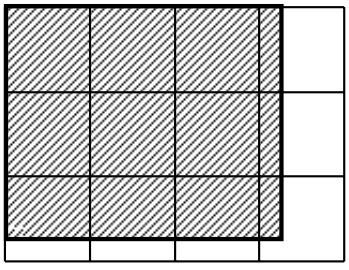

Figure 5.20: An image (shaded) divided into tiles.

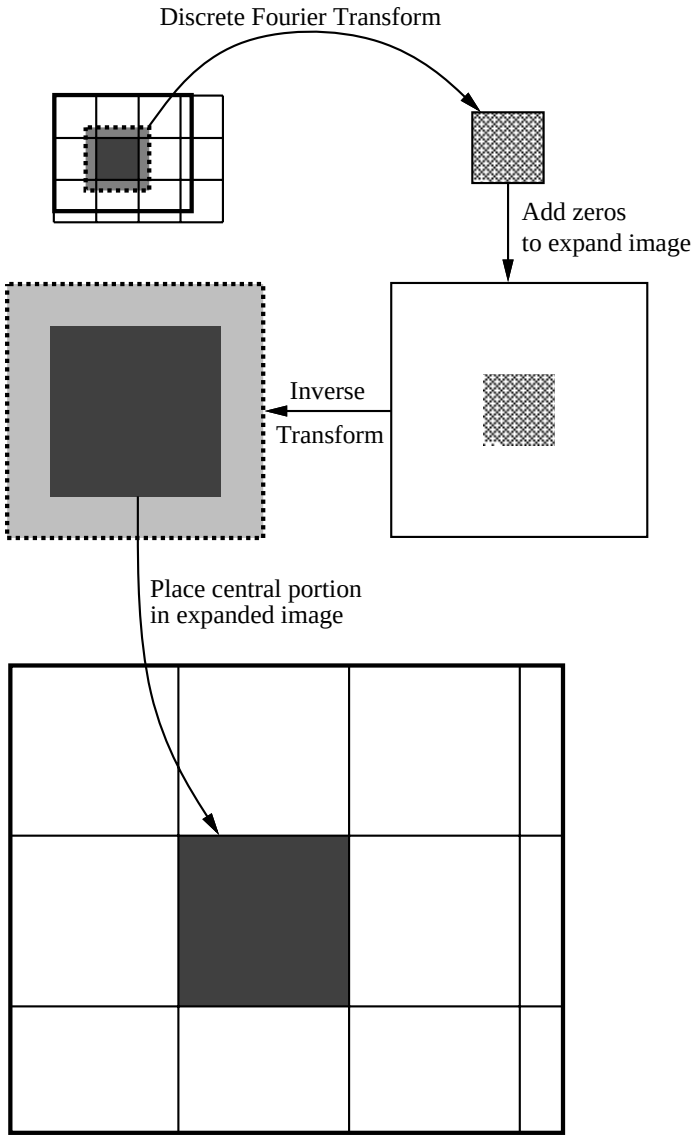

Figure 5.21: Using a tiled DFT expansion. Each tile is individually expanded, within its local context, and the appropriate expanded portion put into the expanded image.

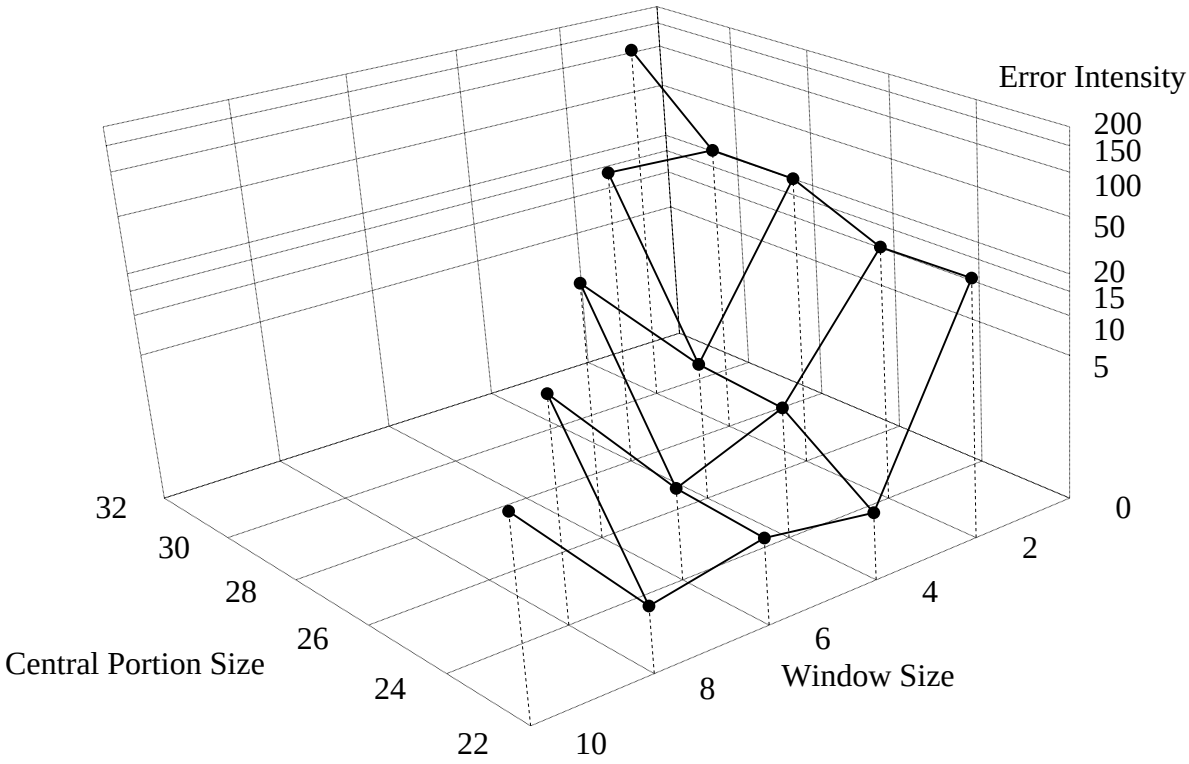

Figure 5.22: The values in table 5.1. Error intensity is the height of the largest ripple in intensity values, ranging from 0 to 255. This is graphed on a logarithmic scale. Only values for which Central Portion Size + Window Size ≤ 32 were evaluated.

As with the untitled version, if we use a DFT expansion, we are faced with edge effects. The DFT of a tile implicitly assumes that the infinite image is that tile replicated to infinity. The central quarter of the expanded tile will probably be unaffected by these edge effects but transforming an image twice the size of the useful portion in both dimensions is quite an overhead. It would be better if the useful portion was a larger proportion of the whole tile.

Here the edge effects solutions come into play. We could apply a DCT, or linearisation and a DFT to the tile, both of which would markedly increase the size of the usable inner portion of the tile. Further, windowing is a viable proposition here because the windowed pixels will be in the unused outer portion of the tile. An experiment has been performed to ascertain the best size of window and central portion given a tile size of 32×32 pixels. A completely black image was enlarged with windowing designed to fade the image off to white. Thus any artifacts in the expanded image will be extremely obvious as non-black pixels. This experiment gives a feel for the maximum errors likely due to windowing. In practice windowing should be done to a mid-grey, halving these errors; but many people prefer to window off to an extreme, usually black, and so it is necessary to record these maximum errors.

The results of this experiment are tabulated in table 5.1 and graphed in figure 5.22. The window size refers to the number of pixels in a row (or column) that are windowed. Half this number are windowed at each end of a row or column.

Any combination which has an intensity error less than three produces no visible artifacts. If windowing is done to a mid-grey than any combination with an intensity error under six produces no visible artifacts. Therefor any combination of an $n \times n$ central portion in a 32×32 tile is good provided $n \leq 26$ and the window width is greater than 2 and less than $32 - n$. Besides requiring no visible artifacts we also require the largest possible central portion relative to the tile size. Thus

Window Size	Central Portion Size				
	30	28	26	24	22
2	200 ± 0.5	57.8 ± 0.2	57.0 ± 0.2	30.8 ± 0.2	31.6 ± 0.1
4	$\times$	62.8 ± 0.2	4.24 ± 0.01	3.70 ± 0.01	0.98 ± 0.005
6	$\times$	$\times$	29.2 ± 0.1	1.68 ± 0.005	1.46 ± 0.005
8	$\times$	$\times$	$\times$	16.7 ± 0.05	0.91 ± 0.005
10	$\times$	$\times$	$\times$	$\times$	10.75 ± 0.03

Table 5.1: The maximum height of the ripples caused by DFT reconstruction. These heights are measures in intensity levels on a scale from 0 (no ripples) to 255. Obviously there was little point in testing cases where the windowing intruded into the central portion, so these entries are marked with a cross. The values in this table are graphed in figure 5.22.

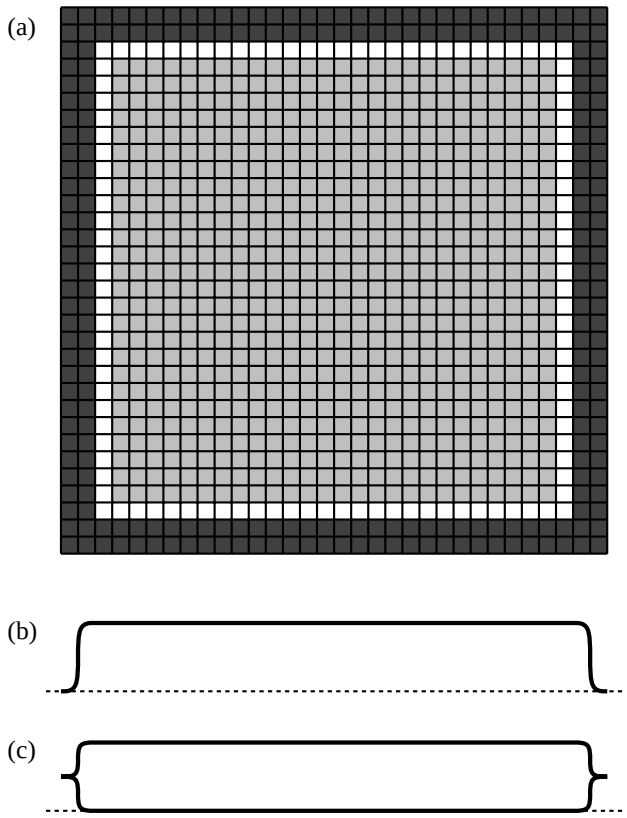

Figure 5.23: (a) a 26×26 pixel tile within a 32×32 pixel context, the outer two pixel wide border is windowed using the window function shown in (b). (c) shows the actual effect of this window which fades the function off to a mid-grey value.

we chose a 26×26 central portion in a 32×32 tile with a four pixel window (that is a two pixel wide cosine half bell windowed border around the tile) and fading to a mid-grey. This is illustrated in figure 5.23.

Speed and storage savings

If the tiles are of size $L \times L$ and the image to be expanded is of size $N \times N$ then this tiling method reduces the time required from $O(N^2 \log N)$ to $O(N^2 \log L)$. The memory required to perform the transforms is also reduced, from $O(N^2)$ to $O(L^2)$. The memory required to store the expanded image remains at $O(N^2)$. However, each pixel in the expanded image store only need be accessed

once in the expansion process, whilst each element in the transform memory must be accessed. $2+2\log_2 L$ times (for an untiled transform $L = N$). There is also the possibility that the expanded image could be generated a few tiles at a time, as required, rather than as a whole, which is what the untiled version must do.

The tiled version of the algorithm thus makes a big difference to the amount of transform memory required for the transform. With a 256×256 pixel image split in to 32×32 tiles, a sixty-fourth of the memory is required, reducing the required 4MB of random access memory quoted on page 164 to 64kB.

If the whole operation can be carried out in random access memory then little difference is made to the time taken to expand the image. In the example in the previous paragraph the time is reduced by thirty percent if 32×32 non-overlapping tiles are used and *increased* by nine percent if a 26×26 pixel central portion is used in a 32×32 tile. However, if the untiled version is swapping in and out of virtual memory then the tiled version can run considerably faster.

Implementation in hardware

Fraser [1989a] notes that the FFT is a time-intensive process, which perhaps explains why this method of reconstruction has been neglected. However the advent of very fast FFT hardware means that FFT interpolation is feasible.

As an example, dataβ produce a dedicated FFT processor which can perform a 1024 point FFT every 700μs [Data Beta, 1992]. To enlarge a 256×256 image to 1024×1024 using this processor would take 753ms. Using 32×32 non-overlapping tiles would take 525ms, and using overlapping 32×32 tiles with a 26×26 pixel central portion would take 819ms.

Theoretical ramifications of tiling

By tiling the image we destroy the theoretical basis behind applying the DFT or DCT to the whole image as a way of performing sinc reconstruction. Applying the DFT or DCT to a tile gives an approximation to this reconstruction. The untiled version gives an approximate sinc reconstruction based on all of the information in the image, the tiled version gives an approximate sinc reconstruction based on local information only. We can consider the entire image to be a large tile taken from an infinite, non-repeating picture. In this scenario the tiled version of the process is a scaled-down version of the untiled version with the advantage that most of the tiles can be placed in some sort of context.

In spite of this it is surprising that the tiled and untiled algorithms give virtually identical results. This observation lends weight to the hypothesis that it is local information that is important in determining the intensity surface's values, rather than any globally encoded intensity information.

5.5 Summary

We have seen how DFT expansion can be used, with a local piecewise polynomial reconstructor, to generate a near perfect sinc reconstructed intensity surface in $O(N^2 \log N)$ time.

We have examined two areas where improvements can be made to the existing method. The first, the edge effect problem, has several solutions, one of which led to the use of the DCT in place of the DFT, with better intensity surface quality near edges. This also laid the foundation for the use of any transform in performing the necessary expansion. The second, the need for time and space savings, led to a tiling solution, which dramatically reduces the amount of memory required to perform the transforms and, where virtual memory must be used for a non-tiled version, can lead to speed improvements also.

Chapter 6

A priori knowledge reconstruction

If we have some *a priori* knowledge about the image we are resampling then we may be able to reconstruct a better intensity surface than we could without this knowledge.

A priori knowledge comes in two forms:

1. Knowledge about how the image was sampled;
2. Knowledge about the image's content.

The majority of this chapter is concerned with finding an exact reconstruction of the image in one particular case where both these are known. Before progressing to this we look at what can be achieved when only the first is known.

6.1 Knowledge about the sampler

Most images are captured by some physical device. Knowledge of that device's sampling process gives the potential to invert the process and restore what would have been produced by single point sampling the original intensity surface, or at least a closer approximation to it than that produced by the device. The closer an image is to the single point sampled image, the better many of the NAPK reconstructors discussed in the previous three chapters will work.

Much effort has been expended over the years on image restoration, the attempt to produce a better image from a less good one. Such a process could be applied to an image which could then be reconstructed using a NAPK method.

Referring back to figure 2.3 we can add this restoration process to the figure, and add also the theoretically equivalent path of single point sampling, as shown in figure 6.1. This inversion of the capture process could be built into the reconstructor, giving an APK reconstructor by combining a restorer and a NAPK reconstructor.

6.1.1 Inverting the sampling filter

All capture devices implement some form of area sampling. This sampling can be thought of as convolving the intensity surface with a sampling filter, followed by single point sampling the resulting intensity surface (section 2.5.1). If this sampling filter can be inverted, and the inversion implemented, then it can be used for image restoration and hence APK reconstruction. This process is illustrated in figure 6.2, in the frequency domain.

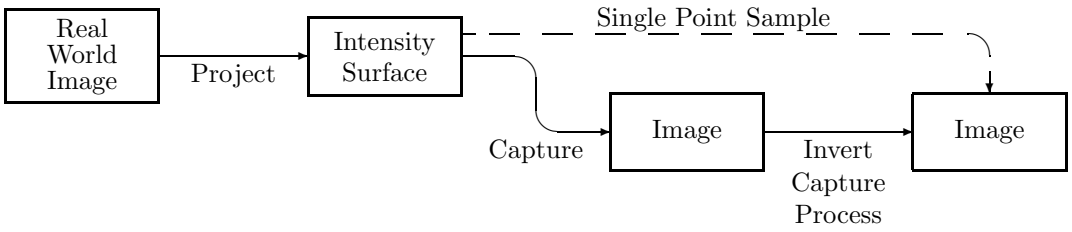

Figure 6.1: The image capture process, and how inverting the capture produces a better image. The first two stages are taken directly from figure 2.3. A real world image is projected to an intensity surface which is captured by some area sampling process. Inverting this sampling produces an image which is as if the intensity surface had been single point sampled.

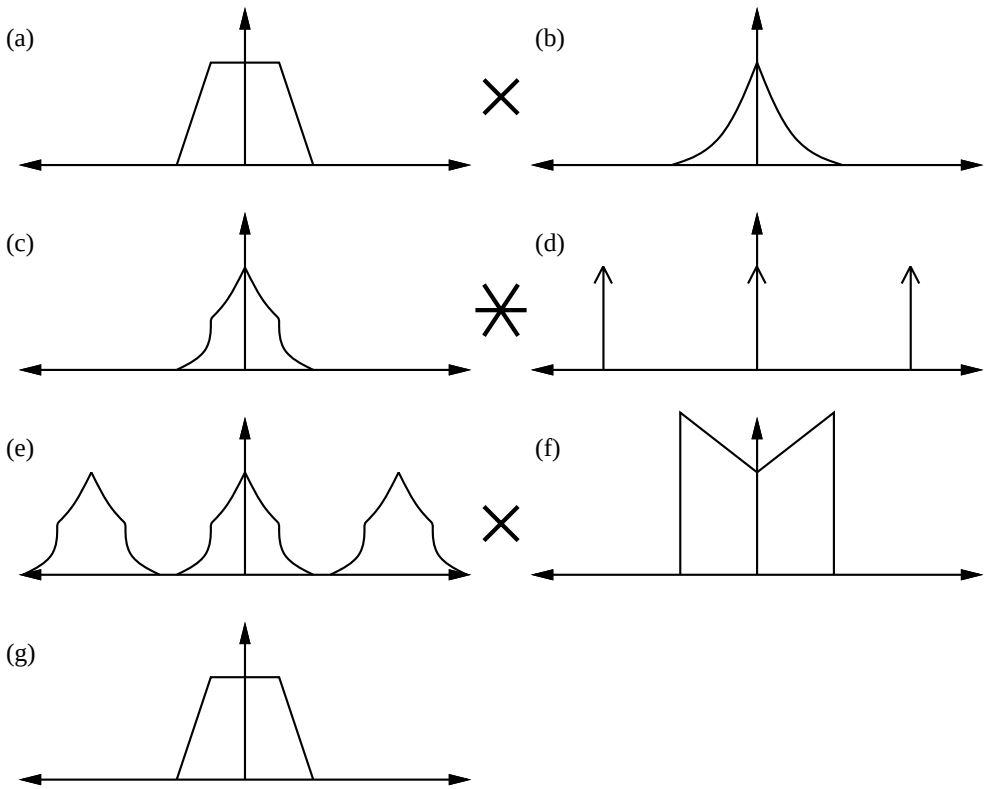

Figure 6.2: Frequency domain illustration of area sampling and APK reconstruction. The Fourier transform of the continuous intensity surface, (a), is multiplied by the area sampler's Fourier transform, (b), giving a filtered intensity surface, (c). This is sampled by convolving with a comb, (d), to give the sampled, filtered image, (e). Inverting (b) gives (f). If (e) is multiplied by (f) then we get (g), an exact reconstruction of (a).

If the sampling filter has frequency spectrum $S(\nu)$ then the inverted filter could be given the spectrum $I_1(\nu) = \frac{1}{S(\nu)}$. If $S(\nu)$ extends beyond the folding frequency then this will have the undesirable effect of amplifying copies of the central component of the image's spectrum. So, the desired form of this inverted filter is:

$$I_2(\nu) = \frac{B_1(\nu)}{S(\nu)}$$

That is: the ideal filter's spectrum, $B_1(\nu)$, multiplied by the inverted sampling filter's spectrum, $\frac{1}{S(\nu)}$. $I_2(\nu)$ can be implemented as convolution in the spatial domain, if the inverse filter's kernel can be determined. Or it can be approximated using the DFT, with the inverse filtering being performed in the frequency domain and an appropriate NAPK reconstruction method applied to the resulting image. The DFT reconstruction methods of the previous chapter could be combined with this DFT restoration to produce an improved reconstructed intensity surface.

The problem with this method is that all practical sampling filters fall off as they move away from zero. Thus the inverse filter amplifies those frequencies near the folding frequency. It is these frequencies in the image which have the smallest amplitudes and which are most affected by noise and any aliasing which may occur. The frequencies near zero, which are least amplified by the inverse filter, are those which are at least affected by these two problems. Therefore inverse filtering amplifies any noise and aliasing artifacts present in an image. It is thus unsuitable for all images except those with very low noise and practically no aliasing.

6.1.2 Modified inverted sampling filter

Oakley and Cunningham [1990] have considered the problem of finding the best reconstruction filter given the sampling function. They develop an error measure which they claim is a good approximation to the visual quality of the reconstructed images [*ibid.*, p.191]. By minimising this measure over all images they produce a formula for the optimal reconstruction filter. In one dimension it is:

$$I(\nu) = \frac{K(\nu)S^*(\nu)}{\frac{1}{\Delta x}\sum_{n=-\infty}^{\infty}\left|S\left(\nu + \frac{n}{\Delta x}\right)\right|^2} \tag{6.1}$$

where $S^*(\nu)$ is the complex conjugate of $S(\nu)$; Δx is the sample spacing in the spatial domain; and $K(\nu)$ is the Fourier transform of the ideal reconstruction filter. Here 'ideal reconstruction filter' means the filter you would like to convolve the *original* intensity surface with to produce the reconstructed intensity surface. Several such functions are of interest:

1. $K(\nu) = 1$; that is: the reconstructed intensity surface should be as close as possible to the original intensity surface. Oakley and Cunningham [1990] call this a restoration case. This reconstruction filter is highly sensitive to noise [*ibid.*, p.180]. Note that, if the sampling filter is bandlimited to below the folding frequency then the reconstruction filter generated by equation 6.1 is equal to both $I_1(\nu)$ and $I_2(\nu)$, except for a multiplicative constant. A second restoration filter is where $K(\nu)$ is the statistically optimal Wiener filter for the continuous image formation case. This produces an implementation of the Wiener filter which is corrected for the effects of sampling.

2. $K(\nu)$ is a low-pass filter. Here the reconstructed intensity surface approximates as closely as possible the original intensity surface convolved with the low pass filter. Of special interest is the case where $K(\nu) = B_1(\nu)$. The reconstructed intensity surface will approximate a perfectly low-pass filtered version of the original intensity surface. It is instructive to note that the sum of the squares in the denominator of equation 6.1 is the sampling filter squared in the frequency domain, then sampled in the spatial domain and transformed into the

frequency domain. Thus the function:

$$\frac{S^*(\nu)}{\sum_{n=-\infty}^{\infty} \left|S\left(\nu + \frac{n}{\Delta x}\right)\right|^2}$$

is closely related to $\frac{1}{S(\nu)}$ with some modification to take into account the fact that the image is *sampled*, not just an intensity surface filtered by $S(\nu)$. If $S(\nu)$ is bandlimited to below the folding frequency then

$$\frac{S^*(\nu)}{\sum_{n=-\infty}^{\infty} \left|S\left(\nu + \frac{n}{\Delta x}\right)\right|^2} = \frac{1}{S(\nu)}$$

3. $K(\nu) = S(\nu)$. The reconstructed intensity surface here is the original surface convolved by the sampling filter — thus producing the theoretical surface generated just before single point sampling occurred. Oakley and Cunningham [1990, p.181] call this "matched reconstruction" or the "interpolating case". If $S(\nu)$ is bandlimited to below the folding frequency than the resampling filter is a box function: $I(\nu) = \Delta x B_1(\nu)$. This means that the reconstructed intensity surface is the same as that produced by convolving the image with the sinc function.

Both Oakley and Cunningham [1990] and Boult and Wolberg [1992] have generated implementations of matched reconstructions filters. These filters have been based on rectangular and hexagonally sampled Gaussian filters [Oakley and Cunningham, 1990] and on box and cubic B-spline filters [Boult and Wolberg, 1992]. Both claim that their derived reconstruction filters perform better than the best NAPK reconstructors, notably better than the Catmull-Rom cubic interpolant.

6.2 Knowledge about the image content

It is possible that a better reconstruction can be achieved if we know something about the image's content. This is true for image restoration; Oakley and Cunningham [1990, p.180] state that:

> "In general, successful image restoration relies not only on correct linear processing, but on the the exploitation of prior knowledge about the image source."

In the image resampling field itself, Ward and Cok [1989, p.264] hypothesise:

> "If there is sufficient *a priori* knowledge of the content of an image, the visual quality can be improved by using interpolation functions that use this *a priori* information. For example, if the original image is known to consist of uniform areas and edges, interpolated pixels can be constrained by some rule to be close in value to some of the neighbouring pixels."

This is an interesting idea but Ward and Cok do not take it any farther.

In the fields of image understanding and computer vision much work has, and is, been done on trying to extract features from a digital image. If an accurate list of features could be extracted then it could be used to drive a renderer which would generate a transformed image. This process is illustrated in figure 6.3. This is analagous to the reconstruct–transform–sample decomposition in figure 1.14, the difference being that the intensity surfaces are replaced by scene descriptions. Unfortunately, the generation of a detailed enough scene description is extremely difficult for even the simplest scenes and so this process would appear to be impractical for image resampling, except in the case of very limited sets of images.

Figure 6.3: A three stage decomposition for a resampler which analyses an image into a scene description, transforms this and then renders it. Compare figure 1.14.

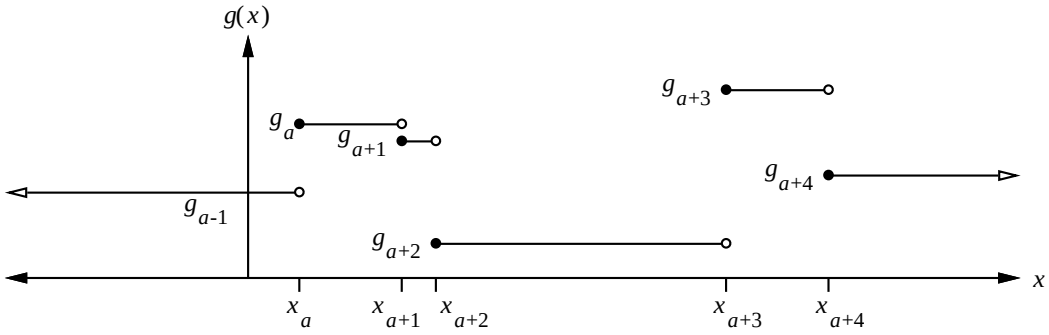

Figure 6.4: The general intensity curve input to one-dimensional sharp edge reconstruction. It consists of areas of constant intensity separated by sharp discontinuities.

To illustrate the type of algorithm that could be developed we will consider a simple case. In this case we limit the class of images to those which consist of areas of constant intensity bounded by infinitely sharp edges. These images will be sampled using an exact-area sampler on a square pixel grid.

We begin by considering the one-dimensional case before progressing to the two-dimensional case.

6.3 One-dimensional sharp edge reconstruction

The general intensity curve in the one-dimensional case consists of a series of plateaux of constant intensity separated by sharp discontinuities. Such an image is shown in figure 6.4. It can be described mathematically as:

$$g(x) = g_c,\ x_c \leq x < x_{c+1} \tag{6.2}$$

where $(\ldots,(x_{-1},g_{-1}),(x_0,g_0),(x_1,g_1),\ldots)$ is an ordered set of ordered pairs of position and intensity information. The pairs are ordered on position values: $x_c < x_{c+1}$, and the intensity values fall in the range $0 \leq g_c \leq 1$.

6.3.1 The black and white case

To simplify matters we begin by considering only the black and white case where $g_c = 0$ or $g_c = 1$. Zero is taken to be black, and one, white. We start by looking at the simplest case: a single edge between a black area and a white area (see figure 6.5). This can be represented as the set $((-\infty,0),(x_1,1),(\infty,\phi))$ where ϕ is an arbitrary value which is never used.

Without loss of generality we can consider sampling with unit spacing, and with position x_1 between zero and one ($0 \leq x_1 < 1$). If the samples are represented as $\{\hat{g}_n, n \in \mathcal{Z}\}$ then sample $\hat{g}_n$ is taken at point $x = n + \frac{1}{2}$ [Heckbert, 1990a]. This disparity between continuous and discrete coordinates, illustrated in figure 6.6, greatly simplifies many of the calculations on them.

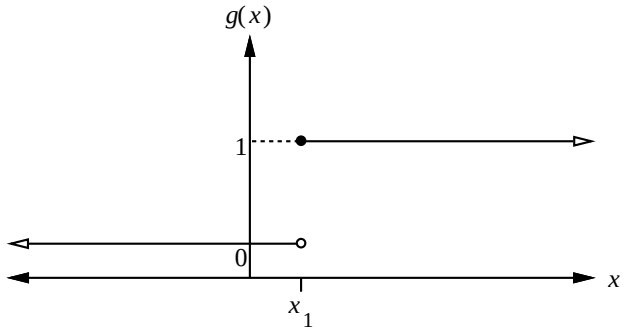

Figure 6.5: The black and white case with a single edge. The edge is at x_1. To the left the intensity curve is blank (0), and to the right, (1).

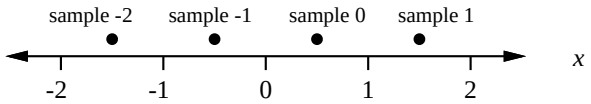

Figure 6.6: The positions of the discrete samples relative to the continuous coordinate system [after Heckbert, 1990a, fig 1]

If the function shown in figure 6.5 is point sampled then the sample values will be:

$$\begin{aligned} \hat{g}_n &= 0,\ n < 0 \\ \hat{g}_0 &= \begin{cases} 0, & x_1 < \frac{1}{2} \\ 1, & x_1 \geq \frac{1}{2} \end{cases} \\ \hat{g}_n &= 1,\ n > 0 \end{aligned}$$

The information about the discontinuity's position is lost here. It is only possible to say where the edge occurred to within $\pm\frac{1}{2}$.

However, we want to use exact-area sampling which is equivalent to convolving with a box filter followed by point sampling (section 2.5.1). Convolving the intensity curve with this box filter produces the function in figure 6.7.

Point sampling this function produces the sample values:

$$\begin{aligned} \hat{g}_n &= 0,\ n < 0 \\ \hat{g}_0 &= 1 - x_1 \\ \hat{g}_n &= 1,\ n > 0 \end{aligned}$$

The information about the position of the discontinuity is now encoded in $\hat{g}_0$. It can be exactly reconstructed from that value:

$$x_1 = 1 - \hat{g}_0 \tag{6.3}$$

A similar situation holds in the case where $g(x) = 1,\ x < x_1$ and $g(x) = 0,\ x \geq x_1$, shown in figure 6.8. Here the sample values will be:

$$\begin{aligned} \hat{g}_n &= 0,\ n < 0 \\ \hat{g}_0 &= x_1 \\ \hat{g}_n &= 1,\ n > 0 \end{aligned}$$

And the discontinuity can be reconstructed exactly as being at:

$$x_1 = \hat{g}_0 \tag{6.4}$$

Thus, in either case, we can exactly reconstruct the curve from the image.

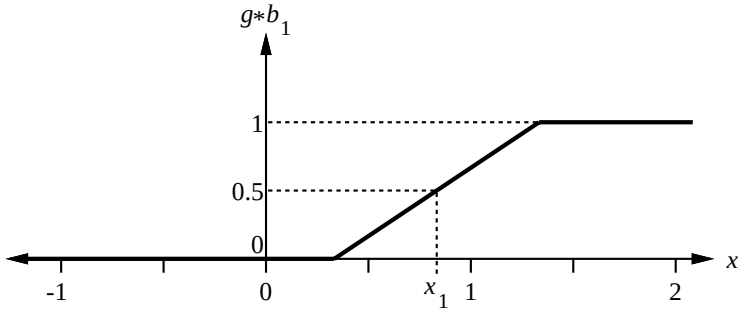

Figure 6.7: The intensity curve of figure 6.5 convolved with a box filter of width one.

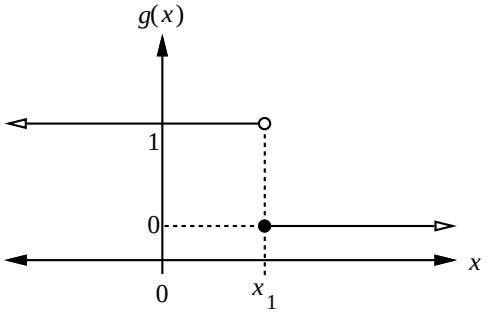

Figure 6.8: The other single edge black and white case, white to the left of the discontinuity and black to the right.

Black and white case — many edges

If we extend this to a situation where there are many edges alternating the intensity between black and white then we can apply the above result in the following way. The original function, $g(x)$, is represented by its exact-area samples $\{\ldots, \hat{g}_{-1}, \hat{g}_0, \hat{g}_1, \ldots\}$. The function that is reconstructed from these samples is, $g_r(x)$. $g_r(x)$ can be generated in a piecewise manner as follows:

Algorithm 1
For every pixel, a:

If $\hat{g}_a = 0$ then $g_r(x) = 0,\ a \le x < a+1$

If $\hat{g}_a = 1$ then $g_r(x) = 1,\ a \le x < a+1$

If $0 < \hat{g}_a < 1$ then

if $\lim_{x \to a^-} g_r(x) = 0$ *or* $\lim_{x \to (a+1)^+} g_r(x) = 1$ then

$$g_r(x) = \begin{cases} 0, & a \le x < a+1-\hat{g}_a \\ 1, & a+1-\hat{g}_a \le x < a+1 \end{cases}$$

if $\lim_{x \to a^-} g_r(x) = 1$ *or* $\lim_{x \to (a+1)^+} g_r(x) = 0$ then

$$g_r(x) = \begin{cases} 1, & a \le x < a+\hat{g}_a \\ 0, & a+\hat{g}_a \le x < a+1 \end{cases}$$

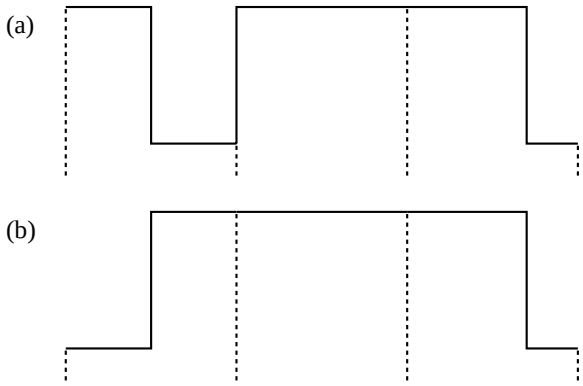

Figure 6.9: Two ways of interpreting the sample sequence 0.5, 1.0, 0.7, if each pixel is allowed to contain one edge. Only (b) is possible if edges are constrained to be at least one sample space apart.

This algorithm will not give an exact reconstruction for all possible $g(x)$. In theorem 3 we see what restrictions must be put on $g(x)$ for $g_r(x)$ to be an exact reconstruction, that is: to ensure that $g_r(x) = g(x)$. The last part of this algorithm shows that, in addition to the intensity level of the edge pixel, one extra bit of information is required to uniquely determine the location of the edge. This bit is the orientation of the edge: whether it is rising from zero to one, or falling from one to zero. The orientation can be ascertained from the orientation of the reconstructed function in either of the adjacent pixels. A single zero or one pixel is required in the entire infinite sequence to fix the orientation for *all* edges. This information can then be propagated through the sequence to produce $g_r(x)$.

An alternative representation of $g_r(x)$ would be to find the values $(\ldots, (x_{-1}, g_{-1}), (x_0, g_0), (x_1, g_1), \ldots)$ which define $g(x)$ (equation 6.2). This can be done from $g_r(x)$, as produced by algorithm 1. An algorithm to *directly* generate the (x_c, g_c) pairs must be constructed so as to take into account the possibility of edges which fall exactly at pixel boundaries. Here the pixels either side of the edge will have sample values zero and one indicating the discontinuity, rather than a single pixel with a value between zero and one indicating it[1]. Notice that algorithm 1 implicitly deals with this situation in its first two cases.

Theorem 3 *Algorithm 1 exactly reconstructs $g_r(x) = g(x)$ if adjacent edges in $g(x)$ are spaced more than one sample space apart. That is: $x_{c+1} - x_c > 1, \forall c$.*

Proof: if $x_{c+1} - x_c > 1, \forall c$ then:

1. No pixel can contain more than one edge, thus ensuring that any grey pixel codes the position of one, and only one, edge. This edge can be reconstructed using orientation information and equation 6.3 or 6.4.

2. Any edge occurring at a pixel boundary generates a zero sample value on one side and a one sample value on the other. This ensures that no dichotomies arise in the reconstruction. For example, if we imposed the lesser restriction that each pixel could only contain a single edge (but that the edges could be any distance apart) then the sample sequence $\ldots, 0.5, 1, 0.7, \ldots$ could be interpreted in two different ways, as can be seen in figure 6.9, whereas the tighter restriction imposed here permits the unique interpretation in figure 6.9(b).

3. Orientation information can be generated by any pair of adjacent pixels. If their sample

[1]The assumption that the samples on either side will have values zero and one is valid if the conditions in theorem 3 are adhered to.

values are $\hat{g}_c$ and $\hat{g}_{c+1}$ then the following table gives the orientation information:

$\hat{g}_c$	$\hat{g}_{c+1}$	$\lim_{x\to(c+1)^-} g_r(x)$	$\lim_{x\to(c+1)^+} g_r(x)$
0	–	0	–
1	–	1	–
–	0	–	0
–	1	–	1
α	$\beta > 1-\alpha$	1	1
α	$\beta < 1-\alpha$	0	0

where $0 < \alpha, \beta < 1$. We can never have a situation where $\beta = 1-\alpha$ because this would mean that two edges were exactly one sample space apart which is not allowed.

From this information we can produce an algorithm which generates the exact reconstruction, $g_r(x)$ from local information, rather than depending on some global method to propagate the orientation information back and forth along the number line. Such an algorithm is essential for the reconstruction of a finite length sequence of samples because it is possible to conceive of a situation where no zero or one samples would occur within a finite length to provide the orientation information for algorithm 1. The improved algorithm, for a sequence of infinite length, is:

Algorithm 2
For every pixel, c:

If $\hat{g}_c = 0$: $g_r(x) = 0,\ c \le x < c+1$

If $\hat{g}_c = 1$: $g_r(x) = 1,\ c \le x < c+1$

If $0 < \hat{g}_c < 1$:

If $\hat{g}_{c-1} < 1-\hat{g}_c$: $g_r(x) = \begin{cases} 0, & c \le x < c+1-\hat{g}_c \\ 1, & c+1-\hat{g}_c \le x < c+1 \end{cases}$

If $\hat{g}_{c-1} > 1-\hat{g}_c$: $g_r(x) = \begin{cases} 1, & c \le x < c+\hat{g}_c \\ 0, & c+\hat{g}_c \le x < c+1 \end{cases}$

An algorithm to find the ordered pairs that define $g(x)$ is:

Algorithm 3
1. For every pixel, c:

If $\hat{g}_c = 0$ and $\hat{g}_{c-1} = 1$: output $(c, 0)$

If $\hat{g}_c = 1$ and $\hat{g}_{c-1} = 0$: output $(c, 1)$

If $0 < \hat{g}_c < 1$:

If $\hat{g}_{c-1} < 1-\hat{g}_c$: output $(c+1-\hat{g}_c, 1)$

If $\hat{g}_{c-1} > 1-\hat{g}_c$: output $(c+\hat{g}_c, 0)$

2. Sort the ordered pairs, (x_i, g_i), which have been output, into an ordered set on their x-values.

Finite-length black and white functions

A finite length function can be defined as

$$g(x) = g_c,\ x_c \le x < x_{c+1},\ c \in \{0, 1, 2, ..., N\} \tag{6.5}$$

where: $((-\infty, g_0), (x_1, g_1), (x_2, g_2), \ldots, (x_N, g_N), (+\infty, \phi))$ is an ordered set of ordered pairs, $x_c < x_{c+1} - 1$. $g_{N+1} = \phi$ is irrelevant, as its value is never used.

$g(x)$ is defined over all real numbers; a finite length version of $g(x)$ must be defined over at least $x \in [\lceil x_1 \rceil - 1, \lfloor x_N \rfloor + 1)$ giving at least samples $\hat{g}_{\lceil x_1 \rceil - 1}, \hat{g}_{\lceil x_1 \rceil}, \ldots, \hat{g}_{\lfloor x_N \rfloor - 1}, \hat{g}_{\lfloor x_N \rfloor}$. The reason for these limits is to ensure that even an edge at $x_1 = \lfloor x_1 \rfloor$ or $x_N = \lceil x_N \rceil$ can be detected.

The algorithms to reconstruct $g(x)$ from its samples are very similar to algorithm 2 and algorithm 3. The main difference is that the first pixel is a special case. Note that the algorithms given below only work if there are at least two samples in the sample set. Edge effects are avoided by assuming that the intensity value at either end of the sequence continues to infinity. This is explicit in the definition of $g(x)$ (equation 6.5).

Algorithm 4
To reconstruct $g_r(x)$ from samples $\hat{g}_a, \hat{g}_{a+1}, \ldots, \hat{g}_{b-1}, \hat{g}_b$:
For every value $c \in \{a, a+1, \ldots, b-1, b\}$:

If $\hat{g}_c = 0$: $g_r(x) = 0, c \le x < c + 1$

If $\hat{g}_c = 1$: $g_r(x) = 1, c \le x < c + 1$

If $0 < \hat{g}_c < 1$:

If $c = a$:

If $\hat{g}_{c+1} > 1 - \hat{g}_c$: $g_r(x) = \begin{cases} 0, & c \le x < c + 1 - \hat{g}_c \\ 1, & c + 1 - \hat{g}_c \le x < c + 1 \end{cases}$

If $\hat{g}_{c+1} < 1 - \hat{g}_c$: $g_r(x) = \begin{cases} 1, & c \le x < c + \hat{g}_c \\ 0, & c + \hat{g}_c \le x < c + 1 \end{cases}$

If $c \neq a$:

If $\hat{g}_{c-1} < 1 - \hat{g}_c$: $g_r(x) = \begin{cases} 0, & c \le x < c + 1 - \hat{g}_c \\ 1, & c + 1 - \hat{g}_c \le x < c + 1 \end{cases}$

If $\hat{g}_{c-1} > 1 - \hat{g}_c$: $g_r(x) = \begin{cases} 1, & c \le x < c + \hat{g}_c \\ 0, & c + \hat{g}_c \le x < c + 1 \end{cases}$

This algorithm exactly reconstructs the values of $g(x)$ over the range $a \le x < b$, given the following conditions:

1. $x_c < x_{c+1} - 1,\ \forall c \in \{0, 1, ..., N\}$ (that is: all adjacent edges are greater than one sample space apart);
2. $a < b$ (that is: at least two samples)
3. $a \le \lceil x_1 \rceil - 1$ and $b \ge \lfloor x_N \rfloor$ (that is: enough information to adequately reconstruct the edges at both ends).

The last contstraint allows us to exactly reconstruct the intensity surface over the entire number line. If we only need the values of $g(x)$ for $a \le x < b$, they can be relaxed to:

$$a \le \lfloor x_1 \rfloor \ \text{ and } \ b \ge \lceil x_N \rceil - 1$$

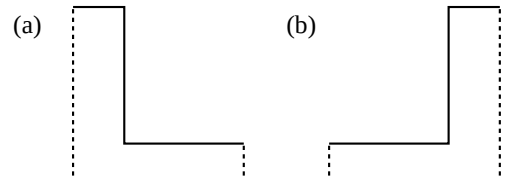

Figure 6.10: The two possible interpretations of a grey pixel value for a single pixel.

The need for constraint 1 was determined in theorem 3, and the need for constraint 2 is implicit in algorithm 4 requring two adjacent pixels to ascertain the edge position in certain cases. If there is only one pixel then we cannot extract the orientation information and thus there are two possiblities for a grey pixel, as illustrated in figure 6.10.

The finite length algorithm to find the edge positions (that is: the (x_c, g_c) pairs) is similar to algorithm 3. To exactly reconstruct $g(x)$ it requires constraints 1, 2, and 3 as given above.

Algorithm 5
To reconstruct $g_r(x)$ from samples $\hat{g}_a, \hat{g}_{a+1}, \ldots, \hat{g}_{b-1}, \hat{g}_b$:

1. Set $n \leftarrow 0$, $x_0 \leftarrow -\infty$
2. If $\hat{g}_a = 0$: $g_0 \leftarrow 0$
   If $\hat{g}_a = 1$: $g_0 \leftarrow 1$
   If $0 < \hat{g}_a < 1$:
   (a) $n \leftarrow 1$
   (b) If $\hat{g}_{a+1} < 1 - \hat{g}_a$: $g_0 \leftarrow 1$, $x_1 \leftarrow a + \hat{g}_a$, $g_1 \leftarrow 0$
   If $\hat{g}_{a+1} > 1 - \hat{g}_a$: $g_0 \leftarrow 0$, $x_1 \leftarrow a + 1 - \hat{g}_a$, $g_1 \leftarrow 1$
3. For $c = a + 1$ to b:
   If $\hat{g}_c = 0$ and $\hat{g}_{c-1} = 1$:
   (a) $n \leftarrow n + 1$
   (b) $g_n \leftarrow 0$, $x_n \leftarrow c$
   If $\hat{g}_c = 1$ and $\hat{g}_{c-1} = 0$:
   (a) $n \leftarrow n + 1$
   (b) $g_n \leftarrow 1$, $x_n \leftarrow c$
   If $0 < \hat{g}_c < 1$:
   (a) $n \leftarrow n + 1$
   (b) If $g_{n-1} = 0$: $g_n \leftarrow 1$, $x_n \leftarrow c + 1 - \hat{g}_c$
   If $g_{n-1} = 1$: $g_n \leftarrow 0$, $x_n \leftarrow c + \hat{g}_c$
4. $x_{n+1} \leftarrow \infty$, $g_{n+1} \leftarrow \phi$
5. $g_r(x) = g_z, x_z \leq x < x_{z+1}, z \in \{0, 1, 2, \ldots, n\}$

We now present an example of how algorithm 5 works:

$$\begin{array}{rl} \text{Let} & ((x_0, g_0), (x_1, g_1), (x_2, g_2), (x_3, g_3), (x_4, g_4), (x_5, g_5)) \\ = & ((-\infty, 0), (0.4, 1), (2.2, 0), (3.4, 1), (5, 0), (\infty, \phi)) \end{array} \tag{6.6}$$

This defines $g(x)$ as illustrated in figure 6.11

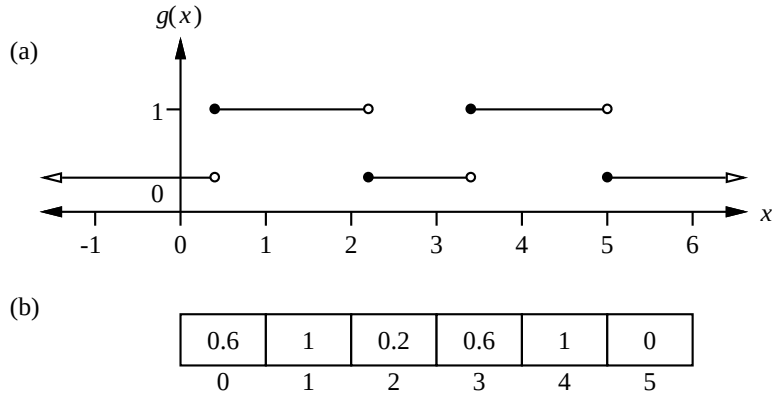

Figure 6.11: The intensity curve used in the example on page 181 is shown in (a). It is defined by equation 6.6 and equation 6.5. The finite image sampled from this intensity curve is shown in (b).

Taking $\hat{g}_n, n \in \{0,1,2,3,4,5\}$ we get:

$$\hat{g}_0 = 0.6, \hat{g}_1 = 1, \hat{g}_2 = 0.2, \hat{g}_3 = 0.6, \hat{g}_4 = 1, \hat{g}_5 = 0$$

Stepping through algorithm 5:

Step		Actions
1.		$n \leftarrow 0, x_0 \leftarrow -\infty$
2.	(a)	$n \leftarrow 1$
	(b)	$g_0 \leftarrow 0, x_1 \leftarrow 0.4, g_1 \leftarrow 1$
3.$(c = 1)$		
3.$(c = 2)$	(a)	$n \leftarrow 2$
	(b)	$g_2 \leftarrow 0, x_2 \leftarrow 2.2$
3.$(c = 3)$	(a)	$n \leftarrow 3$
	(b)	$g_3 \leftarrow 1, x_3 \leftarrow 3.4$
3.$(c = 4)$		
3.$(c = 5)$	(a)	$n \leftarrow 4$
	(b)	$g_4 \leftarrow 0, x_4 \leftarrow 5$
4.		$x_5 \leftarrow \infty, g_5 \leftarrow \phi$

In step 5, $g_r(x)$ is specified by the ordered set of ordered pairs:

$$((-\infty, 0), (0.4, 1), (2.2, 0), (3.4, 1), (5, 0), (\infty, \phi))$$

which is identical to the specification of the original intensity curve, $g(x)$ (equation 6.6).

6.3.2 The grey level case

The extension to grey levels immediately increases the amount of information required to locate an edge's position. In the black and white case we require the intensity value of the pixel in which the edge falls (hereafter called the 'edge pixel') plus one bit of orientation information to ascertain whether the edge is a rise from zero to one or a fall from one to zero. In the grey level case, where the original function is defined in equation 6.2, we require three pieces of information to exactly locate an edge. These three are the intensity of the edge pixel and the intensities of the grey level plateaux on either side of the edge. In the absence of any other information *we assume that these latter two values are provided by the two pixels immediately adjacent to the edge pixel*. This situation is illustrated in figure 6.12.

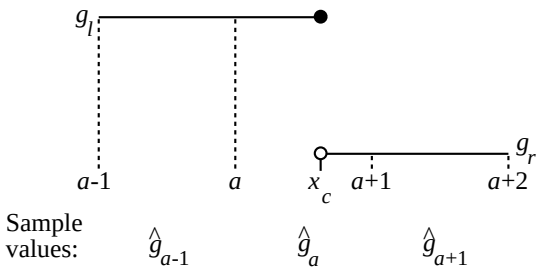

Figure 6.12: An edge in the grey level case. The intensity to the left of the edge is g_l, to the right, g_r. The three sample values are: $\hat{g}_{a-1} = g_l$, $\hat{g}_a = g_r + (x_c - a)(g_l - g_r)$, and $\hat{g}_{a+1} = g_r$.

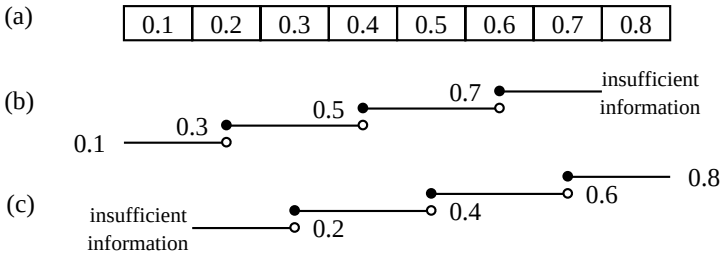

Figure 6.13: Two possible ways of reconstructing the same finite-length sequence of pixel values. (a) shows a sequence of pixel values. (b) and (c) show the two possible ways of reconstructing these values. Note that each case has one pixel in which there is insufficient information to decide what happens within that pixel. Also, it is every second pixel that contains an edge.

We can find the position of the edge from the three sample values as:

$$x_c = a + \frac{\hat{g}_{a+1} - \hat{g}_a}{\hat{g}_{a+1} - \hat{g}_{a-1}} \tag{6.7}$$

and the value of the plateau in the intensity curve immediately to the right of this edge as $g_c = \hat{g}_{a+1}$. Therefore, to exactly reconstruct an edge, *there must be a single edge within the edge pixel and no edges within the two adjacent pixels.* We will assume that this is the case for all edges in the intensity curve, thus no edge pixel will be adjacent to any other edge pixel.

How then do we ascertain which are edge pixels and which are not? For simplicity consider only the cases where no edges occur at pixel boundaries (we will shortly examine the special case where they do occur here). The problem is that we cannot determine from an individual sample's value whether it is an edge pixel or not. In the black and white case it is simple: an edge pixel has a value between zero and one, whilst a non-edge pixel has a value of either zero or one (remember, we are not considering edges that occur at pixel boundaries). In this grey-scale case it is simple to invent a finite-length sequence which is ambiguous. For example the set of samples $0.1, 0.2, 0.3, 0.4, 0.5, 0.6, 0.7, 0.8$ can be reconstructed in two possible ways, shown in figure 6.13.

It proves to be easiest to identify pixels which do *not* contain edges and to ascertain from these which pixels do contain edges. There are two cases where a pixel can be definitely said not to contain an edge:

1. if an adjacent pixel has the same value as this pixel then neither can contain an edge;
2. if both adjacent pixels have different values to this pixel and they are either both greater or both lesser values than this pixel's value, then this pixel does not contain an edge.

If a pixel's value is zero or one, then one of these two cases will always be true.

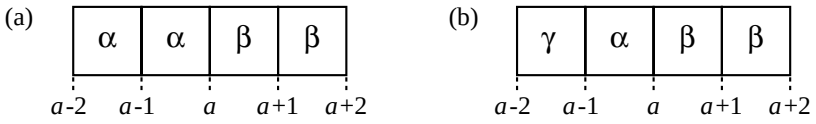

Figure 6.14: The arrangement required to identify an edge at a pixel boundary is shown in (a): two pixels either side of the edge with the same intensity. (b) shows a situation that can be interpreted wrongly. If $\gamma < \alpha < \beta$ then an edge will be found in the α pixel rather than an edge at $x = a$ and one in the γ pixel, as occurred in the original intensity curve.

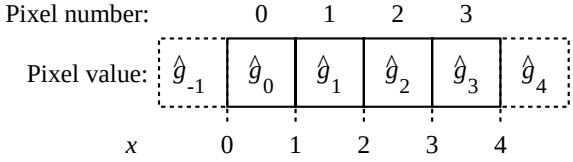

Figure 6.15: The situation for a four-pixel sequence.

Having found a single non-edge pixel, the entire infinite length becomes an unambiguous encoding of $g(x)$. The only case where no non-edge pixel could be identified using the above rules is where the sample values continuously ascend or descend, never reaching one or zero at either end.

Let us now consider the case of an edge at a pixel boundary. Equation 6.7 can still be used to find the edge position. But, to prevent ambiguity, there must be two samples of equal value on either side of the edge, giving a sequence of four samples with the edge in the middle of the sequence. Figure 6.14 shows the ambiguity which arises if this constraint is not obeyed.

This constraint, and the constraint that the two pixels adjacent to an edge pixel may not be edge pixels, can be drawn into a single rule: that any two edges in the original image must be farther than two sample spaces apart. That is, in equation 6.2:

$$x_{a+1} - x_a > 2 \tag{6.8}$$

It is debatable whether this equation should have $\geq$ rather than $>$. With the black and white case we found that the greater than without the equality allowed us to unambiguously reproduce the reconstructed surface from any pair of sample values. Proceeding on that precedent, we will attempt to find some unambiguous reconstruction from a finite-length set of contiguous samples, assuming that equation 6.8 holds.

Is there an unambiguous reconstruction from a four-pixel sequence?

The shortest length which can contain two potential pairs of edges is four pixels long. If these four pixels contain either of the two situations described on page 183 then the original function can be unambiguously reconstructed over at least the central two pixels (the outer two may require one extra pixel of information in order for us to apply equation 6.7). In the cases where neither situation occurs the four sample values will be either increasing or decreasing. Without loss of generality we can take the increasing case with the left-most pixel being pixel zero, as illustrated in figure 6.15.

We know the values of $\hat{g}_0, \hat{g}_1, \hat{g}_2, \hat{g}_3$. They are related by:

$$0 < \hat{g}_0 < \hat{g}_1 < \hat{g}_2 < \hat{g}_3 < 1$$

The values of $\hat{g}_{-1}$ and $\hat{g}_4$ are unknown, but are used in some of the intermediate formulae.

There are two possibilities: either edges occur in pixels 0 and 2 or in pixels 1 and 3. We want to find some way of distinguishing between these two. The only constraint on the original function

Possible edge pixels	Number of cases	Percent of cases
0 and 2	1,167,877	29.8%
1 and 3	1,092,634	27.9%
Both	793,406	20.2%
Neither	867,308	22.1%
Total	3,921,225	100.0%

Table 6.1: The results for a four pixel long sequence, with pixels having values of $0.01n$, $n \in \{1, 2, \ldots, 99\}$. The table shows the number of cases in which edges could occur in pixels 0 and 2 only, pixels 1 and 3 only, either of these cases, or neither of them.

is that any two edges must be more than two sample spaces apart. Therefore we need to find the potential edge locations, $x_0; x_2$ and $x_1; x_3$, and the distances between these pairs of edges $\Delta_{0,2}$ and $\Delta_{1,3}$. The edge locations can be found using equation 6.7 and the distance between edges thus become:

$$\Delta_{0,2} = 2 + \frac{\hat{g}_3 - \hat{g}_2}{\hat{g}_3 - \hat{g}_1} - \frac{\hat{g}_1 - \hat{g}_0}{\hat{g}_1 - \hat{g}_{-1}} \tag{6.9}$$

$$\Delta_{1,3} = 2 + \frac{\hat{g}_4 - \hat{g}_3}{\hat{g}_4 - \hat{g}_2} - \frac{\hat{g}_2 - \hat{g}_1}{\hat{g}_2 - \hat{g}_0} \tag{6.10}$$

The distance between edges must be greater than two, so, to ensure unambiguous reconstruction either $\Delta_{0,2} > 2$ *or* $\Delta 1, 3 > 2$. If *both* inequalities are true, then either case could hold and reconstruction is ambiguous. A problem with finding when these inequalities hold is that the unknown value $\hat{g}_{-1}$ appears in equation 6.9 and $\hat{g}_4$ in equation 6.10. If we set the former to 0 and the latter to 1, we maximise the values of $\Delta_{0,2}$ and $\Delta_{1,3}$. We need to know these maxima in order to ascertain if unambiguous reconstruction can be achieved given just the values $\hat{g}_0$, $\hat{g}_1$, $\hat{g}_2$, and $\hat{g}_3$. Setting these two values to these extrema gives us the following conditions:

1. For it to be possible for edges to be located in pixels 0 and 2, we require:

$$\frac{\hat{g}_3 - \hat{g}_2}{\hat{g}_3 - \hat{g}_1} - \frac{\hat{g}_1 - \hat{g}_0}{\hat{g}_1} > 0 \tag{6.11}$$

2. For it to be possible for edges to be located in pixels 1 and 3, we require:

$$\frac{1 - \hat{g}_3}{1 - \hat{g}_2} - \frac{\hat{g}_2 - \hat{g}_1}{\hat{g}_2 - \hat{g}_0} > 0 \tag{6.12}$$

It can easily be shown that both conditions can be true for some combinations of sample values, for example: $\hat{g}_0 = \frac{1}{20}$, $\hat{g}_1 = \frac{2}{20}$, $\hat{g}_2 = \frac{4}{20}$, and $\hat{g}_3 = \frac{9}{20}$ produces, in equation 6.11: $\frac{3}{14} > 0$, and in equation 6.12: $\frac{1}{48} > 0$.

To give some idea of what is going on, an experiment was performed using all possible values of $\hat{g}_0, \hat{g}_1, \hat{g}_2, \hat{g}_3 \in \{0.01, 0.02, 0.03, \ldots, 0.98, 0.99\}$. This gave the results shown in table 6.1. In nearly 26% of the cases where one of the edge cases is possible, the other is possible too. Therefore the inequalities in equation 6.9 and equation 6.10 do not effectively arbitrate between the two cases.

Longer sequences

An obvious extension to this idea is to use a larger context to determine where the edges fall. Rather than explicitly extend to a five pixel context, then to a six pixel context, and so on, we present the general case, for an n pixel context.

Possible edge pixels	Number of cases	Percent of cases
Even only	9,349,562	12.4%
Odd only	35,036,048	46.5%
Either	2,624,600	3.5%
Neither	28,277,310	37.6%
Total	75,287,520	100.0%

Table 6.2: The results for a five pixel long sequence, with pixels having values of $0.01n$, $n \in \{1, 2, \ldots, 99\}$. The table shows the number of cases in which edges could occur in the even numbered pixels only, the odd numbered pixels only, either even or odd, or neither even nor odd.

Possible edge pixels	Number of cases	Percent of cases
Even only	189,397,344	15.9%
Odd only	179,280,225	15.0%
Either	8,826,079	0.74%
Neither	814,548,752	68.3%
Total	1,192,052,400	100.0%

Table 6.3: The results for a six pixel long sequence, with pixels having values of $0.01n$, $n \in \{1, 2, \ldots, 99\}$. The table shows the number of cases in which edges could occur in the even numbered pixels only, the odd numbered pixels only, either even or odd, or neither even nor odd.

Given n consecutive pixel values: $\hat{g}_0, \hat{g}_1, \ldots, \hat{g}_{n-1}$, such that $0 < \hat{g}_a < 1$ and $\hat{g}_a < \hat{g}_{a+1}$, and given that any two edges will be greater than two sample spaces apart:

1. For it to be possible for the edges to the edges to be in the even numbered pixels, we require:

$$\delta_{0,2} > 0,\ \delta_{2,4} > 0,\ \ldots,\ \begin{cases} \delta_{n-3,n-1} > 0, & n \text{ odd} \\ \delta_{n-4,n-2} > 0, & n \text{ even} \end{cases}$$

2. For it to be possible for the edges to occur in the odd numbered pixels, we require:

$$\delta_{1,3} > 0,\ \delta_{3,5} > 0,\ \ldots,\ \begin{cases} \delta_{n-3,n-1} > 0, & n \text{ even} \\ \delta_{n-4,n-2} > 0, & n \text{ odd} \end{cases}$$

where:

$$\delta_{a-1,a+1} = \frac{\hat{g}_{a+2} - \hat{g}_{a+1}}{\hat{g}_{a+2} - \hat{g}_a} - \frac{\hat{g}_a - \hat{g}_{a-1}}{\hat{g}_a - \hat{g}_{a-2}}$$

and the two required but unknown pixel values are set to:

$$\begin{aligned} \hat{g}_{-1} &= 0 \\ \hat{g}_n &= 1 \end{aligned}$$

When $n = 5$, both cases are possible for, for example: $\hat{g}_0 = 0.2$, $\hat{g}_1 = 0.3$, $\hat{g}_2 = 0.4$, $\hat{g}_3 = 0.5$, and $\hat{g}_4 = 0.7$. With these values: $\delta_{0,2} = \frac{1}{6}$, $\delta_{1,3} = \frac{1}{6}$, and $\delta_{2,4} = \frac{1}{10}$.

When $n = 6$, both cases are still possible. For example, with $\hat{g}_0 = 0.01$, $\hat{g}_1 = 0.02$, $\hat{g}_2 = 0.03$, $\hat{g}_3 = 0.05$, $\hat{g}_4 = 0.1$, and $\hat{g}_5 = 0.3$: $\delta_{0,2} = \frac{1}{6}$, $\delta_{1,3} = \frac{3}{14}$, $\delta_{2,4} = \frac{2}{15}$, and $\delta_{3,5} = \frac{4}{63}$.

For $n = 5$ and $n = 6$ similar experiments were performed to that for $n = 4$. The results of these are shown in tables 6.2 and 6.3. For the case of $n = 6$ we would expect an equal number of cases for even only and odd only. The difference in table 6.3 is most likely due to bias in the particular 1.2 billion samples we took.

Obviously the proportion of situations where either case could be true declines as n increases from 4 to 6; but the fact that there are still situations where either case is possible means that we cannot use these inequalities to arbitrate between the cases.

We have been unable to find a proof which shows that, for any length, there are always situations where both cases are possible, or that there is a length for which it is possible to unambiguously arbitrate between the two cases. However the series of sample values: $\hat{g}_a = \ln(ca + k)$, with suitable choices for c and k, appears to provide situations where either case could be true for very large n. For example: $c = 0.001$, $k = 1.001$ provides a situation where both cases are true for any n, $n \leq 1717$. To discover if a logarithmic sequence can produce a situation where both cases are true for arbitrarily large n seems an insoluble problem in itself. For example, computer calculations show that $c = 10^{-4}$ and $k = 1 + 10^{-4}$ gives a situation where either case could be true for $n \leq 17,181$, whilst $c = 10^{-6}$ and $k = 1 + 10^{-6}$ does not give such a situation for any n.

In the face of this failure to find an unambiguous reconstruction from a finite-length sequence, what can we say?

Firstly, with $n = 6$, only about 2.3% of the situations where one case could be true can also represent the other cases. Thus, we could use $n = 6$ and, in ambiguous situations, depend on pixels beyond these six to provide sufficient contextual information to unambiguously reconstruct. This option would succeed almost always, but, as we have seen, even with a very long sequence of samples there exist situations which are ambiguous over the entire sequence. Secondly, these calculations have been based on the assumption that any two adjacent edges are greater than two sample spaces apart (equation 6.8). We could increase this limit. The simplest way to ensure unambiguous reconstruction for a finite-length sequence is to have one known non-edge pixel in the sequence. Non-edge pixels can be identified using one of the two rules on page 183. Pixels obeying the second rule are impossible to ensure for any length of sequence with *any* minimum limit on the distance between adjacent edges. It is possible to ensure that at least one non-edge pixel can be identified using the first rule, provided that:

$$x_{a+1} - x_a > 2 + \frac{1}{\left\lfloor \frac{n-1}{2} \right\rfloor} \tag{6.13}$$

for a sequence of n pixels.

This condition ensures that, in most cases, there are adjacent pixels in the sequence of n pixels which can be identified as non-edge pixels using the first rule on page 183. In the remaining cases, where no two adjacent pixels have the same value, we can be sure that the pixels at the extreme ends of the sequence are both non-edge pixels. This latter situation only occurs when n is odd, The limiting value can obviously be made closer to two by increasing the length of the sequence.

6.3.3 Practical reconstruction

To perfectly reconstruct a function from a sequence of samples we need to convert the above results to a practical algorithm. One such algorithm considers sequences of three pixels, thus requiring all edges to be greater than three sample spaces apart. By considering longer sequences a smaller minimum distance can be used, and by considering all N samples a distance very close to two could be achieved for large enough N.

The algorithm for three pixel sequences is:

Algorithm 6
Given a sequence of samples: $\hat{g}_a, \hat{g}_{a+1}, \ldots, \hat{g}_b$, generated from a function $g(x)$, where $g(x)$ is described by equation 6.2, and the ordered set of pairs is $((-\infty, g_0), (x_1, g_1), \ldots, (x_m, g_m), (\infty, \phi))$. Then an exact reconstruction, $g_r(x)$, can be made from the samples in the range $x \in [a + 1, b)$, if:

1. $b - a \geq 2$ (at least three samples);
2. $x_{c+1} - x_c > 3$, $\forall c \in \{1, 2, \ldots, m - 1\}$ (all adjacent edges greater than three sample spaces apart).

$g_r(x)$ is generated piecewise as follows:

For every value $c \in \{a+1, a+2, \ldots, b-2, b-1\}$:

If $\hat{g}_{c-1} = \hat{g}_c$ or $\hat{g}_{c+1} = \hat{g}_c$
then $g_r(x) = \hat{g}_c,\ c \leq x < c+1$

If $\hat{g}_{c-1} \neq \hat{g}_c$ and $\hat{g}_{c+1} \neq \hat{g}_c$
then $g_r(x) = \begin{cases} \hat{g}_{c-1}, & c \leq x < c+\epsilon \\ \hat{g}_{c+1}, & c+\epsilon \leq x < c+1 \end{cases}$ where $\epsilon = \frac{\hat{g}_{c+1} - \hat{g}_c}{\hat{g}_{c+1} - \hat{g}_{c-1}}$

If $\hat{g}_a = \hat{g}_{a+1}$
then $g_r(x) = \hat{g}_a,\ a \leq x < a+1$
otherwise $g_r(x)$ is undefined for $a \leq x < a+1$

If $\hat{g}_b = \hat{g}_{b-1}$
then $g_r(x) = \hat{g}_b,\ b \leq x < b+1$
otherwise $g_r(x)$ is undefined for $b \leq x < b+1$

You will note that this algorithm perfectly reconstructs the original function in the range $x \in [a+1, b)$. It is undefined in the range $x \in [a, a+1)$ and $x \in [b, b+1)$ if there are edges in pixels a and b respectively. This is a manifestation of the edge effect problem — there is not enough information to exactly reconstruct the function in these two end pixels. An equivalent algorithm to find the (x_i, g_i) pairs will be unable to ascertain the values at the extreme ends of the range of pixels in the same situations.

An alternative strategy is to allow adjacent edges to be closer together but insist that no edge occur in either of the pixels at the extreme ends of the sample sequence. These changes to the criteria would enable us to *always* exactly reconstruct an intensity curve.

This final, one-dimensional algorithm, exactly reconstructs the entire original function, provided that the original function obeys the given criteria.

Algorithm 7
Given a set of samples: $\hat{g}_a, \hat{g}_{a+1}, \ldots, \hat{g}_{b-1}, \hat{g}_b$ generated from a function $g(x)$, an exact reconstruction, $g_r(x)$, of $g(x)$ can be generated by this algorithm provided:

- $g(x)$ is generated by equation 6.2 from the ordered set of ordered pairs: $((-\infty, g_0), (x_1, g_1), (x_2, g_2), \ldots, (x_m, g_m), (\infty, \phi))$ where $x_c < x_{c+1}$, $\forall c \in \{1, 2, \ldots, m-1\}$;
- $x_{c+1} - x_c > 2$, $\forall c \in \{1, 2, \ldots, m-1\}$;
- $a + 1 \leq x_1$;
- $x_m < b$.

$g_r(x)$ is generated by:

1. $m \leftarrow 0$
   $x_0 \leftarrow -\infty$
   $g_0 \leftarrow \hat{g}_a$
   previous $\leftarrow$ NotEdge
2. For $c \leftarrow a+1$ to $b-1$:
   If $\hat{g}_c \neq \hat{g}_{c-1}$ and previous = NotEdge
   then:
   (a) $m \leftarrow m + 1$

(b) $g_m \leftarrow \hat{g}_{c+1}$,
$x_m \leftarrow c + \frac{\hat{g}_{c+1} - \hat{g}_c}{\hat{g}_{c+1} - \hat{g}_{c-1}}$,
previous $\leftarrow$ Edge

otherwise:
previous $\leftarrow$ NotEdge

3. $x_{m+1} \leftarrow \infty$, $g_{m+1} \leftarrow \phi$

4. $g_r(x) = g_e,\ x_e \leq x < x_{e+1},\ e \in \{0, 1, 2, \ldots, m\}$

For an infinite length sequence all that need be done is to identify a single non-edge pixel and apply this algorithm forward toward positive infinity and a slightly modified version of it backward toward negative infinity. Thus, provided that there is a single identifiable non-edge pixel in the infinite image, a perfect reconstruction can be generated. As equation 6.8 must be true in this algorithm, an identifiable non-edge pixel will almost certainly appear in an infinitely long sequence.

6.3.4 Use in resampling

If we are resampling functions of the type described by equation 6.2 then the above algorithms give an exact reconstruction of the original function. This is better than any of the NAPK methods could do with this particular set of original functions, and even better than the APK methods disscussed in section 6.1, because neither the sampling kernal nor the original function are band limited. The band-unlimited nature of these functions is discussed in the next section.

The final algorithm in the previous section (algorithm 7) generates a *description* of the function which can be transformed and the new description rendered as illustrated by figure 6.3. Thus the resampled version is as accurate as it could possibly be, having been rendered from an exact description of the function.

6.3.5 Relationship to sampling theory

It is well known that *any* function, $f(x)$, can be exactly reconstructed from single point samples, $\hat{f}_i$, provided that the highest spatial freqency in $f(x)$ has wavelength longer than two sample spacings (section 2.4.1). If, without loss of generality, we take the sample spacing to be one, then this condition is that the highest spatial frequency is less than one half. Perfect reconstruction is performed by convolving the samples by an appropriate sinc function.

The algorithms given in this chapter have shown that *any* function, $g(x)$, which can be defined by equation 6.2 can be exactly reconstructed from its exact-area samples $\hat{g}_i$, provided that any two edges in the image are greater than two sample spaces apart and that there is at least one identifiable non-edge pixel in the sample set. Perfect reconstruction in this case is performed by algorithm 7 modified for an infinite set of samples, as explained on page 189.

The sets of functions which can be exactly reconstructed by these two methods are disjoint except for the trivial case $f(x) = g(x) = K$, a constant. This can be proven by noting that, except for the trivial case, $g(x)$ always contains sharp edges, which require infinite frequencies to generate whilst $f(x)$ must always be bandlimited.

Classical sampling theory produces criteria for perfect reconstruction based on Fourier transform theory [Shannon, 1949]. The resulting method of perfect reconstruction is a simple mathematical process: convolution of the samples by a sinc function. The method of perfect reconstruction presented here, on the other hand, consists of an algorithm which generates a description of the original function.

	Sinc Reconstruction	Sharp Edge Reconstruction
Original function	$f(x) = \int_{-\infty}^{\infty} F(\nu) e^{i2\pi\nu x} d\nu$	$g(x) = g_a,\ x_a \leq x < x_{a+1}$
Specified by	its spectrum: $F(\nu)$	an ordered set of ordered pairs of edge position and intensity level information: $((-\infty, g_{-\infty}), \ldots, (x_{-1}, g_{-1}), (x_0, g_0), (x_1, g_1), \ldots, (\infty, \phi))$.
Restrictions on the specification	$\lvert\nu\rvert < \frac{1}{2}$, this is equvailent to $\lvert\lambda\rvert > 2$ where the wavelength $\lambda = \frac{1}{\nu}$	$x_{c+1} - x_c > 2,\ \forall c$, plus at least one identifiable non-edge pixel
Sampling method	Single point sampling	Exact area sampling
Reconstruction method	Convolution by a sinc function	Using algorithm 7 extended to the infinite case
Comments	Only works for an infinite set of samples	Can work on both infinite and finite sets, to work on a finite set requires an extra restriction, that is: no edge in the first or last pixel in the set

Table 6.4: Comparison of sinc and sharp edge reconstruction assuming unit spaced samples.

A further difference between the two is in the types of function and types of sampling which are used. Classical sampling theory considers a function to be a (finite) sum of sinusoids, whilst the process described in this chapter considers a piecewise constant function. The former is typical of audio and AC electrical signals, whilst the latter is typical of visual signals. Classical sampling theory considers single point samples, while this process considers exact-area sampling which is a good approximation to the form of sampling employed by a charge coupled device (CCD) sensor [Kuhnert, 1989] or by a microdensitometer with appropiate aperture shape [Ward and Cok, 1989], both image capture devices. A summary of the differences between the two perfect reconstruction is given in table 6.4.

The effect of errors

Two types of error beset these algorithms: one due to the finite number of samples, the other due to errors in the sample values themselves. Sinc reconstruction will only work for an infinite number of samples. A finite set causes edge effects, which must be dealt with using one of the methods in chapter 4 to produce an approximately correct reconstruction. Exact grey scale reconstruction can deal with finite numbers of samples, as described in algorithm 7 or algorithm 6.

Errors in the sample values themselves, from whatever source, prevent either method from producing an exact reconstruction of the original function. Sinc reconstruction degrades gracefully as the magnitude of the error increases. With small errors in the sample values sinc still produces a good approximation to the original function.

Exact grey scale reconstruction, on the other hand, degrades gracefully as quantisation error increases but fails completely for any other type of error. This failure is due to an inability to ensure that adjacent non-edge pixels have the same intensity, a fact which is assumed by all the algorithms. With only quantisation errors, adjacent non-edge pixels will have the same intensity, but it will be a quantised version of the correct intensity. With other errors, it is possible to modify the reconstruction algorithm to take into account an error distribution over the sample values; perhaps by considering two adjacent pixels to have the same grey-value if their values lie within a certain

distance of each other. Such a modification is left for future work.

An analysis of the algorithm's performance for quantisation errors shows that, if the two grey levels either side of an edge quantise to the same qunatisation level, then that edge cannot be reconstructed at all: it 'dissappears'. All other edges will tend to move slightly. The smaller the difference in grey level either side of the edge, the larger the maximum possible difference in edge position between the original and the reconstructed functions, but the less visible the edge to the eye and so possibly, the less the eye will care about the shift. For N quantisation levels, when Δg, the difference between adjacent grey levels, is $\Delta g \gg \frac{1}{N-1}$; this maximum shift in edge position is approximately $\pm\frac{1}{\Delta g\,(N-1)}$. See appendix B.9 for details.

We have demonstrated that, in an error-free system, a class of intensity curves can be exactly reconstructed by sharp edge reconstruction, which cannot be exactly reconstructed by classical sampling theory methods. We now consider if such a class exists for two-dimensional intensity surfaces.

6.4 Two-dimensional sharp edge reconstruction

The original intensity surface in this case consists of areas of constant intensity bound by sharp edges. The image is produced by taking exact-area samples off this intensity surface. We will consider a square pixel grid and, without loss of generality, unit spaced samples. Thus if the original function is $g(x, y)$, then $\hat{g}_{i,j}$ is taken over the area $i \leq x < i + 1, j \leq y < j + 1$; that is:

$$\hat{g}_{i,j} = \int_i^{i+1} \int_j^{j+1} g(x, y)\, dy\, dx$$

A good deal of research has been done on locating the positions of edges in images. These tend to be developed for and tested on real, noisy images, and give approximate locations of edges in the image. By constrast we are here assuming a perfectly sampled, perfect intensity surface — thus no errors appear in the sample values. The aim is to ascertain whether, in the absence of any errors, perfect reconstruction is possible. If so, what criteria must the original intensity surface obey for perfect reconstruction to be possible.

6.4.1 Single point sampling case

Before looking at exact-area sampling, we examine how much information we can extract from a single point sampled image. Here a pixel's sample value is the value of the intensity surface at the pixel's center. An edge will thus be identifiable as being close to where adjacent pixels have different intensities.

In the one-dimensional case the edge occurs in a single pixel, and thus the error in edge position is $\pm\frac{1}{2}$ sample spaces. In the two dimensional case, an infinitely long edge will pass through an infinite number of pixels. Thus there is potential to extract accurate information about the line's slope and position by considering more of the evidence than a single pixel's worth.

Theorem 4 *If we have an intensity surface containing a single, infinitely long straight edge, single point sampled over all $\mathcal{Z}^2$, then the slope of that edge can be exactly determined, whilst its position may have some inaccuracy.*

Proof: Consider only edges with a slope between zero and one:

$$y = mx + c,\ 0 \leq m \leq 1$$

where the area below the edge is white and above it is black. All other cases can be transformed into this case by rotation of $90n^\circ, n \in \mathcal{Z}$ and/or reflection in the line $y = 0$.

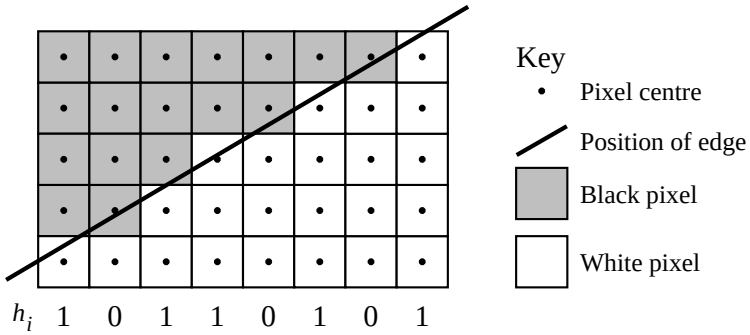

Figure 6.16: An example of a single point sampled single edge. The h_i are a Rothstein code for the edge.

For every integer x-coordinate we define a number h_i, which is either one or zero, depending on the values of the pixels near the edge. To ascertain the value of h_i we first find j such that $\hat{g}_{i,j} \neq \hat{g}_{i,j+1}$, then:

$$h_i = \begin{cases} 1, & \hat{g}_{i-1,j} \neq \hat{g}_{i,j} \\ 0, & \hat{g}_{i-1,j} = \hat{g}_{i,j} \end{cases}$$

Part of an edge is illustrated in figure 6.16, with the h_i values given underneath. A value of 1 indicates that this column contains the first white pixel on a row, a value 0 indicates that it does not.

$\ldots, h_{-1}, h_0, h_1, h_2, \ldots$ is a Rothstein code describing the line [Weiman, 1980; Rothstein and Weiman, 1976]. The slope of the line is the number of 1s in the sequence divided by the total number of digits in the sequence:

$$m = \lim_{k \to \infty} \frac{\sum_{i=-k}^{k} h_i}{\sum_{i=-k}^{k} 1} \tag{6.14}$$

If the sequence of h_i values is aperiodic then equation 6.14 converges on the real value of m [Rothstein and Weiman, 1976, p.123]. A finite length fragment gives an approximation to the real slope [*ibid.*, p.110]. These statements are also true for a periodic sequence of h_i values, but in this case the value of m is rational. If the length of a period is q and each period contains p 1s then the slope is [*ibid.*, p.109]:

$$m = \frac{p}{q}$$

Thus the slope of the edge can be exactly determined, in all cases, because we have an infinite number of h_i values.

If h_i is periodic (that is: m is rational) then the position, c, can only be determined to within some error bounds. If the slope is expressed as $m = \frac{p}{q}$ with p and q relatively prime then c can be determined with an error of $\pm\frac{1}{2q}$. This is illustrated in figure 6.17. The truth of this error bound can be seen by finding the y-intercepts, y_i, of the edge with each of the sampling lines; $y = i + \frac{1}{2},\ i \in \mathcal{Z}$. The fractional parts of these values repeat with period q, and within a period they are evenly spaced. Thus, if the fractional part of y_i is $e_i = y_i - \lfloor y_i \rfloor$, then, because $y_{i+1} = y_i + \frac{p}{q}$, we can write, for some e_n:

$$e_n = o + \frac{np \bmod q}{q} \tag{6.15}$$

where n is chosen so that $e_n < \frac{1}{q}$ and thus o, the offset from zero, is such that $o < \frac{1}{q}$.

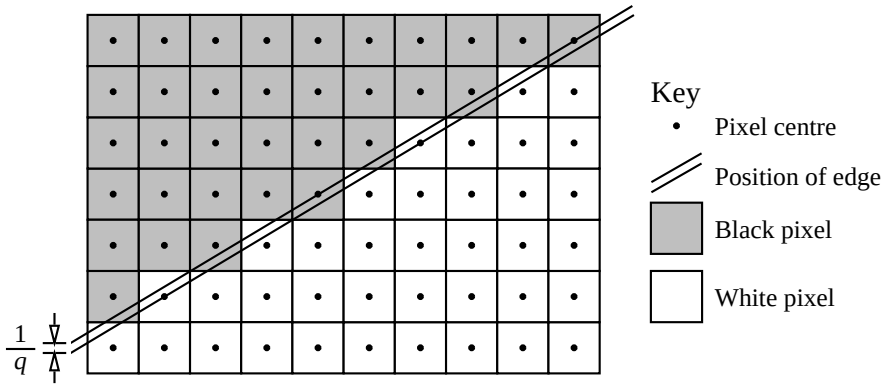

Figure 6.17: The error bounds on the position of a line of rational slope, in this case the slope $m = \frac{p}{q} = \frac{3}{5}$. The line can be positioned anywhere over a vertical distance of $\frac{1}{q}$.

The values of e_i are periodic, with period q. They are also evenly distributed. The minimum difference between any two different values of e_i is $\frac{1}{q}$. Thus o can range over values up to $\frac{1}{q}$ apart and yet the same sample values will be generated. The error in the position, c, is plus or minus half this number, that is $\pm\frac{1}{2q}$.

If we wish to know the positional error in the direction perpendicular to the edge, rather than along the y-axis then, given that the error along the y-axis is $\epsilon_y = \pm\frac{1}{2q}$, then the positional error perpendicular to the edge is:

$$\epsilon_\perp = \pm\frac{1}{2\sqrt{p^2+q^2}}$$

If the sequence h_i is aperiodic (that is: m is irrational), then we can condider the situation as q goes to infinity:

$$\lim_{q\to\infty} \epsilon_\perp = 0$$

Therefore, there exists only one possible position for a line of irrational slope, and c can be exactly determined in this case. QED.

For a finite length edge the slope can only be determined approximately. When a sequence of m h_i values are available, $h_1, h_2, \ldots, h_n$, then the slope is approximated by:

$$\check{m} = \frac{\sum_{i=1}^{n} h_i}{n}$$

We can see that a good approximation to the line's slope and position can be obtained from the single point sample case. Can the exact-area sample case improve on these results?

6.4.2 Exact area sampling — black and white case, single edge

Given an image, area sampled from an intensity surface consisting of a single edge between an area of constant intensity zero and an area of constant intensity one, what can we say? Firstly the position of the edge can be approximately determined from the location of the grey pixels in the image. The edge must pass through all these grey pixels in the image. We call such pixels 'edge pixels'. Secondly, the exact slope and positions of the edge should be determinable from a finite number of pixel values. (In the single point sample case an infinite number of pixel values were requried to exactly determine the slope, and there existed situations where the position could not be exactly determined).

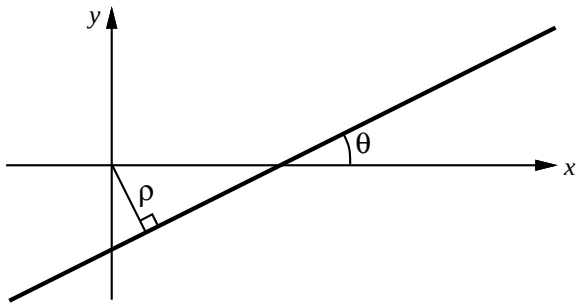

Figure 6.18: The (ρ, θ) parameterisation of a straight line. θ is the angle the line makes with the positive x-axis, ρ is the perpendicular distance from the line to the origin.

Hypothesis: *The position and slope of a single, infinitely long, straight edge between an area of constant intensity zero and an area of constant intensity one can be exactly determined from two exact-area sample values.*

This hypothesis has its foundation in the recognition that only two numbers are required to exactly specify a straight line. In section 6.3.1 we saw that a single number specified the position of a sharp edge in one dimension and that this positional information was coded in a single pixel values (plus one extra bit of orientation information which could be derived from a neighbouring pixel). Here we will see that the slope and direction of a straight line are indeed coded in the sample values of two adjacent edge pixels plus some extra bits of orientation information, which can be derived from neighbouring pixels. Because of the need for this orientation information, the hypothesis is incorrect, but it is not far from the truth.

The equation of a straight line

Three parameterisation of a straight line, which prove useful when determining the position of an edge, are:

1. $y = mx + c$, the standard equation of the line, using the slope, m, and y-intercept c, as the parameters. This equation for a straight line has problems in that a vertical line cannot be represented and a small change in m makes a large difference in the line when m is small and a small difference in the line when m is large, meaning that an error measure on m (or on c which has a similar problem) is difficult.

2. $x = t\cos\theta + \rho\sin\theta$, $y = t\sin\theta - \rho\cos\theta$, using parameters ρ and θ. ρ is the perpendicular distance from the line to the origin, and θ is the angle the line makes with the positive x-axis (figure 6.18). These two parameters are better than m and c in that they render a uniform description for any position and orientation (error bounds will be the same for all orientations and positions) and have no special case (such as the vertical lines in the previous case) [Kitchen and Malin, 1987]. However, they can also make the algebra more difficult.

3. $x = x_0 t$, $y = y_0(1 - t)$. The two parameters x_0 and y_0 are the x- and y-intercepts of the line as shown in figure 6.19(a). This parameterisation can represent any line except one for which $x_0 = y_0 = 0$, or a vertical or a horizontal line which does not pass through the origin. An alternative parameterisation using the same philosophy is that shown in figure 6.19(b) using y_0 and y_1, the y-intercepts of the line at $x = 0$ and $x = 1$ respectively. This gives: $x = t$, $y = (1 - t)y_0 + ty_1$. This parameterisation cannot represent vertical lines.

   Neither of these parameterisations renders a uniform description for all positions and orientations. In the former, for example, when either parameter is close to zero, a small change in the other will cause a large change in the line. However, both of these very similar parametrisations prove useful in the ensuing work.

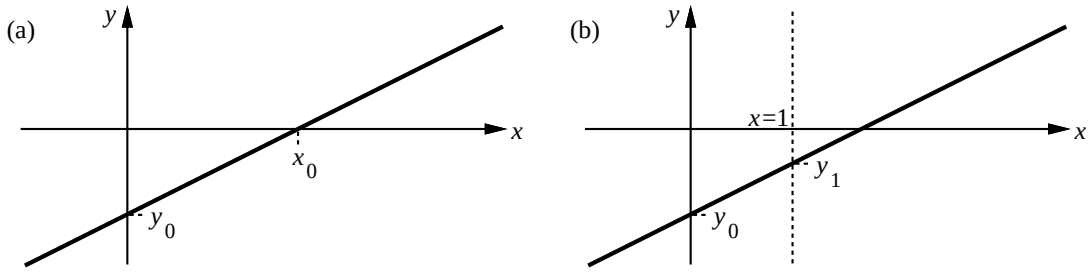

Figure 6.19: Two intercept parameterisations of a straight line. (a) in terms of its x- and y-axis intercepts, x_0 and y_0. (b) in terms of two y-intercepts, y_0 and y_1.

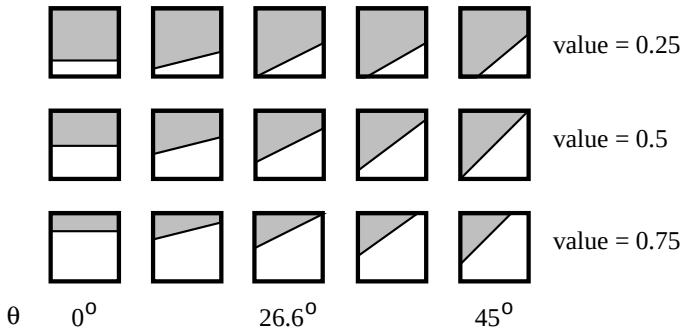

Figure 6.20: A single edge pixel's value can represent an edge at any orientation. Here we see three pixel values (0.25, 0.5, and 0.75) each with five of the many possible edges that could pass through the pixel.

All three parameterisations completely determine the position and slope of a line in two parameters. It is therefore not unreasonable to expect that two pixel values will also completely determine the position and slope of the edge.

What can one pixel value tell us?

To again simplify matters we consider only an edge with slope between zero and one, and with black (intensity zero) above it and white (intensity one) below it. All other possible situations can be transformed into this set of situations by reflection and/or rotation. The single edge pixel will have a grey value between zero and one. Its value reduces the set of possible edges through the pixel from an infinite set to a smaller, but still infinite, set. Examples are shown in figure 6.20. The ambiguity in the line's slope and position can be removed by considering the value of an adjacent edge pixel.

Before doing this we classify edge pixels into three groups based on how the edge passes through the pixel. Type I pixels have the edge passing through their bottom and right sides (figure 6.21(a)). Type II have the edge passing through the left and right sides (figure 6.21(b)), and Type III have the edge passing through the left and top sides (figure 6.21(c)). No other combination of sides can occur for an edge with slope between zero and one. Edges passing through the bottom-left or top-right corner can be considered to be of any appropriate type.

If we now apply a local coordinate system to the pixel, with the origin at the bottom left corner and the pixel of size 1×1 (figure 6.21(a)), then we can describe the edge simply using the third of our three parameterisations of a straight line on page 194. These descriptions are shown in figure 6.21(b), (c), and (d).

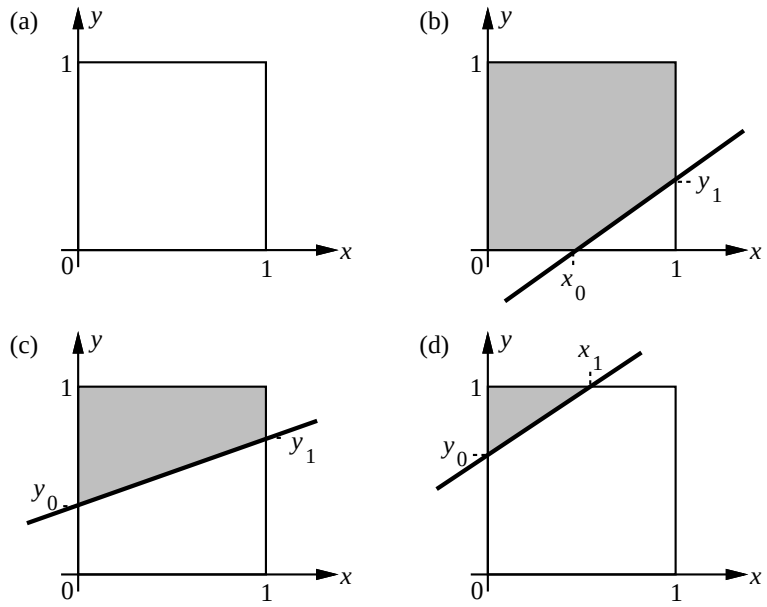

Figure 6.21: The coordinate system for a pixel and the three types of pixel. (a) Local coordinate system for the pixel. (b) Type I pixel, parameterised by x_0 and y_1. (c) Type II pixel, parameterised by y_0 and y_1. (d) Type III pixel, parameterised by y_0 and x_1.

Case	Third intercept calculation
I.II	$y_2 = y_1(1 + \frac{1}{1-x_0})$
I.III	$x_2 = 1 + \frac{1-y_1}{y_1}(1 - x_0)$
II.II	$y_2 = 2y_1 - y_0$
II.III	$x_2 = \frac{1-y_0}{y_1-y_0}$
III.I	$y_2 = y_0 + \frac{1-y_0}{x_1}$

Table 6.5: How the third intercept is calculated from the first two in all five possible cases.

The sample value, A, for each type of pixel can easily be determined using these simple formulae:

$$A_{\mathrm{I}} = \frac{1}{2}(1 - x_0)y_1 \tag{6.16}$$

$$A_{\mathrm{II}} = \frac{1}{2}(y_0 + y_1) \tag{6.17}$$

$$A_{\mathrm{III}} = 1 - \frac{1}{2}x_1(1 - y_0) \tag{6.18}$$

The information that can be gathered from two adjacent edge pixels

Given an edge pixel we will consider also the next edge pixel to the right, or, if this is not an edge pixel, then the next edge pixel above. This gives the five possible situations shown in figure 6.22. No other situations are possible given the restrictions we have placed on edge orientation. In each case the third intercept is given the subscript 2 in order to save confusion and unify the notation for all cases. This third intercept can be derived from the other two, because the first two uniquely define the lines. These derivations are shown in table 6.5.

Given the two pixel values, call the left one, A, and the right, B, it is possible to recover the values

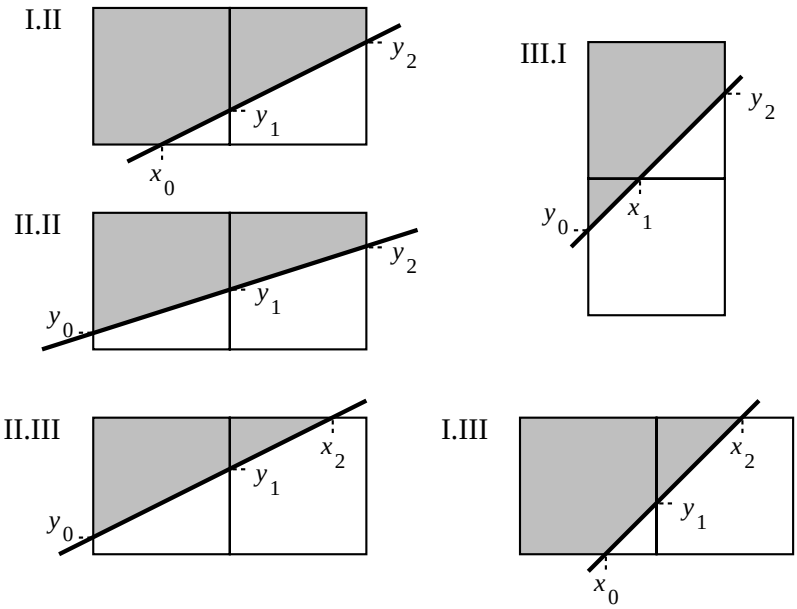

Figure 6.22: The five possible arrangements of two adjacent edge pixels for a line of slope between zero and one. Each is named by the types of the two pixels ordered from left to right, or bottom to top. The origin is always considered to be at the bottom left corner of the bottom left pixel.

of the first and second intercepts, thus uniquely determining the edge position and slope from the two pixels' values.

Case II.II

This is the simplest case. The pixel values are given by:

$$\begin{aligned} A &= \frac{1}{2}(y_0 + y_1) \\ B &= \frac{1}{2}(y_1 + y_2) \\ &= \frac{1}{2}(3y_1 - y_0) \end{aligned}$$

where the last step is produced by replacing y_2 with its equivalent equation in table 6.5.

Some fairly simple algebra leads to the results:

$$\begin{aligned} y_0 &= \frac{1}{2}(3A - B) \\ y_1 &= \frac{1}{2}(A + B) \end{aligned}$$

From these, and table 6.5, we can also find y_2:

$$y_2 = \frac{1}{2}(3B - A)$$

The other four cases are not as simple as this. Rather than show the working here we present only the start and end of the algebraic manipulation.

Case I.II

The equations for the pixel values are:

$$\begin{aligned} A &= \frac{1}{2}(1-x_0)y_1 \\ B &= \frac{1}{2}(y_1+y_2) \\ &= y_1 + \frac{y_1}{2(1-x_0)} \end{aligned}$$

which produce these equations for the intercepts:

$$\begin{aligned} y_1 &= -2A + 2\sqrt{A^2+AB} \\ x_0 &= 1 - \frac{2A}{-2A+2\sqrt{A^2+AB}} \end{aligned}$$

For the denominator to be zero in the latter equation requires $A = B = 0$, which means that the edge passes along the lower boundary, rather than intercepting it, so the value of x_0 is undefined. Such a situation should be considered as case II.II, not case I.II.

Case I.III

The equations for the pixel values are:

$$\begin{aligned} A &= \frac{1}{2}(1-x_0)y_1 \\ B &= 1 - \frac{1}{2}(x_2-1)(1-y_1) \\ &= 1 - \frac{1}{2}\frac{(1-y_1)^2}{y_1}(1-x_0) \end{aligned}$$

which produce these equations for the intercepts:

$$\begin{aligned} y_1 &= \frac{\sqrt{A}}{\sqrt{A}+\sqrt{1-B}} \\ x_0 &= 1 - 2A - 2\sqrt{A(1-B)} \end{aligned}$$

For the denominator to be zero in the equation for y_1 requires $A = 0$ and $B = 1$, which implies that the slope of the line is greater than one. Therefore this situation cannot arise.

Case II.III

The equation for the pixel values are:

$$\begin{aligned} A &= \frac{1}{2}(y_0+y_1) \\ B &= 1 - \frac{1}{2}(1-y_1)(x_2-1) \\ &= 1 - \frac{1}{2}(1-y_1)\left(\frac{1-y_0}{y_1-y_0} - 1\right) \end{aligned}$$

which produce these equations for the intercepts:

$$\begin{aligned} y_1 &= 1 + 2(1-B) - 2\sqrt{(1-B)^2 + (1-A)(1-B)} \\ y_0 &= 1 - 2(1-A) - 2(1-B) + 2\sqrt{(1-B)^2 + (1-A)(1-B)} \end{aligned}$$

III.I	I.III
y_0	$2 - x_2$
x_1	$1 - y_1$
y_2	$2 - x_0$
A	B
C	A

I.II	II.III
x_0	$2 - x_2$
y_1	$1 - y_1$
y_2	$1 - y_0$
A	$1 - B$
B	$1 - A$

II.II	II.II
y_0	$1 - y_2$
y_1	$1 - y_1$
y_2	$1 - y_0$
A	$1 - B$
B	$1 - A$

Table 6.6: The equivalences between the various cases. Note that II.II is equivalent to itself. Substituting the values in the right hand column in the place of those in the left hand column in the left hand case's equations will produce the right hand case's equations.

Case III.I

This is different from the other four cases in that it uses the pixel above pixel A, rather than to the right. We will identify this pixel's value as C. The pixel to the right has value $B = 1$. The equations for the pixel values are:

$$\begin{aligned} A &= 1 - \frac{1}{2}(1 - y_0)x_1 \\ C &= \frac{1}{2}(1 - x_1)(y_2 - 1) \\ &= \frac{1}{2}\frac{(1 - x_1)^2}{x_1}(1 - y_0) \end{aligned}$$

which produce these equations for the intercepts:

$$\begin{aligned} x_1 &= \frac{\sqrt{1 - A}}{\sqrt{1 - A} + \sqrt{C}} \\ y_0 &= 1 - 2(1 - A) - 2\sqrt{(1 - A)C} \end{aligned}$$

For the denominator to be zero in the equation for x_1 requires $A = 1$ and $C = 0$, which means that the edge passes along the boundary between the two pixels, rather than intercepting it, so the value of x_1 is undefined. Such a situation should be considered as case II.II, not case III.I.

Equivalences between cases

In figure 6.22 we can see that cases I.II and II.III are very similar. By a substitution of variables one case can be made equivalent to the other, thus linking the sets of equations for the two cases. The same is true of cases I.III and III.I. The equivalences are shown in table 6.6. Substituting the values in the right hand column in the place of those in the left hand column in the left hand case's equations will produce the right hand case's equations.

Identifying the case

Given the edge pixel, of value $0 < A < 1$, if the next pixel to the right is not an edge pixel (that is: $B = 1$) then we know that we have case III.I. The pixel, of value C, above pixel A is used in the calculation. If $C = 0$ and $B = 1$ then the edge passes through the top right corner of the pixel. Case III.I still calculates the intercepts correctly; they are:

$$\begin{aligned} x_1 &= 1 \\ y_0 &= 2A - 1 \end{aligned}$$

If $0 < B < 1$ then we could be dealing with any of the other four cases. Fortunately the values A and B uniquely identify which to apply.

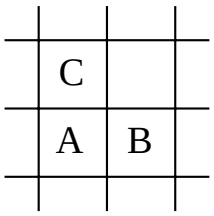

Figure 6.23: The arrangement of pixels A, B, and C.

I.II	I.III	II.II	II.III
$0 \leq x_0 \leq 1$	$0 \leq x_0 \leq 1$	$0 \leq y_0 \leq 1$	$0 \leq y_0 \leq 1$
$0 \leq y_1 \leq 1$	$0 \leq y_1 \leq 1$	$0 \leq y_1 \leq 1$	$0 \leq y_1 \leq 1$
$0 \leq y_2 \leq 1$	$1 \leq x_2 \leq 2$	$0 \leq y_2 \leq 1$	$1 \leq x_2 \leq 2$

Table 6.7: The restrictions on the values of the parameters in the four cases which use pixels A and B.

Possible values of A and B are restricted to lie in the square:

$$0 \leq A \leq 1$$

$$0 \leq B \leq 1$$

Further restrictions are produced by making the slope of the edge lie between zero and one: a minimum slope of zero means that

$$A \leq B$$

A maximum slope of one affects only case, I.III, where it implies that $x_2 - x_1 \geq 1$ (in the other three cases the slope can never exceed one). Working through the algebra of this gives us the restriction:

$$B \leq \frac{1}{2} - A + \sqrt{2A},\ 0 \leq A \leq \frac{1}{2}$$

These four restrictions define the boundary in figure 6.24 within which A and B must lie. The other lines in figure 6.24 are set by restricting the values of the intercepts in each case to lie within the boundaries listed in table 6.7. These lines bound the areas with which each case deals.

Some involved algebraic manipulation or a dense sampling of A, B pairs will determine which areas within the boundary are dealt with by each case. Figure 6.25 shows these areas. They do not overlap and completely fill the area within the boundary. The boundaries between the various areas are where the edge passes through the corner of one of the pixels. These are illustrated in figure 6.26, along with the situations that occur at the boundaries of the whole area.

These results are all well and good for edges with a slope between zero and one, allowing us to exactly reconstruct the line from two adjacent sample values. It leaves the question of how to identify the orientation of a general edge so that it can be transformed to this case and its intercepts determined.

Identifying the orientation

Given two edge pixels A and B, arranged as shown in figure 6.23, the orientation of the edge can be determined to one of two octants. This is shown in figures 6.27 and 6.28. A similar diagram can be drawn for edge pixels A and C arranged as in figure 6.23. Examples are given in figure 6.29. To determine which of these two choices is correct we require more information than supplied by the two pixel values.

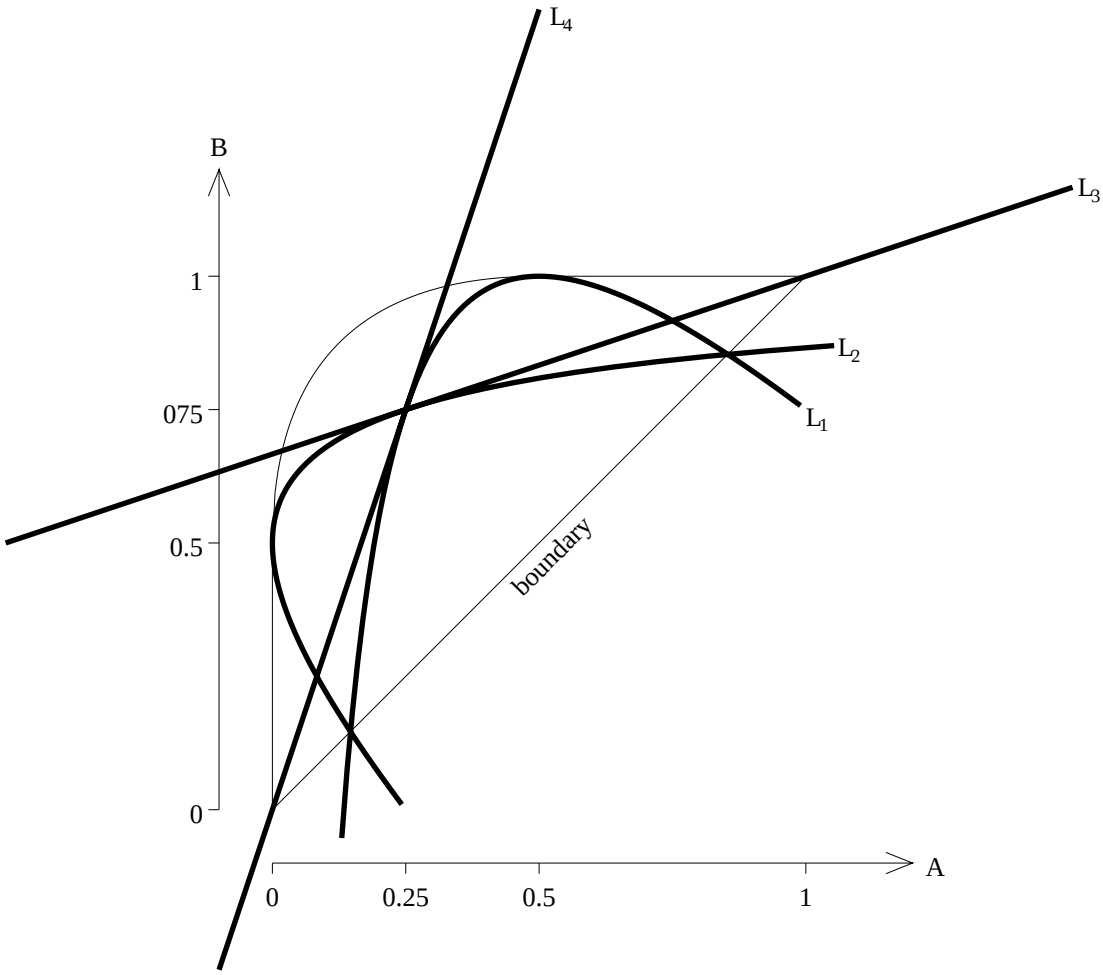

Figure 6.24: The restrictions on A and B values for the various cases, this figure shows the bounding lines of the areas covered by each case. The light line shows the boundary within which A, B pairs must lie, the equations defining this boundary are given in the text. The other four lines are generated by imposing the restrictions in table 6.7. They are:

L_1: $B = 2 - A - \frac{1}{4A}$
L_2: $A = \frac{(B-\frac{1}{2})^2}{1-B}$
L_3: $B = 1 - \frac{1}{3}(1 - A)$
L_4: $B = 3A$

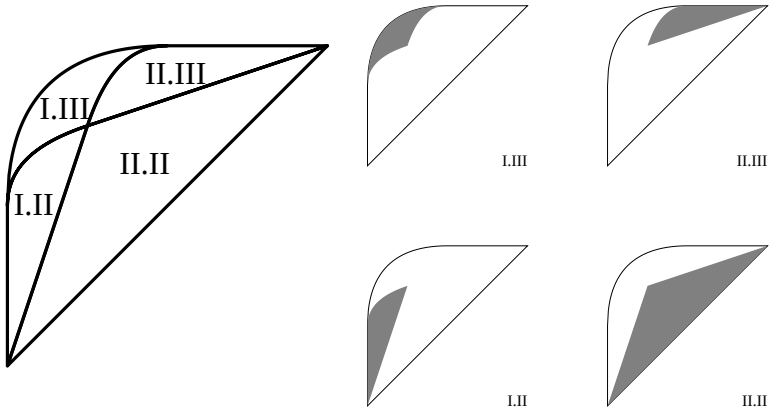

Figure 6.25: The four disjoint areas covered by the four cases.

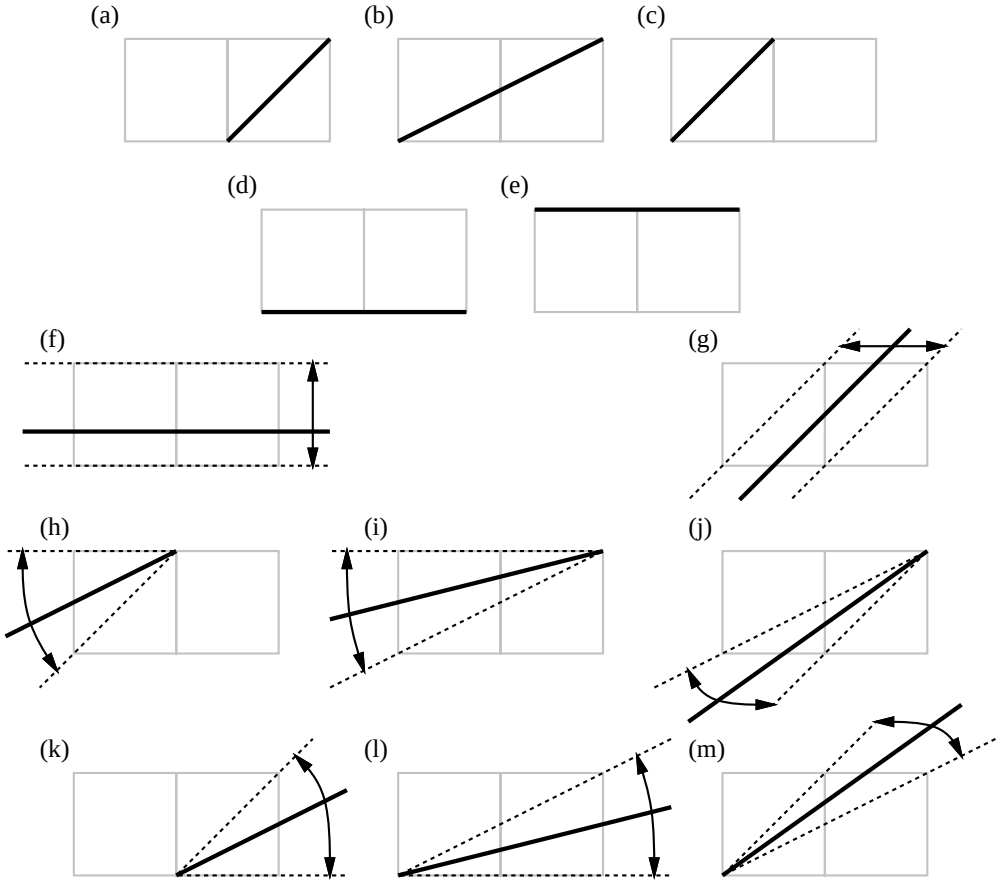

Figure 6.26: The special cases, on boundaries in figure 6.25. They are defined by their locations in (A, B) space. (a) $(0, \frac{1}{2})$, the point on the left boundary where I.II meets I.III; (b) $(\frac{1}{4}, \frac{3}{4})$, the point in the middle where all four regions meet; (c) $(\frac{1}{2}, 1)$, the point on the top boundary where I.III and II.III meet; (d) $(0, 0)$, the bottom left corner; (e) $(1, 1)$, the top right corner; (f) moving along the boundary line $A = B$ from $(0, 0)$ to $(1, 1)$; (g) moving around the boundary from $(0, \frac{1}{2})$ to $(\frac{1}{2}, 1)$; (h) moving along the top boundary from $(\frac{1}{2}, 1)$ to $(1, 1)$; (i) moving along L_3 from $(\frac{1}{4}, \frac{3}{4})$ to $(1, 1)$; (j) moving along L_2 from $(0, \frac{1}{2})$ to $(\frac{1}{4}, \frac{3}{4})$; (k) moving up the left boundary from $(0, 0)$ to $(0, \frac{1}{2})$; (l) moving along L_4 from $(0, 0)$ to $(\frac{1}{4}, \frac{3}{4})$; (m) moving along L_1 from $(\frac{1}{4}, \frac{3}{4})$ to $(\frac{1}{2}, 1)$.

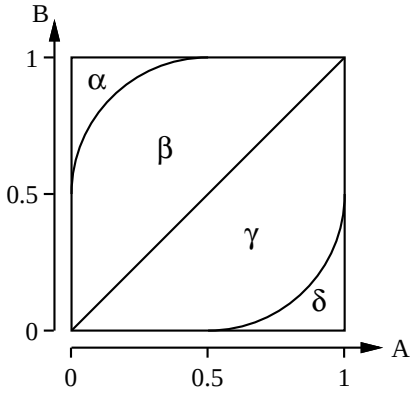

Figure 6.27: These are four areas of A, B space: corresponding to four pairs of octants. We have been considering area β. An edge in any area can be identified to be in either of two possible locations, shown in figure 6.28.

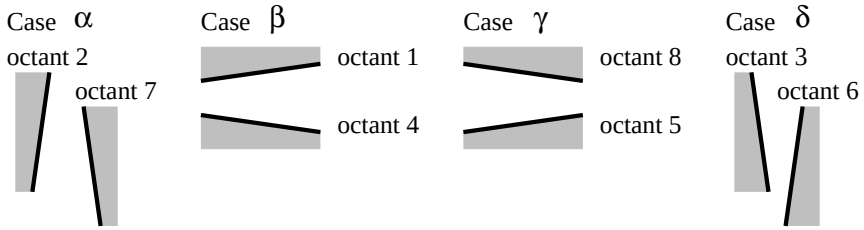

Figure 6.28: The four areas in figure 6.27 can identify an edge to be one of just two possibilities. In each case these two edges lie in two different quadrants. Examples are shown here for each case.

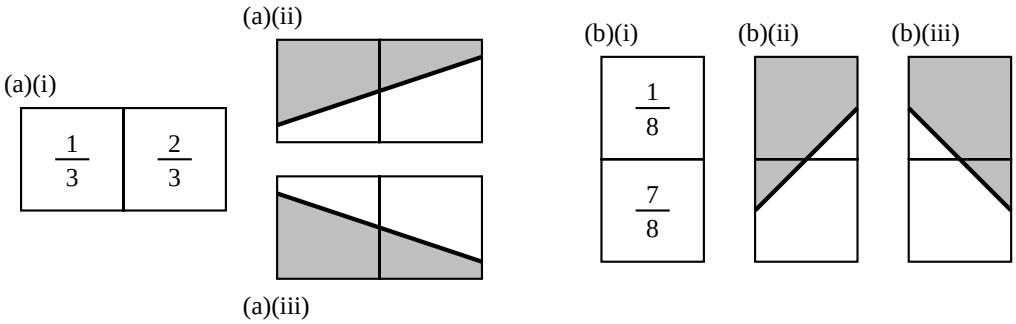

Figure 6.29: Two examples of the two possibilities for a given pair of adjacent grey pixel values. (a)(i) can represent either (a)(ii) or (a)(iii), (b)(i) can represent either (b)(ii) or (b)(iii).

κ	C	λ
	A	B
μ		ν

Figure 6.30: The 3×3 context of the edge pixel A, with the pixel labels used in the text.

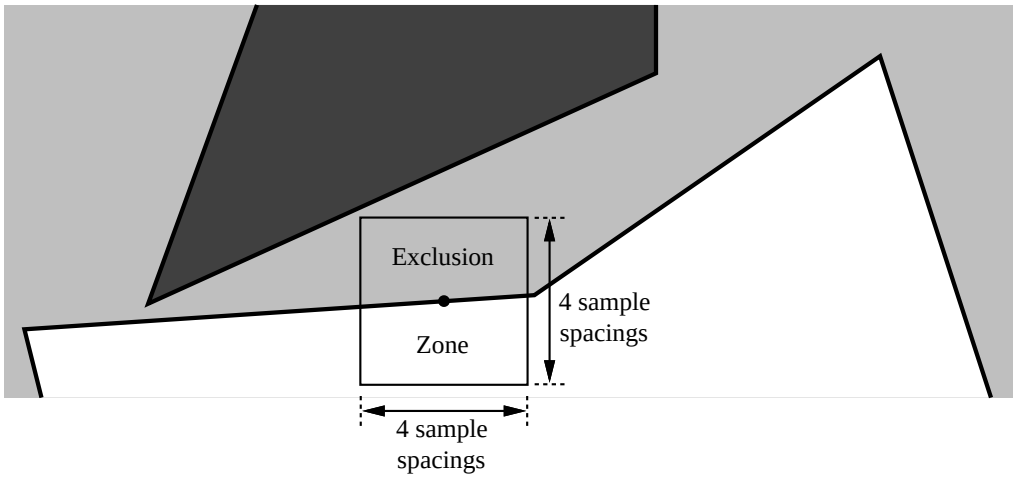

Figure 6.31: To ensure that every edge generates at least one edge pixel at the centre of a 3×3 context through which no other edge passes, there must be at least one edge point on every edge such that no other edge passes through a 4×4 sample spacing 'exclusion zone' cantered on that edge point.

If we pick a single edge pixel and use the 3×3 pixel region around it we can be certain to get the orientation right. The 3×3 region is illustrated in figure 6.30. If the 3×3 region is rotated and reflected so that $\kappa \leq \lambda \leq \mu \leq \nu$ then we can be certain that the edge is in the first octant. We can then apply our equations to A and B (or A and C, if $B = 1$) and then transform the results back to the correct octant. Note that, after rotation and reflection, $\kappa = 0$ and $\nu = 1$.

6.4.3 Extension to grey scale — single edge

A single edge, where the intensity on either side may have any value, can be exactly reconstructed as easily as a black and white edge. Taking a 3×3 area, as in figure 6.30. Again rotate and reflect it so that $\kappa \leq \lambda \leq \mu \leq \nu$. Then, if $A \neq \kappa$ and $A \neq \nu$, A is an edge pixel. All values in the 3×3 square can be modified so that $\kappa = 0$ and $\nu = 1$. Taking o to be the old pixel value and m, the modified pixel value, the modification is simply

$$m = \frac{o - \kappa}{\nu - \kappa}$$

for each pixel value. The edge can now be found in the same way as for the black and white case.

6.4.4 Extension to many edges

Many edges in an intensity surface means that it consists of areas of constant intensity separated by sharp edges. Provided every edge generates at least one edge pixel at the centre of a 3×3 block of pixels through which no other edges run, then the method of the previous section can be used to find the slope and position of all the edges in the image.

To ensure that every edge generates at least one block of pixels of this type there must be at least one position along the edge such that no other line passes inside a square of side four sample spacings centred at that point. An example is given in figure 6.31. A 4×4 region is required because we do not necessarily know where the pixel edges are going to fall, but we can be sure that there will be a 3×3 pixel block inside this 4×4 exclusion zone, and that the central pixel of this block will contain this edge point, thus this central pixel will be an edge pixel.

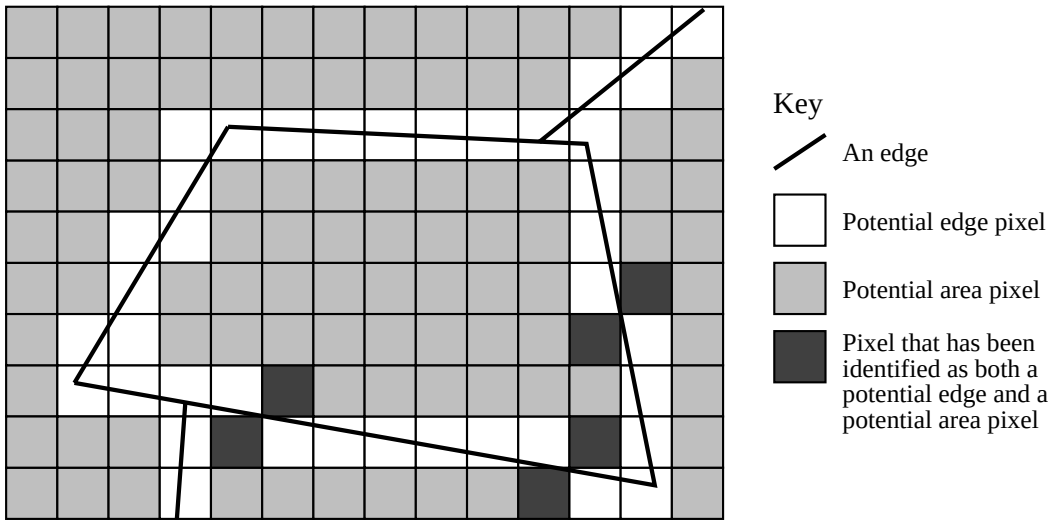

Figure 6.32: The algorithm discussed in the text would classify the pixels as shown for this combination of edges.

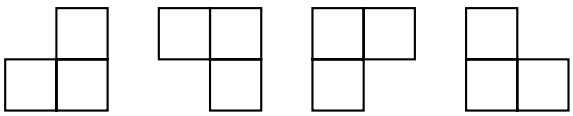

Figure 6.33: No edge can generate three edge pixels of the same intensity in any of these L-shaped arrangements.

How edge pixels are found

This restriction on the original intensity surface ensures that there will be at least one 3×3 pixel block for every edge through which no other edge passes. This allows us to calculate the slope and position of the edge. The problem is now to separate those 3×3 blocks which contain a single edge from those which contain no edges or which contain two or more edges.

One solution to this problem is to first find all of the four-connected areas of constant intensity and mark all of the eight-connected neighbours of this area as potential edge pixels. An example is shown in figure 6.32. The second step is to apply our equations to the 3×3 region around each potential edge pixel (and any pixels which were not identified as either potential edge pixels or area pixels). The edge information is only retained for those regions for which it is consistent with the pixel values. This gives us the position and slope of all edges in the image.

These two steps need some fleshing out. The first step, area-finding, is achieved by a single observation and a modification of a well-known algorithm. The observation is that no single edge can generate three edge-pixels *of the same intensity* in an L-shaped arrangement (those illustrated in figure 6.33). Such an arrangement of three pixels can thus be assumed to be part of an area or caused by a combination of several edges. In the first case none of the three pixels is an edge pixel, in the latter, none is at the centre of a 3×3 block containing only a single edge. Thus no pixel identified by this method need be passed to the second step.

A pixel from an L-shaped block of three of the same intensity can be used as the seed to a flood-fill algorithm [Foley *et al*, pp.979–982]. Every pixel in the filled area is identified as a possible area pixel and every pixel not in, but eight-connected to, the area is identified as a possible edge pixel. This process is repeated until all identifiable areas have been flood-filled. If an L-shaped block is generated by multiple edges the whole algorithm should still work, because neither these pixels, nor any pixel of the same intensity four-connected to them, will uniquely identify a single edge.

Note that some pixels may be identified as both possible edge pixels and possible area pixels (for example: when an edge falls on a pixel boundary), this is not a problem and, for the next stage, these pixels should be treated as possible edge pixels.

In the second step every possible edge pixel is processed individually. All pixels that have not been identified as possible edge or possible area pixels must also be processed. Such pixels may arise in a small single pixel wide area with no L-shaped group of pixels in it.

An attempt is made to rotate and reflect the 3×3 region centred on each pixel so that $\kappa \leq \lambda \leq \mu \leq \nu$ in figure 6.30. If this is impossible then we can be certain that more than one edge pixel passes through this region, otherwise we apply our equations to generate a slope and direction for an edge, along with the intensity on either side of the edge. These four values can then be used to generate pixel values for all nine pixels in the region. If these match the true pixel values then there is only one edge in the region and we can output the edge parameters and the grey values either side of the edge, otherwise we ignore these values. This will generate the parameters for all of the edges in the image (duplicate sets of parameters can be discarded).

This process gives us the slope and positions of all the edges in the image, because every edge has at least one pixel in a 3×3 area which will uniquely identify it. As a byproduct the process gives us the intensities of the areas either side of each edge. What it does not give us are the end points of the edges. However, for a scene to be consistent all areas must be of constant intensity and bound by straight edges. Hence it should be possible for an algorithm to be devised which generates the end points of all the edges given the image, the slopes and positions of all the edges, and the grey values either side of each edge; all of which can be derived from the above methods and equations. Such an algorithm has not been developed, it is left for future work. Some idea of how if could operate is given below:

> Every edge's edge pixels are rendered assuming that it is the only edge in the image. The values produced are compared with the values in the image and all correct values noted as being pixels through which this edge is likely to be the only edge. The pixels at either end of a run of such edge pixels are likely to contain two or more edges. Such end pixels can be rendered using all suitable edges in the description. If the correct value is generated it is likely that the edges used pass through the pixel. Intersections between edges must be found to render these pixel values and these intersections are likely to be the ends of lines. When three or more edges pass through a pixel all combinations of intersections may need to be tried to find the correct one.

Without designing such an algorithm it is impossible to say whether or not any extra restrictions must be placed on the input intensity surface to allow for exact reconstruction.

6.4.5 Discussion

Whether or not extra restrictions are required, this work shows that there exists a class of two-dimensional intensity surface which can be exactly reconstructed from their exact-area sampled images. Apart from the trivial, constant intensity surface, no member of this class can be exactly reconstructed from its single point sampled image using classical sampling theory.

Such an exact reconstruction would be extremely useful in resampling as it allows the resampling to produce the best possible resulting image. However, the class of intensity surfaces that can be exactly reconstructed by this method is extremely limited.

Real images

Several types of real image could potentially be exactly reconstructed by these methods. For example: printed matter (text and diagrams) and especially cartographic documents (maps) may

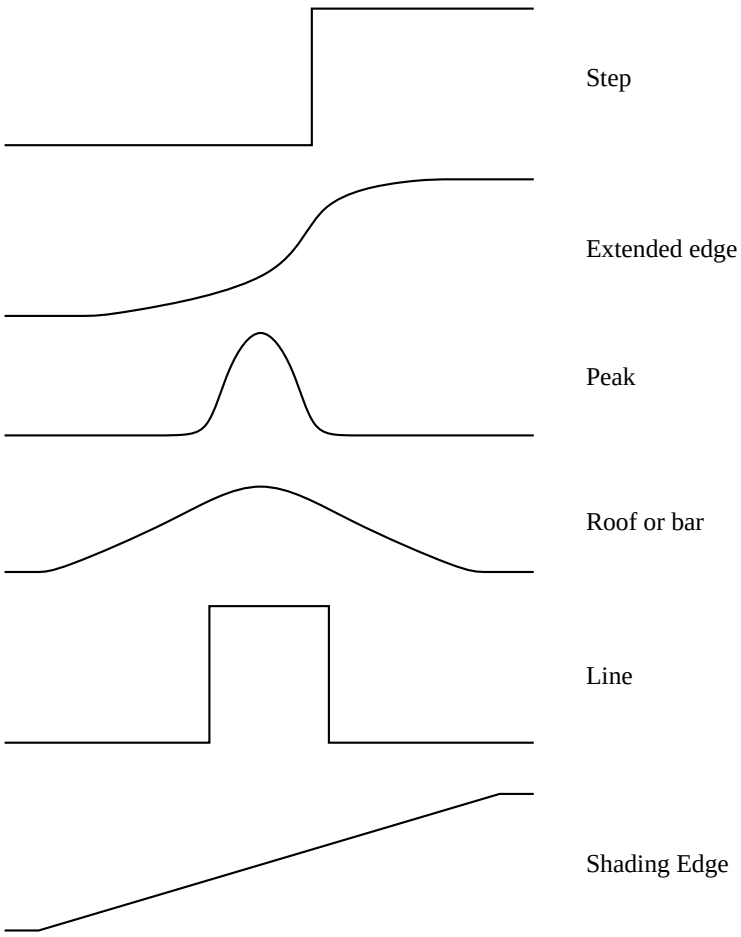

Figure 6.34: Several different types of edge which occur in real images. Only the step and line edges are adequately modelled in our exact reconstruction process (after Marr [1976] and Horn [1977]).

meet the requirement for areas of constant intensity separated by sharp edges. The ability to scan a map into a computer and get an exact digital representation would be extremely useful. Unfortunately, the nature of the maps (for example line widths of 0.1mm or finer are common-place [Woodsford, 1988]) means that an extremely high-resolution scan would be required to produce an image which met our criteria for exact reconstruction. There is the additional problem that the task does not just involve finding edges, but requires significant intelligence in recognising what each area of colour and each edge represents (information on the problems involved in digitising maps may be found in Waters [1984, 1985], Woodsford [1988], Laser-Scan [1989] and Waters, Meader and Reinecke [1989]).

Real images of real scenes, as opposed to real images of two dimensional 'flat' scenes (books, paper, maps) pose difficulties. A major problem is that the things we humans perceive as edges may bear little resemblance to the sharp discontinuity used to model an edge in this work. Horn [1977] discusses edges in real scenes and explains how different edges in real scenes produce different intensity profiles. He and Marr [1976] classify the different types of edge, some of which are shown in figure 6.34. Only two of these types match our model of an edge as a discontinuity.

Despite these problems with applying our work to real images, the process developed here produces interesting theoretical results in that a class of intensity surfaces which cannot be exactly reconstructed by classical sampling theory can be exactly reconstructed by these methods and equations.

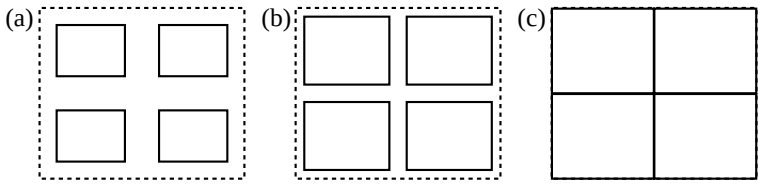

Figure 6.35: Layout of CCD sensors. The solid lines show the receptive area of each pixel's sensor. (a) common CCD sensor, (b) advanced CCD sensor, (c) ideal CCD sensor. (After Kuhnert [1989] fig 3.)

Errors

As in the one-dimensional case, the introduction of errors causes problems. Again, quantisation error introduces an inaccuracy into the calculated edge parameters, while other errors require parameter calculations based on probabilities rather than being deterministic as they have been in the above discussion.

The advantage here over the one-dimensional case is that every line has many edge pixels and each pair of these can be used to estimate the slope and position of the line (note that not only adjacent pairs of edge pixels can be used, but *any* two edge pixels provided we know their types (I, II, or III) and their relative position). Also the position of all the edge pixels in the pixel grid gives bounds on the slope and position of the line, because the line has to pass through all of its edge pixels. Therefore we can expect to be able to generate a fairly accurate approximation from a noisy image provided that none of the edges are very short.

Other published work

Klassman [1975] considered the case of thick lines. These can be considered as two parallel edges between which lies a black region and outside which lie two white regions. Klassman's results indicated that, even with no errors in the pixel values, there will always be an error in the estimated position of the line no matter how thick it is. Our process, on the other hand, would be able to exactly find the position the line provided its width is such that the 4×4 exclusion zone constraint is satisfied for some point on each edge.

Kuhnert [1989] considers rectangular pixels as used in a CCD device, he gives three types of CCD cell, shown in figure 6.35. We have been using an ideal CCD-sensor layout (figure 6.35(c)). Kuhnert uses the advanced layout (figure 6.35(b)). He considers an edge between two areas of constant intensity but concludes that his model of the sensor does not permit a unique conclusion on the position and slope of the edge. He says that this is unsurprising given that the original intensity surface violates the sampling theorem. However, we have seen here that exact reconstruction of such an intensity surface is possible, given exact-area sampling.

Hyde and Davis [1983] consider a similar situation to ours: a single edge, of finite length, between two areas of constant intensity. They use two least-squares edge estimation techniques, assuming some noise in the image. The first step, which they assume is done for them, is to identify the edge pixels. Then, one technique gives the least-squares edge fitted to the centres of the edge pixels, that is: no intensity information is utilised. This is similar to the black and white case discussed in section 6.4.1. The second technique gives a least-squares fit based on the intensity values of the edge pixels. The sum of the squares of the difference between the true intensity values and the estimated intensity values, is minimised.

Their conclusion is that the differences between the two techniques are not significant enough to warrant the use of the second, more costly technique. That is: taking the intensity values into consideration gives little advantage over simply using the position of all the edge pixels to calculate the edge's parameters. Compare this with our method which gives the exact position of an edge,

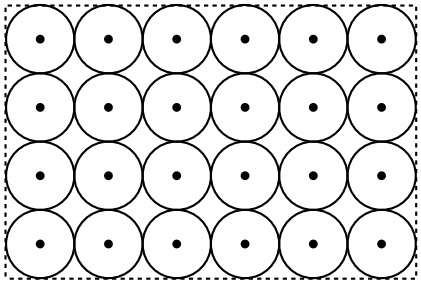

Figure 6.36: Kiryati and Bruckstein [1991] use exact-area sampling over abutting circular areas. The dots are the pixel centres, the circles are the pixel areas. (After Kiryati and Bruckstein [1991] fig 1.)

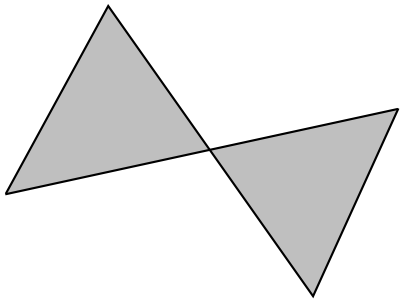

Figure 6.37: A case which violates the restrictions of Kiryati and Bruckstein's [1991] exact reconstructor.

using grey-level information. However, it must be said that our method does not take noise into account whilst Hyde and Davis assume a noisy image.

Kitchen and Malin [1989] consider a single, infinitely long, straight edge between areas of intensity zero and one, which has been exact-area sampled. This study the behaviour of several common edge operators on this step edge. Their results show that none of these operators gives a particularly good approximation to the correct orientation or position of the edge. The principle conclusion is that, even under ideal conditions, the common edge operators are not very accurate.

The most recent piece of research is that of Kiryati and Bruckstein [1991]. They consider a similar situation to ours, except that they use exact-area sampling in *abutting* circular pixels, as shown in figure 6.36. Their work is detailed and they show that, given an intensity surface which obeys certain restrictions, an exact reconstruction can be made from its circular exact-area sampled image. This again shows that classical sampling theory is not the final arbiter of which intensity surfaces can be exactly reconstructed from their images and which cannot. One interesting point is that Kiryati and Bruckstein's restrictions exclude intensity surfaces like that shown in figure 6.37. Provided the six edges in this intensity surface are long enough that each has a point surrounded by a 4×4 zone excluding all the other edges, there seems no reason why the algorithms outlined in this chapter could not exactly reconstruct this image.

6.4.6 Extensions

Three possible extensions to the described reconstructor are:

1. To make it more useful this algorithm could be altered to recognise sharp edges between areas of slowly varying intensity. Then exact reconstruction could be used at the edges and some local reconstructor in the slowly varying parts. Cumani, Grattoni and Guiducci [1991] have tried a similar idea for image coding: exactly storing the image near sharp edges and

storing very little information in the slowly varying areas between regions. Such an idea could be tried with resampling where the intensity surface in the slowly varying regions is reconstructed differently to that near the edges.

2. A straight edge can be represented by two parameters. A circle by three. An extension could be made to find a circle's parameters from three pixel values on the circle's edge. Preliminary results show that the algebra involved in these computations is considerably more involved than that for straight edges.

3. Two problems with images that have been enlarged using good NAPK reconstructors are: (1) the straight edges become blurry; and (2) textured areas do not reveal any finer texture (for example, enlarging a tree produces a blurry tree, you do not see more of the tree's structure). Kajiya and Kay [1989] call this effect 'the painter's illusion'. The image gives the impression that more detail is there at the sub-pixel level than is actually present. When the image is enlarged this lack of fine detail becomes readily apparent. The work in this section has attempted to solve the first of the two problems. An extension would be to tackle the second: how to reconstruct, or resample, a textured region so that the resampled image is visually acceptable.

6.5 Summary

We have seen that, given knowledge about how an image was sampled, a better reconstructed intensity surface can be generated. The bulk of this chapter dealt with sharp edge reconstruction. We have proven that, for a certain set of one-dimensional intensity curves, exact reconstruction is possible from the exact area sampled image of an intensity curve in the set. We have also given strong evidence that a similar result holds in two dimensions.

The significance of this result is two-fold. Firstly, it shows that classical sampling theory is not the final word on which intensity surfaces can be exactly reconstructed from images. Secondly, it indicates that a good reconstruction of this particular class of *real* intensity surface may be possible.

Chapter 7

Transforms & Resamplers

In this chapter we draw together the threads of reconstruction, sampling, and transformation. We discuss the overall resampler, the measurement of quality, and some points about transforms in general.

The transform is at the heart of the resampling. The other two sub-processes can be considered as simply format converters (chapter 1) allowing the transform to be performed in the continuous domain, where it is simple, rather than in the discrete domain, where it is complicated. In general the transform moves intensity information around but neither loses nor adds any information. Reconstruction and sampling, on the other hand, tend to be lossy operations.

Thus, it is the choice of reconstructor and sampler which determines the quality of the overall resampler. These should therefore be the best possible, regardless of the transform. For certain classes of images there are perfect reconstruction and sampling processes, but, for the average image, such perfect processes do not exist. So we must content ourselves with the best imperfect resampler that we can implement.

Before we continue we need to note that, in chapter 1, a resampler consisted of a specific reconstructor, transform, and sampler. Often however, we will wish to discuss the same reconstructor and sampler coupled with many different transforms, or some class of transforms. In these cases we still speak of a resampler but it is one in which the transform can be any of a set of transforms or sometimes any transform at all, whilst the reconstructor and sampler remain fixed.

7.1 Practical resamplers

In general the better the reconstructor or sampler, the more difficult it is to implement and so we need to trade off between a good reconstructor or sampler and an easily implemented one. We need to make as many simplifications as possible, with the least effect on quality in order to produce a quick, practical, and good resampler.

For certain transforms it transpires that changing the reconstructor or changing the sampler makes little difference on the overall result of the resampling, while changing the other can make a great difference. Heckbert [1989, pp.51–52] shows that, for large magnifications, the reconstruction method dominates the resampler and the sampler is irrelevant, so it may as well be a single point sampler for simplicity. He also shows that for large minification the sampling method dominates, and the reconstructor is irrelevant. In this case we can use a simple reconstructor with much the same effect as a complex one.

For a resampler which may have to cope with both large magnifications and large minifications, we require either a good reconstructor and a good sampler, or some sort of combination where a

switch is made from a good magnification resampler to a good minification resampler as the scale factor passes through one [Heckbert, 1989, p.52].

Near a scale factor of one, the evidence indicates that changing the sampler makes little or no difference to the quality of the resampled image[1], and that there is little to choose between the quality offered by the better reconstructors. With a magnification factor near one, reconstruction by nearest-neighbour produces noticeable artifacts and reconstruction by linear interpolation often gives a blurry result, but other methods produce few, if any artifacts (see section 7.3.2 which discusses the effect of reconstructors at large scale factors compared with their effect at a scale factor of one). Therefore, good samplers are required for minification, and good reconstructors required for same-scale operations and magnification.

7.1.1 Restricted resamplers

While theoretical resamplers can be applied to any transform, a practical resampling method may only be applicable to a limited set of transforms. A resampler employing point sampling can be used with any invertible transform provided that the reconstructor can give the value of the original intensity surface at an arbitrary point. An invertible transform here is one for which any output point can be mapped, by the computer program, to a point in the input intensity surface. Many transforms are covered by this restriction. Those which are not can be closely approximated by transforms which are.

Practical resamplers which employ area sampling tend to be more restricted in the types of transforms they can be used with. This restriction is due to their implementation, discussed in section 1.8.2. Greene and Heckbert [1986], for example, consider a resampler composed of a Gaussian reconstructor and a Gaussian area sampler. This resampler only works with affine transforms. However, a local affine approximation to the true transform can be used, allowing the reconstructor to approximate the correct results for a wide range of transforms. Other area sampling resamplers give a transform-dependent approximation to a transform-independent sampler. Such resamplers include those developed by Crow [1984], Glassner [1986], and Fournier and Fiume [1988]. Their starting point in algorithm development is a transform-independent area sampler. The final algorithm has a transform-dependent area sampler in order to be practical.

Williams [1983] has an interesting approach to approximating a nearest-neighbour reconstruction/exact area sampling resampler. If we look at his entry in appendix A, we see that his method is equivalent to point sampling off a three-dimensional reconstructed volume. The first two dimensions are the usual spatial coordinates whilst the third dimension, d, is related to the size of the output pixel projected back onto original image space. The volume is created by first minifying the image several times (by a nearest-neighbour reconstruction/exact area sampling resampler) to generate an image pyramid. Each image in the pyramid is then reconstructed by linear interpolation and the whole volume filled in by linear interpolation between the intensity planes in the pyramid (figure 7.1).

7.1.2 Resampler equivalences

The implementation of an area sampler, described in section 1.8.2, is possible because of the equivalence of two different decompositions. In general, any resampler can be decomposed in many different ways; the transform remaining the same but the reconstructor and sampler being different. As an example, consider a resampler consisting of nearest-neighbour reconstruction, a

[1]The evidence, indicating this result for samplers, is in the papers which discuss resampling for geometric correction of images. Such correction does not require large scale changes and none of these papers discuss any form of sampling other than single point. Our own observations indicate that an exact area sampler makes no appreciable difference in near-same scale transforms, compared with single point sampling, unless a nearest-neighbour reconstructor is used.

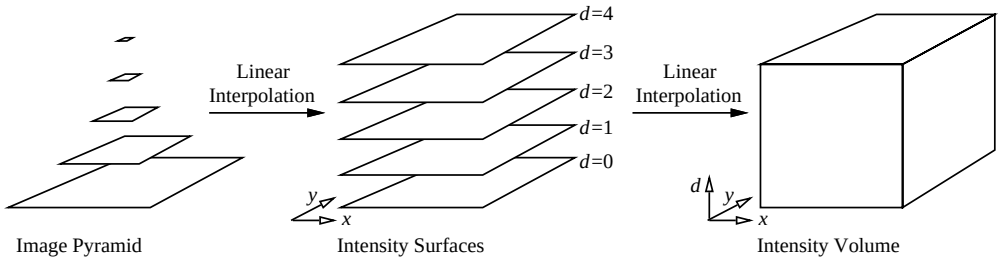

Figure 7.1: Williams' [1983] reconstructor. An image pyramid is formed by nearest-neighbour/exact area scaling by a factor of two, several times. Each level of the pyramid is then enlarged by linear interpolation, and then the third dimension is filled in by linear interpolation between the resulting intensity surfaces.

	Reconstruction Filter	Transform	Sampling Filter
(a)		translation	
(b)		translation	
(c)		translation	

Figure 7.2: Three equivalent decompositions of the same reconstructor: (a) nearest-neighbour/exact area, (b) linear/single point, and (c) delta-function/triangle filter.

translation, and exact area sampling. This same resampler can be decomposed into linear interpolation and single point sampling; or into Dirac delta function reconstruction and triangle filtered area sampling. These three decompositions are illustrated in figure 7.2, for one dimensional signals. If we now change the transform, these three decompositions are no longer equivalent. For example: take a resampler with nearest-neighbour reconstruction, scaling transform, and exact area sampling. Its equivalent decomposition with point sampling is shown in figure 7.3. The reconstructor depends on the scale of the transform. This equivalence can lead to confusion. Durand and Faguy [1990] for example, mistakenly equate scaling using nearest-neighbour reconstruction and exact area sampling with scaling using linear intepolation and single point sampling, when this equivalence is only correct for a scale factor of one.

For a general transform using transform-independent reconstruction and area sampling, the equivalent decomposition with single point sampling will have a reconstructor that is transform-dependent. We hypothesise that, given a transform-independent reconstructor, an arbitrary transform, and a transform-independent sampler, any equivalent resampler will have a transform-dependent reconstructor and/or a transform-dependent sampler. This hypothesis shows why area sampling resamplers are so much more difficult to implement than point sampling ones. It is because, in the method of section 1.8.2, the area sampler has to be converted to a point sampler to be implementable, and so the reconstructor in the equivalent point sampling resampler is transform-dependent, and hence difficult to implement.

7.2 Transform dimensionality

Resampling has been applied to one-, two-, and three-dimensional images. One use of resampling is in texture mapping where a two-dimensional image is mapped onto a three-dimensional surface which is then projected onto a two-dimensional plane, giving an overall 2D to 2D transform. Image warping and rectification are also generally 2D to 2D transforms.

For any dimensionality the theory is much the same. However, resamplings where a many di-

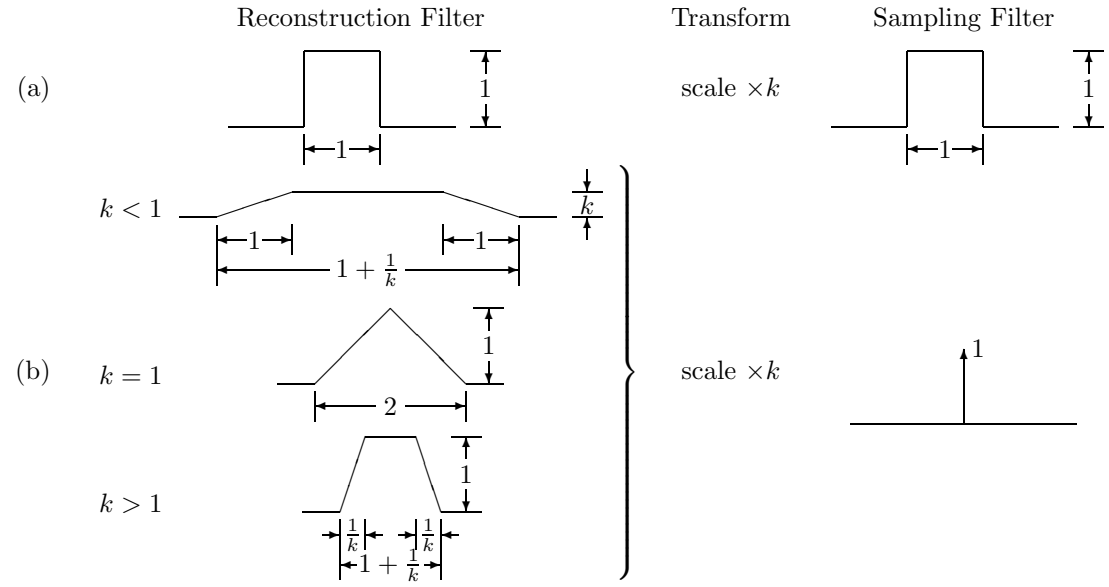

Figure 7.3: Two equivalent decompositions of the same reconstructor: (a) nearest-neighbour/exact area, (b) a transform-dependent reconstructor combined with point sampling. A third decomposition could be generated with delta-function reconstruction and a transform-dependent sampler.

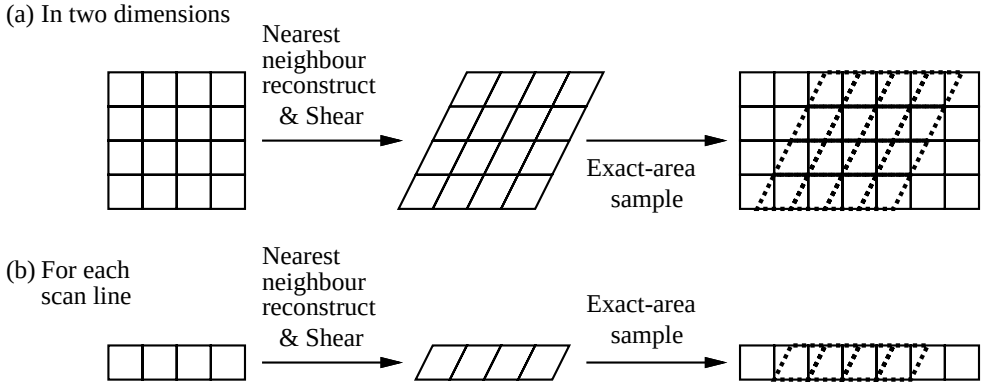

Figure 7.4: A shear transform, with nearest-neighbour reconstruction and exact area sampling. (a) The 2D resampling; (b) the $1\frac{1}{2}$D resampling process for a single scanline.

mensional transform is split into two or more one-dimensional passes are a special case (see section 1.7.5). There are two types of one-dimensional resampling used in such multipass algorithms on two-dimensional images. We have choosen to call these 1D resampling and $1\frac{1}{2}$D resampling.

In 1D resampling each scan-line is treated as a one-dimensional resampling problem. That is: the scan-line has length but not breadth [Euclid, 300BC]. It is thus easy to use the one-dimensional theory to develop resamplers for this case. In $1\frac{1}{2}$D resampling each scan-line is considered to be one pixel wide, and the transform applied to it does not necessarily have to be the same across the entire width of the line, it is thus a restricted two-dimensional resampling. An example of $1\frac{1}{2}$D resampling is given by Paeth [1990], where he implements rotation as three shears. Each shear is implemented as a one-dimensional resampling on each row or column of the image (figure 7.4). Paeth takes this exact $1\frac{1}{2}$D resampling and approximates it by a 1D nearest-neighbour reconstruction/exact area sampling resampler.

This idea can be extended to, for example, three dimensions. With one-dimensional resampling, in 3D, we can either have a breadth-less 1D resampling, or a volume with cross-section of size a

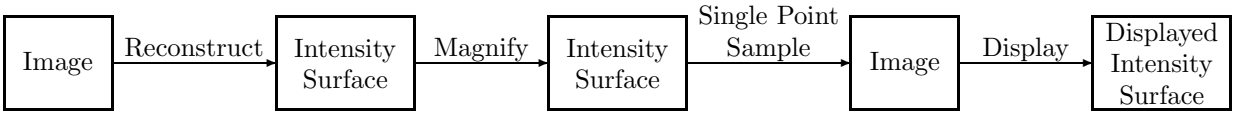

Figure 7.5: The reconstruction process we want to evaluate is on the left, we would like to view the intensity surface that it produces. The other three processes are needed for us to be able to view an approximation to the reconstructed intensity surface on a physical display device.

pixel width by a pixel width. This could be called $1\frac{2}{3}$D resampling.

7.3 Evaluation of reconstructors and resamplers

In chapter 3 we said that reconstructors are evaluated either on their visual results or on their mathematical properties. But how do we visually evaluate a reconstructor? It produces an intensity surface which cannot be represented inside the computer and cannot be displayed directly unless a piece of hardware is built which takes the discrete image as input and produces the reconstructed intensity surface in a form that can be viewed directly by the eye. In general, such a piece of hardware would be impossible, or at best, expensive and difficult to build.

The usual way to visually assess reconstructors is to resample an image using the appropriate reconstructor, a magnification, and single point sampling, and then display this much larger image on an ordinary CRT [Andrews and Patterson, 1976; Schreiber and Troxel, 1985; Mitchell and Netravali, 1988; Wolberg, 1990; Boult and Wolberg, 1992]. The process involved is shown in figure 7.5. The intensity surface we are evaluating is therefore not the intensity surface which we view, but is separated from it by a sampling and another (probably dissimilar) reconstruction.

How valid are the results of this type of evaluation? We can conclude that they are adequate if the effects of the sampling and the display reconstruction are small compared to the effects of the reconstructor we are studying. Such a situation will arise under a significant magnification of the intensity surface and when the displayed intensity surface is viewed from sufficient distance that the display's reconstruction effects are not noticeable (see the discussion in section 7.3.1 on the effect of viewing distance on the perceived intensity surface).

The former point about significant magnification is justified because of two results of insufficient magnification. The first is that, under low magnification, the sampling significantly affects the result. For small magnification the combination of a reconstructor and sampler can produce very different results to those expected from considering the reconstructor alone. This happens because the combination of reconstructor and sampler generate a discrete reconstructor with different properties to the continuous one. The solution is to either magnify by a large factor (for example: $\times 8$), which ameliorates this problem; or to magnify by an irrational factor (for example: $\times e$ or $\times \pi$), which randomly distributes errors across the magnified image rather than producing a regular error pattern. The latter solution is not preferred because the error is still there, it is just not as obvious because it is random [Cook, 1986].

The second reason for using a large magnification factor is so that the reconstruction filter is large compared to the display reconstruction filter. This means that the display reconstruction filter has little effect on the overall filter, and so what we see is very similar to the reconstruction filter which we are trying to evaluate. If we assume that the display reconstructs using a typical Gaussian convolved with a box filter[2], then the overall reconstruction filter viewed is shown in figure 7.6 for various magnification factors of a linear interpolant.

Thus, for our results to be valid we need large magnification. A factor of four is the minimum

[2]the box filter is the nearest-neighbour reconstruction used in most display drivers, and the Gaussian is the blur caused by the phosphor spot on a CRTs surface.

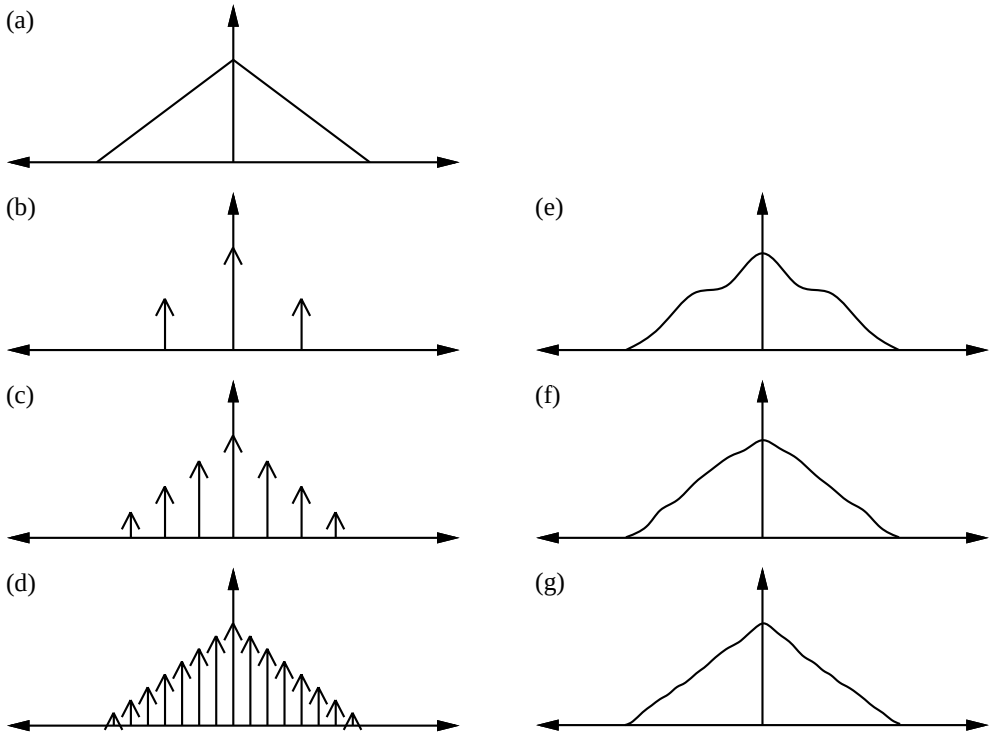

Figure 7.6: The effect of magnification factor on displaying a reconstructors results. On the left is the linear interpolation filter, (a), whose effects we are trying to view. After sampling this becomes (b) for magnification by 2, (c) for magnification by 4, and (d) for magnification by 8. Reconstruction by the display's Gaussian∗box reconstructor gives an overall reconstructor shown in (e), (f) and (g). As the magnification factor increases, so the overall reconstructor better approximates (a), the reconstructor we are trying to evaluate.

that will be useful, eight is better. Andrews and Patterson [1976] used a factor of 16, which is the largest factor recorded in the literature.

Whilst useful for evaluating reconstructors, enlargement of this nature is not a particularly useful function of resampling. By enlarging a function to, say, four times its size in both dimensions, we are basically using the original as a compressed version of the resampled image. It is possible to achieve much higher quality reproduction, using the same number of bits of information, by using a better compression method than sampling at one quarter of the frequency and reproducing the original by resampling. However, Reed, Algazi, Ford and Hussain [1992] have used such resampling as *part* of a more complex compression method. First, the image is subsampled at an eighth the resolution in each dimension, and this minified image encoded and transmitted. Secondly the difference between the original image and this small image enlarged by cubic interpolation is quantised, encoded and transmitted. At the receiver, the minified image is decoded and enlarged by the same resampling method, and the difference image is decoded and added back to the enlarged image.

Resampling cannot create extra information. So reconstruction is the process of arranging the available information in the best possible way. By enlarging an image we stretch the available information over a wide area and the artifacts of the reconstruction method become readily apparent. This is why we use enlargement to subjectively study reconstruction methods, it is a way of getting a handle on what the reconstructed surface actually looks like. However, in practical applications, it is desirable to have as much information as possible available. Thus, if we know beforehand the range to which we may have to transform our original image, then we should ensure that the original contains as many, if not more, samples than the final image will require. This ensures that we will be discarding information rather than having to 'fill in the gaps', and thus

our final image will contain the maximum amount of information possible. This is a tall order because often we do not know what transformations will have to be performed on an image when it is captured. However, if the choice exists between recapturing the image at higher resolution or resampling it to higher resolution, then recapturing it is by far more preferable from the point of view of image quality.

It is interesting to consider an application where the size of the final image is roughly known before the original is captured. Venot *et al* [1988] and Herbin *et al* [1989] describe a system for the registration of medical images. The normal process is that two or more images are captured over the period of treatment and registered with one another to track the progress of healing. The first image to be captured is the standard. Subsequent images are then taken over a period of weeks and are registered against the standard. Venot *et al* [1988, p.300] give their default range of scale factors to be 0.8 to 1.2. This implies that they expect subsequent images to be at roughly the same scale as the first. This is a sensible assumption: too much larger than the original and excessive processing would be required to reduce it down to size and, more importantly, with a fixed size image some of the necessary parts of the second image could be lost off the edges (for example: the edge of a region of scar tissue could fall outside the image's edge). Much smaller than the original and there would be insufficient detail in the second image, it would need to be enlarged too much, and of course no extra information would be available.

Our recommendation is that, ideally, the second image should be a little larger than the first to allow for some information loss during the resampling process. Some information is bound to be lost in this process, so having more than enough to start with will partly compensate for the quality degradation due to the resampling.

7.3.1 Display artifacts

Now, consider the effect of the display reconstructor on the resampled image. Pavlidis [1990] and Blinn [1989b] both say that it is the display reconstructor which causes at least some of the rastering effects in the continuous intensity surfaces that we view. This is certainly true. Pavlidis [1990] suggests that we could improve the performance of our graphics displays by using a better reconstructor between the digital image and the displayed intensity surface. Such an idea merits consideration, but there are two factors which may make it impractical or unnecessary.

The first is that this idea cannot be implemented easily with CRT technology. A better reconstructor than the box convolved with a Gaussian that is currently used could be designed for reconstruction along a raster scan line, by altering the digital to analogue converter used to drive the CRT. But it is difficult to see how it could be made to work between scan lines, because the reconstruction method in this direction is inherent in the CRT and cannot be altered by changing the process which drives the display. Perhaps extra scan lines could be used between the true ones?

The second is that, regardless of the reconstruction method, from a great enough distance, the reconstructed image looks the same. Using nearest-neighbour, linear, Catmull-Rom and FFT reconstruction we found that the four magnified versions were indistinguishable when a single pixel subtended a visual angle of less than about 2 minutes. Thus, provided the CRT is always viewed from at least this distance (50–60cm for a typical display), rastering effects caused by the display should be undetectable. As we cannot guarantee that the display will always be viewed from at least this distance, there is value in Pavlidis' suggestion, although it may require non-CRT display technology to implement.

As to worries about evaluating resampled images on an imperfect display device: (1), the image will always have to be displayed somehow, so that it may be a good thing to evaluate it on a typical display; (2), if we are worried about it, we can enlarge the image using any reconstructor we think desirable, and then view the image on the display from a much greater distance, ameliorating the effects of the display reconstructor, as discussed earlier.

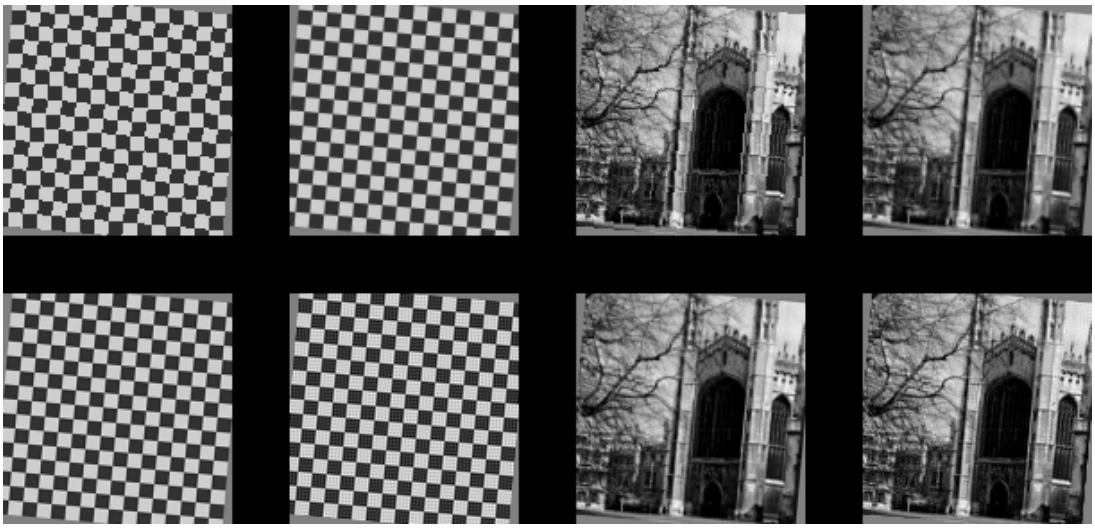

Figure 7.7: Two images rotated by 5° using four reconstructors and single point sampling. In both cases: top left: nearest-neighbour; top right: linear interpolation; bottom left: Catmull-Rom cubic interpolation; bottom right: FFT interpolation.

7.3.2 Judging a resampler by its reconstructor's quality

Resamplers are evaluated visually by examining the displayed resampled image and comparing it with the displayed original image (as in figure 1.8). They are evaluated mathematically by comparing the original and resampled images in some way, or by considering the mathematical features of the whole resampler.

Resamplers are often evaluated by considering only their reconstructors and assuming that the quality of the resampler depends solely on the quality of the reconstructor. We have already seen that this is not necessarily a valid assumption.

One practical example of this error of reasoning, occurred in the following situation. Four reconstruction methods, nearest-neighbour, linear, Catmull-Rom and an FFT method, were used with single point sampling. Three different transformations were used: magnification by a factor of four, and rotation by five and forty-five degrees. The first transformation is a standard way of assessing the quality of different reconstructors [Mitchell and Netravali, 1988; Andrews and Patterson, 1976]. The results from the magnification (figures 7.9 and 7.10) indicated that the FFT method is inferior to the Catmull-Rom method. The nearest-neighbour and linear methods are inferior also[3].

The results from the rotation by 5 degrees (figure 7.7) however, indicate that the FFT method is as good as the Catmull-Rom method. The nearest-neighbour and linear methods are still inferior[4].

However, when rotating by forty-five degrees, all four methods produce virtually identical results (figure 7.8). The trained eye can pick up some blurriness in the linear version and some minor defects in the nearest-neighbour version but these are almost negligible.

The point here is that a resampling method cannot be judged on its reconstructor alone, as some are wont to do, but rather on the reconstructor, transform, *and* sampler. Here we see that reconstructors of widely differing quality can produce resamplers of similar quality because the transform and sampler are such that the differences in reconstructor quality are negligible in the overall resampler. Obviously, from this, there are situations where a low quality reconstructor will be just as effective as a high quality one. The best example of this is in minification, where the quality of

[3]The main problems with the reconstructors are: blockiness (nearest-neighbour), blur (linear) and ringing (FFT).

[4]Nearest-neighbour produces a lot of obvious 'jaggies', linear produces a slightly blurry image.

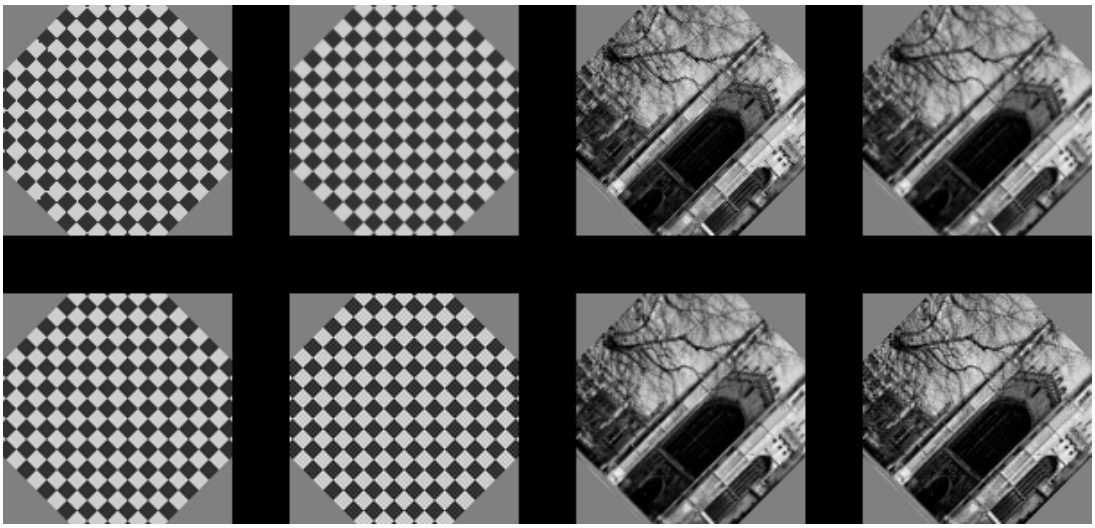

Figure 7.8: Two images rotated by 45° using four reconstructors and single point sampling. In both cases: top left: nearest-neighbour; top right: linear interpolation; bottom left: Catmull-Rom cubic interpolation; bottom right: FFT interpolation.

the sampler is important, and the quality of the reconstructor is practically irrelevant.

7.3.3 Artifacts in resampled images

Mitchell and Netravali [1988] consider several artifacts which can occur in a resampled image: sample frequency ripple, anisotropic effects, ringing, blurring, and aliasing. If we are comparing different type of resampler, (for example: linear against cubic against FFT reconstructors), rather than searching for, say, the best cubic reconstructor, then we can assume that the first two problems have been designed out of the resampler. These two tend to be easy to remove early on in resampler design. If they do occur, the solution is to use a better reconstructor. This leaves us with several artifacts which may occur in an image, Mitchell and Netravali's latter three plus an additional few. They all have their causes and most can be corrected for:

- Aliasing — caused by bad sampling. May be corrected by sampling well, or may be desirable in certain cases (for example: the exact reconstruction method in chapter 6 required an aliased image as input).

- Ringing — caused by a combination of aliasing and near 'perfect' reconstruction. May be corrected by using a less than perfect reconstructor (for example: Catmull-Rom cubic, rather than sinc) or by not using aliased images. May also be caused by a well sampled image and near perfect reconstruction giving a result that is exactly correct, but which we conceive to be very wrong (see section 2.7).

- Rastering — an artifact caused by bad reconstruction. Most noticeable with nearest-neighbour reconstruction where it produces the well-known 'jaggy' effect (for example, figure 7.10(top left)). The solution is to use a better reconstructor.

- Blurring — caused by certain types of reconstruction. Notably, all strictly positive reconstructors produce blurred results. The solution is to use a reconstructor with negative lobes, or an exact reconstructor, as in chapter 6. The former solution can lead to negative intensities. There is a trade-off here, between removing blur and wanting to be certain of always having positive intensities.

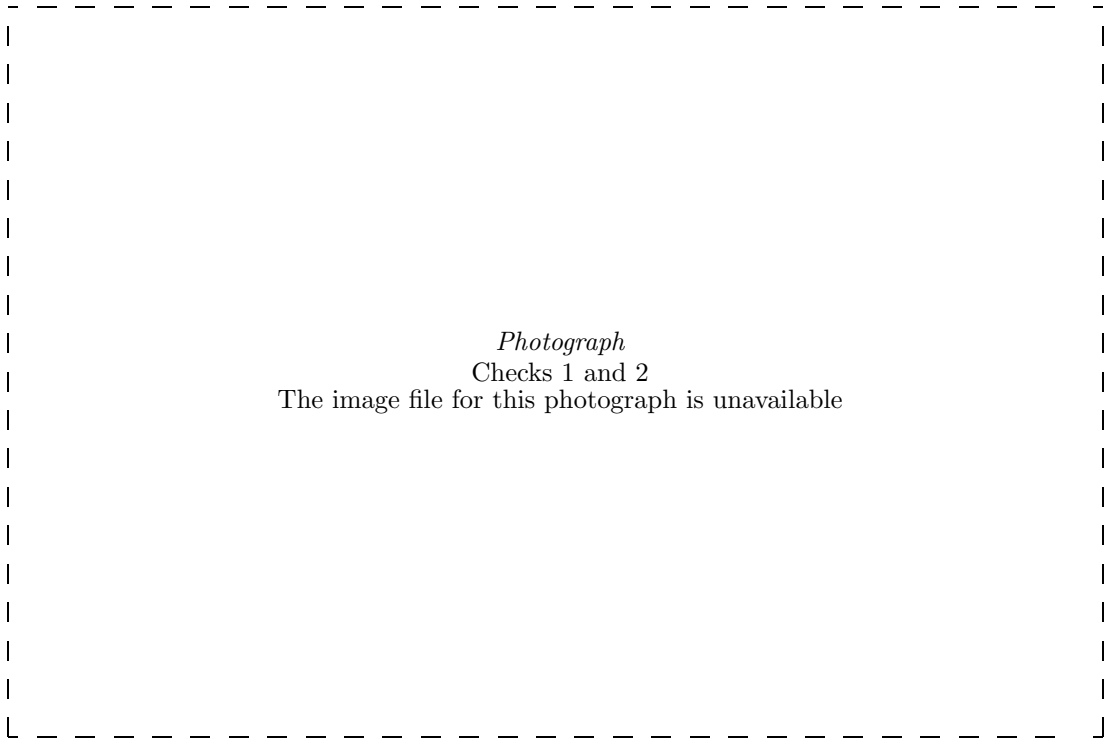

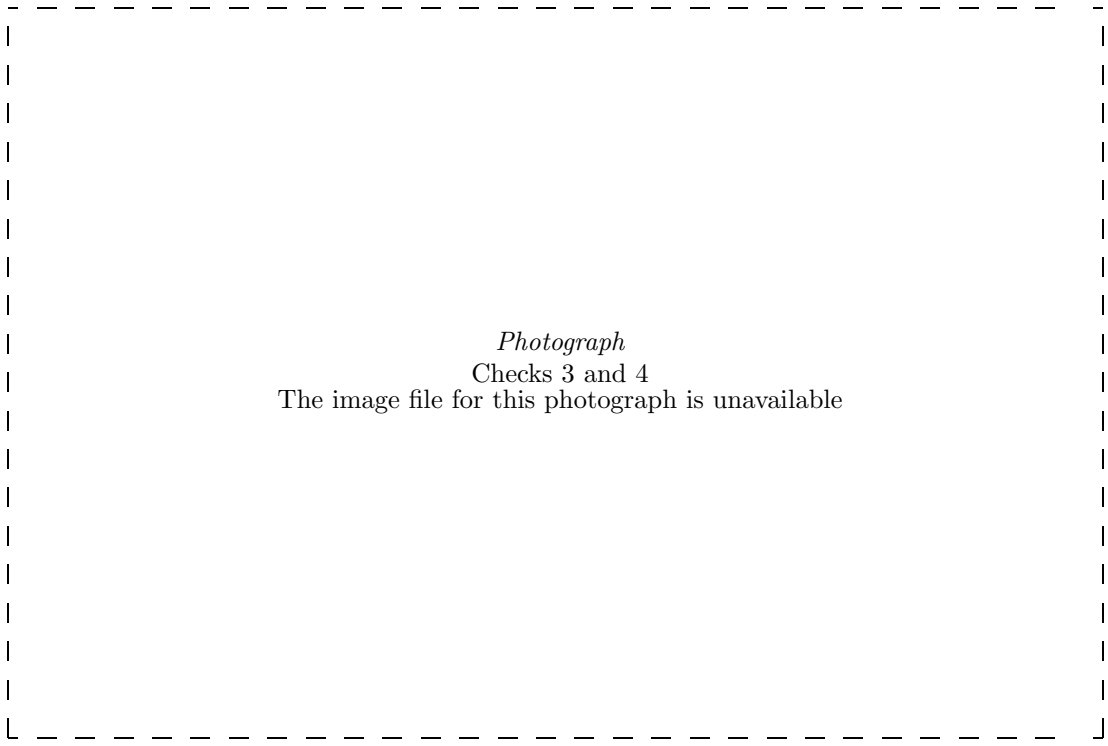

Figure 7.9: A checkerboard image enlarged fourfold using four reconstructors and single point sampling. Top left: nearest-neighbour; top right: linear interpolation; bottom left: Catmull-Rom cubic interpolation; bottom right: FFT interpolation. For this particular image the nearest-neighbour method gives an exact reconstruction, an unusual occurrence.

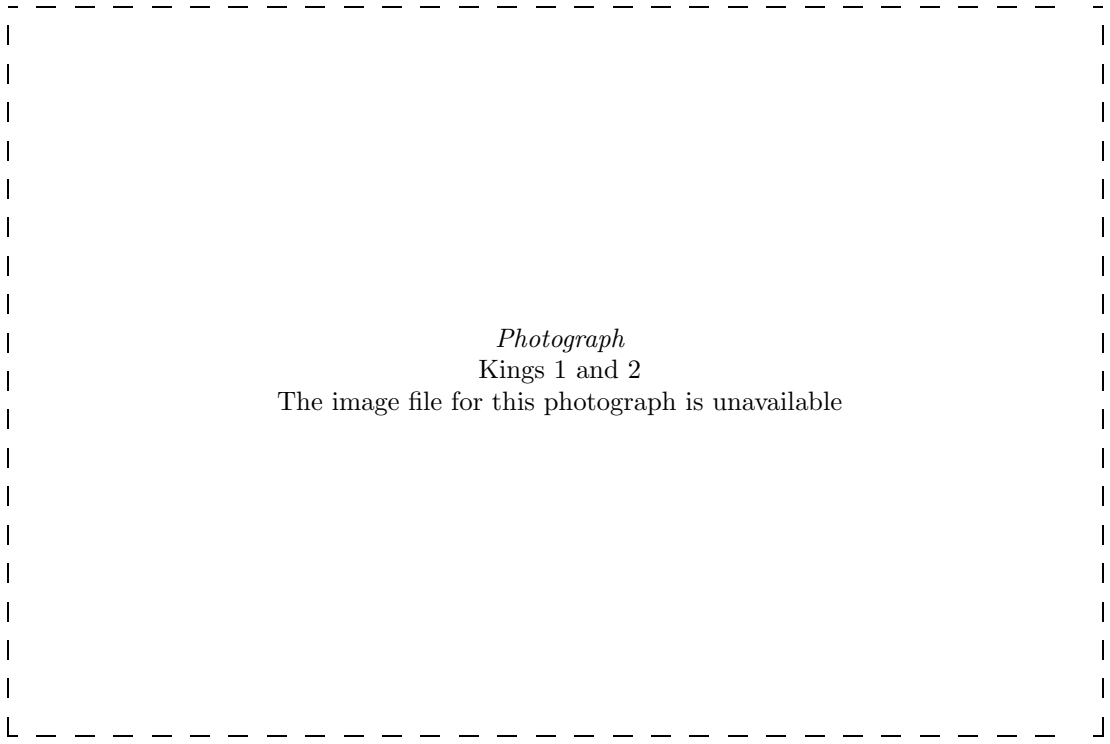

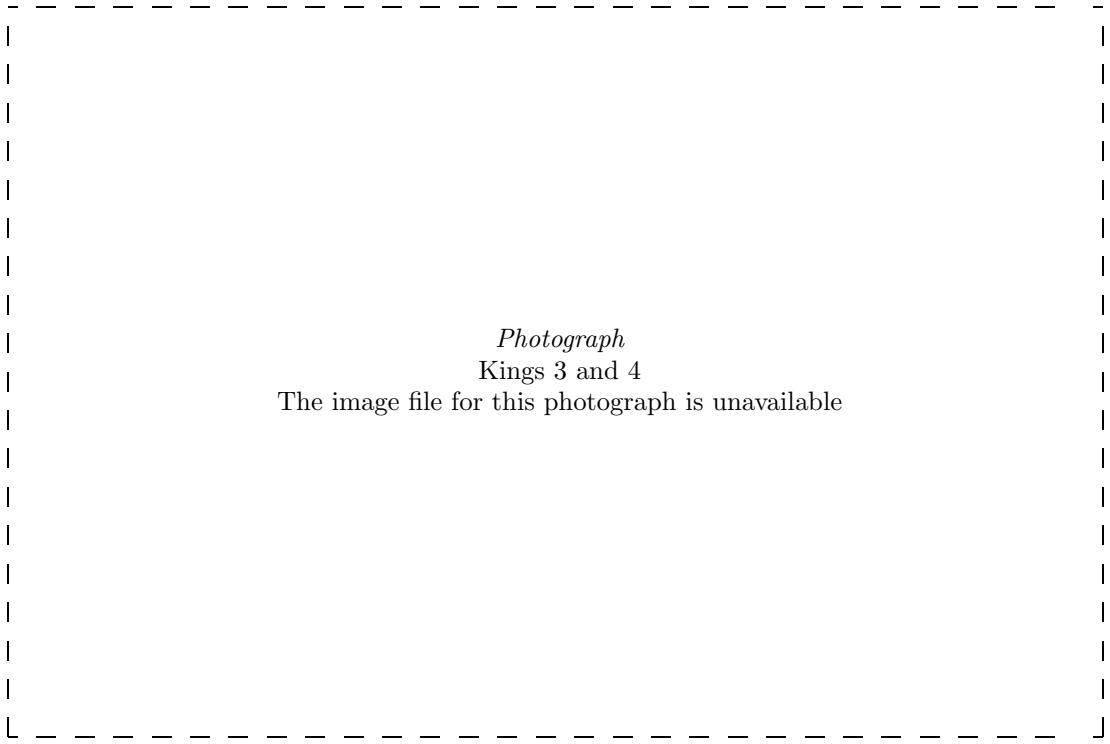

Figure 7.10: A captured image enlarged fourfold using four reconstructors and single point sampling. Top left: nearest-neighbour; top right: linear interpolation; bottom left: Catmull-Rom cubic interpolation; bottom right: FFT interpolation.

- Missing detail — this was mentioned at the end of chapter 6. It occurs when a textured region is enlarged and no extra detail becomes apparent. There is no obvious solution to this problem.
- Blurry edges — occur, under magnification, even with good reconstructor. They are due to a lack of information about edge position. One solution to this was developed in chapter 6.

These last two artifacts are due to the original image being a representation at a specific scale of an intensity surface. Magnifying the image reveals the lack of underlying detail in this representation. ('the painter's illusion' [Kajiya and Kay, 1989]). There are certain methods which try to produce underlying detail. One is the exact reconstructor of chapter 6 which can reconstruct straight edges. Another is the fractal compression technique [Sloan, 1992] which represents an image as a set of fractal definitions. This allows an image to be magnified and produce finer detail than was in the original. There is of course, no guarantee that this fine detail will be accurate. In general, we cannot access any underlying detail and so must content ourselves with the information that exists in the original image.

7.3.4 Quality measures

One very useful tool in the evaluation of resamplers would be a single number which could be calculated from an image, or images, which would indicate the quality of the resampling. For example, say we had a quality measure which we could apply to a single image. When we generate several resampled images from the same original, using the same transform but different resamplers, we could calculate this measure for them. Ideally, the measure should order the resampled images in order of increasing visual quality.

In practice, subjective visual judgements are often used. For example, Mitchell and Netravali [1988] used subjective visual judgement by experts to assess image quality. Vogt [1986] and Fiume [1989] both bemoan the lack of a formal measure of goodness, which thus leaves it up to a human to make arbitrary statements about how good an image is. Vogt especially comments that it is difficult to compare more than four images at one time without losing judgement.

Pratt [1978] discusses qualitative measures of image quality. He says that they are desirable because:

- they form a basis for the design and evaluation of imaging systems;
- they eliminate the cumbersome, and often inaccurate efforts of image rating by human observers;
- they can form the framework for the optimisation of image processing systems.

He goes on to comment that, unfortunately, developing such quantitative measures is tricky and that, while much progress has been made, the measures that have been developed are not perfect. Counter-examples can often be generated that possess a high quality rating but that are subjectively poor in quality and vice-versa. He claims that the key to the formulation of better image quality measures is a better understanding of the human visual system. At the present time, Pratt states that the most common and reliable judgement of image quality is subjective rating by human observers.

Nagioff [1991] discussed the problem for comparing image compression techniques. She concluded that the best way of judging image quality, to date, is root mean square difference between compressed and original versions combined with visual inspection, but that neither on its own is a sufficiently good quality measure.

The image quality measures that have been developed, can be divided into two classes [Pratt, 1978]:

- bivariate — a numerical comparison between two images;
- univariate — a numerical rating assigned to a single image based upon measurements on that image.

Many bivariate measures have been used. One such is the root mean square difference. In image resampling we are faced with the problem that we cannot use difference measures of this type because the original and resampled images are not aligned. A solution to this problem is to resample the image and then resample the resampled image to realign it with the original. Hammerin and Danielsson [1991] and Parker *et al* [1983] do this to get mean square differences for rotated images. The argument here is that the degradation in both rotations is roughly the same and so the mean square difference is a valid measure of the quality of a single rotation.

Unfortunately, this argument fails when the transform involves a scale change. Magnifying an image and reducing an image are very different operations and an algorithm that is good at one can be hopeless at the other. For example, we performed an experiment in which an image was magnified and reduced, and the root mean square difference between the original and the doubly resampled image calculated. This was done for a range of magnifications and a number of resamplers. The results are shown in appendix C. The worst resampler (nearest-neighbour reconstruction/single point sampling) performed the best in this test because it allows the original image to be exactly reproduced for any magnification factor greater than one, yet it produces the worst magnified image. The better resamplers produced worse numerical results on this test, but better visual results in the magnified images. Thus the root mean square difference between an image and its doubly resampled version is not a good measure of quality for transforms involving any sort of scale change.

What is required is a univariate quality measure, one which can be calculated for a single image. Such a measure is likely to be very hard to find. Pratt [1978 pp.175-176] only gives one true univariate measure, the 'equivalent rectangular passband measure', and he says that this has not proven to be well correlated with subjective testing. One possible candidate is the mean intensity level. However, this should be constant for all images resampled from the same source, and so is unlikely to be a good discriminator between resamplers.

Oakley and Cunningham [1990, p.191] claim that their accuracy metric is closely related to the visual quality of the results. They propose to present a future paper discussing the relationship between the theoretical and visual performance of the optimal reconstruction filter generated using this accuracy metric.

To give some idea of the relative merits of various possible measures, we performed experiments, comparing five different quality measures, on six different images, using four different resamplers, over a range of rotations from zero to forty-five degrees.

The first quality measure was root mean square difference between a doubly rotated image and the original; it is a valid measure here because there is no scale change in the transform. The other four were calculated from the central portion of a single, resampled image. These were determined as follows:

Three were measures of image entropy. One was the entropy itself, defined as:

$$H = -\sum_{i=0}^{N-1} p_i \ln p_i$$

where p_i is the probability that a pixel will have intensity i and N is the number of intensity levels.

Entropy was chosen because it is often proposed as a measure of the amount of information in an image. It is debatable how well this information measure relates to image quality. What it does measure is the minimum number of bits per pixel required to encode the image, with no relationships between adjacent pixels taken into consideration.

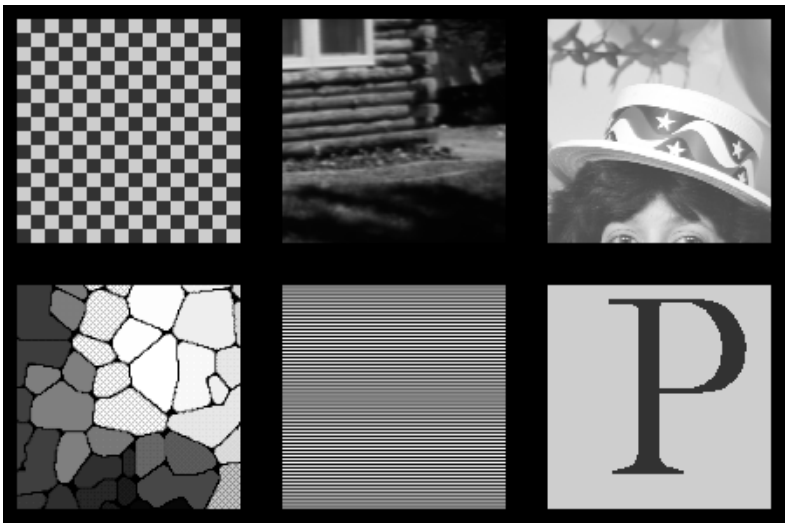

Figure 7.11: The six images used in the quality measure experiment. See text for a description of the images.

The other two entropy measures do take adjacent pixel values into consideration. One of these was the entropy of the differences between a pixel's intensity and each of its four-connected neighbours' intensities. This we termed the 'difference entropy'. The third entropy measure was second order entropy which uses the probability that a pixel will be a certain intensity given the intensity of one of its four-connected neighbours.

The hypothesis in choosing these measures is that it is not so much the absolute intensity of each pixel that is important in image quality, but the relative intensities; the eye being more sensitive to intensity differences (for example: edges), than to absolute intensities.

The fifth potential quality measure that was tested was developed based on the same hypothesis. The concept behind this is to take the weighted root mean square of the difference between each pixel and every other pixel:

$$I = \sqrt{\frac{\sum_i \sum_{j \neq i} (f_i - f_j)^2 \times w_{i,j}}{\sum_i \sum_{j \neq i} w_{i,j}}}$$

The weights, $w_{i,j}$, were set to be the inverse square of the distance between the two pixels. The measure we actually implemented in our experiment is an approximation to this, which considers only a pixel's eight-connected neighbours. A low value of this measure should indicate a smooth image and a high value a heavily corrugated one.

Figure 7.11 shows the six images used in the experiment. Images 1 and 6 have only two intensity levels (a dark and a light grey, not black and white) and hence very low entropies. Images 2 and 3 are extracts from natural images, one of a log cabin and one of a woman with some party decorations in the background. Image 4 is extracted from a piece of computer art with many grey levels and some patterned areas. Image 5 is a computer generated sine wave, sampled very close to its Nyquist limit. It is thus a pathological case for which we would expect any resampler to fail except one using sinc reconstruction.

Four resamplers were tested, all using single point sampling. The reconstructors involved were nearest-neighbour, linear interpolation, Catmull-Rom cubic interpolation, and FFT/Catmull-Rom interpolation, which approximates sinc reconstruction. The results of the experiments are graphed in appendix C.

The visual evidence indicates that the Catmull-Rom and FFT methods give similar results, both producing acceptable resampled (rotated) images, the linear interpolant often gives blurry results and the nearest-neighbour gives results which usually contain obvious jaggy artifacts, most noticeable along edges.

Analysis of the results in appendix C gives some interesting information about these resamplers and the images they produce:

1. Apart from pathological image 5, the RMS difference between original and doubly resampled images remains almost constant for the linear, Catmull-Rom, and FFT methods for all images at all rotation angles. This indicates that there is something inherent in these methods which causes the differences, rather than an angle-dependent factor. For nearest-neighbour the RMS difference climbs as the angle increases. This indicates that, as the angle increases, more and more pixels are being lost or moved to the wrong location by this method.

2. The nearest-neighbour method preserves all the entropy measures, some extremely precisely, even in cases where the other methods produce widely different values. This is presumably due to the fact that nearest-neighbour does not produce any new (interpolated) pixel values, merely moves the old ones to new locations, and adjacent pixels in the original image usually remain adjacent in the resampled image.

3. The other three methods increase the entropy of the image. Image 1 is an interesting case here. In order to produce a visually acceptable resampled image, the resamplers produce an image with far more entropy than the original. The Catmull-Rom and FFT methods depend on the side lobe sharpening effect to produce sharp edges, requiring a far larger range of pixel values than the original which simply had sharp edges. Two very different ways of producing the same visual result.

   This data implies that more 'information' is required to represent a resampled image than is required to represent the original. This is not an intuitive result as no resampling process can increase the amount of real information in an image, in fact they tend to lose information. This data could thus mean that a resampler compensates for this lost information by producing an image which generates the correct visual stimulus in a more complex way than the original.

4. The other two entropy measures also increase with the linear, Catmull-Rom, and FFT methods. The exceptions to this are the two natural images (2 and 3) with linear interpolation, where the entropy reduces. This may be due to linear interpolation's tendency to blur (smooth) an image, reducing the differences between adjacent pixels, but, if this is so, why is the same effect not apparent in the artificial images?

5. Of all the entropy measures, the FFT result is always higher than the linear result except in the case of image 5's second order entropy and the Catmull-Rom result is higher than linear in all but image 3's entropy, where they are the same. The FFT and Catmull-Rom methods are not as consistently ordered: in images 2, 3, 4 and 6 the FFT value is always higher than Catmull-Rom's. In images 1 and 5 it is not. Quite how this relates to subjective image quality has yet to be tested. We suspect that there is a relation but a probabilistic rather than a consistent one.

6. The final 'smoothness' measure gives interesting insights. The nearest-neighbour method produces a less smooth (higher value) or similarly smooth image to the original. Linear and Catmull-Rom give smoother images, perhaps indicating that they blur the original in the resampling. Linear consistently produces a smoother image than Catmull-Rom. Catmull-Rom, in turn, consistently produces a smoother image than the FFT method. The most surprising result is that the FFT method gives almost exactly the same value for the resampled image as for the original in three of the six images. The consistent ordering provided by this measure, except for the nearest neighbour case, gives some hope that it may be a step toward a useful quality measure. Further work is required to confirm or contradict this view.

While these results are interesting, they have not given us a conclusive quality measure. It may yet prove possible to find a good univariate measure.

7.4 Summary

In a resampler, it is the reconstructor and sampler which cause degradation in the image. For transforms which minify the image, good sampling is required; for transforms which magnify, good reconstruction is required; and for same-scale transforms, the quality of both reconstructor and sampler have little effect on the overall quality of the resampler, except that skeleton, delta function, or nearest-neighbour reconstruction cause obvious degradation.

If the required transform is known before the original image is captured, then it should be captured slightly larger than the final image will be in order to ensure that no magnification is required. This will maximise the information in the resampled image.

When subjectively evaluating visual reconstructor quality, the image should be magnified using that reconstructor, before displaying it on a display device. This minimises the effect of the sampler and the display on the displayed intensity surface.

Subjective image quality is difficult to evaluate mathematically, especially as a univariate measure is required for measurements on any resampler which involves a scale change. We experimented with four univariate measures, and commented on our results. However, we could draw no definite conclusions. Further work is required on these measures, especially on the last 'smoothness' measure, in order to discover their true utility.

Chapter 8

Summary & Conclusions

We have examined many facets of digital image resampling, concentrating on the reconstruction sub-process. In this final chapter we summarise the main results and conclusions, briefly mention other results, and end with three suggestions for future research.

8.1 Major results

In the area of piecewise local polynomials we have shown that zero-phase, piecewise local quadratics can be derived. Of the two that we did derive, one gives practically identical visual quality to the Catmull-Rom cubic interpolant, which is the best all-round piecewise local cubic interpolant. This quadratic can be evaluated in about 60% of the time of the cubic, giving a significant time saving in situations where we require the Catmull-Rom's visual quality.

Moving to non-local reconstructors, we have derived the kernels of the interpolating cubic B-spline and interpolating Bezier cubics, and shown them to be the same. This kernel has allowed us to create an efficient way of extending the one-dimensional cubic B-spline to a two-dimensional reconstructor.

For edge extension, we concluded that replication or windowed extrapolation are the best methods, with constant extension the fastest. With sinc reconstruction: constant edge extension, or windowed extrapolation, are the only practicable edge extension methods, giving an $O(N^4)$ resampling time for an $N \times N$ image. However, FFT reconstruction reduces this to $O(N^2 \log N)$, with replication edge extension. We have provided solutions to two major problems with FFT reconstruction: (1) Edge effects, for which four solutions were presented. The fourth, DCT reconstruction, uses reflection edge extension and paves the way for us to show when and how a general transform can be used for image reconstruction. (2) Time and storage requirements, for which a tiling solution was developed. The tiled version greatly reduces the memory required for performing the transform, and, when the untiled version must be executed using virtual memory, the tiled version can reduce the time requirement as well. The fact that the tiled version gives very similar visual results to the untiled version gives weight to the hypothesis that local, rather than global information is important in image reconstruction.

In *a priori* knowledge reconstruction, we considered one particular set of one-dimensional intensity curves, coupled with one particular type of sampling. Here we proved that, given certain conditions on the original intensity curve, it can be exactly reconstructed from its exact area samples. These intensity curves cannot be exactly reconstructed using classical sampling theory. For the two-dimensional case the evidence strongly suggests that a similar proof can be found.

Finally, drawing the strands together, we show that the quality of the resampler is not dependent solely on the quality of its reconstructor, but on all three sub-processes. We have performed

some experimental work on measuring the quality of an image, which is a step in the search for a univariate quality measure for images.

8.2 Other results

An analysis of the factors involved in designing piecewise local polynomials has been given, showing that it is very difficult to include all of the desirable factors in a single piecewise local polynomial reconstructor.

An analysis of several infinite reconstructors has shown that all decay exponentially, except sinc, allowing them to be truncated locally with negligible loss of quality. Sinc can be windowed locally, greatly changing its nature, or non-locally, which does not solve the problem of undesirable ripples being generated near edges in non-bandlimited images. We have proven the result that no finite image can be bandlimited.

The three-part decomposition developed in chapter 1 has underpinned all of the other work in this dissertation. We believe it has shown its utility throughout all this work.

8.3 Future work

We could extend the work on piecewise local polynomials to fifth and higher orders, to ascertain whether such extension is worthwhile. Our opinion is that there is probably little to gain from such extension, and that, to achieve better reconstruction, methods other that piecewise local polynomials must be considered.

The work on the two-dimensional sharp edge reconstructor in section 6.4 has stopped short of a working implementation. Development of such an implementation, following the outline given in section 6.4, is a necessary piece of future work.

Finally, more analysis of the quality measures examined in section 7.3.4 is required. Special attention should be paid to the 'smoothness' measure to ascertain its utility.

Appendix A

Literature Analysis

Many resamplers have been considered over the years. This appendix contains a table of the resamplers considered in many of the papers in the field. Each set of resamplers is decomposed into its three constituent parts, as described in chapter 1 (figure 1.14). We have deliberately omitted the books and surveys on the subject as these consider a very large number of resamplers and draw heavily on the papers listed here. Specifically omitted are Heckbert [1986a], Heckbert [1989], Wolberg [1990] and Foley *et al* [1990].

Reference	Reconstructors	Transforms	Samplers
Andrews and Patterson [1976]	Nearest-neighbour; linear; approximating quadratic B-spline; approximating cubic B-spline; four-piece piecewise linear.	Scaling $\times 16$. Further experiments with nearest-neighbour and linear reconstruction only: scaling $\times 8$, $\times 4$, $\times 2$ and $\times 1$.	Single point.
Bier and Sloan [1986]	*Don't say.*	Mapping a two-dimensional image onto a three-dimensional surface via an intermediate simple three-dimensional surface (plane, box, cylinder, or sphere).	*Don't say.*
Blinn [1989b]	Nearest-neighbour; linear; Gaussian; sinc; Lanczos windowed sinc.	*None* (frequency domain analysis of reconstructors).	*None* (frequency domain analysis of reconstructors).
Boult and Wolberg [1992]	Linear; interpolating cubic B-spline; Catmull-Rom; cubic interpolant ($a = -1$); quadratic APK reconstructor based on rectangular and Gaussian area samplers; two piece cubic APK reconstructor based on rectangular area sampler.	Scaling by 8.	Single point.
Braccini and Marino [1980]	Nearest-neighbour.	Rotation; scaling; general affine; non-affine; four-point transformations.	Single point.
Catmull and Smith [1980]	*Don't say* (but see e.g. Smith [1981, 1982]).	Two-pass, one-dimensional rotation; rational linear; bilinear.	*Don't say* (but see e.g. Smith [1981, 1982]).
Crow [1984]	Linear.	Arbitrary.	Exact area sampling over a rectangle in the *original* image space, this area based on the size and position of the final pixel inverse mapped into original image space.

Reference	Reconstructors	Transforms	Samplers
Durand [1989]	Nearest-neighbour on an abutting circular pixel grid, zero between the circles.	Rotation.	Exact area on an abutting circular pixel grid.
Durand and Faguy [1990]	Nearest-neighbour; quadratic and cubic B-splines.	Scaling by a rational factor.	Exact area.
Fant [1986]	Nearest-neighbour; nearest-neighbour/linear crossbred.	Arbitrary 1D transforms in multi-pass operations.	Exact area.
Feibush, Levoy and Cook [1980]	Linear.	Perspective.	Single point, exact area, Gaussian.
Fournier and Fiume [1988]	Piecewise polynomials (and arbitrary reconstructors).	Conformal; perspective.	Piecewise polynomial approximations to various sampling filters; specifically Gaussian, sinc and difference of Gaussian.
Fraser [1987, 1989a, 1989b]	FFT/Catmull-Rom with and without windowing; Catmull-Rom; cubic interpolation with $a = 0$ and $a = -1$; linear.	Rotation (one pass 2D and two pass 1D).	Single point; sinc filtering.
Fraser, Schowengerdt and Briggs [1985]	Nearest-neighbour; Catmull-Rom.	Two-pass, one-dimensional, separable operations: specifically rotation and third-order polynomial warping. Also the transpose operation required between the two passes.	Single point.
Frederick and Schwartz [1990]	see Williams [1983].	Conformal mapping. Either (a) directly (if the mapping is invertible), or (b) approximately via triangulation and two-dimensional linear interpolation over the triangles.	see Williams [1983].
Glassner [1986]	Nearest-neighbour.	Arbitrary (none specifically analysed).	An approximation to exact area sampling.

Reference	Reconstructors	Transforms	Samplers
Goshtasby [1989]	Nearest-neighbour.	Correction of image deformation using a Bezier patch method (local scaling is $\times 0.97$–$\times 1.03$ ($\pm 3\%$), thus little change in scale; shearing is also involved but no transformation is of high magnitude).	Single point.
Greene and Heckbert [1986]	Gaussian.	Perspective.	Gaussian.
Hammerin and Danielsson [1991]	Linear; 2-, 4- and 8-point cubic splines.	One-pass (2D), two-pass (1D) and three-pass (1D) rotation.	Single point
Hanrahan [1990]	Catmull-Rom cubic interpolation (but discusses the theory of perfect reconstruction).	Three-dimensional affine transformations (but discusses two-dimensional and more complex three-dimensional transformations).	Single point (but discusses pre-filtering).
Heckbert [1986b]	Linear.	Arbitrary.	Various area samplers over a rectangle in the *original* image space, this area based on the size and position of the final pixel inverse mapped into original image space.
Herbin *et al* [1988]	see Venot *et al* [1989]		
Hou and Andrews [1978]	Cubic B-splines. Also briefly mentions nearest-neighbour, linear, quadratic B-splines, polynomial interpolation and sinc interpolation. Compares nearest-neighbour, linear, interpolating cubic B-spline and approximating cubic B-spline for magnification. Compares cubic B-spline with sinc for minification.	Scaling $\times r$, $r \in \mathcal{R}$ (in software). Scaling $\times \frac{M}{N}$, $M, N \in \mathcal{Z}$ (in hardware).	Single point.

Reference	Reconstructors	Transforms	Samplers
Keys [1981]	Linear and Catmull-Rom (also briefly looks at nearest-neighbour; sinc; six-point cubic and piecewise cubic Lagrange interpolant).	Scaling $\times 5\frac{15}{32}$ (horizontally), $\times 5\frac{1}{4}$ (vertically) for linear and Catmull-Rom reconstruction.	Single point.
Lee [1983]	Linear; interpolating cubic B-spline and restoring cubic B-spline (also discusses nearest-neighbour, Catmull-Rom, and sinc).	Scaling $\times z$, only integral values of z are used by Lee but the method is not restricted to integers.	Single point.
Maeland [1988]	Interpolating cubic B-spline; linear; cubic convolution with $a = 0$ (two point cubic), $a = -\frac{1}{2}$ (Catmull-Rom), $a = -\frac{3}{4}$ (also mentions $a = -1$).	Arbitrary — no specific transformation discussed.	Single point.
Maisel and Morden [1981]	Sinc.	Two pass 1D rotation (frequency domain analysis).	Single point.
Mitchell and Netravali [1988]	Two parameter family of cubic reconstructors; 30 unit wide windowed sinc.	Scaling.	Single point.
Namane and Sid-Ahmed [1990]	Find the border pixels of the character, scale these pixels, interpolate between the scaled points and fill in the character.	Scaling (note that the reconstructor and transform are intimately tied together. All processing is in the discrete domain, no continuous intensity surface is produced in this method).	Single point (note that this processing is performed on a binary image and produces a binary image).
Oakley and Cunningham [1990]	A matched APK reconstructor based on a Gaussian area sampler; compared against Catmull-Rom cubic and nearest-neighbour.	Scaling.	Single point.

Reference	Reconstructors	Transforms	Samplers
Oka, Tsutsui, Ohba, Kurauchi and Tago [1987]	Nearest-neighbour.	Block affine approximation to general transformation.	Minimum enclosing rectangle of pixel preimage (approximating exact area area sampling).
Paeth [1986, 1990]	Nearest-neighbour.	Three pass 1D rotation.	Approximation to exact area (both 1D and $1\frac{1}{2}$D); triangle and higher order sampling filters.
Park and Schowengerdt [1982]	Nearest-neighbour; linear; cubic with $a = -1$; sinc.	*None* (frequency domain analysis of reconstructors).	*None* (frequency domain analysis of reconstructors).
Park and Schowengerdt [1983]	Nearest-neighbour; linear; cubic interpolating piecewise polynomials (including Catmull-Rom); sinc.	*None* (frequency domain analysis of reconstructors).	*None* (frequency domain analysis of reconstructors).
Parker, Kenyon and Troxel [1983]	Nearest-neighbour, linear, approximating cubic B-spline, cubic convolution with $a = -\frac{1}{2}$ (Catmull-Rom) and $a = -1$ (also mentions $a = -\frac{3}{4}$).	General two-dimensional transformations. Specific examples used are rotation and subpixel translation. Applied to image registration.	Single point.
Ratzel [1980]	See Schreiber and Troxel [1985].		
Reichenbach and Park [1982]	Mitchell and Netravali's [1988] two parameter family of cubics.	*None* (frequency domain analysis of reconstructors).	*None* (frequency domain analysis of reconstructors).
Schafer and Rabiner [1973]	Digital filters: Lagrange interpolation; linear interpolation; optimum FIR interpolation.	Scaling $\times\frac{M}{N}$, $M, N \in \mathcal{Z}$.	Single point.
Schreiber and Troxel [1985] (based on Ratzel [1980])	Nearest-neighbour; linear; truncated Gaussian; truncated sharpened Gaussian; truncated sinc; approximating cubic B-spline; two types of sharpened cubic B-spline.	Scaling $\times 5$ (also scaling by other factors to find best sharpened Gaussian prefilter and best sharpened Gaussian reconstructor).	Single point.
Smit, Smith and Nichols [1990]	FFT; FFT with ARMA algorithm; nearest-neighbour.	Scaling $\times 2^k$, $k \in \mathcal{Z}$ (with potential to truncate result to a sub-image).	Single point.

Reference	Reconstructors	Transforms	Samplers
Smith [1981]	Sinc.	Scaling.	Single point; sinc filtered sampling.
Smith [1982]	Catmull-Rom; approximating cubic B-spline; various windowed sincs.	Scaling and arbitrary.	*None* (discussion of reconstruction and transforms only).
Smith [1987]	*Not stated* (but see e.g. Smith [1981, 1982]).	Two-pass; one-dimensional superquadric; bi-cubic and bi-quadratic warps.	*Not stated* (but see e.g. Smith [1981, 1982]).
Trussell *et al* [1988]	Inverse sinc.	Correction of one-dimensional sample position errors.	Single point.
Turkowski [1990]	Nearest-neighbour; linear; two Gaussians; two Lanczos windowed sincs.	Scaling $\times 2, 3, 4$; $\times \frac{1}{2}, \frac{1}{3}, \frac{1}{4}$.	Single point.
Venot *et al* [1988], Herbin *et al* [1989]	*Don't say.*	Registration of two-dimensional images. Translation, rotation, scaling, included in a general transform which also allows for grey-scale manipulation.	*Don't say.*
Ward and Cok [1989]	Linear; Catmull-Rom (with and without coefficient bins); Hamming windowed sinc.	Scaling $\times \frac{3}{2}$, $\times 2$ and $\times 4$ (all three reconstructors). Non-seperable and seperable rotation (Catmull-Rom only).	Single point.
Watson [1986]	FFT	Scaling.	FFT
Weiman [1980]	Nearest-neighbour.	Rotation, scaling, shearing by multi-pass 1D algorithms.	Exact area.

Reference	Reconstructors	Transforms	Samplers
Williams [1983]	A three-dimensional intensity volume is produced. It is generated by linear interpolation between two-dimensional intensity planes. Each plane is generated by two-dimensional linear interpolation between sample points created by a two-dimensional nearest-neighbour/exact area resampling (minification by $2^n, n \in \{0, 1, 2, 3, \ldots\}$) of the original image.	General. Any transformation although ones with highly non-symmetrix (non-square) pixel preimages do not work well.	Single point sampling into the three-dimensional volume using spatial (x and y) coordinates and a "depth" coordinated wich is related to the size of the destination pixel mapped onto the original image.
Wolberg and Boult [1989]	see Fant [1986].	Arbitrary two-pass 1D transformations specified by spatial lookup tables.	see Fant [1986].

Appendix B

Proofs

B.1 The inverse Fourier transform of a box function

(section 2.4.1)

$$\begin{aligned}
s(x) &= \int_{-\infty}^{\infty} \mathrm{Box}(\nu) e^{i2\pi\nu x}\, d\nu \\
&= \int_{-\nu_b}^{\nu_b} e^{i2\pi\nu x}\, d\nu \\
&= \frac{1}{i2\pi\ x} e^{i2\pi\nu x}\Big|_{-\nu_b}^{\nu_b} \\
&= \frac{1}{i2\pi\ x}\left(e^{i2\pi\nu_b x} - e^{-i2\pi\nu_b x}\right) \\
&= \frac{1}{i2\pi\ x}\left(\cos(2\pi\nu_b x) + i\sin(2\pi\nu_b x) - (\cos(2\pi\nu_b x) - i\sin(2\pi\nu_b x))\right) \\
&= \frac{1}{i2\pi\ x}\left(2i\sin(2\pi\nu_b x)\right) \\
&= \frac{\sin(2\pi\nu_b x)}{\pi x} \\
&= 2\nu_b \mathrm{sinc}(2\nu_b x)
\end{aligned}$$

$\mathrm{sinc}(x)$ is defined in the literature as either $\mathrm{sinc}(x) = \frac{sin(x)}{x}$ or as $\mathrm{sinc}(x) = \frac{sin(\pi x)}{\pi x}$. In this thesis we will stick with the latter.

B.2 The Fourier transform of the sinc function

(section 5.1)

The sinc function is defined as:

$$h(x) = N\frac{\sin \pi N x}{\pi N x},\ N > 0$$

It's Fourier transform is:

$$H(\nu) = \int_{-\infty}^{\infty} h(x) e^{-i2\pi\nu x}\, dx$$

$$\begin{aligned} &= \int_{-\infty}^{\infty} N \frac{\sin(\pi N x)}{\pi N x} \left[\cos(2\pi\nu x) - i \sin(2\pi\nu x)\right] \\ &= \frac{1}{\pi} \int_{-\infty}^{\infty} \frac{\sin(\pi N x)\cos(2\pi\nu x)}{x}\, dx - \frac{i}{\pi} \int_{-\infty}^{\infty} \frac{\sin(\pi N x)\sin(2\pi\nu x)}{x}\, dx \\ &= \frac{1}{\pi} A(x,\nu) - \frac{i}{\pi} B(x,\nu) \end{aligned}$$

Let $y = \pi N x$. Thus: $x = \frac{y}{\pi N}$ and $\frac{dy}{dx} = \frac{1}{\pi N}$.

$$\begin{aligned} A(x,\nu) &= \int_{-\infty}^{\infty} \frac{\sin(\pi N x)\cos(2\pi\nu x)}{x}\, dx \\ &= \int_{-\infty}^{\infty} \frac{\sin(y)\cos(2y/N)}{y}\, dy \end{aligned}$$

sin is an odd function, $\frac{1}{y}$ is an odd function, and cos is an even function, therefore the function that is being integrated is even, and so:

$$\begin{aligned} A(x,\nu) &= 2\int_{0}^{\infty} \frac{\sin(y)\cos(2y/N)}{y}\, dy \\ &= \begin{cases} 0, & \left|\frac{2\nu}{N}\right| > 1 \\ \frac{\pi}{2}, & \left|\frac{2\nu}{N}\right| = 1 \\ \pi, & \left|\frac{2\nu}{N}\right| < 1 \end{cases} \end{aligned}$$

[Dwight 858.9]

$$\begin{aligned} B(x,\nu) &= \int_{-\infty}^{\infty} \frac{\sin(\pi N x)\sin(2\pi\nu x)}{x}\, dx \\ &= \frac{1}{2}\int_{-\infty}^{\infty} \frac{\cos(\pi(N-2\nu)x)}{x}\, dx - \frac{1}{2}\int_{-\infty}^{\infty} \frac{\cos(\pi(N+2\nu)x)}{x}\, dx \end{aligned}$$

[Dwight 401.07]

Now, cos is an even function and $\frac{1}{x}$ is an odd function, so the equation inside each of the integrals is odd, meaning that each integral equates to zero ($\int_{-\infty}^{0} \frac{\cos kx}{x}\, dx = -\int_{0}^{\infty} \frac{\cos kx}{x}\, dx$).

Thus:

$$B(x,\nu) = 0$$

and therefore:

$$H(\nu) = \begin{cases} 1, & |\nu| < \frac{N}{2} \\ \frac{1}{2}, & |\nu| = \frac{N}{2} \\ 0, & |\nu| > \frac{N}{2} \end{cases}$$

B.3 Derivation of $a = -2 + \sqrt{3}$

(section 4.5.1)

From Rasala [1990] we know that:

$$a_k = -\frac{f_{m-k}}{f_m}$$

where $f_i = -4f_{i-1} - f_{i-2}$, $f_0 = 1$, $f_1 = -3$ or -4.

For i very large:

$$\begin{aligned}
\frac{f_{i-1}}{f_i} &= \frac{f_{i-1}}{(-4f_{i-1} - f_{i-2})} \\
&= -\frac{1}{4 + \frac{f_{i-2}}{f_{i-1}}} \\
&= -\frac{1}{4 - \frac{1}{4 + \frac{f_{i-3}}{f_{i-2}}}} \\
&= -\frac{1}{4 - \frac{1}{4 - \frac{1}{4 - \frac{1}{\ddots}}}}
\end{aligned}$$

From this we can see that:

$$\lim_{i \to \infty} \left(\frac{f_{i-1}}{f_i} - \frac{f_{i-2}}{f_{i-1}} \right) = 0$$

and so,

$$\begin{aligned}
\lim_{m \to \infty} a_1 &= \lim_{m \to \infty} -\frac{f_{m-1}}{f_m} \\
&= \lim_{m \to \infty} \frac{1}{4 - \frac{f_{m-2}}{f_{m-1}}} \\
&= \lim_{m \to \infty} \frac{1}{4 - \frac{f_{m-1}}{f_m}} \\
&= \frac{1}{4 - \lim_{m \to \infty} a_1}
\end{aligned}$$

which implies that the limit of a_1 as m goes to infinity is: $a_1 = 2 \pm \sqrt{3}$.

Now, the value of a_2 as m goes to infinity can be defined in terms of this limit of a_1:

$$\begin{aligned}
a_2 &= -\frac{f_{m-2}}{f_m} \\
&= a_1 \times \frac{f_{m-2}}{f_{m-1}} \\
&= -a_1^2 \ (m \to \infty)
\end{aligned}$$

A similar argument for the general case as m goes to infinity is:

$$\begin{aligned}
a_n &= -\frac{f_{m-n}}{f_m} \\
&= -\frac{f_{m-1}}{f_m} \times \frac{f_{m-2}}{f_{m-1}} \cdots \times \frac{f_{m-n}}{f_{m-n+1}} \\
&= -(-a_1)^n \\
&= -(a)^n \ (m \to \infty)
\end{aligned}$$

where $a = -a_1 = -2 \mp \sqrt{3}$.

The case $a = -2 - \sqrt{3}$ gives a divergent series of a_i values, while the case $a = -2 + \sqrt{3}$ gives a converging series. Thus:

$$a = -2 + \sqrt{3}$$

B.4 The Straightness Criteria

(Section 3.5.3)

For first order continuity:

Given m sample points, $f_{\alpha-a}, f_{\alpha-a+1}, \ldots, f_{\alpha}, \ldots, f_{\alpha+b}$, all having the same value, f_α, we want the reconstructed segment dependent on these m values to be $f(x) = f_\alpha$.

Thus:

$$\begin{aligned} f_x &= f_\alpha \sum_{i=-a}^{b} \sum_{j=0}^{n-1} k_{i,j} t^j \\ &= f_\alpha, \ \forall t \in \mathcal{T} \\ \mathcal{T} &= \begin{cases} [0,1), & m \text{ even} \\ [-\frac{1}{2}, \frac{1}{2}), & m \text{ odd} \end{cases} \end{aligned}$$

where: $\alpha = \left\lfloor \dfrac{x - x_0}{\Delta x} \right\rfloor$ and $t = \dfrac{x - x_\alpha}{\Delta x}$.

This implies that:

$$\sum_{i=-a}^{b} \sum_{j=0}^{n-1} k_{i,j} t^j = 1$$

which gives us the result that:

$$\begin{aligned} \sum_{i=-a}^{b} k_{i,j} &= 0, \ \forall j \in \{1, 2, \ldots, n-1\} \\ \sum_{i=-a}^{b} k_{i,0} &= 1 \end{aligned}$$

which is equation 3.13.

For second order continuity:

Given m sample points, $f_{\alpha-a}, f_{\alpha-a+1}, \ldots, f_{\alpha}, \ldots, f_{\alpha+b}$, having value $f_{\alpha+i} = f_\alpha + i\delta$, we want the reconstructed segment dependent on these m values to be $f(x) = f_\alpha + t\delta$.

Thus:

$$\begin{aligned} f(x) &= \sum_{i=-a}^{b} \sum_{j=0}^{n-1} k_{i,j} t^j (f_\alpha + i\delta) \\ &= f_\alpha + t\delta, \ \forall t \in \mathcal{T} \\ \mathcal{T} &= \begin{cases} [0,1), & m \text{ even} \\ [-\frac{1}{2}, \frac{1}{2}), & m \text{ odd} \end{cases} \end{aligned}$$

where: $\alpha = \left\lfloor \dfrac{x - x_0}{\Delta x} \right\rfloor$ and $t = \dfrac{x - x_\alpha}{\Delta x}$, as before.

This implies that:

$$f_\alpha + t\delta = f_\alpha \sum_{i=-a}^{b} \sum_{j=0}^{n-1} k_{i,j} t^j + \delta \sum_{i=-a}^{b} \sum_{j=0}^{n-1} i k_{i,j} t^j$$

and so:

$$f_\alpha = f_\alpha \sum_{i=-a}^{b} \sum_{j=0}^{n-1} k_{i,j} t^j \tag{B.1}$$

$$t\delta = \delta \sum_{i=-a}^{b} \sum_{j=0}^{n-1} i k_{i,j} t^j \tag{B.2}$$

Equation B.1 is the same as for first order straightness, and so equation 3.13 holds for second order straightness as well. Equation B.2 reduces to the following results:

$$\begin{aligned} \sum_{i=-a}^{b} i k_{i,j} &= 0, \ \forall j \in \{0, 2, 3, \ldots, n-1\} \\ \sum_{i=-a}^{b} i k_{i,1} &= 1 \end{aligned}$$

which is equation 3.14.

B.5 Proof that a signal cannot be simultaneously of finite extent in both the frequency domain and the spatial domain

(section 4.3)

Assume that $f(x)$ and $F(\nu)$ are a Fourier transform pair. Further assume that $f(x)$ is real, of finite extent, and infinitely piecewise differentiable:

$$f(x) \in \mathcal{R}$$

$$f(x) = 0, |x| > x_K$$

and that $F(\nu)$ is bandlimited:

$$F(\nu) = 0, |\nu| > \nu_N$$

$$\begin{aligned} F(\nu) &= \int_{-\infty}^{\infty} f(x) e^{-i2\pi\nu x} \, dx \\ &= \int_{-x_K}^{x_K} f(x) e^{-i2\pi\nu x} \, dx \\ &= \frac{f(x) e^{-i2\pi\nu x}}{-i2\pi\nu} \Big|_{-x_K}^{+x_K} - \frac{1}{(-i2\pi\nu)} \int_{-x_K}^{x_K} f'(x) e^{-i2\pi\nu x} \, dx \\ &\qquad \text{[Dwight, 79]} \\ &= \frac{f(x) e^{-i2\pi\nu x}}{-i2\pi\nu} \Big|_{-x_K}^{+x_K} - \frac{f'(x) e^{-i2\pi\nu x}}{(-i2\pi\nu)^2} \Big|_{-x_K}^{+x_K} + \frac{1}{(-i2\pi\nu)^2} \int_{-x_K}^{x_K} f''(x) e^{-i2\pi\nu x} \, dx \\ &= e^{iax} \left(\frac{f(x)}{ia} - \frac{f'(x)}{(ia)^2} + \frac{f''(x)}{(ia)^3} - \frac{f'''(x)}{(ia)^4} + \cdots \right) \Big|_{-x_K}^{x_K}, a = -2\pi\nu \\ &= (\cos(ax) + i \sin(ax)) \left(\frac{f(x)}{(ia)} - \frac{f'(x)}{(ia)^2} + \frac{f''(x)}{(ia)^3} - \frac{f'''(x)}{(ia)^4} + \cdots \right) \Big|_{-x_K}^{x_K} \\ &= \quad \cos(ax) \left(\tfrac{f'(x)}{a^2} - \tfrac{f'''(x)}{a^4} + \cdots \right) \Big|_{-x_K}^{x_K} \\ &\quad + \quad \sin(ax) \left(\tfrac{f(x)}{a} - \tfrac{f''(x)}{a^3} + \cdots \right) \Big|_{-x_K}^{x_K} \\ &\quad + \quad i \cos(ax) \left(-\tfrac{f(x)}{a} + \tfrac{f''(x)}{a^3} - \cdots \right) \Big|_{-x_K}^{x_K} \\ &\quad + \quad i \sin(ax) \left(\tfrac{f'(x)}{a^2} - \tfrac{f'''(x)}{a^4} + \cdots \right) \Big|_{-x_K}^{x_K} \end{aligned}$$

$$\begin{aligned}
= & \quad \cos(ax)\phi(a,x)|_{-x_K}^{x_K} \\
& + \quad \sin(ax)\chi(a,x)|_{-x_K}^{x_K} \\
& + \quad i\cos(ax)(-\chi(a,x))|_{-x_K}^{x_K} \\
& + \quad i\sin(ax)\phi(a,x)|_{-x_K}^{x_K} \\
= & \quad \cos(ax_K)(\phi(a,x_K)-\phi(a,-x_K)) \\
& + \quad \sin(ax_K)(\chi(a,x_K)+\chi(a,-x_K)) \\
& + \quad i\cos(ax_K)(-\chi(a,x_K)+\chi(a,-x_K)) \\
& + \quad i\sin(ax_K)(\phi(a,x_K)+\phi(a,-x_K))
\end{aligned} \tag{B.3}$$

Where:

$$\phi(a,x) = \left(\frac{f'(x)}{a^2} - \frac{f'''(x)}{a^4} + \cdots\right)$$

and:

$$\chi(a,x) = \left(\frac{f(x)}{a} - \frac{f''(x)}{a^3} + \cdots\right)$$

Now, if we set equation B.3 to be zero outside the bandlimit of $F(\nu)$ (as we assumed) and remember that $f(x)$ is a real function, then we find that:

$$\begin{aligned}
\phi(a,x_K) &= -\phi(a,-x_K),\ |a| > \nu_N/2\pi \\
\phi(a,x_K) &= \phi(a,-x_K),\ |a| > \nu_N/2\pi \\
\chi(a,x_K) &= -\chi(a,-x_K),\ |a| > \nu_N/2\pi \\
\chi(a,x_K) &= \chi(a,-x_K),\ |a| > \nu_N/2\pi
\end{aligned}$$

These four equations show that:

$$\begin{aligned}
\phi(a,x_K) &= 0,\ |a| > \nu_N/2\pi \\
\phi(a,-x_K) &= 0,\ |a| > \nu_N/2\pi \\
\chi(a,x_K) &= 0,\ |a| > \nu_N/2\pi \\
\chi(a,-x_K) &= 0,\ |a| > \nu_N/2\pi
\end{aligned} \tag{B.4}$$

Taking equation B.4 as an example:

$$\begin{aligned}
\phi(a,x_K) &= \left(\frac{f'(x_K)}{a^2} - \frac{f'''(x_K)}{a^4} + \frac{f^{(v)}(x_K)}{a^6} - \cdots\right) \\
&= 0,\ |a| > \nu_N/2\pi
\end{aligned}$$

which gives the following equalities:

$$\begin{aligned}
f'(x_K) &= 0, \\
f'''(x_K) &= 0, \\
f^{(v)}(x_K) &= 0 \\
&\vdots
\end{aligned}$$

This gives us the result:

$$\phi(a,x_K) = 0,\ \forall a$$

A similar argument holds for $\phi(a,-x_K)$, $\chi(a,x_K)$ and $\chi(a,-x_K)$. From these and equation B.3 it can be seen that:

$$F(\nu) = 0,\ \forall \nu$$

which implies that:

$$f(x) = 0,\ \forall x$$

So there exists only one trivial case in which the original assumption holds, that is $f(x) = 0$ and $F(\nu) = 0$. Therefore the Fourier transform of a real, finite-extent function, $f(x)$ cannot be bandlimited, unless $f(x) = 0$. Further, the Fourier transform of a bandlimited function, $F(\nu)$ cannot be a real, finite-extent function, unless $F(\nu) = 0$.

B.6 The Fourier transform of a finite-extent comb

(section 4.3)

Let the finite extent, one-dimensional comb function, $d(x)$, be defined as:

$$d(x) = \sum_{j=-b}^{b} \delta(x - j\Delta x)$$

Its Fourier transform is:

$$\begin{aligned}
D(\nu) &= \int_{-\infty}^{\infty} \sum_{j=-b}^{b} \delta(x - j\Delta x) e^{-i2\pi\nu x}\, dx \\
&= \sum_{j=-b}^{b} e^{-i2\pi\nu j\Delta x} \\
&= \sum_{j=-b}^{b} \cos 2\pi\nu j\Delta x - i \sin 2\pi\nu j\Delta x \\
&= \cos 0 + 2\sum_{j=1}^{b} \cos 2\pi\nu j\Delta x \qquad \text{[sin odd, cos even]} \\
&= 1 + 2\sum_{j=1}^{b} \cos 2\pi\nu j\Delta x \\
&= 1 + 2\frac{\cos(b+1)\pi\nu\Delta x \, \sin b\pi\nu\Delta x}{\sin \pi\nu\Delta x} \qquad \text{[Dwight 420.2]} \\
&= 1 + \frac{\sin((2b+1)\pi\nu\Delta x)}{\sin \pi\nu\Delta x} + \frac{\sin(-\pi\nu\Delta x)}{\sin \pi\nu\Delta x} \qquad \text{[Dwight 401.05]} \\
&= 1 + \frac{\sin((2b+1)\pi\nu\Delta x)}{\sin \pi\nu\Delta x} - 1 \\
&= \frac{\sin((2b+1)\pi\nu\Delta x)}{\sin \pi\nu\Delta x}
\end{aligned}$$

In two-dimensions:

$$\begin{aligned}
d(x,y) &= d(x) * d(y) \\
&= \sum_{j=-b_x}^{b_x} \sum_{k=-b_y}^{b_y} \delta(x - j\Delta x, y - k\Delta y)
\end{aligned}$$

Implying that the two-dimensional Fourier transform is:

$$\begin{aligned}
D(\nu_x, \nu_y) &= D(\nu_x) \times D(\nu_y) \\
&= \frac{\sin((2b_x+1)\pi\nu_x\Delta x)}{\sin \pi\nu_x\Delta x} \times \frac{\sin((2b_y+1)\pi\nu_y\Delta y)}{\sin \pi\nu_y\Delta y}
\end{aligned}$$

B.7 The not-a-knot end-condition for the B-spline

(section 4.5)

The cubic B-spline function (equation 4.11) is:

$$f(x) = \sum_{i=-1}^{2} \left(\sum_{j=0}^{3} k_{i,j}\, t^j \right) g_{\alpha+i}$$

The third derivative of this is:

$$\begin{aligned} f'''(x) &= 6 \sum_{i=-1}^{2} k_{i,3}\, g_{\alpha+i} \\ &= -g_{\alpha-1} + 3g_\alpha - 3g_{\alpha+1} + g_{\alpha+2} \end{aligned}$$

The not-a-knot condition requires $f'''(x)$ to be continuous at x_1 and x_{n-2}. At x_1:

$$\begin{aligned} -g_{-1} + 3g_0 - 3g_1 + g_2 &= -g_0 + 3g_1 - 3g_2 + g_3 \\ \Rightarrow g_{-1} - 4g_0 + 6g_1 - 4g_2 + g_3 &= 0 \end{aligned} \tag{B.5}$$

We know that (equation 4.12):

$$f_i = \frac{1}{6}(g_{i-1} + 4g_i + g_{i+1})$$

For f_0 we can write $6f_0 = g_{-1} + 4g_0 + g_1$. Subtracting this from equation B.5 gives:

$$-8g_0 + 5g_1 - 4g_2 + g_3 = -6f_0 \tag{B.6}$$

For f_2 we can write $6f_2 = g_1 + 4g_2 + g_3$. Subtracting this from equation B.6 produces:

$$-8g_0 + 4g_1 - 8g_2 = -6f_0 - 6f_2 \tag{B.7}$$

And for f_1 we can write $48f_1 = 8g_0 + 32g_1 + 8g_2$. Adding this to equation B.7 gives:

$$36g_1 = 48f_1 - 6f_0 - 6f_2 \tag{B.8}$$

Making equation B.8 a function of g_1 gives us:

$$g_1 = \frac{1}{6}(8f_1 - f_0 - f_2)$$

QED

A similar derivation holds for g_{n-2}.

B.8 Timing calculations for the B-spline kernel

(section 4.5.4)

In the first method we need to sum 113 terms (assuming we adopt the diamond shaped kernel discussed on page 139). Each term is of the form:

$$V_i W_j f_{x-i,y-j}$$

Where 15 V_i and 15 W_j values must be precalculated as follows:

$$\begin{aligned} V_i &= v_{i,3}r^3 + v_{i,2}r^2 + v_{i,1}r^1 + v_{i,0} \\ W_i &= w_{j,3}t^3 + w_{j,2}t^2 + w_{j,1}t^1 + w_{j,0} \end{aligned}$$

Operation	Method 1	Method 2	M1/M2
Multiplies	320	113	3×
Adds	202	112	2×
Table lookups	120	113	1×
Function value lookups	113	113	1×

Table B.1: Timing calculations for the two ways of implementing the interpolating cubic B-spline.

where i and j range from -7 to 7, $v_{i,n}$ and $w_{j,n}$ are retrieved from a table, and the r^n and t^n terms are precalculated.

From this we find that we require 320 multiples, 202 adds, 120 table lookups and 113 function value lookups for each intensity surface value calculation.

Using the second method, each coefficient is calculated by summing 113 products of a table lookup ($a^{|i|+|j|}$) and a function value lookup ($f_{x-i,y-j}$). This makes the requirement 113 multiples, 112 adds, 113 table lookups and 113 function value lookups, per coefficient.

These values are laid out in table B.1, from which we can conclude that the first method's calculation is 2 to 3 times as long as the second method's, thus $2c < k_1 < 3c$.

B.9 The error in edge position due to quantisation

section 6.3.5

The edge's position is given by:

$$x_m = c + \frac{\hat{g}_{c+1} - \hat{g}_c}{\hat{g}_{c+1} - \hat{g}_{c-1}}$$

(equation 6.7).

Without loss of generality, take $c = 0$:

$$x_m = \frac{\hat{g}_1 - \hat{g}_0}{\hat{g}_1 - \hat{g}_{-1}} \tag{B.9}$$

With quantisation, the values of $\hat{g}_{-1}$, $\hat{g}_0$, and $\hat{g}_1$ in equation B.9 are quantised:

$$\begin{aligned} \hat{g}_{-1} &= Q(g_l) \\ \hat{g}_0 &= Q(g_r + \epsilon(g_l - g_r)) \\ \hat{g}_1 &= Q(g_r) \end{aligned}$$

The quantisation function is:

$$Q(g) = \frac{1}{N-1} \langle (N-1)g \rangle$$

The error caused by this is $\pm\frac{1}{2(N-1)}$, so:

$$Q(g) = g \pm \frac{1}{2(N-1)} \tag{B.10}$$

Substituting equation B.10 into equation B.9 gives:

$$x_m = \frac{g_r \pm \frac{1}{2(N-1)} - (g_r + \epsilon(g_l - g_r) \pm \frac{1}{2(N-1)})}{g_r \pm \frac{1}{2(N-1)} - g_l \pm \frac{1}{2(N-1)}}$$

$$\begin{aligned} &= \frac{\epsilon(g_r - g_l) \pm \frac{1}{(N-1)}}{g_r - g_l \pm \frac{1}{(N-1)}} \\ &= \frac{\epsilon(\Delta g) \pm \frac{1}{(N-1)}}{\Delta g \pm \frac{1}{(N-1)}} \end{aligned} \tag{B.11}$$

where: $\Delta g = g_r - g_l$.

If $\Delta g \gg \frac{1}{N-1}$ then equation B.11 becomes:

$$\begin{aligned} x_m &\approx \frac{\epsilon(\Delta g) \pm \frac{1}{(N-1)}}{\Delta g} \\ &= \epsilon \pm \frac{1}{\Delta g(N-1)} \end{aligned}$$

As x_m is an approximation to ϵ, the error in x_m is $\pm\frac{1}{\Delta g(N-1)}$ provided $\Delta g \gg \frac{1}{N-1}$.

Appendix C

Graphs

The graphs are unavailable in this online version of the report owing to the way in which they were produced.

This appendix contains the results used in section 7.3.4. There are two sets of experimental results. The first consists of three graphs showing the root mean square difference between an image and its doubly resampled image, for a range of magnification factors (each image is magnified by this factor and then minified by the inverse of the factor). The three images used are reproduced in figure C.1.

The second set of results consists of thirty graphs. There are five sets of graphs, one for each of the quality measures investigated. Each set contains six graphs, one for each of the six images involved in the experiments. These images are reproduced in figure 7.11.

Note that the fifth measures, called 'smoothness' in section 7.3.4 is here called 'bumpiness'.

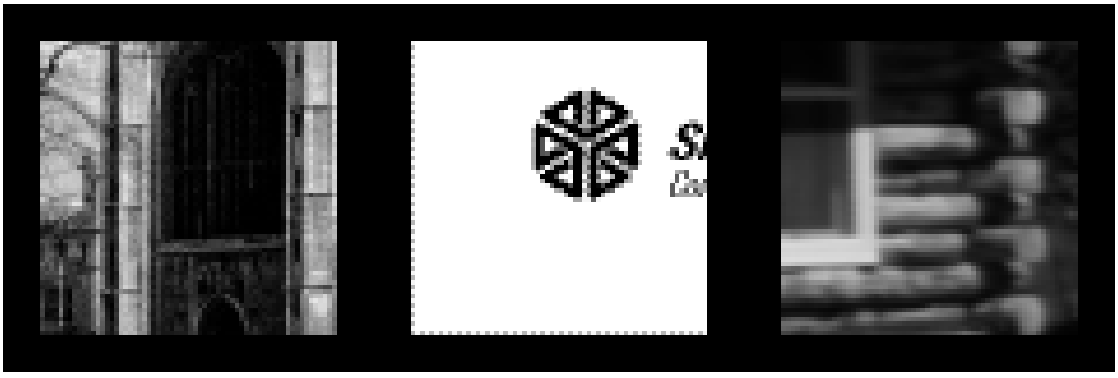

Figure C.1: The three images used in the first experiment.

Appendix D

Cornsweet's figures

This appendix should have contained two photocopies of Cornsweet's [1970] figures 11.2 and 11.3. Unfortunately, we were unable to get permission to copy these figures before the dissertation was bound. Instead we present approximations to Cornsweet's figures, which attempt to illustrate the same effect. The two images in each photograph (figures D.1 and D.3) are generated from different intensity distributions (shown in figure D.2), but, in each case, they give approximately the same visual sensation.

Figure D.1: Two intensity curves which produce roughly the same response from the human visual system. The profiles of the edges in the two images are shown in figure D.2(a) and (b) (left and right images respectively). Note that, in the right hand image, the intensity at the centre of the stripe is the same as the intensity at the left and right edges of the image. (After Cornsweet [1970] fig 11.2).

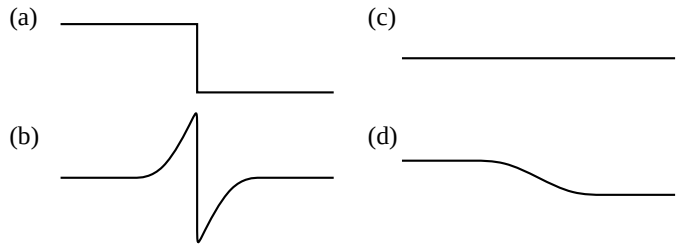

Figure D.2: The intensity profiles of the edges (a) and (b) in figure D.1; (c) and (d) in figure D.3.

Figure D.3: Two intensity curves which produce roughly the same response from the human visual system. The profiles of the 'edges' in the two images are shown in figure D.2(c) and (d) (left and right images respectively). The left hand image has no edges, while the right has slowly changing edges one quarter and three quarters of the way across the image. Thus, in the right hand image, the intensity at the centre of the image is not the same as the intensity at the left and right edges, even thought it looks virtually the same. (After Cornsweet [1970] fig 11.3).

Glossary

Approximant a *reconstructor* that does not necessarily interpolate the *image samples*. Compare *interpolant*.

Area sampler a *sampler* which uses *intensity surface* values over some area to provide a value for each *pixel* in the *image*. Compare *point sampler*.

Decomposition dividing a process into *sub-processes* in order to better understand the process. In this dissertation decomposition is applied to the image resampling process, notably decomposing it into three sub-processes: *reconstruction*, *transform*, and *sampling*.

Destination image the *image* that is output by a resampling process, also called *resampled image* or *final image*.

Filter in an *area sampler* there is an equivalence that allows us to represent the sampler as a filter combined with *single point sampling*, such that the filter is the function that is convolved with the *intensity surface* before single point sampling the filtered surface. Some *point samplers* can also be represented in this way. Some *reconstructors* can be represented by filters, so that the *reconstructed intensity surface* that they produce is the convolution of the filter with the *image*. Also called *kernel* or 'filter kernel'.

Final image the *image* that is output by a resampling process, also called *destination image* or *resampled image*.

Final intensity surface the *intensity surface* generated by *transforming* the *original intensity surface*. The *final image* is generated from it by *sampling*.

Hedgehog an omnivorous mammal renowned for its prickliness.

Image in this dissertation 'image' almost exclusively refers to a discrete image. A continuous image is known as an *intensity surface*.

Image samples the sample values that make up a discrete *image*. Also called *pixels* or *pixel values*.

Intensity surface a continuous surface in three dimensions, with two spatial dimensions and one intensity dimension. There is a many-to-one mapping from two-dimensional spatial coordinates to intensity values. Can be extrapolated to an intensity volume (three spatial dimensions and one intensity dimension) or to a colour surface (where colour dimensions replace the single intensity dimension). Also known as 'continuous image'.

Interpolant a *reconstructor* that interpolates the *image samples*. Compare *approximant*.

Kernel an abbreviation of 'filter kernel' (see *filter*).

Original image the *image* that is input to the resampling process, also called *source image*.

Original intensity surface the *intensity surface* generate from the *original image* by *reconstruction*.

Pixel (a) a single sample value in an *image*; (b) the theoretical area represented by such a sample value in an *intensity surface* which generates, or is generated by, that image. Also called 'pel'.

Point sampler a *sampler* which only uses *intensity surface* values at a countable set of points to provide a value for each *pixel* in the *image*. Compare *area sampler*.

Reconstruction applying a *reconstructor* to an *image* to produce an *intensity surface*.

Reconstructor a process which reconstructs a continuous *intensity surface* from a discrete *image*.

Resample to take a discrete *image* and produce another *image* which appears to be a spatially transformed version of the first.

Resampled image the *image* that is output by a resampling process, also called *final image* or *destination image*.

Resampler a process which performs image resampling.

Sampler a process which produces a discrete *image* from a continuous *intensity surface*.

Sampling applying a *sampler* to an *intensity surface* to produce an *image*.

Single point sampler a *point sampler* which uses a single *intensity surface* value to provide a value for each *pixel*.

Source image the *image* that is input to a resampling process, also called *original image*.

Sub-process a process that forms part of a larger process. Sub-processes are generated by *decomposition* of some process. Also called: a 'part' or 'stage' of the larger process.

Transform a process which takes a continuous *intensity surface* and produces another, transformed, intensity surface from it.

Warp a synonym for *resample*, used more in computer graphics work; whilst 'resample' is used more in signal processing work.

Bibliography

The reference style used in this dissertation follows these rules:

1. A reference is given by the author's name, or authors' names, followed by the date of publication and sometimes extra information as to the location within the quoted work of the particular item referenced.

2. If the context requires a direct reference to the paper then the name(s) are placed in the text, with the other material placed in square brackets immediately after the name(s). If an indirect reference is required then all the information appears inside square brackets.

3. A work with three or more authors should be referenced by all the authors' names the *first* time it is referred to. Subsequent references use the first author's name followed by "*et al*" in place of all the other names.

This last rule has been bent in the case of Venot, Devaux, Herbin, Lebruchec, Dubertret, Raulo and Roucayrol [1988] and Herbin, Venot, Devaux, Walter, Lebruchec, Dubertret and Roucayrol [1989]. These are always referred to as Venot *et al* [1988] and Herbin *et al* [1989] respectively.

To aid those working at the University of Cambridge, there is a reference mark at the end of many of the entries in this bibliography which shows where the referenced work may be found. Abbreviations used in these references are:

CLL Computer Laboratory Library
SPL Scientific Periodicals Library
UL University Library

Adobe, [1985a] *PostScript Language Reference Manual*, Addison-Wesley, Reading, Massachusetts, USA, ISBN 0–201–10174–2.

Ahmed, N., Natarajan, T. and Rao, K.R. [1974] "Discrete cosine transform", *IEEE Transactions on Computers*, Vol. C–23, No. 1, Jan, 1974, pp.90–93. CLL

Andrews, H.C. and Patterson, C.L. (III) [1976] "Digital interpolation of discrete images", *IEEE Transactions on Computers*, Vol. C–25, No. 2, Feb, 1976, pp.197–202. CLL

Bier, E.A. and Slone, K.R.(Jr) [1986] "Two-part texture mappings", *IEEE Computer Graphics and Applications*, Sept, 1986, pp.40–53. CLL

Binkley, T. [1990] "Digital dilemmas", *LEONARDO*, Digital Image—Digital Cinema Supplemental Issue, 1990, pp.13–19. CLL

Bley, H. [1980] "Digitization and segmentation of circuit diagrams", *Proceedings of the First Scandanavian Comference on Image Analysis*, Studentlitteratur, Lund, Sweden, 1980, pp.264–269. UL 348:8.c.95.1213

Blinn, J.F. [1989a] "What we need around here is more aliasing", *IEEE Computer Graphics and Applications*, Jan, 1989, pp.75–79. CLL

Blinn, J.F. [1989b] "Return of the jaggy", *IEEE Computer Graphics and Applications*, Mar, 1989, pp.82–89. CLL

Blinn, J.F. [1990] "Wonderful world of video", *IEEE Computer Graphics and Applications*, Vol. 10, No. 3, May, 1990, pp.83–87. SPL E0.2.96

Boult, T.E. and Wolberg, G. [1992] "Local image reconstruction and sub-pixel restoration algorithms", *CVGIP: Image Understanding*, in press.

Braccini, C. and Marino, G. [1980] "Fast geometrical manipulations of digital images", *Computer Graphics and Image Processing*, Vol. 13, 1980, pp.127–141. SPL E0.2.13

Brewer, J.A. and Anderson, D.C. [1977] "Visual interaction with Overhauser curves and surfaces", *Computer Graphics*, Vol. 11, No. 2, Summer, 1977, pp.132–137.

Brown, E.F. [1969] "Television: the subjective effects of filter ringing transients", *Journal of the Society of Motion Picture and Television Engineers (SMPTE),* Vol. 78, No. 4, Apr, 1969, pp.249–255. SPL E0.2.24

Catmull, E. [1974] "Computer display of curved surfaces", *Proceedings of the Conference on Computer Graphics, Pattern Recognition and Data Structure*, Los Angeles, California, May 14–16, 1974, IEEE, New York, 1975, IEEE Catalogue Number 75CHO981–1C, pp.11–17.
Also reprinted as: *Tutorial and Selected Readings in Interactive Computer Graphics*, H. Freeman (ed), IEEE, 1980, IEEE Catalogue Number EHO 156–0, pp.309–315.

Catmull, E. and Rom, R. [1974] "A class of local interpolating splines", *Computer Aided Geometric Design*, R.E. Barnhill and R.F. Riesenfeld (eds.), Academic Press, New York, ISBN 0–12–079050–5, pp.317–326.

Catmull, E. and Smith, A.R. [1980] "3-D transformations of images in scanline order", *Computer Graphics*, Vol. 14, No. 3, 1980, pp.279–285.

Chen, W-H. and Pratt, W.K. [1984] "Scene adaptive coder", *IEEE Transactions on Communications*, Vol. COM–32, No. 3, Mar, 1984, pp.255–232. CLL

Chiou, A.E.T. and Yeh, P. [1990] "Scaling and rotation of optical images using a ring cavity", *Applied Optics*, Vol. 29, No. 11, 10^{th} Apr, 1990, pp.1584–1586. SPL F1.2.3

Chu, K-C. [1990] "B3-splines for interactive curve and surface fitting", *Computers and Graphics*, Vol. 14, No. 2, 1990, pp.281–288. SPL E0.1.34

Cook, R.L. [1986] "Stochastic sampling in computer graphics", *ACM Transactions on Graphics*, Vol. 5, No. 1, Jan, 1986, pp.51–72. CLL

Cornsweet, T.N. [1970] *Visual Perception*, Academic Press, 1970, Library of Congress Catalogue Card No. 71–107570.
Physiological Lab. Library C6.143A

Crow, F.C. [1977] "The aliasing problem in computer-generated shaded images", *Communications of the ACM*, Vol. 20, No. 11, Nov, 1977, pp.799–805 CLL

Crow, F.C [1978] "The use of grayscale for improved raster display of vectors and characters", *Computer Graphics*, Vol. 12, No. 3, Aug, 1978, pp.1–5. CLL

Crow, F.C. [1984] "Summed-area tables for texture mapping", *Computer Graphics*, Vol. 18, No. 3, Jul, 1984, pp.207–212. CLL

Cumani, A., Grattoni, P. and Guiducci, A. [1991] "An edge-based description of colour images", *CVGIP: Graphical Models and Image Processing*, Vol. 53, No. 4, Jul, 1991, pp.313–323. CLL

Data Beta [1992] Product Description; Data Beta Ltd, Unit 7, Chiltern Enterprise Centre, Theale, Berkshire, United Kingdom RG7 4AA.

Durand, C.X. [1989] "Bit map transformations in computer 2-D animation", *Computers and Graphics*, Vol. 13, No. 4, 1989, pp.433–440. SPL E0.1.34

Durand, C.X. and Faguy, D. [1990] "Rational zoom of bit maps using B-spline interpolation in computerized 2-D animation", *Computer Graphics Forum*, Vol. 9, No. 1, Mar, 1990, pp.27–37 CLL

Dwight, H.B. [1934] *Tables of Integrals and other Mathematical Data*, The MacMillan Company, New York, 1934. CLL X14

Euclid [300BC] *Elements.*

Fang, Z., Li, X. and Ni, L.M. [1989] "On the communication complexity of generalised 2-D convolution on array processors", *IEEE Transactions on Computers*, Vol. 38, No. 2, Feb, 1989, pp.184–194. CLL

Fant, K.M. [1986] "A non-aliasing, real-time spatial transform technique", *IEEE Computer Graphics and Applications*, Jan, 1986, pp.71–80. SPL E0.2.96

Fiume, E.L. [1986] "A mathematical semantics and theory of raster graphics", PhD thesis, technical report CSRI–185, Computer Systems Research Group, University of Toronto, Toronto, Canada M5S 1A1 CLL V106–669
Published, with minor additions, as Fiume [1989].

Fiume, E.L. [1989] *The Mathematical Structure of Raster Graphics*, Academic Press, San Diego, 1989, ISBN 0–12–257960–7.
Based on Fiume [1986].

Feibush, E.A., Levoy, M. and Cook, R.L. [1980] "Synthetic texturing using digital filters", *Computer Graphics*, Vol. 14, 1980, pp.294–301.

Foley, J.D. and van Dam. A. [1982] *Fundamentals of Interactive Computer Graphics*, Addison-Wesley, Reading, Massachusetts, USA, 1982, ISBN 0–201–14468–9.

Foley, J.D., van Dam, A., Feiner, S.K. and Hughes, J.F. [1990] *Computer Graphics: Principles and Practice* ('second edition' of Foley and van Dam [1982]), Addison-Wesley, Reading, Massachusetts, USA, 1990, ISBN 0–201–12110–7.

Fournier, A. and Fiume, E.L. [1988] "Constant-time filtering with space-variant kernels", *Computer Graphics*, Vol. 22, No. 4, Aug, 1988, pp.229–238. CLL

Fournier, A. and Fussell, D. [1988] "On the power of the frame buffer", *ACM Transactions on Graphics*, Vol. 7, No. 2, Apr, 1988, pp.103–128. CLL

Fraser, D. [1987] "A conceptual image intensity surface and the sampling theorem", *Australian Computer Journal*, Vol. 19, No. 3, Aug, 1987, pp.119–125. SPL E0.13.3

Fraser, D. [1989a] "Interpolation by the FFT revisited — an experimental investigation", *IEEE Transactions on Acoustics, Speech and Signal Processing*, Vol. 37, No. 5, May, 1989, pp.665–675. SPL E0.2.34

Fraser, D. [1989b] "Comparison at high spatial frequencies of two-pass and one-pass geometric transformation algorithms", *Computer Vision, Graphics and Image Processing*, Vol. 46, No. 3, Jun, 1989, pp.267–283. SPL E0.2.34

Fraser, D., Schowengerdt, R.A. and Briggs, I. [1985] "Rectification of multichannel images in mass storage using image transposition", *Computer Vision, Graphics and Image Processing*, Vol. 29, No. 1, 1985, pp.23–56. SPL E0.2.13

Fredrick, C. and Schwartz, E.L. [1990] "Conformal image warping", *IEEE Computer Graphics and Applications*, Vol. 10, No. 2, Mar, 1990, pp.54–61. SPL E0.2.96

Gardner, I.C. and Washer, F.E [1948] "Lenses of extremely wide angle for airplane mapping", *Journal of the Optical Society of America*, Vol. 38, No. 5, May, 1948, pp.421–431. SPL F1.2.1

Gibbs, A.R. [1992] *Personal communication.*

Glassner, A. [1986] "Adaptive precision in texture mapping", *Computer Graphics*, Vol. 20, No. 4, Aug, 1986, pp.297–306. CLL

Glassner, A.S. [1990b] "Interpretation of texture map indices", *Graphics Gems*, A.S. Glassner (ed.), Academic Press Ltd, San Diego, California, USA, 1990, ISBN 0–12–286165–5.

Gonzalez, R.C. and Wintz, P. [1977] *Digital Image Processing*, Addison-Wesley, 1977, ISBN 0–201–02596–5. CLL U135

Goshtasby, A. [1989] "Correction of image deformation from lens distortion using Bezier patches", *Computer Vision, Graphics and Image Processing*, Vol. 47, 1989, pp.385–394. SPL E0.2.13

Greene, N. and Heckbert, P.S. [1986] "Creating raster omnimax images from multiple perspective views using the elliptical weighted average filter", *IEEE Computer Graphics and Applications*, Vol. 6, No. 6, Jun, 1986, pp.21–27. CLL

Guibas, L.J. and Stolfi, J. [1982] "A language for bitmap manipulation", *ACM Transactions on Graphics*, Vol. 1, No. 3, Jul, 1982, pp.191–214.

Hall, A.D. [1989] "Pipelined logical convolvers for binary picture processing", *Electronics Letters*, Vol. 25, No. 15, 20 Jul, 1989, pp.961–963. SPL E0.1.36

Hall, A.D. [1991] *Personal communication.*

Hall, E.L. [1979] *Computer image processing and recognition*, Academic Press, New York, USA, 1979, ISBN 0–12–318850–4. CLL 1Y88

Hammerin, M. and Danielsson, P-E. [1991] "High accuracy rotation of images", *Contributions to the SSAB symposium, March, 1991*, Report No. LiTH–ISY–I–1161, Department of Electrical Engineering, Linköping University, S–58183 Linköping, Sweden; pp.1–4.

Hanrahan, P. [1990] "Three-pass affine transforms for volume rendering", *Computer Graphics*, Vol. 24, No. 5, Nov, 1990, pp.71–78. CLL

Heckbert, P.S. [1986a] "Survey of texture mapping", *IEEE Computer Graphics and Applications*, Nov, 1986, pp.56–67. CLL

Heckbert, P.S. [1986b] "Filtering by repeated integration", *Computer Graphics*, Vol. 20, No. 4, 1986, pp.315–321. CLL

Heckbert, P.S. [1989] "Fundamentals of texture mapping and image warping", Master's thesis, report number UCB/CSD 89/516, Computer Science Division (EECS), University of California, Berkeley, California 94720, USA; June, 1989.

Heckbert, P.S. [1990a] "What are the coordinates of a pixel?", *Graphics Gems*, A.S. Glassner (ed.), Academic Press, 1990, ISBN 0–12–28616–5, pp.246–248.

Heckbert [1990b] "Texture mapping", lecture presented to the ACM/BCS International Summer Institute, "State of the art in computer graphics", 2–6 July, 1990, Edinburgh, U.K.

Heckbert, P.S. [1991a] "Review of 'Digital Image Warping' [Wolberg, 1990]", *IEEE Computer Graphics and Applications*, Jan, 1991, pp.114–116. CLL

Heckbert, P.S. [1991b] Response to Wolberg [1991] and McDonnell's [1991] replies to Heckbert's [1991a] review of Wolberg's [1990] book ("Letters to the Editor" column), *IEEE Computer Graphics and Applications*, May, 1991, p.5. CLL

Herbin, M., Venot, A., Devaux, J.Y., Walter, E., Lebruchec, J.F., Dubertret, L. and Roucayrol, J.C. [1989] "Automated registration of dissimilar images: application to medical imagery", *Computer Vision, Graphics and Image Processing*, Vol. 47, No.1, Jul, 1989, pp.77–88. SPL E0.2.13

Horn, B.K.P. [1977] "Understanding image intensities", *Readings in Computer Vision*, M.A. Fischler and O. Fischler (eds.), Morgan Kaufmann Publishers Inc., 95 First Street, Los Altos, California 94022, USA, 1987, ISBN 0–934613–33–8.
Originally in *Artificial Intelligence*, Vol.8, No.2, 1977, pp.201–231.

Hou, H.S. and Andrews, H.C. [1978] "Cubic splines for image interpolation and digital filtering", *IEEE Transactions on Acoustics, Speech and Signal Processing*, Vol. ASSP–26, No. 6, Dec, 1978, pp.508–517. SPL E0.2.34

Hyde, P.D. and Davis. L.S. [1983] "Subpixel edge estimation", *Pattern Recognition*, Vol. 16, No. 4, 1983, pp.413–420. SPL E0.0.1

Kajiya, J.T. and Kay, T.L. [1989] "Rendering fur with three-dimensional textures", *Computer Graphics*, Vol. 23, No. 3, Jul, 1989, pp.656–657. CLL

Keys, R.G. [1981] "Cubic convolution interpolation for digital image processing", *IEEE Transactions on Acoustics, Speech and Signal Processing*, Vol. ASSP–29, No. 6, Dec, 1981, pp.1153–1160. SPL E0.2.34

Kiryati, N. and Bruckstein, A. [1991] "Gray levels can improve the performance of binary image digitizers", *CVGIP: Graphical Models and Image Processing*, Vol. 53, No. 1, Jan, 1991, pp.31–39. CLL

Kitchen, L.J. and Malin, J.A. [1989] "The effect of spacial discretization on the magnitude and direction response of simple differential operators on a step edge", *Computer Vision, Graphics and Image Processing*, Vol. 47, No.2 , Aug, 1989, pp.234–258. SPL E0.2.13

Klassman, H. [1975] "Some aspects of the accuracy of the approximated position of a straight line on a square grid", *Computer Graphics and Image Processing*, Vol. 4, No. 3, Sept, 1975, pp.225–235. SPL E0.2.13

Kornfeld, C.D. [1985] "Architectural elements for bitmap graphics", PhD thesis, technical report CSL–85–2, June, 1985, Xerox Corporation, Palo Alto Research Center, 3333 Coyote Hill Road, Palo Alto, California 94304, USA, 1985. CLL V106–900

Kornfeld, C. [1987] "The image prism: a device for rotating and mirroring bitmap images", *IEEE Computer Graphics and Applications*, Vol. 7, No. 5, 1987, pp.21–30. CLL

Kuhnert, K-D. [1989] "Sensor modelling as a basis of subpixel image processing", *Proceedings of the SPIE*, Vol. 1135, "Image Processing III", chair and editor: J.F. Duverney; 27–28 April, 1989, Paris, France, pp.104–111. SPL F1.2.6

Laser-Scan, [1989] "VTRAK", Laser-Scan Laboratories Ltd, Software Product Specification, Jan 12, 1989, issue 1.2. Laser-Scan, Science Park, Milton Rd, Cambridge, CB4 4FY.

Lee, C-H. [1983] "Restoring spline interpolation of CT images", *IEEE Transactions on Medical Imaging*, Vol. MI–2, No. 2, Sept, 1983, pp.142–149.

Lynn, P.A. and Fuerst, W. [1989] *Introductory digital signal processing with computer applications*, John Wiley and Sons, Ltd, Chichester, 1989, ISBN 0–471–91564–5.

Mach, E. [1865] "On the visual sensations produced by intermittent excitations of the retina", *Philosophical Magazine*, Vol. 30, No. 2, Fourth Series, 1865, pp.319–320. SPL A0.1.2

Maeland, E. [1988] "On the comparison of the interpolation methods", *IEEE Transactions on Medical Imaging*, Vol. 7, No. 3, Sept, 1988, pp.213–217. SPL E0.2.103

Maisel, J.E. and Morden, R.E [1981] "Rotation of a two-dimensional sampling set using one-dimensional resampling", *IEEE Transactions on Acoustics, Speech and Signal Processing*, Vol. ASSP–29, No. 6, Dec, 1981, pp.1218–1222. SPL E0.2.34

Mantas, J. [1987] "Methodologies in patternrecognition and image analysis — a brief survey", *Pattern Recognition*, Vol. 20, No. 1, 1987, pp.1–6. SPL E0.0.1

Marion, A. [1991] *An introduction to image processing*, Chapman and Hall, 2–6 Boundary Row, London, 1991, ISBN 0–412–37890–6.

Marr, D. [1976] "Early processing of visual information", *Philosophical Transactions of the Royal Society of London*, Vol. 257, Series B, 1976, pp.483–524.

Martin, G.E. [1982] *Transformation Geometry*, Springer-Verlag, New York, USA, 1982, ISBN 0–387–90636–3.

McDonnell, M. [1991] "Response to Heckbert's [1991a] review of Wolberg's [1990] book", "Letters to the Editor" column, *IEEE Computer Graphics and Applications*, May, 1991, p.4–5.

Mersereau, R.M [1979] "The processing of hexagonally sampled two-dimensional signals", *Proceedings of the IEEE*, Vol. 67, No. 6, Jun, 1979, pp.930–949. CLL

Mitchell, D.P. and Netravali, A.N. [1988] "Reconstruction filters in computer graphics", *Computer Graphics*, Vol. 22, No. 4, Aug, 1988, pp.221–288. CLL

Murch, G.M. and Weiman, N. [1991] "Gray-scale sensitivity of the human eye for different spacial frequencies and display luminance levels", *Proceedings of the Society for Information Display*, Vol. 32, No. 1, 1991, pp.13–17.

Nagioff, O. [1991] *Personal communication.*

Namane, A. and Sid-Ahmed, M.A. [1990] "Character scaling by contour method", *IEEE Transactions on Pattern Analysis and Machine Intelligence*, Vol. 12, No. 6, Jun, 1990, pp.600–606. SPL E0.2.98

Newman, W. and Sproull, R. [1979] *Principles of Interactive Computer Graphics* (second edition), McGraw-Hill, 1979, ISBN 0–07–046338–7.

NMFPT, [1992] National Museum of Film, Photography, and Television, Bradford, West Yorkshire, *personal communication.*

Oakley, J.P. and Cunningham, M.J. [1990] "A function space model for digital image sampling and its application in image reconstruction", *Computer Graphics and Image Processing*, Vol. 49, No. 2, Feb, 1990, pp.171–197. SPL E0.2.13

Oka, M., Tsutsui, K., Ohba, A., Kurauchi, Y. and Tago, T. [1987] "Real-time manipulation of texture-mapped surfaces", *Computer Graphics*, Vol. 21, No. 4, Jul, 1987, pp.181–188. CLL

Olsen, J. [1990] "Smoothing enlarged monochrome images", *Graphics Gems*, A.S. Glassner,(ed.), Academic Press Ltd, San Diego, CA, 1990, ISBN 0–12–286165–5, pp.166–170.

Oskoui-Fard, P. and Stark, H. [1988] "Tomographic image reconstruction using the theory of convex projections", *IEEE Transactions on Medical Imaging*, Vol. 7, No. 1, Mar, 1988, pp.45–58. SPL E0.2.103

Overhauser, A.W. [1968] "Analystical definition of curves and surfaces by parabolic blending", Mathematical and Theoretical Sciences Department, Scientific Laboratory, Ford Motor Company, Report No. SL–68–40, 1968.

Paeth, A.W. [1986] "A fast algorithm for general raster rotation", *Proceedings, Graphics Interface '86/Vision Interface'86*, 26–30 May, 1986, pp.77–81. CLL 1Y712

Paeth, A.W. [1990] "A fast algorithm for general raster rotation", *Graphic Gems*, A.S. Glassner (ed.), Academic Press, 1990, ISBN 0–12–286165–5.

Park, S.K. and Schowengerdt, R.A. [1982] "Image sampling, reconstruction and the effect of sample scene phasing", *Applied Optics*, Vol. 21, No. 17, 1 Sept, 1982, pp.3142–3151. SPL F1.2.3

Park, S.K. and Schowengerdt, R.A. [1983] "Image reconstruction by parametric cubic convolution", *Computer Vision, Graphics and Image Processing*, Vol. 23, No. 3, Sept, 1983, pp.258–272. SPL E0.2.13

Parker, J.A., Kenyon, R.V. and Troxel, D.E. [1983] "Comparison of interpolation methods for image resampling", *IEEE Transactions on Medical Imaging*, Vol. MI–2, No. 1, Mar, 1983, pp.31–39.

Pavlidis, T. [1982] *Algorithms for Graphics and Image Processing*, Springer-Verlag, 1982. CLL 1Y138

Pavlidis, T.[1990] "Re: Comments on 'Stochastic Sampling in Computer Graphics' [Cook, 1986]", Letter to the Editor, *ACM Transactions on Graphics*, Vol. 9, No. 2, Apr, 1990, pp.233–326. CLL

Petersen, D.P. and Middleton, D. [1962] "Sampling and reconstruction of wave-number-limited functions in N-dimensional Euclidean spaces", *Information and Control*, Vol. 5, No. 4, Dec, 1962, pp.279–323. SPL E0.2.121

Pettit, F. [1985] *Fourier Transforms in Action* Chartwell-Bratt (Publishing and Training) Limited, 1985, ISBN 0–86238–088–X. CLL 1Y505

Piegl, L. [1991] "On NURBS: a survey", *IEEE Computer Graphics and Applications*, Jan, 1991, pp.55–71. CLL

Prasad, K.P. and Satyanarayana, P. [1986] "Fast interpolation algorithm using FFT", *Electronics Letters*, Vol. 22, No. 4, 13 Feb, 1986, pp.185–187. SPL E0.1.36

Pratt, W.K [1978] *Digital Image Processing*, John Wiley and Sons, New York, USA, 1978, ISBN 0–471–01888–0. UL 9428.c.3814

Pratt, W.K [1991] *Digital Image Processing* (second edition), John Wiley and Sons, New York, USA, 1991, ISBN 0–471–85766–0.

Press, W.H., Flannery, B.P., Teukolsky, S.A. and Vetterling, W.T. [1988] *Numerical Recipes in C: The Art of Scientific Computing*, Cambridge University Press, Cambridge, 1988, ISBN 0–521–35465–X.

Rabbani, M. and Jones, P.W. [1991] *Digital Image Compression Techniques*, SPIE — The Society of Photo-Optical Instrumentation Engineers, P.O. Box 10, Bellingham. Washington, USA, 1991, ISBN 0–8194–10648–1.

Rasala. R. [1990] "Explicit cubic spline interpolation formulas", *Graphic Gems*, A.S. Glassner (ed.), Academic Press, 1990, ISBN 0–12–286165–5.

Ratliff, F. [1965] *Mach Bands: Quantitative studies on neural networks in the retina*, Holden-Day Inc, San Francisco, USA, 1965.
Psychology Lab. Library: C.6.68A

Ratzel, J.N. [1980] "The discrete representation of spatially continuous images", PhD thesis, Department of Electrical Engineering and Computer Science, Massachusetts Institute of Technology, Cambridge, Massachusetts, USA, Aug, 1980.

Reed, T.R., Algazi, V.R., Ford, G.E. and Hussain, I. [1992] "Perceptually based coding of monochrome and color still images", *Proceedings of the Data Compression Conference*, March 24–27, 1992, Snowbird, Utah, USA; J.A. Storer and M. Cohn (eds.), IEEE Computer Society Press, Los Alamitos, California, USA; ISBN 0–8186–2717–4 (case bound); pp.142–151.

Reichenbach, S.E. and Park, S.K. [1989] "Two-parameter cubic convolution for image reconstruction", *Proceedings of the SPIE*, Vol. 1199, "Visual Communications and Image Processing IV (1989)", pp.833–840.

Richards, P.I. [1966] "Sampling positive functions", *Proceedings of the IEEE (Letters)*, Vol. 54, No. 1, Jan, 1966, pp.81–82. CLL

Robertson, P.K. [1987] "Fast perspective views of images using one-dimensional operations", *IEEE Computer Graphics and Applications*, Vol. 7, No. 2, Feb, 1987, pp.47–56. SPL E0.2.96

Rogers, D.F. and Adams, J.A. [1976] *Mathematical Elements for Computer Graphics*, McGraw-Hill, 1976, ISBN 0–07–053527–2.

Rosenenfeld, A. [1988] "Computer vision: basic principles", *Proceedings of the IEEE*, Vol. 76, No. 8, Aug, 1988, pp.863–868. CLL

Rosenfeld, A. and Kak, A.C. [1982] *Digital Picture Processing* (second edition, two volumes), Academic Press, Orlando, Florida, USA, 1982, ISBN 0–12–597301–2. CLL 1Y213

Rothstein, J. and Weiman, C. [1976] "Parallel and sequential specification of a context sensitive language for straight lines on grids", *Computer Graphics and Image Processing*, Vol. 5, No. 1, Mar, 1976, pp.106–124. SPL E0.2.13

van Sant, T. [1992] "The Earth/From Space", a satellite composite view of Earth, ©Tom van Sant/The Geosphere Project, Santa Monica, California, USA, 800 845–1522.
Reproduced in *Scientific American*, Vol. 266, No. 4, April, 1992, p.6.

Schafer, R.W. and Rabiner, L.R. [1973] "A digital signal processing approach to interpolation", *Proceedings of the IEEE*, Vol. 61, No. 6, Jun, 1973, pp.692–702.

Schoenberg, I.S. [1973] "Cardinal spline interpolation", *Regional Conference Series in Applied Mathematics*, Society for Industrial and Applied Mathematics, (SIAM), Philadelphia, Pennsylvania, USA, Vol. 12, 1973.

Schreiber, W.F. and Troxel, D.E. [1985] "Transformation between continuous and discrete representations of images: a perceptual approach", *IEEE Transactions on Pattern Analysis and Machine Intelligence*, Vol. PAMI–7, No. 2, Mar, 1985, pp.178–186. SPL

Sedgewick, R. [1988] *Algorithms* (second edition), Addison-Wesley, Reading, Massachusetts, USA, 1988, ISBN 0–201–06673–4.

Shannon, C.E. [1949] "Communication in the presence of noise", *Proceedings of the IRE*, Vol. 37, No. 1, Jan, 1949, pp.10–21. SPL E0.2.17

Sloan, A.D. [1992] "Fractal image compression: a resolution independent representation from imagery", *Proceedings of the NASA Space and Earth Science Data Compression Workshop*, March 27, 1992, Snowbird, Utah, USA; J.C. Tilton and S. Dolinar (eds.); NASA Conference Publications; to appear.

Smit, T., Smith, M.R. and Nichols, S.T. [1990] "Efficient sinc function interpolation technique for centre padded data", *IEEE Transactions on Acoustics, Speech and Signal Processing*, Vol. 38, No. 9, Sept, 1990, pp.1512–1517 SPL E0.2.34

Smith, A.R. [1981] "Digital filtering tutorial for computer graphics", Technical Memo, Lucasfilm Ltd, (available from PIXAR, 1001 West Cutting Richmond, CA 94804, USA). Technical Memo No. 27, 1981.

Smith, A.R. [1982] "Digital filtering tutorial, part II", Technical Memo, Lucasfilm Ltd, (available from PIXAR, 1001 West Cutting Richmond, CA 94804, USA). Technical Memo No. 44, 10 May, 1982.

Smith, A.R. [1987] "Planar 2-pass texture mapping and warping", *Computer Graphics*, Vol. 21, No. 4, Jul, 1987, pp.263–272. CLL

Smith, T.G. [1986] *Industrial Light and Magic: the art of special effects*, Virgin Publishing, 338 Ladbroke Grove, London, UK, 1986, ISBN 0–86287–142–5.

Sproull, R.F. [1986] "Frame-buffer display architectures", *Annual Review of Computer Science*, Vol. 1, 1986, pp.19–46. SPL A0.2.39

Trussell, H.J., Ardner, L.L., Moran, P.R. and Williams, R.C. [1988] "Corrections for non-uniform sampling distributions in magnetic resonance imagery", *IEEE Transactions on Medical Imaging*, Vol. 7, No. 1, Mar, 1988, pp.32–44. SPL E0.2.103

TRW, [1988] , *Data Book: Data Converters — DSP Products*, TRW LSI Products Inc., P.O. Box 2472, La Jolla, California 92038, USA, 1988.

Turkowski, K. [1986] "Anti-aliasing in topological color spaces", *Computer Graphics*, Vol. 20, No. 4, Aug, 1986, pp.307–314. CLL

Turkowski, K. [1990] "Filters for common resampling tasks", *Graphics Gems*, A.S. Glassner (ed.), Academic Press, 1990, ISBN 0–12–286165–5.

Venot, A., Devaux, J.Y., Herbin, M., Lebruchec, J.F., Dubertret, L., Raulo, Y. and Roucayrol, J.C. [1988] "An automated system for the registration and comparison of photographic images in medicine", *IEEE Transactions on Medical Imaging*, Vol. 7, No. 4, Dec, 1988, pp.298–303. SPL E0.2.103

Vogt, R.C. [1986] "Formalised approaches to image algorithm development using mathematical morphology", Environmental Research Institute of Michigan, Ann Arbor, Michigan, USA; *personal communication*, 1986.

Ward, J. and Cok, D.R. [1989] "Resampling algorithms for image resizing and rotation", *Proceedings of SPIE*, Vol.1075, "Digital Image Processing Applications", 17–20 Jan, 1989, Y-W. Lin and R. Srinivason (eds.), Los Angeles, California, USA.
Also available: (with colour plates)as: Technical Report 24800H, Hybrid Imaging Systems Division (PRL-PPG), Kodak Research Laboratories, Eastman Kodak Company, Rochester, New York, 14650–2018, USA. SPL F1.2.6.

Waters, R. [1984] "Automated digitising: the 'remaining' obstacles", presented to "Copmputer Graphics in Mapping and Exploration", Computer Graphics '84, Wembley, London, Oct 11, 1984. Laser-Scan, Science Park, Milton Rd, Cambridge, CB4 4FY.

Waters, R. [1985] "LASERTRAK: a vector scanner", presented at AM/FM Keystone Conference, Aug, 1985. Laser-Scan, Science Park, Milton Rd, Cambridge, CB4 4FY.

Waters, R., Meader, D., and Reinecke, G. [1989] "Data Capture for the Nineties: VTRAK", Laser-Scan, 12343F Sunrise Valley Drive, Reston, Virginia 22091, USA.

Watson, A.B. [1986] "Ideal shrinking and expansion of discrete sequences", NASA Technical Memorandum 88202, Jan, 1986, NASA, Ames Research Center, Moffett Field, California 94035, USA.

Weiman, C.F.R. [1980] "Continuous anti-aliased rotation and zoom of raster images", *Computer Graphics*, Vol. 14, No. 3, 1980, pp.286–293. SPL

White, B. and Brzakovic, D. [1990] "Two methods of image extension", *Computer Vision, Graphics and Image Processing*, Vol. 50, No. 3, Jun, 1990, pp.342–352. SPL E0.2.13

Whittaker, E.T. [1915] "On the functions which are represented by the expansions of the interpolation theory", *Proceedings of the Royal Society of Edinburgh*, Vol. 35, Part 2, 1914–1915 session (issued separately July 13, 1915), pp.181–194. SPL A1.1.10

Williams, L.[1983] "Pyramidal parametrics", *Computer Graphics*, Vol. 17, No. 3, Jul, 1983, pp.1–11. CLL

Wolberg, G. [1988] "Geometric tranformation techniques for digital images: a survey", Department of COmputer Science, Columbia University, New York, New York 10027, USA; Technical Report CUCS–390–88, Dec, 1988.

Wolberg, G. [1990] *Digital Image Warping*, IEEE Computer Society Press Monograph, IEEE Computer Society Press, 10662 Los Vaqueros Circle, P.O.Box 3013, Los Alamitos, CA 90720–1264, USA, 1990, ISBN 0–8186–8944–7 (case bound).

Wolberg, G. [1991] "Response to Heckbert's [1991a] review of Wolberg's [1990] book", "Letters to the Editor" column, *IEEE Computer Graphics and Applications*, May, 1991, p.4. CLL

Wolberg, G. and Boult, T.E [1989] "Separable image warping with spatial lookup tables", *Computer Graphics*, Vol. 23, No. 3, Jul, 1989, pp.369–378. CLL

Woodsford, P.A. [1988] "Vector scanning of maps", *Proceesings of IGC Scanning Conference*, Amsterdam, 1988. Laser-Scan, Science Park, Milton Rd, Cambridge, CB4 4FY.

Wüthrich, C.A. and Stucki, P. [1991] "An algorithmic comparison between square and hexagonal based grids", *CVGIP: Graphical Models and Image Processing*, Vol. 53, No. 4, Jul, 1991, pp.324–339. CLL

Wüthrich, C.A., Stucki, P. and Ghezal, A. [1989] "A frequency domain analysis of square- and hexagonal-grid based images", *Raster Imaging and Digital Typography*, Proceedings of the International Conference, Ecole Polytechnique Fédérale, Lausanne, October, 1989; André, J. and Hersch, R.D. (eds.); Cambridge University Press, UK, 1989; ISBN 0–521–37490–1, pp.261–270